Acid Mine Drainage Prediction Techniques and Geochemical Modelling: Case Study on Gold Tailing Dams, West Rand, Witwatersrand Basin Area, South Africa

by

Changhong Wu

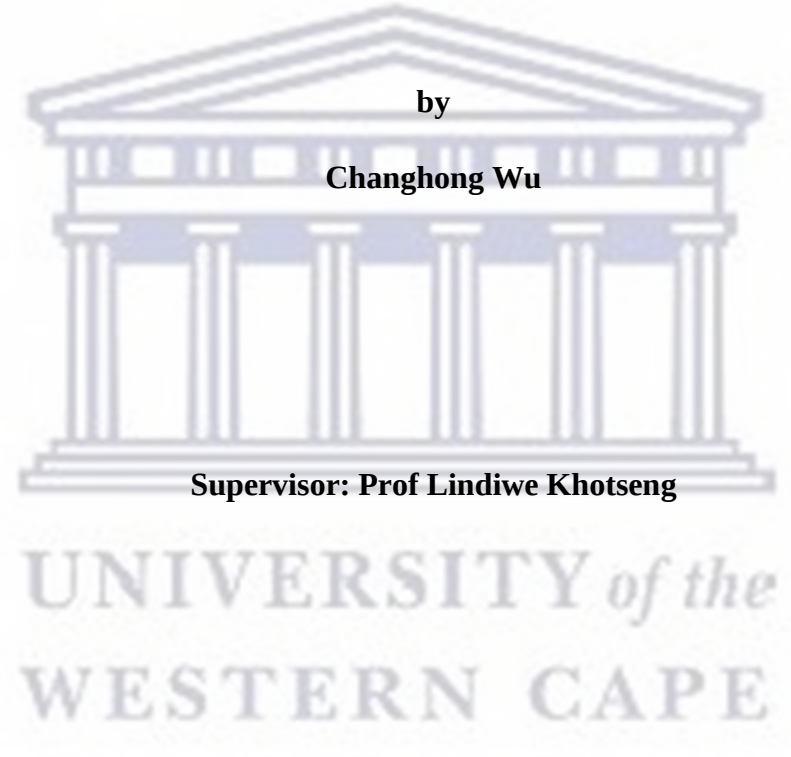

Supervisor: Prof Lindiwe Khotseng

A thesis submitted in partial fulfilment of the requirements for the degree of Doctor of Philosophy Degree of Science in Applied Geology in the Faculty of Natural Sciences at the University of the Western Cape

DECLARATION

I, Changhong Wu, student No: 2371347, hereby declare that this dissertation is my own work. It is being submitted for the Doctor of Philosophy Degree of Science at the Department of Earth Science, Faculty of Natural Sciences, University of the Western Cape, Cape Town, South Africa. It has not been submitted before for any degree or examination in any other University.

Student Signature: 

This of the 20-day February month, 2021

ABSTRACT

Keywords: Acid Mine Drainage; Gold Tailings; Geochemical; Mineralogical; Prediction; West Rand, Witwatersrand

Acid Mine Drainage (AMD) is identified as one of the contributors to environmental hazard in the gold mining region of South Africa, as caused by the mining operational activities performed by mining industries in South Africa. This effect motivates the development of AMD prediction techniques application and geochemistry modelling using gold tailing dams located in West Rand area, Witwatersrand Basin as a case study. Control strategies are devised to assess, understand and measure the acidic potential generation of waste materials in ensuring the right method required to analyse risks caused by AMD to environment. The method encompasses mineralogical and geochemical analysis of 93 samples collected, AMD prediction, test modification and geochemical modelling. This method was appropriately applied to understand the basic mechanisms involved in controlling acid generation, assessing prediction procedure and selecting the right prediction tools.

Study objectives are attained by performing a series of experimental lab tests on the samples collected from the two major tailing dams (Mogale and Gold One_1 tailings). Results derived from the lab experiments (XRD and SEM-EDS) show presence of mineral phases characterised with the surface feature of samples, and unknown substances of samples were identified. Geochemical characterisation was performed by XRF and ICP-MS to determine the major oxides elements and trace elements, respectively. Leco test generate total sulphur and total carbon. Multi-statistical analysis is used to interpret the data derived from geochemical characterisation process to explicate the metal and trace elements distribution and occurrence. Initial samples were screened and categorised based on paste pH and EC using kinetic tests to determine acid-forming and neutralising minerals in samples and static tests to determine acid generation potential in samples.

Net Acid Producing (NAPP) was mathematically calculated from Acid Neutralising Capacity (ANC), Maximum Potential Acidity (MPA) and total Sulphur. Results

obtained from the Paste pH demonstrate that samples collected from 1 meter downward the holes to 10 meters, with a few meters samples in hole T003 at Gold One_1 are non-acidic while the remaining tailing samples are acidic. ANC/MPA ratio was applied to assess the risk of acid generation from mine waste materials. Graphical illustrations of the Acid Base Account (ABA) are plotted to demonstrate the net acidic generation potential trends of samples, which were classified into non-acid forming, potential acid forming and uncertain categories. Results integration between ANC, Single Addition Net Acid Generation (NAG) test and NAPP were used to classify acid generation potential of the samples. Leachate collected from leaching column test were analysed for pH, EC and chemical element by ICP-MS. The leaching column test used to analyse samples (T004) and (T001) collected from the two major tailings was set up for a 4-month experiment.

Study findings present environmental assessment report on the two investigated gold tailing dams in Witwatersrand Basin area. Other findings are improved understanding of the application and limitations of various existing AMD prediction methods for assessment of gold mine waste and conceptual geochemical modelling developed to test appropriate methodology for AMD potential at a given gold mine site.

ACKNOWLEDGEMENTS

Thesis completed in memory of my dearest sister, Jianghong (Helen) Wu, who cannot celebrate my achievement with me. I will always love you forever.

The completion of this study would not have been attained without the ceaseless encouragement and moral supports from my friends and colleagues. Appreciation goes to the gold companies for the site support and funding received from the National Research Foundation throughout this study.

In addition, I am indebted to individuals who in one way or another supported me throughout this study. Thus, my appreciation is expressed below as thus:

- Firstly, my sincere gratitude goes to my exceptional and amiable supervisor, Professor Lindiwe Khotseng for her valuable academic support in the course of completing this study.
- I want to thank my wonderful and considerate former supervisor, Prof Charles Okujeni for his thorough guidance from the start of this study. Professor, your patient, motivation, enthusiasm, and knowledge aided me during this study to the completion of this thesis. I wish you a wonderful retirement life.
- Also, I thank my best friend, Mr Tak Wing Yu, for his unceasing encouragement, support, and attention.
- Mr Oluseyi Abegunde, a PhD student of Earth Science Department, University of the Western Cape, for his friendship and ceaseless support all the way.
- Many thanks go to my editor, Mr Oluwatimilehin Okeowo, he encouraged, persuaded, and aided me to complete my thesis during the COVID-19 pandemic.
- Many thanks to all the members of Applied Geology Department for their valuable assistance and support throughout this study, such wonderful individuals as Dr. A. Said, Prof. Jan van Bever Donker, Prof. Tapas

Chatterjee, Mr. and Mrs. Davids, Mr. Peter Meyer, Ms. Janine Becorney, Mr. Henok Solomon and Ms. Mandy Naidoo.

- Much appreciation goes to the gold mine companies staff, Department of Water and Sanitation for their valuable assistance in approving my access to the tailing dam sites for samples collection.

- I am also grateful to my entire family, my dearest parents and my sister for their incomparable love, resilient care, and valued support since my arrival in South Africa and beyond. Also, my caring husband, Dr Hongze Luo (CSIR) for his love, assistance, support and understanding throughout my course of study.

- Finally, I would like to thank individuals, whom I could not mentioned here. I appreciate your direct or indirect contributions in ensuring that I completed this study.

CONTENTS

LIST OF FIGURES

LIST OF TABLES

GLOSSARY

ABA	Acid Base Accounting
ABCC	Acid Buffering Characteristic Curve: – the relative reactivity of neutralising phases in a sample is determined by slow titration of a sample with HCl.
AMD	Acid Mine Drainage
ANC	Acid Neutralising Capacity in kg H2SO4/t: – determined by acid digestion and back titration with NaOH; ANC is equivalent to neutralisation potential (NP).
AP	Acidic Potential
ARD	Acid Rock Drainage
EC	Electrical conductivity
EDS	Energy dispersive spectroscopy
Eq	Equation
ICP –MS	Inductive Coupled Plasma- Mass Spectroscopy
Kinetic test	Tests devised to measure changes in the geochemical characteristics of a sample over time, focusing on rates of reaction.
Leco	High temperature analytical method routinely used to determine S and C.
MPA	Maximum potential acidity, calculated from total S in kg H2SO4/t
NAG	Net acid generation
NAG to Ph 4.5	NAG acidity titrated to Ph 4.5 in kg H2SO4/t
NAG to Ph 7.0	NAG acidity titrated to Ph 7.0 in kg H2SO4/t

NAPP	Net acid producing potential, calculated from ANG to total S (or MPA), in kg H2SO4/t
NP	Neutralisation Potential
Paste EC	EC of a sample slurry with a solid to water ratio of 1:2
Paste Ph	Ph of a sample slurry with a solid to water ratio of 1:2
QA/QC	Quality Assurance and Quality Control
SEM	Scanning electron microscopy
Static Test	Tests devised to measure the geochemical characteristics of a sample, focusing on capacities to produce or consume acid.
XPS	X-ray photoelectron spectroscopy
XRD	X-ray diffraction
XRF	X-ray fluorescence
ABA	Acid base accounting

CHAPTER ONE

1. INTRODUCTION

1.1 Study Background

There are more than 3500 tailings dams around the world (Baguley, 2020). Tailings are the fine-grained solid residues left after minerals and metals have been extracted from an ore. They are commonly transported as slurry and thickened before being stored in tailings dams. According to Mintek database, over 446 gold tailing dumps covering more than 18 000 ha exist across Johannesburg, while most of the gold retreatment activities occur on the West Rand and in the Free State (Durand, 2012). With more demands from the mining companies to retreat the tailing, hence it is critical to sustain the balance between environmental protection, economic growth and social development (MacRobert, 2018). This can be achieved by demanding for a comprehensive understanding of environmental impacts, and how to predict the problems from the tailings, such as Acid Mine Drainage (AMD).

The dissertation focuses on the AMD Prediction Modelling Development. The research is a case study that involves the use of gold tailing located in West Rand, Witwatersrand Basin area, South Africa. A total of 120 tailing samples, 17 water samples along the tailing streams, 7 sediments samples from the water pond and 13 soil samples from the residential area closed to the tailings were collected to conduct AMD analysis and lab experiments. The study includes three major aspects, which are samples collection and lab experiments, prediction modelling development and environmental impacts assessment. The prediction methods to be considered in this study will include Acid-Base Account, paste pH, Net Acid Generation and leaching column test. The geochemical modelling will give a better knowledge on the application and limitation of different existing AMD prediction methods. An environmental impact assessment of the study area will be accomplished after the modelling development.

1.1.1 Mining and Its Emerging Problem

The discovery of gold in quartz-pebble conglomerates minerals by George Harrison on the farm Langlaagte in Witwatersrand on March, 1886 was the first global awareness on a sequence of rocks that was to become the greatest source of gold on earth, Witwatersrand Supergroup (Nathan & Scobell, 2012). Subsequently, mining became one of the pillar industries globally, as well substantially contribute to social-economic development in South Africa. According to key facts and figures displayed on the website of Minerals Council South Africa, The Witwatersrand Basin remains the largest gold resource in the world today (Gold - Minerals Council South Africa, 2020). Gold sales are one of the global contending markets, where in 2019 gold sales were R72.6 billion (Gold - Minerals Council South Africa, 2020). Mining technology listed The Witwatersrand Basin among the top ten biggest gold mines in the worlds based on the quantity of the gold reserves produced (Gold - Minerals Council South Africa, 2020).

Online report on mining and minerals in South Africa claimed that mining accounts for about 18% of the country's gross domestic product (GDP), with gold solely more than one-third of exports (Kearney, 2012). Today, mining is still playing a remarkable role in the economic development and history of South Africa, as one of the most industrialised countries on the continent of Africa (Gold - Minerals Council South Africa, 2020).

However, some of environmental problems emerged from the large quantities of mine wastes during and after mining operation, such as land desertification, natural disaster and environmental contamination. These problems, such as water pollution, soil and sediments contamination, have become an increasingly important socio-economic issue in South Africa. Experience overseas, Europe and North America, has shown that the costs involved in the remediation of large-scale polluted areas are far too high, owing to too large quantities of contaminated material being treated (Rosner et al., 2001). Industries and governments have invested considerable efforts in formulating appropriate management solutions to tackle these problems In 100 years' times, 2,000 km^3 of mine wastes will be generated (Lottermoser, 2010), and the estimated costs for total worldwide liability, with the current and future

remediation of AMD are approximately US$ 100 billion (Price, 2009), nowadays, even more.

1.2 Preliminary Discussion on AMD

Before the description of AMD, a simple knowledge on Acid Rock Drainage (ARD) was presented by (The Internaitonal Network for Acid Prevention, 2009) as a by-product of the natural oxidation of sulphide minerals together with reactions of the base minerals in the rock, which are exposed to air and water. AMD is generated by those activities that involve the excavation of rock with sulphide minerals (e.g., mining). The process involved in generating these activities is accelerated, because such activities increase the exposure of sulphide minerals to air, water and microorganisms. AMD is produced from the oxidation process of neutral to acidic, with or without dissolved heavy metals, and always contains sulphate as explained by INAP (The Internaitonal Network for Acid Prevention, 2009). The other sources that caused AMD includes tailing dam, waste rock stockpiles, pit walls and underground workings, etc.

1.2.1 AMD Definition

AMD is caused by the atmospheric oxidation of naturally occurring Sulphide minerals, pyrite (FeS_2) in particular, and Pyrrhotite (Fe (1-X) S), Arsenopyrite (FeAsS) as well in the presence of water, with the stoichiometry (Miller, Robertson, and Donohue, 1997) Pyrite is reported as an important mineral that emerged from an acid-generation perspective (Nordstrom and Alpers, 1999). In addition, it is noted that pyrite's concentration, grain size, and distribution may be the most important factor affecting the production of acidic mine waters (Nordstrom and Alpers, 1999). Acidic mine water is usually characterised as low pH, with high sulphate and Fe^{2+} content and oxidation of Fe^{2+} to Fe^{3+}, including the formation of Fe^{2+} and Fe^{3+} hydroxides.

Pyrite oxidation occurs directly from reaction with water and air, or indirectly from reaction with ferric iron. At mining sites, the direct oxidation processes and associated biochemical reactions are the major contributors to AMD. The reaction process for the direct air and water oxidation of pyrite (Hutchision & Ellison., 1992)

is given in the Equation 1 – 3. Equation 4 shows that trivalent ferric iron in solution oxidizes pyrite, which results in acid generation without oxygen (Williams, Rose, Parizek, and Waters, 1982).

$2FeS_2 + 7O_2 + 2H_2O \rightarrow 2Fe_2+ + 2SO_4^{2-} + 4H+$ .....……..... Equation 1.1

$4Fe_2+ + 10H_2O + O_2 \rightarrow 4Fe(OH)_3 + 8H+$ …...…….....……..... Equation 1.2

$2Fe_2+ + O_2 + 2H+ \rightarrow 2Fe_3+ + H_2O$ …….……....……..… Equation 1.3

$FeS_2 + 14Fe_3+ + 8H_2O \rightarrow 15Fe_2+ + 2SO_4^{2-} + 16H+$ …….. Equation 1.4

The above is the simplified pathway for pyrite oxidation. The overall reaction can be written as below:

$4FeS_2 + 15O_2 + 14H_2O \rightarrow 4Fe(OH)_3 + 2H_2SO_4$ .....…..……Equation 1.5

Typical characteristics of AMD are within acidic pH of 1-4, which contains moderate to elevated metals (The Internaitonal Network for Acid Prevention, 2009). Also, some are toxic elements, with elevated sulphate treated for acid neutralisation, metal and sulphate removal (The Internaitonal Network for Acid Prevention, 2009). High acidity rate in AMD increases its mineralization effect on the surrounding rocks. This demonstrates a high degree of mineralization in the acid mine water with many toxic elements. As part of the effects, elemental and non-metallic elements can damage mining production, as well affect the ecological environment in the mining area.

The potential effects of AMD vary with physical and geochemical properties of the waste material produced, how waste is managed, and nature of receiving environment. When acid water is generated it may contaminate groundwater and natural drainage, lowering pH and increasing the concentration of dissolved elements (particularly metals) of environmental concern. Dissolution of metals is a direct consequence of metal sulphide oxidation, wherein acid and metal cations are released as part of the same reactions (e.g. Fe^{2+}, Cu^{2+} and Zn^{2+}). The additional metal release could occur through the interaction of the generated acid with the surrounding minerals. This interaction could increase dissolution and release of

metal ions (in a particular dissolution of alumina-silicates resulting in the release of Al3+). If unchecked, AMD can result in:

- Acute and chronic impacts on aquatic ecosystems.
- Community health risks in soil and plant contamination.
- Contamination of growth horizons in rehabilitation areas, which could lead to re-vegetation failure, increased erosion, and dump stability issues.

1.2.2 AMD Problems in South Africa

AMD is a huge environmental problem facing mining industry in South Africa (Naidoo, 2017). This is due to its persistence and expensiveness, and as a liability for mines after they cease operating (Naidoo, 2017). The mines grind down rock into a fine sand to extract minerals from host rocks (MacRobert, 2018). Once the mineral is extracted, most of this fine sand remains as a by-product called tailings (MacRobert, 2018). Although, as big and robust the mining sector in South Africa, tailings are huge economic and environmental challenges to the country (MacRobert, 2018). The tailings challenges require urgent attention in order to daunt their huge economic and environmental challenges in South Africa (MacRobert, 2018). The mine waste contains large amounts (between 10 and 30 kg/ton) of Sulphate minerals, such as pyrite, which are likely to generate AMD (Rösner & Van Schalkwyk, 2000).

The study area considered for this research is Witwatersrand basin, which covers an area of 1600 km2. This basin led to the event of 400 km^2 of mine tailings dams and 6 billion tons of pyrite tailings containing low-grade uranium (Liefferink, 2012). The potential volumes of AMD within the Witwatersrand mining basin is 350 million litres (Liefferink, 2012). It is recently discovered that mining activities occurring in the Witwatersrand area caused environmental challenges, where mine water discharged affected the Vaal Rivers System as well as the Crocodile River System (Liefferink, 2012), respectively. These environmental challenges are reportedly not rectified, which can eventually lead to a huge crisis hereafter (Liefferink, 2012).

In a report submitted by ministry of the Federation for a Sustainable Environment in 2010, as cited by Liefferink (2012), AMD was discharged from an old inclined shaft that belongs to Harmony Gold. The discharging rate was at 20 million litres per day, while close to 56 million litres per day were discharged during heavy rains (Liefferink, 2012). And the flooding of the Western Basin led to the mass destruction of the ecosystems in the Wonderfonteinspruit and the Tweelopiesspruit. The aftermath of the flooding caused acid water discharges. The persistent discharge of AMD has become a public concern.

AMD generated from the Western Basin is partially treated and discharged into the Tweelopiesspruit at a deplorable quality that caused unsafe downstream pollution of boreholes. The discharged AMD largely polluted the Swartkrans groundwater compartment, which 9 km away from the area. Mine water decant point was discovered at the Randfontein area. The water is decanting from a reclaimed tailing dam and flows northwards to the Krugersdorp Game Reserve and the Cradle of Humankind World Heritage site. Although, in the west of Randfontein, the regular flowing of the untreated mine water affects the whole Vaal river system. As stated in the preceding paragraph, AMD is a potential public risk to scarcity of water resources in South Africa, because its treatment requires huge resources to attain a safe water source for public use. In essence, this calls for great awareness relating to land development and cultivation across the affected areas and beyond; most especially, areas with initial tailing dams' encounters (Gauteng Province areas).

1.2.3 AMD Prediction

Based on the deplorable quantity of AMD discharged in South Africa, it is crucial to develop sustainable management strategies to control its impact on the environment. In this study, the appropriate approach for managing and resolving AMD problems is based on the ability to measure the potential acid for the waste materials, including the techniques suitable for solving the problems. Some parameters are crucial in understanding the efforts needed in selecting most effective and appropriate strategies to prevent AMD, such parameters as total potential acid generated, acid released rate, metal elements transport, contamination zones and associated contaminants, etc.

AMD prediction methods are classified into five groups, which are waste geochemistry comparisons, geological and mineralogical models, geochemical static tests, geochemical kinetic tests and mathematical models (Ferguson, 1986). The main objectives of applying the acid generation prediction are given as: to predict if a waste can generate acid hereafter (measuring the rate of occurrence), and to predict the quantity and quality of the drainage leaving the waste, under both controlled and uncontrolled site conditions. A general phased approach of prediction methods for a study involves the following steps (Hutchision & Ellison., 1992):

- Define the geologic units and define its mineralization.
- Design and implement a material sampling program.
- Conduct laboratory and field testing.
- Evaluate the potential for AMD formation.
- Conduct further sampling and testing.
- Characterise the waste materials in terms of acid generation potential.

The case study site for the gold tailings as specified in this study follows the above steps and built comprehensive modelling to understand all parameters of AMD generation, including prediction during re-treatment operation.

1.3 Problem Statement

Having recent improvement in gold prices globally, with new mining projects being developed and some closed mines (tailings) may soon be operational again, therefore, it is expected that more gold tailings will be reclaimed by mining companies. In relation to this, Vice President of Sibanye's West Rand Tailings Retreatment Project (WRTRP), Grant Stuart declared that more demands are made from the mining company to reclaim those gold tailings, because of the higher sufficient grade of gold-containing of the ore. It is assumed that an initial treatment rate of tailings is 1.4-million tonnes a month by Sibanye's tailings.

Additionally, numerous older waste deposits are reprocessed, and the impact of the tailing dams and sand dumps is a concern; most especially, dust and AMD. The problem is that the impact of the tailings will continue to leach residual chemical

into the environment. And the finer fraction of the tailing deposits could be dispersed as wind-borne around the communities causing air pollution.

The other problem is tailing effects on human being's life. The quantity of tailings dispersed to the communities around the mining areas contain some substantial amounts of complex compounds used in the ore extraction process. And these substances are perceived to be hazardous to the people working or living within the affected environments. With the extraction of lower grade ores to produce gold more waste will be made. Common minerals and elements found in gold tailings include arsenic, calcite, fluorite, barite, radioactive materials, mercury, sulphur, etc. Therefore, the procedural approach for preventing contamination of water resources by the aforesaid metal elements and AMD are highlighted in tailings retreatment procedure.

The monitoring and maintenance of tailings consumed a long-term cost either for a mining company or local government. For example, Harmony Gold Mine (Pty) in 2005 disclosed that despite spending more than Twenty-Eight Million Rands (R28,000,000) on infrastructure and R75,000 on monthly operating cost, the water still contains sulphates of 250 mg per litre after treatment. The third problem is how to develop or implement an affordable approach to control AMD to reduce the huge capital spent to control the impact of AMD on the environment.

However, previous studies done on AMD focused more on coal and metal mines than the gold tailings. The prediction techniques that will be applied in this study is expected to establish a potential acid generation and prediction of gold tailings, especially re-treatment tailings.

1.4 Research Questions

1. What the methods are used to determine the potential acid generation or neutralisation of AMD for the gold tailings samples?
2. What is the effective assessment for the factors that have controlled AMD?
3. What is the economic way to detect a set of AMD prediction methods via a series lab experiments by using gold tailings sample and to test if it is applicable to the gold waste materials?

1.5 Objectives of the Study

Regarding the questions stated in the section 1.4, some objectives are developed to pave the way for the appropriate methodology that could facilitate clear understanding on the impact of gold tailings across the communities around gold mining areas in South Africa. Appropriate application of the methodology will generate results (findings) relevant to validate both the research questions and the study objectives.

The study objectives are enumerated below as follows:

1. Determining the potential for AMD in the study area and particularly to those re-treatment tailing dams,
2. Assessment of the factors that control AMD and evaluating those control measures,
3. Detecting a set of AMD prediction methods and its applicability to the gold waste materials, and
4. Building conceptual modelling to assess environmental impacts, including areas directly affected by gold tailings re-treatment, mine water decanted, and contaminated water resources and soil.

In addition, the study objectives will be determined through a combination of study literatures, samples analysis and experimental works.

1.6 Significance of the Study

The study will confirm an approach which can be used to predict AMD for the gold tailing dam, especially when it is going to be re-treated. The appropriate prediction techniques can reduce the impact of AMD to the local communities, to the aquatic environment, and to the health of human beings. A huge cost of treatment of AMD is a big issue for South Africa gold tailings re-treatment project, different prediction techniques may guide the stakeholders to make an appropriate decision on the AMD treatment plan.

1.7 Expected Outcomes

Prior to the expected outcomes of this study, four major approaches are to be completed to pave the way for an efficient attainment of the results. Enumerated below are the four major approaches considered:

- Investigation of the existing information–related to AMD,
- Field trip,
- Mineralogical and geochemical analysis and lab experiments, and
- Evaluation of analytical and experimental results–applicable to tailing materials and evaluation of the findings.

Therefore, the expected outcomes of this study are highlighted below:

- To produce a mineralogical-geochemically-characterised gold tailings data sets (to attain an improved concept of controlling the potential generation of acid and the geochemical behaviour of gold tailings).
- To recommend an improved concept on various existing acid prediction methods for gold tailings.
- To provide an environmental assessment for gold tailings in the Witwatersrand Basin area.
- To set up an environmental indicator to tailings re-treatment project manager and stakeholder.

1.8 Ethical Considerations

The participants of the study and research are not subjected to harm in any ways whatsoever. Full consent is obtained from the participants prior to the study. The protection of the privacy of research participants has been ensured. The research data is open to the research institutions and students with the appropriated citation. The deception or exaggeration about the aims and objectives of the research have been avoided. Affiliations in any forms, sources of funding, as well as any possible conflicts of interests have been declared (see declaration part). The communication in relation to the study is honesty and transparency. The primary data is my own collection, and any other data has been indicated source.

1.9 Thesis Structure

Chapter 1 encompasses a concise preamble of the background study on mining and its emerging problems. Concise literatures on AMD are presented to offer a simplified knowledge on the impacts of AMD in South Africa. As part of this chapter, other sections such as problem statement, research questions, objectives of the study, significant of the study, expected outcomes, ethical considerations and thesis structure are discussed to clarify the critical state of environmental challenges in relation to mining in South Africa.

Chapter 2 discusses the relevant literatures reviewed for more technical know-how and hypothetical analyses. Also, the general principles for acid generation and neutralisation are discussed at the beginning of this chapter. The acid products and its impacts on the local environment are comprehensibly discussed in the chapter. Other AMD related literatures discussed are mineralogical and geochemical investigations, together with the prediction methods for AMD, which covers their limitation and applicability, mostly focused on Acid-Base Accounting (ABA).

Chapter 3 presents a complete description of the study area. In this chapter, a comprehensive understanding of natural geography, geology, and hydrogeology of the study area are discussed to offer more clarity on the approved case study. And the residence distribution and water resources location are mapped and presented in this chapter as the water, soil and sediments samples collected in the surrounding area for environmental assessment.

Chapter 4 explains the methodologies considered for this study. The chapter demonstrates how the samples were collected from the tailings site using drilling methods. The samples preparation and analytical methods are explicated. The prediction techniques, together with theory and procedures are detailed outline. And the quality assurance of the process is discussed at the end of the chapter.

Chapter 5 comprehensibly discussed mineralogical characterisation, together with the interpretation of the analysis results from XRF, XRD, SED-EDS and ICP-MS. The interpretation includes samples classification by core logging, the major and trace elements examination, total sulphur and total carbonate test.

Chapter 6 discusses the geochemical characterisation, together with the interpretation of the results of the geochemical analysis. The different layers of the tailings of the AMD categories are described, together with the approach adopted in understanding how acid is generated and transported.

Chapter 7 demonstrates a strategic approach towards the development of a conceptual prediction modelling for the environmental assessment by using prediction test results. Both static and kinetic test will be applied to evaluate the level of contamination of the study site by AMD, with the understanding on the condition that acid generation can be predicted for future prevention.

Chapter 8 presents the summary of findings and discussion parts of the study. The objectives and outcomes of the study will be summarised and reviewed thoroughly to ascertain the attainment of the research questions.

Chapter 9 concludes the study. The way forward for the future research of AMD is discussed and recommended.

The dissertation also includes reference and appendix volumes. The appendix is presented with all test results and analysis data.

CHAPTER TWO

2. LITERATURE REVIEW

2.1 Introduction

This chapter discusses literature reviewed on the basic understanding of AMD occurrence mechanisms and assessment techniques required in selecting appropriate tests methods for this study. The key areas that will be discussed in this chapter are given as follow:

- Overview of AMD occurrence mechanisms and their impacts on the environment and society.
- Overview of the previous studies relating to AMD.
- Overview of existing prediction methods applicable to AMD studies.

2.2 AMD Generation

Exposure of sulphide minerals as pyrite to air and water caused acid water after being mined. The physical and geochemical properties of the waste materials will determine the AMD potential (Stewart, 2005). The characteristics of AMD are usually low in pH, high in sulphate and Fe^{2+} is subsequently oxidised to Fe^{3+} to produce Fe^{2+} and Fe^{3+} hydroxides. The pH value of AMD is generally between 2-5. With aforesaid pH range, AMD has demonstrated high acidity rate by having strong dissolution effect on the surrounding rocks. Therefore, environmental impacts emerging from AMD cause metals in solution in both acid or alkaline environment, salinity, and sludge precipitates.

2.2.1 Acid Generation

Emergence of acid in the tailing dams around the gold mining areas are due to the reaction between gold-bearing rocks, water, and oxygen. The gold-bearing rocks, such as Witwatersrand rocks, have large quantity of sulphide minerals. When the minerals encounter water and oxygen, they dissolve to generate large high acidic substance in the water. And in a while, the water becomes highly acidic to dissolve

more minerals in the rock. This type of water is considered harmful to the people's health.

The tailing dams generally contain materials with low ore grade. These materials contain large concentrations of sulphide minerals that may be oxidised to generate a significant source of metal and acid contaminants (Harrison et al., 2010). The problem of sulphide oxidation (or, pyrite oxidation) and associated AMD, with the solution and precipitation processes of metals and minerals, has been a centre of focus over the last 50 years (Dold, 2005). The mineralogical and geochemical interactions are essential aspects required to aid the understanding of the parameters that control AMD formation (Lindsay et al., 2015), as well foster the development of the effective prediction and prevention methods.

Global Acid Rock Drainage Guide defined AMD as a composition formed by the natural oxidation of sulphide minerals, such as pyrite or pyrrhotite, together with reactions of the base minerals in the rock, which are exposed to air and water (The International Network for Acid Prevention, 2009). The use of sulphide minerals for the excavation of rock accelerates the process of generating AMD. In essence, the exposure of this rock to air, water, and microorganisms after being excavated with sulphide minerals will intensify the production of AMD composition.

Explicably, the acidic drainage produced from the oxidation process always contains sulphate, which is a combination of water, oxygen, and bacteria during pyrite oxidation to accelerate the acid performing process. Bacteria, usually Thiobacillus ferrooxidans, act as agents that catalyse the reaction by utilising the sulphur present as a source of energy (Andre, 2010). The end products of the process are sulphuric acid and ferric sulphate, which resulted in a pH of 2.5–3.0.

2.2.2 Pyrite Oxidation

The stability of species depends on the reduction-oxidation (redox) reaction taking place between the ions as shown below. The combination of redox condition and pH makes it possible to predict the dominant species under specific geochemical conditions (Dold, 2005).

$O_2 + 4H^+ + 4e^- \leftrightarrow 2H_2O$ (Reduction)

$$4Fe^{2+} \leftrightarrow 4Fe^{3+} + 4e^{-} \quad \text{(Oxidation)}$$

$$O_2 + 4Fe^{2+} + 4H^{+} \leftrightarrow 4Fe^{3+} + 2H_2O \quad \text{(Redox Reaction)}$$

The reaction of pyrite with oxygen and water solves ferrous sulphate and sulfuric acid. Ferrous iron can further be oxidised to produce additional acidity. Iron and sulphur-oxidising bacteria catalyse these reactions at low pH (Jacobs et al., 2014). This effect increases the rate of reactions by several orders of magnitude (A. Parbhakar-Fox et al., 2013).

Moreover, as previously mentioned, pyrite is oxidised when it is exposed to such elements as oxygen and water, and compounds as hydrogen ion release-acidity, sulphate ions and soluble metal ions are generated as demonstrated in Equation 2.1 (Jennings, 2008). The edge of the water is typically expressed as pH or the logarithmic concentration of hydrogen ion concentration in water (Jennings et al., 2008).

$$SFeS_2 + 7O_2 + 2H_2O \rightarrow 2Fe^{2+} + 4SO_4^{2-} + 4H^{+} \quad \text{…… Equation 2.1}$$

Further oxidation of Fe2+ (ferrous iron) to Fe3+ (ferric iron) occurs when sufficient oxygen is dissolved in the water or when the water is exposed to adequate atmospheric oxygen (Jennings, 2008). The process is demonstrated in Equation 2.2.

$$2Fe^{2+} + \frac{1}{2}O_2 + 2H^{+} \rightarrow 2Fe^{3+} + H_2O \quad \text{…….. Equation 2.2}$$

Ferric iron can be precipitated as $Fe(OH)_3$. A red-orange precipitate was seen in waters affected by AMD. And it can react directly with pyrite to produce more ferrous iron and acidity (Jennings, 2008) as demonstrated in Equation 2.3 and Equation 2.4.

$$2Fe^{3+} + 6H_2O \rightarrow 2Fe\,(OH)_3(s) + 6H^{+} \quad \text{…….....……..... Equation 2.3}$$

$$14Fe^{3+} + FeS_2\,(s) + 8H_2O \rightarrow 2SO_4^{2-} + 15Fe^{2+} + 16H^{+} \quad \text{……..... Equation 2.4}$$

When ferrous iron is produced (Equation 2.4) in the present of sufficient dissolved oxygen, the cycle of reactions in both Equation 2.2 and Equation 2.3 is perpetuated (Younger, Banwart, & Hedin, 2002). Without dissolved oxygen, Equation 2.4 will

be completed and water will show elevated levels of ferrous iron (Younger, Banwart, & Hedin, 2002). Bacteria, particularly Thiobacillus ferrooxidans, can significantly accelerate the rates of chemical reactions (Equation 2.2, Equation 2.3, and Equation 2.4). Another microbe, Ferroplasma Acidarmanus, was identified in the production of acidity in mine waters (McGuire, Edwards, Banfield & Hamers, 2001). The kinetics of each reaction is different, which fundamentally depends on the conditions that prevail in the tailings (Dold, 2005). The hydrolysis and precipitation of iron hydroxides will produce most of the acid in this process. If pH is lower than 3.5, then Fe(OH)3 is unstable and Fe3+ remains in solution (Dold, 2005).

2.2.3 Factors Influence AMD

The four basic controls on acid generation rates in a given rock type (Jacobs et al., 2014) are water availability, oxygen availability, mineralogy (sulphide mineral presence) and physical characteristics (Stewart, 2005).

2.2.3.1 Water Factor

The reaction processes involving pyrite mineral, water and oxygen as developed by (Evangelou, 1995) are represented below as chemical reaction equations.

$$FeS_2 + \frac{7}{2}O_2 + H_2O \rightarrow Fe^{2+} + 2SO_4^{2+} + 2H^+ \quad \text{Equation 2.5}$$

$$Fe^{2+} + \frac{1}{4}O_2 + H^+ \rightarrow Fe^3 + \frac{1}{2}H_2O \quad \text{Equation 2.6}$$

$$Fe^{3+} + 3H_2O \rightarrow Fe\,(OH)_3 + 3H^+ \quad \text{Equation 2.7}$$

$$FeS_2 + 14Fe^{3+} + 8H_2O \rightarrow 15Fe^{2+} + 2SO_4^{2-} + 16H^+ \quad \text{Equation 2.8}$$

Typical run-of-mine waste contains sufficient water for the oxidation of the contained sulphides. Water is a crucial element, with a unique transportation mechanism for acid and dissolved products, which as well involves acid production rate (Stewart, 2005).

2.2.3.2 Oxygen Factor

Oxygen serves as a primary element (H Coetzee et al., 2007) that influences the formation of acid in any dumped wastes. In addition, oxygen is transported by

advection and diffusion (Stewart, 2005). Advection, a bulk movement of gas with difference in total pressure of the gas is also called ‘mass flow’. The pressure differences may be caused by temperature gradients, barometric pressure changes in the atmosphere and wind gusts over the waste rock surface (Revuelta, 2018). Advective oxygen conveys within the waste rock is greatly affected by the gas permeability of the dump; most importantly, by the gas permeability of the surface layer (Revuelta, 2018). When the surface layer and mess are sufficiently permeable, mass flow can convey oxygen into the dump and maintain high oxygen concentration there (Gold One International Limited, 2013). When advection is the predominant air transport mechanism (Howard & Heymans, 2000), then mineralogy becomes the dominant influence on variation in acid generation rate (Brough et al., 2013).

As part of the formation process, convection is seen as a contributing factor within the outer face and crest of mining dumps as evident by gas venting, which tends to be confined to zones near the range of the waste dumps (Miller, Robertson & Donohue, 1997). Also, convection can develop in pockets or inclined layers of coarse-grained material within the immediate dump surface (Brough et al., 2013). In addition, diffusion is described by (Miller, 1997) as "the gaseous flow is a result of a difference in concentration, or partial pressure, of components of a gaseous mixture". Water acts as a significant barrier to oxygen as well used directly at many mines to cover sulphuric tailings (Stewart, 2005). Accordingly, the proportion of water to air in waste rock pore spaces will significantly influence oxygen diffusion. The rate of oxygen diffusion through spoils will primarily be a function of depth and percentage moisture saturation (Miller, Robertson & Donohue, 1997).

2.2.3.3 Sulphide Mineral (Pyrite)

As mineral reactions create AMD; then, mineralogy is a significant control on the resultant leachate composition and severity of acidity (Stewart, 2005). Thus, mineralogical considerations for AMD include:

- Existence of mineral species, with their relative rates of acid generation or acid neutralisation.
- Crystal morphology.

- Mechanisms and controls of sulphide oxidation at particle scale.
- Surface chemistry and formation of passivating layers on sulphide surface.

The aforesaid mineralogical considerations comprise of different minerals with different acid generation or neutralising capacities and reaction rates. Amongst the common metallic sulphide minerals, pyrite and pyrrhotite contribute hugely to the world acidic drainage (Blowes & Jambor. 1997). Key sulphide minerals are listed below:

- Pyrite (Iron Pyrites),
- Marcasite (white iron pyrite),
- Chalcopyrite (Copper Pyrites),
- Pyrrhotite (Magnetic Pyrites),
- Bornite (Peacock Copper Ore),
- Chalcocite (Copper Glance),
- Tetrahedrite (Gray Copper Ore), and
- Galena.

The relative characteristics of the acid forming and consuming minerals in the waste material types determine the ability of a waste material to produce acid (Jamieson et al., 2015). In essence, quantity and reaction rates of the minerals must be considered. Suppose acid-neutralising minerals are adequate material for the potential release of acid from the sulphide minerals (Price, 2009). Although, it is possible that the material is a non-acid producing except if the buffering rates demonstrated by the neutralising mineral are slower than that of acid generation rates (Price, 2009). Where acid generation rates exceed acid neutralisation rates, net acid production will emerge. Pope (Pope & Weber, 2013) demonstrated that significant dissolution of silicate minerals requires low pH conditions (pH $\leq$2).

2.2.3.4 Crystal Morphology

Mineral crystal formation is another factor that influence AMD. This factor affects the reactive surface area; thus, the reaction rate is considered as a function of mass (Stewart, 2005). Laboratory studies performed on sulphur oxidation mechanisms by the International Network for Acid Prevention (2009) revealed the reaction rates

on a particle mass basis are directly proportional to the available surface area; the smaller the grain size, the higher the reaction rate per unit mass.

In West Rand area, pyrite in gold tailings is a fine-grained, which is commonly considered framboidal. Pyrite is highly reactive due to its high surface area as the volume of its grain size increases. According to the International Network for Acid Prevention (2009), sedimentary pyrite is more reactive than hydrothermal pyrite; although, the group suggested that differences in the crystal structure were used with the surface area to determine the differences in reactivity (The International Network for Acid Prevention, 2009).

2.2.3.5 Bacteria

Bacteria are the last factor to be discussed as one of the factors that influence AMD. A group of researchers, In (Jacobs, 2014) described the bacteria as site-specific strains of Thiobacillus ferrooxidans with huge influence on the process of AMD by using the sulphur (S) present as a source of energy. Similar description was given in subsections 2.2.1 and 2.2.2 as important agents that use sulphur (S) as the energy to accelerate chemical reactions. The bacteria are autotrophic (autophytic), which means that they obtain their nutritional needs from the atmosphere (nitrogen, oxygen, carbon dioxide and water) and minerals (sulphur and phosphorus) (Usher et al., 2003). These bacteria are not catalysts by true definition but do act as accelerating agents provided that their habitat conditions are at or close to optimal. Notwithstanding, they are most crucial factor in generating acid drainage (The International Network for Acid Prevention, 2009).

2.2.4 AMD Products

Pyrite (FeS2) is a common sulphide mineral oxidation that take place in several steps involved in the process of generating such AMD products as ferrihydrite ($5Fe_2O_3.9H_2O$), schwertmannite (between $Fe_8O_9(OH)_6SO_4$, and $Fe_{16}O_{16}(OH)_{10}(SO_4)_3$), goethite (FeO(OH)), including the more stable secondary jarosite ($KFe_3(SO_4)_2(OH)_6$) and hematite (Fe_2O_3). The products depend on the geochemical conditions (Nordstrom & Alpers, 1999). The possible secondary minerals formed at neutral pH after complete oxidation and neutralisation of pyrite

is Ferric hydroxides and sulphate and gypsum. Smith and Bridges (1991) summarised and specified that other processes involving reactions of other sulphides and sulphur forms (thiosalts and anaerobic reactions) play significant roles in an acid generation.

2.2.5 Acid Neutralisation

The acid neutralisation process involves AMD essential minerals (calcite ($CaCO_3$) or dolomite (Ca, $MgCO_3$) that interact with acid and produces metallic ions (Fe^{3+} and Cu^{2+}, Zn^{2+}, Pb^{2+} and As^{3+}), which react to form hydroxides as precipitates by the general reaction eventually.

$M^n + nOH^- = M(OH)_n$ ……. Equation 2.9

Where:

OH- = hydroxyl ion, and

M(OH)n = Metal hydroxide (precipitates).

This over-simplification represents chemical neutralisation as it occurs by human intervention rather than an accurate portrayal of natural occurrence, where the precipitation products are usually carbonates and sulphates and their hydrated or hydroxyl-complex forms. In nature, acid generating minerals (e.g. pyrite) often occur in close association with acid-neutralising minerals (e.g. calcite ($CaCO_3$) and dolomite (Ca, $MgCO_3$)), and acid produced from pyrite is neutralised by these minerals. In this chemical reaction process, the gypsum ($CaSO_4.2H_2O$) is the most formed sulphate that is sparingly soluble in water, as well contributes to elevated sulphate levels in the ground and surface waters.

Other minerals, which include some silicates (e.g., plagioclase feldspar) may also neutralise the acid produced by sulphide mineral oxidation. However, this process is relatively slow compared to the neutralisation by carbonates. The geologists determined the acid-producing and acid-neutralising mineral contents of many samples from a proposed mine site and analysed the results by a method called acid-base accounting (ABA).

In commercial practice, AMD is neutralised with lime (CaO) to reduce acidity and precipitate metals (Singh, 2014). This is an expensive and long-term necessity. Essentially, the acid together with Fe (III) can dissolve minerals and mobilise elements in the tailings (Smuda et al., 2007). In the process, the acid produced, and the elements mobilised react with acid-neutralising minerals like carbonates or silicates. Also, acid neutralising reactions increase the pore-water pH.

2.2.6 AMD Impacts

This subsection discusses the impacts of AMD on the mining industry and ecological environment. The discussion covers areas such as contamination of surface water resources and groundwater resources, damage on soil and sediments and more wastes with reclamation, effect on higher social expectations and financial cost. All these are discussed in the subsections below.

2.2.6.1 Surface Water Resources

One of the impacts of AMD is the contamination of the surface water resources. The consequence of this impact is a massive death of fish, algae and plankton caused by acidic water with a pH < 5.0, even lower, which directly affects the quality of rivers/streams and aquatic organisms (Jennings, 2008). More so, heavy metals in the acidic water accumulate within the aquatic organism system. And this effect aggravates the toxicity of the aquatic organism system (Rosner, 2001). AMD characterised by acidic metalliferous conditions in water is reported to be responsible for physical, chemical and biological degradation of stream habitat (Jennings, 2008). Once acid drainage is generated, metals are released into the surrounding environment which become readily available to biological organisms. A standard weathering product of sulphide oxidation is the formation of ferric hydroxide ($Fe(OH)_3$). This compound is a red/brown coloured precipitate found in miles of streams affected by AMD (Price, 2009). Ferric (Iron) hydroxides may physically coat the surface of stream sediments and streambeds that destroy habitat, diminish availability of clean gravels used for spawning and reduce fish food items (Jennings, 2008). Surface water contaminated by AMD, which regularly contains elevated concentrations of metals, can be toxic to aquatic organisms by rendering the streams devoid of receiving and breeding most living creatures (Jacobs, 2014).

2.2.6.2 Groundwater Resources

The contaminated surface water is easily and directly infiltrated into shallow groundwater. This affects the groundwater resources, and groundwater contamination is extremely hard to be treated.

2.2.6.3 Soil and Sediments

The infiltration of the contaminated water damaged soil aggregate structure. This impact caused soil compaction and crops were withered. AMD with low pH has severe corrosion damage effects on the pumping parts, pipes, tunnels, and other equipment. Additionally, AMD caused deterioration of the underground mining operating environment. In this case, desulphurisation occurs in AMD discharging procedure, which generate toxic hydrogen sulphide that endangers mining workers' health.

2.2.6.4 More Wastes with Reclamation

With the advanced use of new extraction technology these days, however, an increasingly smaller amount of metals in the ore (lower grades of ores) can be extracted profitably (Zhu & Anderson, 2002). This means that for a given amount of metal, an increase amount of waste is produced (Zhu & Anderson, 2002).

2.2.6.5 Higher Social Expectations

As the AMD discharges into the local aquatic system, the precipitation of ferric hydroxide changes the colour of waterbed and water body into reddish-brown. Due to this effect, the natural view and even historical heritage environment were affected. Meanwhile, in 2009 and to date, South African media have called the attention of the community on the issues emanating from AMD in the newspaper. Therefore, such issues identified were low water quality, land instability, soil, and sediments contamination, weed invasion and public safety hazards (Durand, 2012).

2.2.6.6 Financial Cost

Mining companies normally incur significant costs at mine sites after the minerals have been extracted and the mine is closed (Deloitte Touche Tohmatsu, 2003). Reclamation and other environmental obligations frequently arise during ongoing

operations (Deloitte Touche Tohmatsu, 2003). Chile has been a major producer of copper and gold for hundreds of years, out of 659 mines approximately 50% are abandoned and this situation inevitably poses serious threats to the natural environment and community life (Chilean Copper Commission, 2001). There are between 100 000 and 500 000 small and mid-size abandoned hard rock in the West of USA; in the eastern USA, mining of high sulphur coals in Appalachian states has polluted 11 000 miles of streams and rivers and has endangered drinking water sources (Chilean Copper Commission, 2001). The remediation cost has been estimated at between 32-72 billion of the US dollars (Zhu & Anderson, 2002).

The US Department of Energy estimated that approximately 38 million cubic meters of groundwater are contaminated by uranium mill processing or mill tailings (Zhu and Anderson, 2002). In Norway, historical mining of copper sulphides has made tens of kilometres of streams and rivers barren of aquatic life. In Canada, there are an estimated 351 million tons of waste rocks, 510 million tons of sulphide tailings. The remediation of the AMD environmental problem is estimated to cost Canada about Canadian dollars 3 billion. The estimated costs for total worldwide liability associated with the current and future remediation of AMD are approximately US $ 100 billion (A. K. Parbhakar-Fox et al., 2014). Governments have introduced stringent environmental and rehabilitation requirements, the public has become more environmentally conscious and demanding, and mining companies themselves have introduced their own codes of environmental practice: this results is caused the future cash outlays can indeed be significant (Deloitte Touche Tohmatsu, 2003)

2.3 Early Related Studies to AMD

There are different topics related to research and case studies on AMD. These studies are AMD generation, formation, its impacts, trace elements, and toxic metal elements transportation and mobility. Others are geochemical static and kinetic tests, and AMD treatment techniques. The three crucial areas related to this study are discussed in the subsections.

2.3.1 Studies of AMD Generation and Its Impacts

Early studies done on tailings were related to mine wastes dumped into local rivers, lakes and coastal inlets (Thompson, 1975). These tailings ponds were reported to have environmental impacts on the local aquatic life (Bouiet, 1997). Another researcher, Lesaca (1975) monitored transition-metal concentration (Fe, Ni, Cu, Hg) in natural waters that were used as tailings disposal sites in the Philippines. This study discovered that the siltation effect of tailings affects the ecology of the aquatic environment. Moreover, the study further mentioned that water quality degradation has adversely affected the agricultural areas and fishing industry.

Other related studies on tailings reviewed covered the production of AMD and its adverse effect on surrounding environments. In relation to the aforesaid, (Amari, Valera & Essarraj, 2014) carried out a study on the causes and treatment of AMD to abate its adverse effect on the surrounding environs. In this study, some case studies were evaluated to pinpoint the causes of AMD as well proffer appropriate ways of abating the impact of AMD. Similarly, (Heikkinen, 2009) studied the pollution of a watercourse impacted by AMD in the Imgok creek of the Gangreung coalfield in Korea. Another related study was done by Espana et al. (2005) on the AMD in the Iberian Pyrite Belt (Odiel river watershed, Huelva, SW Spain). This study covered geochemistry, mineralogy, and environmental implications of AMD.

2.3.2 Transportation and Mobility of Toxic Metal Elements of AMD

Mineralogy and geochemistry studies of mine tailings have been published in the early 20th century. The implementation of the MEND (Mine Environment Neutral Drainage) program in Canada shows that the Canadian mining community is aware of the environmental problems plaguing the mining industry. The mining community is willing to work adequately to mitigate and eradicate the adverse effect of the AMD on the surrounding environs. However, the "typical" oxidised tailings with the differing depth are identified, and minerals like goethite, lepidocrocite, ferrihydrite, jarosite and gypsum.

There were some studies done on the transportation and mobility of toxic metal elements of AMD. A group of researchers, Shu et al. (2001), carried out study on

the acidification of lead/zinc mine tailings and its effect on heavy metal mobility. Another similar study was carried out by Smuda et al. (2007) on the mineralogical and geochemical study of element mobility at the sulphide-rich excelsior waste rock dump from the polymetallic Zn–Pb–(Ag–Bi–Cu) deposit. The aforesaid related studies were experimented to have a clear interpretation of the element mobility in the generation of AMD and its adverse effect on the surrounding environs.

2.3.3 Prediction Methodologies for AMD

The prediction methodologies used for AMD in previous studies were thoroughly understudied to have a clear picture of the best and improved prediction approach towards mitigating the impact of AMD on the surrounding environs. Other areas studied are mineralogical studies, tailing impoundment modelling and remedial engineering (Frind & Molson, 1994).

Most importantly, under the prediction methods some tests were conducted such as static test and kinetic test. In relation to the static test, Sobek test method was previously demonstrated by Sobek et al. (1978). Sobek test is described as a typical acid potential and neutralisation potential calculation method Sobek et al. (1978). This test method was developed earlier than the other related tests. It is a simple, efficient, and economic assessment for the water quality.

Also, acid-base calculation in Sobek test is done under the conditions of high acidity and temperature (Sobek, 1978). In essence, silicate with low activity could probably dissolve under the aforesaid conditions. Sobek's acid-base analysis produced an overestimation of the neutralisation potential of the samples that are inconsistent with the actual environment. Lawrence (1990) proposed an improved calculation method for acid-base, where the temperature in acid absorption is low in calculating acid generation and neutralisation with controlled acidity pH at 2.0-2.5. In effect, maximum potential acidity (MPA) is contextual to the calculation of the sulphide–sulphur in the sample rather than total sulphur, which makes the result of the calculation of acid and alkalinity closer to the actual environment.

Lapakko (1994) mentioned that the limitation of an improved method of acid-base as acid production of active silicates is not considered in the calculation. This may

be because the calculation of acid neutralisation potential was too high or too low. Due to this effect, therefore, Lawrence and Scheske (1997) proposed a new method of calculating NP value based on sample mineral composition. Paktunc (1999) reviewed and moderated the technique by establishing the calculation on the mineral composition of the sample. MNP value of a single mineral is significant in evaluating the long-term neutralisation behaviour of neutralising minerals. This is useful in long-term slow dissolution of balancing minerals, which is significantly appropriate for the overall acid discharge of AMD.

Sobek test is problem with siderite when calculating acid generation and neutralisation. In recent years, some moderated methods were proposed and tested to offer a better understanding on the calculation of acid generation and neutralisation. Earliest perspective by Meek (1981) demonstrated that when the sample containing siderite is subjected to the acid-base titration test to calculate the ANC, then the acid absorption solution should be filtered and a little 30% H2O2 should be added before the dripping to promote the oxidation of Fe. In addition, Skousen et al. (1997) mentioned the filtering of acid absorption solution and adding 30% H_2O_2. A research institute in the University of South Australia, Ian Wark Research Institute (2002) added fizz rating, new acid-base calculation classification, as well as adding H_2O_2 to promote the completed oxidation of siderite. Two studies done by Weber et al. (2004) and Weber et al. (2004) equally confirmed the moderation of acid-base calculation. For those samples containing siderite, adding H_2O_2 can obtain more accurate ANC value. The purpose of filtering the acid absorption before adding H_2O_2 is to deter the oxidation of pyrite in the sample to generate acid as well reduces any impact on neutralising the acid potential and ANC calculations.

Aside the use of static test, kinetic test is another type of test used in the prediction methods for AMD to identify the acid generation. Types of kinetic test developed are B.C Research Confirmation, Modified Confirmation, Shake Flask, Soxhlet Extraction, Humidity Cell, Column Test, Pilot Scale and Carbon Pressure (Hutchision & Ellison., 1992). Leaching column test is an extension of kinetic test in quantifying the reaction rate and leachate chemistry to determine the acid generating potential. Weber et al. (Webber, P.A., Thomas, W. M., Skinner, R. St.,

Smart, 2004) introduced the required procedures of leaching column test as 1-2 kg of the sample, sieved less than 7mm, leaching time from few weeks to maximum five years. Other essential procedures are dry and wet cycle once a week (usually four cycles per month), add distil water 200ml when it is a damp cycle (dry the samples by using a heating lamp). And collect leachate monthly by making sure that the entire leaching process is carried out with sufficient air supply. The leach column experiment can provide a series of geochemical information such as the reaction rate of minerals, the quality of acid production, the persistence of acid generation, the leaching of elements and the formation of secondary minerals, etc.

According to general practice in leaching column test, the mineral samples or soil samples are doing leachate by distilling water with weekly dry-wet cycle. The filtrate leachate and solid sample after leaching can be collected to analyse the migration of pollutants. The leaching column test period can be planned in accordance with the waste materials. Weber et al. (2004) leaching test was continuously operational from 1-5 years; for example, the leaching column test carried out by Dubiková et al. (2002) only lasted 30 weeks in the acidification experiment and Skousen et al. (1997) set up Soxhlet Extraction leaching test which only lasted for two months.

2.4 AMD Prediction Methods

Environmental impacts of water decanting out of the waste rocks, tailings containing pyrite or other sulphides, and the water containing acid and heavy metal infiltrated are global problems caused by mining industry. Accurate prediction of acid production potential of waste rocks and tailings is considered appropriate towards reducing environmental damage and waste disposal costs. This approach could facilitate the implementation of the best waste ecological management practices to attain a safer environment.

AMD prediction methodologies, including static and kinetic experimental methods have been applied and practised at the mining site and laboratory in many countries for more than 40 years. The Field and Laboratory Methods Applicable to Overburdens and Mine soils was published in 1978 (Sobek et al., 1978). The evaluation of those prediction methods has been published to improve the practices.

Many studies proved that choosing only one process cannot accurately evaluate whether a sample is producing acid. Basically, most static methods are more than 80% accurate in predicting AMD from waste rock and tailings. Additionally, the static method is simple, convenient, fast, and low cost.

On the other hand, the kinetic experiment is used to simulate the geochemical weathering process of waste rock, but its technique to tailings with acceleration and the experimental conditions are different (Landers & Usher, 2012). In this case, the weathering process of waste rock and tailings is discussed from different perspectives, and AMD prediction effect is relatively accurate. The ability to predict acid generation from mine wastes enhances the development of appropriate control measures. Besides, the implementation of these measures will prevent the formation of AMD. Therefore, the extensive use of two or more methods can offer more accurate evaluation results.

As discussed above with regard to past studies, concise details of the AMD prediction methods as related to this study are enumerated below (Hutchision & Ellison., 1992).

- Geographical comparisons rely on extrapolating waste geochemistry of mines in the same geographic area.
- The rationale of the method of paleoenvironmental and geological investigation assumes that areas with similar geological formation have the identical potential for an acid generation.
- Geochemical static tests are the short-term batch laboratory tests that compare the acid generation and the neutralisation capacity of a material.
- Geochemical kinetic tests are longer-term laboratory tests that produce leachate for analysis and reflect the rate of acid generation of material.
- Conceptual models can be used to extrapolate the rates of acid generation and neutralisation beyond the time frame of the laboratory tests.

2.4.1 Geological and Mineralogical Characterisation

The first phased approach for prediction is to identify the geological control of the mining site and characterise its mineralization. Also, the investigation of geological

and mineralogical characteristics is useful for obtaining a preliminary indication of acid generation potential (Brough et al., 2013). It is necessary to characterise the waste material by identifying the lithological units (A. Parbhakar-Fox et al., 2013). And the next step is to describe the basic geochemical properties, range and type of mineralization that are present in each of the lithological units (Hutchision & Ellison., 1992). But, the aforesaid usually have different characteristics in terms of acid generation and neutralisation potential (Hutchision & Ellison., 1992).

The detailed mineralogy of sedimentary materials of gold sequences will vary in accordance with the geology of the source rocks for the sedimentary material accumulated, structural and metamorphic processes that took place after deposition (Price, 2009). The typical minerals associated with gold sequences are listed as pyrite, marcasite, calcite, dolomite, ankerite, siderite, quartz, clay, goethite, hematite, and gypsum. Among the common minerals, it is the occurrence of pyrite and the carbonates (Changul et al., 2010) (calcite, dolomite, ankerite and siderite) that are most influential on AMD and its prediction (Amari, K., Valera, P., Hibti, M., Pretti, S., Marcello, A., Essarraj, 2014).

2.4.2 Prediction Test

There are two main types of tests used in assessing acid production potential, which are static tests and kinetic tests. These two types of tests intend to provide information on the potential risk of acid production. Static tests focus on the capacities of a given sample to produce acid, but not account for rates of reaction (Stewart, 2005). Kinetic tests attempt to model relative rates of reaction of acid-forming and acid neutralising minerals (Stewart, 2005).

Static tests are simple and relatively inexpensive tests that provide qualitative information on the balance between acid generation and acid-neutralising processes of a sample (Zhao et al., 2010). The major static tests used include paste pH and EC, acid-base accounting (ABA), and net acid generation (NAG) test and its variations. Geochemical tests form the most reliable basis for characterising waste materials (Schippers, 2007). And this type of tests is commonly used in predicting whether a particular waste will generate acid (Marescotti, 2010). More so, they can be used in defining the level of control measures required to prevent, control or

contain acid generation (Jacobs et al., 2014). One vital advantage of static tests is potential to be used as an initial screening process to separate materials that are not acid generating from those that require more thorough kinetic testing before conclusions can be drawn.

In contrast, kinetic tests can provide real-time data on the kinetics and rate of acid generation and acid-neutralising reactions under laboratory-controlled (Stewart, 2005). More information on metal release and drainage quality can be obtained through the kinetic tests. In relation to this, the various treatment options can be evaluated after combining the results of kinetic tests and static tests. The preliminary kinetic tests include Kinetic NAG, Humidity cells, but only leach columns test is considered applicable in this study.

2.4.2.1 Acid-Base Accounting (ABA)

ABA involves the subtraction of an acid-neutralising capacity from a maximum potential acidity of a sample (Hageman et al., 2015). Results are expressed as a net producing or acid consuming power per mass unit of rock with the unit kg H2SO4/t (Stewart, 2005). Also, minerals that can produce acid (acid potential (AP)) can as well neutralise acid (neutralising potential (NP)) in mine waste. Understanding the relative influence of these two parameters can lead to an estimation of the net acid-producing potential (NAPP) or net neutralising potential (NNP). It is essential to be able to predict if or if not a geological unit has the capacity of generating acid (Dold, 2005). This as well is a deciding factor for other treatment strategies of the material (Dold, 2005). A simple ABA would be to measure the total sulphur and total carbon contents in a sample by assuming that the total sulphur value represents the pyrite content and the full carbon represents the calcite content (Dold, 2005).

NAPP = MPA - ANC …….…… Equation 2.10

Where:

MPA is maximum potential acidity = % Sulphur * 30.6

ANC is acid neutralizing capacity.

From Equation 2.10, if the result of NAPP is negative, then, it indicates that the sample's acid-neutralising capacity is stronger than maximum potential acidity to prevent acid generation. Conversely (Stewart, 2005), if the NAPP is positive, then, it indicates that acid may be generated. The stoichiometric conversion factor of 30.6 assumes that all sulphur is present as pyrite, while all sulphide oxidises to completion (Stewart, 2005), according to the pyrite oxidation reaction given in Equation 2.11.

$$FeS_2 + \frac{15}{4}O_2 + H_2O \rightarrow Fe(OH)_3 + 2SO_4^{2-} + 4H^+ \quad \text{..... Equation 2.11}$$

From the above equations it is summarised the static tests that were from the start of the development until further moderation as the following:

B.C. Research Initial: this test provides a quantitative measure of the net acid-producing potential by comparing the maximum acid generating potential with the capacity of the sample to consume acid, based on the assumption of complete sulphur oxidation. AP is calculated from a total sulphur analysis, and it is expressed as an equivalent sulphuric acid calcium carbonate weight percentage e.g., kg of H_2SO_4 or $CaCO_3$ per ton of waste. The whole sulphur analyses are conducted in a Leco furnace that heats the sample to liberate and measure all sulphur-bearing forms, which includes organic sulphur, sulphides, and sulphates.

NP is determined by sulphuric acid titration of a slurry of finely ground waste material from its natural pH to a pH of 3.5. And it is expressed in the same units as AP. The acid generation potential of a sample is assessed by subtracting AP and NP two values.

Sobek Test: the Basic Sobek test, as explicated by Weber et al. (2005), is similar to the B.C Research Initial, but incorporates some refinements to the total sulphur analysis and potentially increasing the value of AP estimated. The Modified Sobek Test only uses the iron sulphide content to determine the AP of the material. This test usually results in a lower and more realistic AP value.

Alkaline Production Method: in this test, the NP of waste is evaluated by determining its alkaline production potential. The total sulphur content determines AP.

Hydrogen Peroxide Test: the purpose of the Hydrogen Peroxide is to determine the amount of pyrite in a sample. The test is performed by observing the oxidation rates of material with a known pyrite content by comparing the rate of chemical oxidation to a standard curve. The quality of chemical oxidation is determined by measuring the rate at which the actual pH of the reagent reacts with the sample changes.

Net Acid Production Test: This test was developed by Acid Rock Drainage Prediction Manual, 1991. The test directly evaluates the net acid generating potential. This method uses hydrogen peroxide to oxidise the sulphides contained in the waste, and it is expressed as kg $CaCO_3$ equivalent per ton of garbage. With regard to this, static tests can be used to provide a preliminary indication of the net acid generating potential of waste by allowing the materials to be categorised as non-acid generating waste, possibly acid-generating waste and acid-generating waste (Skousen et al., 2000).

2.4.2.2 Net Acid Generation (NAG) Test

NAG test returns information on acid production capacities like ABA test. The test is performed by adding hydrogen peroxide solution to a pulverised sample of rock to accelerate the oxidation of the sample and its contained minerals (Mine & Request, 2008). The focus of the test is to return information on the oxidizable sulphide portion and its interaction with any neutralising phases present (Stewart, 2005). Samples have either a positive NAG capacity or no capacity, which is zero. The NAGpH is the pH of the solution after the rapid oxidation reaction is complete, and then the solution is allow to cool (Hughes, 2013).

The rapid oxidation is an attempt to approximate weathering processes, as well supply more information on available sulphide rather than a theoretical maximum such as the NAPP test. During the oxidation and the final heating step, the inherent buffering of the sample can react with the acid produced (Stewart, 2005). This approximately accounts for the effect of available neutralizing capacity (Stewart, 2005). After the completion of the reaction, the resulting solution is titrated against NaOH to determine the remaining acidity. In this case, the result is the balance of the chemical interaction of available acid-producing capacity with acid consuming capacity (Hageman et al., 2015). Morin and Hutt (2001) emphasised that the NAG

test is not valid as a standalone test, but it is not different from ABA or other prediction tools. All required concurrent testing with other methods could be used to overcome inherent limitations in each of the individual tests.

The single addition NAG test involves the addition of 250 ml of 15% hydrogen peroxide (H_2O_2) to 2.5 g of pulverised sample. The sample can react overnight. The entire sample is boiled (for approximately 2 hours) to remove excess hydrogen peroxide and encourage the release of inherent neutralising capacity. Once the sample has cooled, the pH and acidity of the NAG liquor are measured. There are potential interferences with this test. Samples containing organic materials have the potential to interfere with peroxide oxidation tests in two ways (Price, 2009). The carbonaceous material may release organic acids when exposed to hydrogen peroxide. This effect causes an anomalous low pH. Besides, the organic carbon may preferentially consume the hydrogen peroxide and cause incomplete oxidation of reactive sulphide. Also, the temperature rise observed in the single addition NAG test causes boiling results from catalytic decomposition of peroxide, which may occur before all the reactive sulphides have been oxidised (Stewart et al. 2003).

2.4.2.3 Paste pH and EC

Paste pH and electrical conductivity (EC) are measurements on samples water pastes used to provide information about the existing geochemical state of samples and prediction AMD potential. Paste pH & EC method does not involve any oxidation of the sample apart from the one that occurs in the sample before testing (Stewart, 2005). Sample pastes are commonly used in the measurement of sample pH and salinity.

The values obtained indicate the acidity/alkalinity (pH) and the presence of ARD reaction products (EC) in the sample at the time of measurement (Stewart, 2005). For very reactive samples, these methods have the potential to reflect the acid-forming potential of a sample. Jocobs 2014 and Sobek, 1978 described the application of paste pH and EC methods in mine soil and overburden assessment by using pulverised sample at ratios of 2 parts solid to 1 part water (by weight) or saturation, with measurement performed once the reading stabilises. Miller and

Jeffery (1995) described a paste pH and EC method as a method that involves the mixing of deionised water with pulverised sample at a ratio of 1 part solid to 2 parts water and leaving the mixture to calm overnight before measurement.

Morin and Hutt (2001) proposed a rinse pH method similar to the Sobek et al. (1978) method, but making use of the -2mm fraction from the received sample to appropriately represent the in-situ surface behaviour of the sample. This is applicable to soils and placed waste rock, where in-situ measurements are relevant. This type of test does not apply to samples collected from fresh rock in the areas to be mined, since they are not in situ where in their behaviour after sampling and storage will not reflect in-situ processes (Stewart, 2005).

Nonetheless, the advantage of these tests is that they are relatively simple and cost-effective to carry out (Stewart, 2005). While the disadvantage of using them on fresh rock samples is that they do not represent a total acid potential but reflect part oxidation of the sample prior to testing. Samples containing reactive minerals will be most responsive in this test, whereas the time of exposure is likely to influence the results.

A low paste pH measurement (<pH 4) for a sample may be a clear indication that a sample is already acid-forming, but a neutral paste pH measurement does not demonstrate any indication of the acid potential of a sample (Stewart, 2005). Acid forming samples that contain slow reacting sulphides or acid buffering minerals, or ones that are tested after a limited time of exposure could possibly produce neutral paste pH results. Thus, the technique is inadequate in its application because it can only detect acid-forming samples, but not reliable in detecting non-acid forming samples (Stewart, 2005).

2.4.2.4 Leach Columns Test

Kinetic tests involved ageing or "weathering" of samples under laboratory-controlled or onsite conditions to simulate the time-varying chemical changes that occur in waste. The tests attempt to model relative rates of reaction of acid-forming and acid neutralising minerals. Furthermore, the tests also determine typical constituent concentrations that occur in the acid drainage, as well evaluate the

effectiveness of proposed AMD control and treatment methods such as covers, liming, layering, inundation and chemical addition. The results of these tests could be that significant or negligible rate of acid generation could be severe or controls would be required over an extended period (Jacobs et al., 2014).

Clearly, kinetic tests need to be conducted over more extended periods than some other tests. This process is expected to exceed several months. Laboratory short-term tests generally provide qualitative information on drainage water quality (Brough et al., 2013). The primary kinetic test includes Kinetic NAG, Humidity cells and Leach columns. The Kinetic NAG and Leach columns tests will be applied in this study. Among these two, leach columns involve the cyclic addition of known quantities of water to bulk samples in controlled laboratory conditions. The kinetic tests provide information on relative reaction rates of acid generating and acid-neutralising properties of a given material and the possible release rates (loadings) of acid, metals and other contaminants associated with ARD.

In this process, the rates of watering and cycle times are essential to the operation of the leach columns, which depend significantly on the objective of the testing. Price (Price, 2009) carried out an experiment to simulate the result of the inundation of the previously oxidised sample that involves complicated water cycling. When dealing with primary rock and prediction of oxidation rates, complicated water cycling is not required. A leach column, however, is too small and shallow to simulate complex dump oxidation and water flow rates at depths below the surface (Evangelou, 1995). If oxidation rates and relative reactivities of samples are required, standard cycling of dry and wet intervals is probably sufficient (Plumlee, 2009). In that case, the dry interval is needed to allow free access of air throughout the sample for oxidation, while the wet interval is used to rinse out the secondary minerals to enable measurement of constituent loads.

Consequently, the resulting oxidation rates from this approach can be used to model the effects of varying moisture saturation, water balance (seasonal variations) and oxygen concentration in a dump on the final rate of acid production (Wels, Lefebvre & Robertson, 2003). Usually, the oxidation rate is based on the sulphate load in the leachate, which may lead to underestimation where secondary products, particularly

jarosite, are accumulated in the solid. Usher et al. (2003) mentioned that sulphide oxidation rate can be quantified by oxygen consumption with a known starting gas volume in a more enormous sealed column.

2.5 Assessment Modelling Development

This involves the development of conceptual models range from simple to complex. The simple models include a best-fit curve that can be extended beyond the time range of the test results. The complex models theoretically simulate the acid generation and consumption processes that are calibrated using laboratory or field test data (Landers & Usher, 2012).

2.6 Conclusion

The literature reviews have documented a wide variety of test methodologies available for practise in this study. Each test has its own set of constraints, which requires an integrative testing approach to execute a detailed assessment of AMD potential at selected tailing sites (Stewart, 2005). However, the following application of AMD test methodologies are expected to be thoroughly discussed in this study:

- S species need to be considered when assessing ABA (NAPP) data.
- A less personal check on the ANC fizz rating will assist consistency of results.
- The ANC test is not substantially affected by silicates and aluminosilicate.
- The presence of siderite needs to be accounted for in ANC determinations.
- Use of ABA (NAPP) or NAG techniques in isolation are insufficient in predicting AMD potential, wherein an integrative approach is required.

CHAPTER THREE

3. STUDY AREA

3.1 Description of the Study Area and Sample Site

The study area is in West Rand, Witwatersrand Rand Basin, Gauteng Province, South Africa. The latitude is from 26.094906 S to 26.158580 S, while the longitude is from 27.681951 E to 27.774426 E. Within this area, as indicated in Figure 3.1, the three gold tailings assessed in this study are Mogale tailing (located in Krugersdorp area), Gold One_1 tailing and Gold One_2 tailing (both located in Randfontein area).

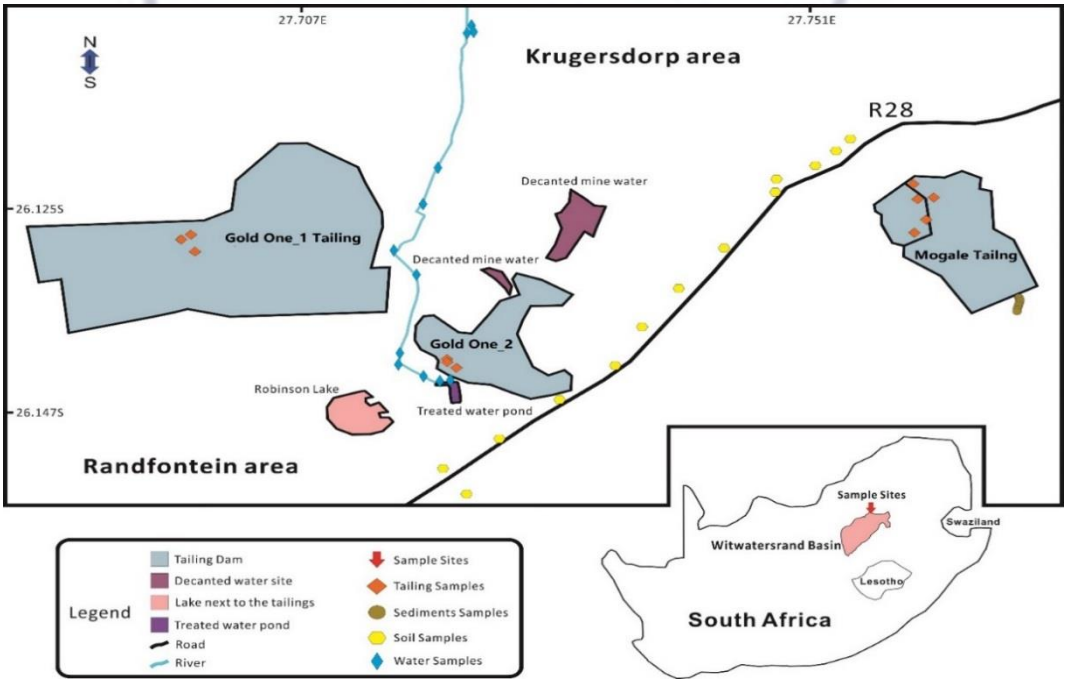

Figure 3.1: Study area and sample sites

As indicated in the diagram, the Gold One_1 tailing is closed to the Krugersdorp Game Reserve. And necessary study samples like tailing samples, sediments samples, water samples and soil samples were collected from the study area. More so, important information in the diagrams are all indicated in symbols to aid easy comprehension. Mogale tailing was formerly owned by Mogale Gold Company located in the south-east of the Krugersdorp. And Gold One_1 tailing and Gold

One_2 tailing formerly belonged to Gold One Pty Ltd located in the north of the Randfontein area. Both companies have changed their names by merging with some other companies.

3.2 Gold Mining History of Witwatersrand

History and status of gold tailings in South Africa is crucial in understanding the actual inception of gold mining activities that led to its existence. This discussion is limited to the Witwatersrand, West Rand, and its cities. A book authored by Potgieter and Mendelsoha (2001) provided a brief written history of mining in Witwatersrand goldfield. In 1853, over 160 years ago, Peter Jacob Marais found gold in the Jukskei and Crocodile rivers to the north of the present Johannesburg. The book mentioned that early development and exploration of the goldfield in Johannesburg's vicinity were in a large quantity due to capital originating from Kimberley, Pietermaritzburg, and Paarl (Figure 3.2).

The first gold mining company founded was registered in Kimberley in September 1886 as the Witwatersrand Gold Mining of William Knight. The actual development of the conglomerate reefs of the Witwatersrand did not begin, until 1887. The official mining operations for real gold was initiated in April of 1887. Jubilee Gold Mining Company was the first company to erect the first stamp battery to crush main reef ore. The Witwatersrand goldfield proper stretches from Randfontein eastwards for about 80 km to the vicinity of Springs (Whiteside, Glasspool, Hiemstra, Pretorius, & Antrobus, 1976).

In 1886, a huge concentration of gold in pebble reefs was traced around the entire Witwatersrand Basin, where 40,000 tons of gold were officially produced till 1985 (Potgieter & Mendelsoha, 2001). It was reported that Witwatersrand reefs have produced close to 55% of globally mined golds in the international market since 1886. In addition, parts of the 5-10 grams per ton of rocks of gold globally marketed.

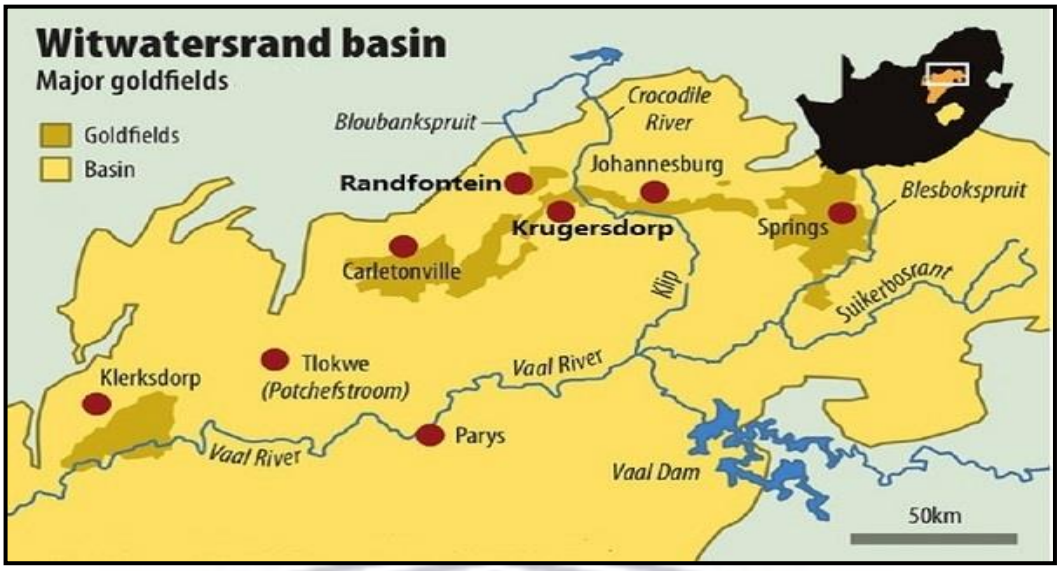

Figure 3.2: Major Goldfields in Witwatersrand Basin

(Source: Department of Water Affairs and Forestry, South Africa)

were economically mined from great depths of the ground through efficient and coordinated mining techniques developed in South Africa (Potgieter & Mendelsoha, 2001).

3.3 West Rand and Gold Cities

The West Rand area, where three sampled tailings located, became a settlement area for the Europeans after the discovery of a gold-bearing reef in 1886. And this event triggered the gold rush that led to the founding of Johannesburg. This is a region with a long history of gold and uranium mining. The West Rand covers 4,066 km^2 area to the west of Randfontein and to the east of Roodepoort. The map section previously displayed in Figure 3.2 shows the location of all towns and nature reserve in the West Rand area. The Krugersdorp Game Reserve, the Kromdraai Conservancy and Cradle of Humankind are all in this area. The northern section of the West Rand, including Mogale City and Cradle of Humankind form part of the Magaliesberg range of ridges. In this area, the ridges are considered to be ecologically sensitive; therefore, the sustainability of these ridges depends on the survival of many species and the overall biodiversity of the region (Coetzee, 2007) due to the negative environmental impacts emanating from the mining activities.

Figure 3.3: Mining City Krugersdorp

Figure 3.4: Mining City Randfontein

(Source: Pictures were taken at the study site)

The two major mining cities with mining operations are displayed in Figure 3.3 and Figure 3.4. It is noted that mining operations occurred around Randfontein in the West Rand goldfield, within a triangular area bounded by the Rietfontein fault far to the east. This is one of the oldest areas of mining in the Witwatersrand Basin which comprises four interconnected mines: namely, Harmony Gold Randfontein Operations, Mogale Gold Pty Ltd, Metmin Pty Ltd and DRD Gold Company.

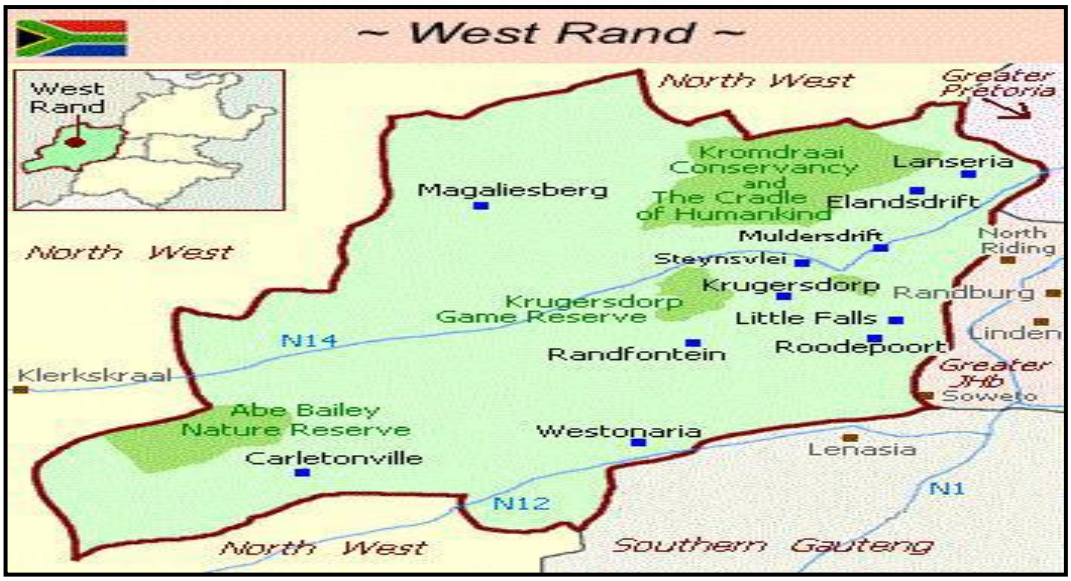

Figure 3.5: West Rand Map

(Source: Accommodation South Africa)

In addition, four local municipalities are instituted in the West Rand goldfield areas, which are Mogale City, Merafong City, Randfontein Local Municipality and Westonaria Local Municipality. The mining site, Mogale tailings, is in the Krugersdorp under the jurisdiction of Mogale City Municipality, while Gold One_1 and Gold One_2 tailings are within the Randfontein Local Municipality. Figure 3.5 presents the map of local municipalities in the West Rand.

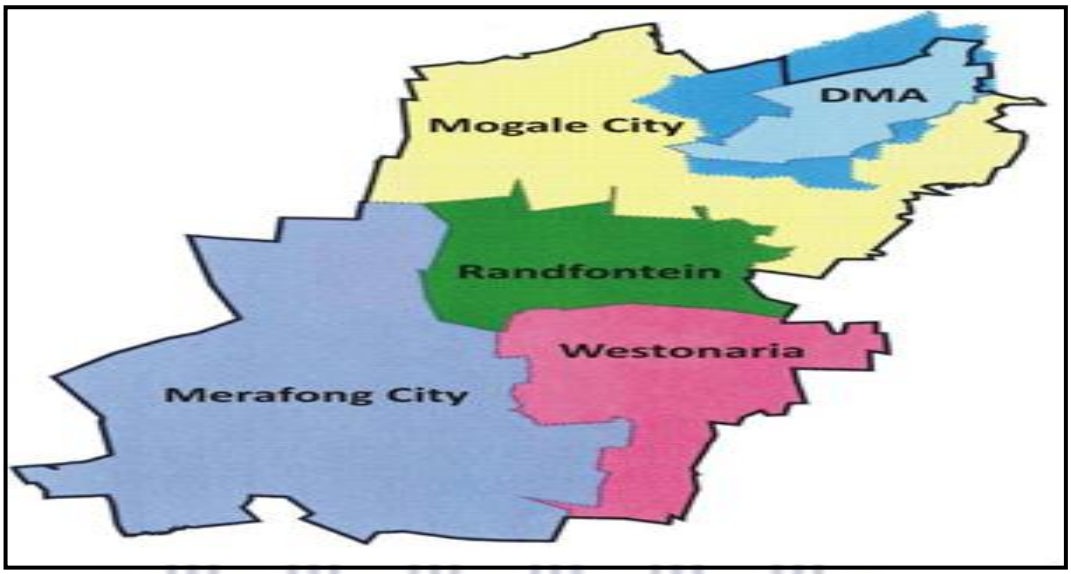

Figure 3.6: Local Municipalities in the West Rand

(Source: Picture adapted from the Municipality of the West Rand)

Randfontein is a gold mining town established in 1890 to serve as a new mining community (Nesbitt, 2013), situated 45km west of Johannesburg in western Gauteng, South Africa. Further review revealed that J.B. Robinson, then known mining financer, bought the farm Randfontein and inaugurated the Randfontein Estates Gold Mining Company in 1889 (Nesbitt, 2013). Also, the gold mining town was administered by Krugersdorp until it became a municipality in 1929 (Hobbs & Cobbing, 2007) . The population of the town was 149,286 in 2011, with an average elevation of 1709m above sea level and total cover area of 475km2 (Coetzee, 2009) regional road (R28) route that connects Krugersdorp with Vereeniging passes through Randfontein (Figure 3.6). This road is locally called Main Reef Road through central Randfontein.

Another gold city, Krugersdorp is a mining city founded in 1887 after the discovery of gold in the Witwatersrand in 1886. Currently, Krugersdorp is no longer a standalone municipal government after being integrated into Mogale City Local Municipality (Figure 3.6).

3.4 Tailings

As part of the assessments conducted, study area covers 11.72km from West to East and 4.85 km from North to South. The tailings are man-made features and do not possess any geological structure. The tailings are the waste products emanating from the processing of gold and uranium ores of the Witwatersrand Supergroup, with their composition. Thus, this reflects the major constituents of the Witwatersrand Basin. Further assessment shows that the surrounding area comprises residence complex, informal settlement, and Krugersdorp Game Reserve.

The tailings within the study area consist mainly of quartz sand and slimes with low concentrations of gold, uranium, and sulphur. The officer conducting the sites assessment claimed that the history of the tailings is about 50 years old, and gold occurs in the concentration of 0.26g/t and above. The size of the site where samples were collected is about 9.32 km2. Based on the assessment, the three sites are observed with large heaps of fine tailings. The three tailings are described the subsections 3.4.1, 3.4.2 and 3.4.3, respectively.

3.4.1 Mogale Tailing

Mogale tailing is the first of the three tailings assessed in this study (Figure 3.7). The size of the tailing is about 2.3 km2, with a depth thickness of 75 meters. Mogale tailings operated by Mogale Gold are 1L23-25, 1L12-15, 1L28, West Wits Pit (Figure 3.8). These areas are collectively referred to as the "Randfontein Cluster" (Nesbitt, 2013).

Figure 3.7: Mogale tailing site

Figure 3.8: Mogale tailing partly operational

(Source: Pictures were taken at the study site)

In addition, it is reported that approximately 126 million tons of a resource were generated from Randfontein Cluster, which are expected to last 20 years for the extraction (Nesbitt, 2013). The re-treatment of tailings project has the potential to contribute significantly to the social, economic and environmental aspects of the Krugersdorp and Randfontein areas (Nesbitt, 2013).

3.4.2 Gold One_1 Tailing

Gold One_1 is a gold tailing assessed in Randfontein area, with an area size of about 3.97 km2 (Figure 3.9 and Figure 3.10). Gold One_1 is a dual-listed mid-tier mining group with gold operations involving gold and uranium prospects across Southern Africa. According to report from Gold One International Limited (2013), the company purchased Rand Uranium (Pty) Limited as well acquired one of the world's most advanced uranium projects.

Figure 3.9: Gold One_1 Tailing site

Figure 3.10: Gold One_1 Tailing site

(Source: Pictures were taken at the study site)

The acquisition of these companies will enable Gold One International Limited in having adequate resources needed to recover uranium, gold and sulphur from the Cooke Tailings Dam and underground ores (Gold One International Limited, 2013). The Gold One Mine was gold mine started in 1900 and originally with 330 hectors. The mining manager on site told that the Gold One Mine was established in 1900 and it has generated 120 million tons of tailings. He also confirmed that the reclamation plan for the tailings will be starting soon in 2021.

3.4.3 Gold One_2 Tailing

Gold One_2 is a gold tailing with area size of approximately 3.05 km^2 (Figure 3.11 and Figure 3.12). The area is one of the operating mines of Gold One and Gold Fields. The re-treatment of the site is part of the Tailings Treatment Project that was signed in 2010. The project is a low-grade gold and uranium recovery project that focuses on the existing tailings storage facilities. As reported in an integrated annual review report prepared by (Durand, 2012) Gold One and Gold Fields declared a mineral resource of 475.6 million tons in tailings storage facilities in December 2010. This storage facilities contains gold mineral resources of 4.5 million ounces and uranium mineral resources of 53.6 million pounds (Ewart, 2011)

Figure 3.11: Gold One_2 tailings operational

Figure 3.12: Gold one_2 tailing decanted water

(Source: Pictures were taken at the study site)

3.5 Geographic Setting

South Africa has a diverse biome with different features of landscapes in a dominated plateau area. Among the dominated plateau areas, only Highveld has the largest sub-region of 1200 to 1800 meters high. In the North, the Highveld is covered with a series of rock formations known as the Witwatersrand. West Rand is on the North of the Witwatersrand, a dry savanna sub-region, known as the Bushveld. It is characterised by open grassy plain with scattered trees and bushes. The elevation of the area varies between about 900 and 1200 meters above sea level. Therefore, this is the area where study samples were collected.

Climatically, the Greater Witwatersrand is temperate with moderate rainfall of 500-900 mm annually, most of it falling during the warmer months from October to March (Whiteside, Glasspool, Hiemstra, Pretorius & Antrobus, 1976). The climate of the study area is subtropical with cold, dry winter and pleasantly warm summer. And there is more precipitation in the summer than the winter season. The rainfall starts from October to April in the summer season, and the winter season receives less precipitation from May to September. The climatic data illustrated above were obtained from the Johannesburg Weather Station (JHB BOT TUINE STATION), including temperature, rainfall, wind speed and air pressure. This climatic condition

covers through the study areas with coordinates of -26.10S to -26.16S, and 27.68E to 27.77E. The weather data were processed to obtain the average values for each criterion from 2003 to 2012. The data will be carefully analysed to deduce its impacts on the AMD generation.

A graphical illustration of the average temperature (°C) of the study area is given in Figure 3.13. The graph demonstrates the distribution of maximum and minimum average temperatures across twelve months from 2003-2012. This represents the summary of the climatic information processed as obtained from the Johannesburg Weather Station.

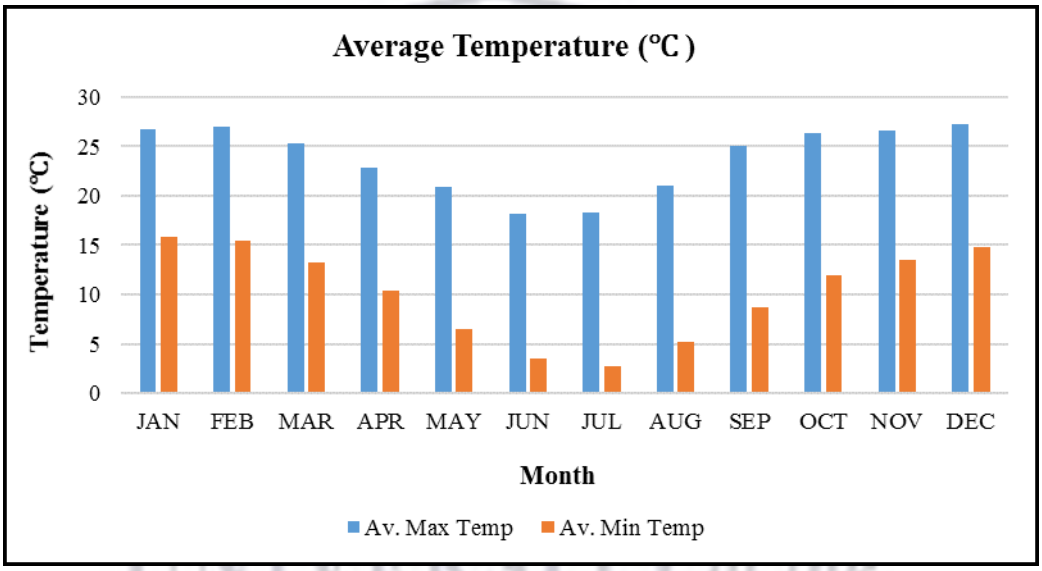

Figure 3.13: Average maximum and minimum temperature of the study area from 2003 to 2012

From the graph, average maximum temperatures of 27.32°C and 21.09°C were exhibited in the summer and winter months, respectively. Regarding average minimum temperatures exhibited for summer and winter months, 11.97°C was exhibited in the summer months and 2.77°C was exhibited in the winter months. Further observation shows that there were drastic drops in the average maximum and minimum temperature values from April to August. This demonstrates the impact of climate change on the wintertime.

Similar approach was used to compute the monthly average rainfall (mm) for the same coverage years. As graphically illustrated in Figure 3.14, it is observed that

most rainfall occurred in the summertime than any other time, from October (48.26 mm) of the preceding year to March (67.14 mm) of the subsequent year. But only four months have higher measurement of rainfall water within these periods, which are December (107.56 mm), January (143.8 mm), February (72.74 mm) and March (67.14 mm).

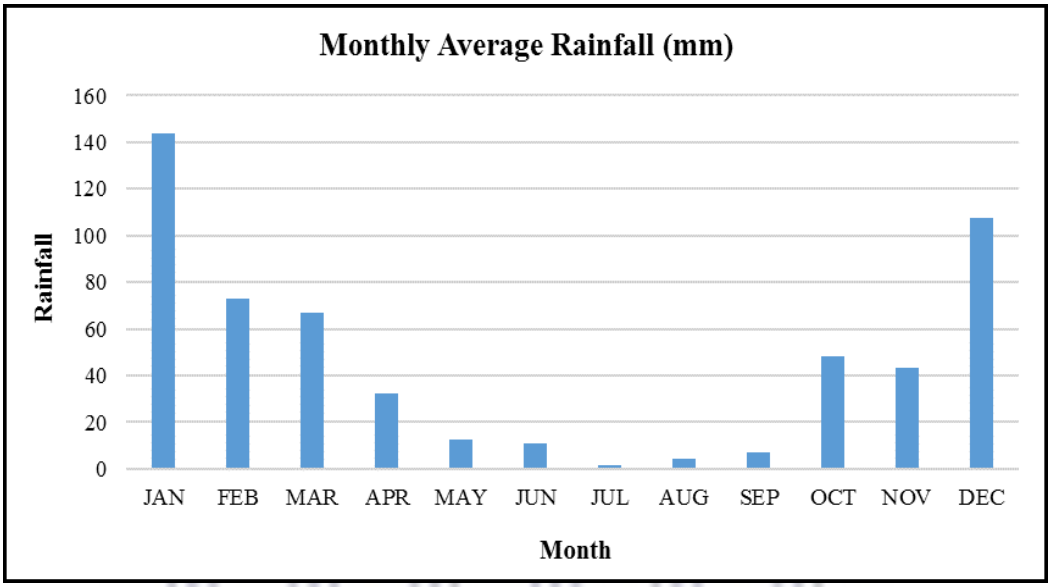

Figure 3.14: Summary of the monthly average rainfall of the study area from 2003 to 2012

Further observation shows a drastic decrease in monthly average rainfall in wintertime, May (12.61 mm), June (11.14 mm), July (1.34 mm), August (4.54 mm) and September (6.96 mm) more than any other time. And thunderstorms of short duration are accompanied with most rainfall in the summertime. Considering the annual rainfall for the coverage years, 551.99 mm average annual rainfall was deduced under intense season, with a potential evaporation of about 1600 mm/annum.

With the intention of having a clear understanding of the rainfall effect across the coverage years, both the total rainfall and average rainfall (mm) were plotted together against the years as displayed in Figure 3.15. The total rainfall is represented in clustered column graph and the average rainfall is represented in line graph. Both total and average rainfalls demonstrated similar data distribution shape from 2003 to 2012, which indicates no variation in the data collected (Figure 3.15).

According to the graphical results, highest total and average rainfalls were recorded in 2010 (906.6 mm, 75.55 mm), followed by 2008 (746.8 mm, 62.23 mm) and 2009 (613.4 mm, 51.12 mm), respectively. Lowest total and average rainfalls were recorded in 2003 (363.4 mm, 30.28 mm), followed by 2012 (378.6 mm, 31.55 mm) and 2004 (438.5 mm, 36.54 mm).

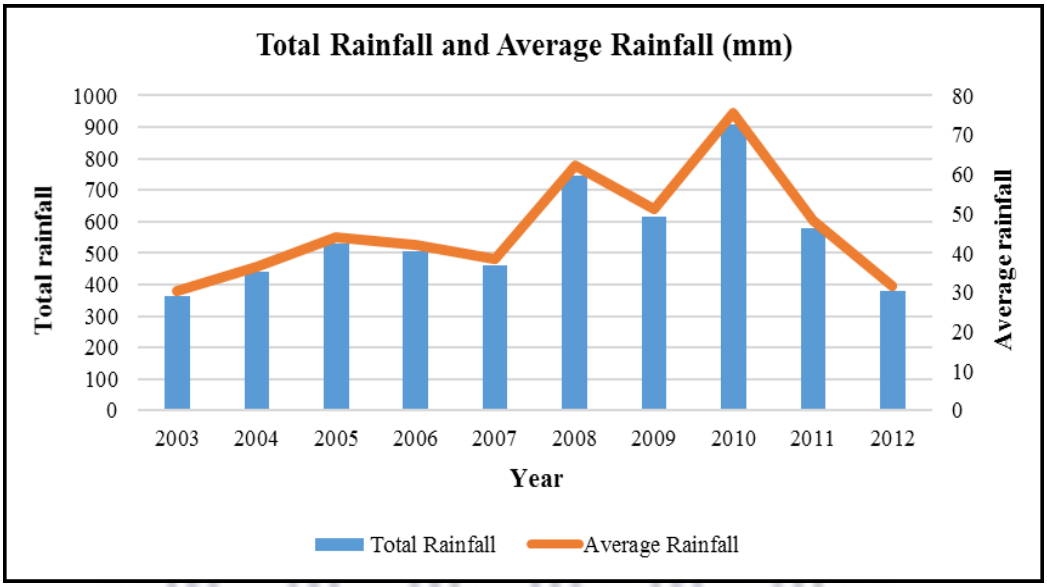

Figure 3.15: Summary of the total rainfall and average rainfall of the study area from 2003 to 2012

Overall observation presents that Randfontein receives an average of about 726 mm of rain per year, with most rainfall occurring during summer. June is the driest month, while the wettest month is January, with about 120 mm. Randfontein's average maximum temperatures range from 16.8°C in June to 27.7°C in January. The region is the coldest in July, when the mercury drops to 0.1°C on average in the night, with temperature as low as -8.0°C. Maximum temperatures in mid-summer can peak around 35 to 37°C. Randfontein has temperature greater than Johannesburg and Krugersdorp. Observably, Randfontein can be 3°C to 4°C colder at night in winter and 2°C to 3°C warmer in the day in summertime than Johannesburg and Krugersdorp.

Wind speed is another parameter assessed in the study area over the coverage years. Average wind speed (m/s) is graphically represented in Figure 3.16, where high wind speeds were recorded in the summertime than the wintertime. The distribution

shape displayed is similar to the distribution shape obtained in the monthly average rainfall (Figure 3.14), where fewer rainfall droplets were measured in wintertime. December recorded highest wind speed data of 1.35 m/s, followed by November and October with equal proportions of 1.31 m/s each. July recorded lowest wind speed data of 0.39 m/s, followed by May and June with 0.43 m/s and 0.46 m/s, respectively.

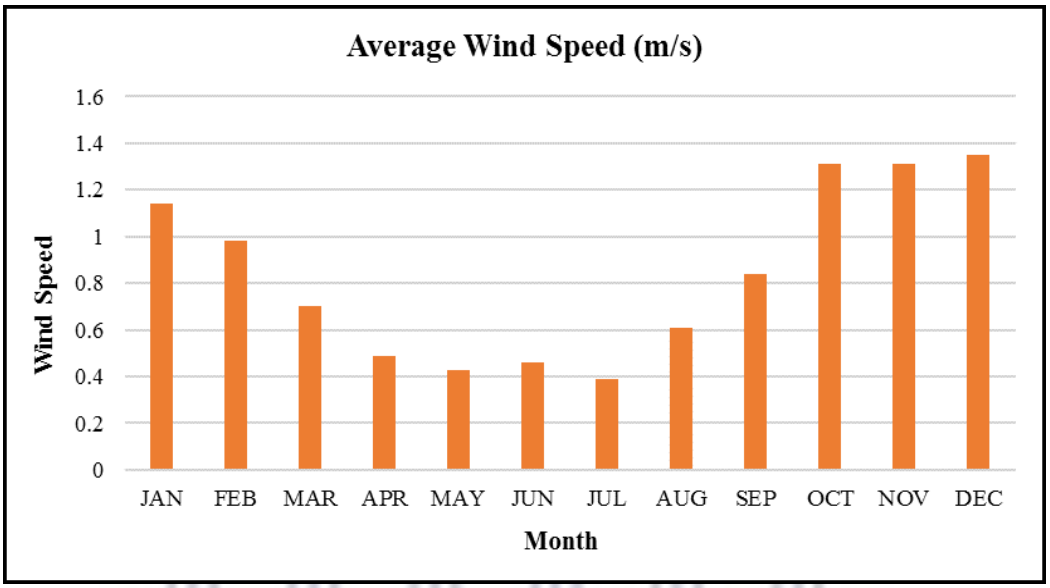

Figure 3.16: Summary of the average wind speed of the study area from 2003 to 2012

Further observation indicates that wind speed drops from January to May, and a slight increment was demonstrated in June but that appeared not to be enough. Then, a drastic increase in the wind speed was observed from August to December. The data of the wind include wind direction and wind speed.

Air pressure was part of the climatic parameters assessed at the study area. Average air pressure was measured, computed, and plotted to simplify its impact on the study area. From the graphical illustration in Figure 3.17, it is observed that average air pressure (hPa) increases from January (840.3 hPa) to a peak value of 845.72 hPa in July, and decreases down to December (839.97 hPa).

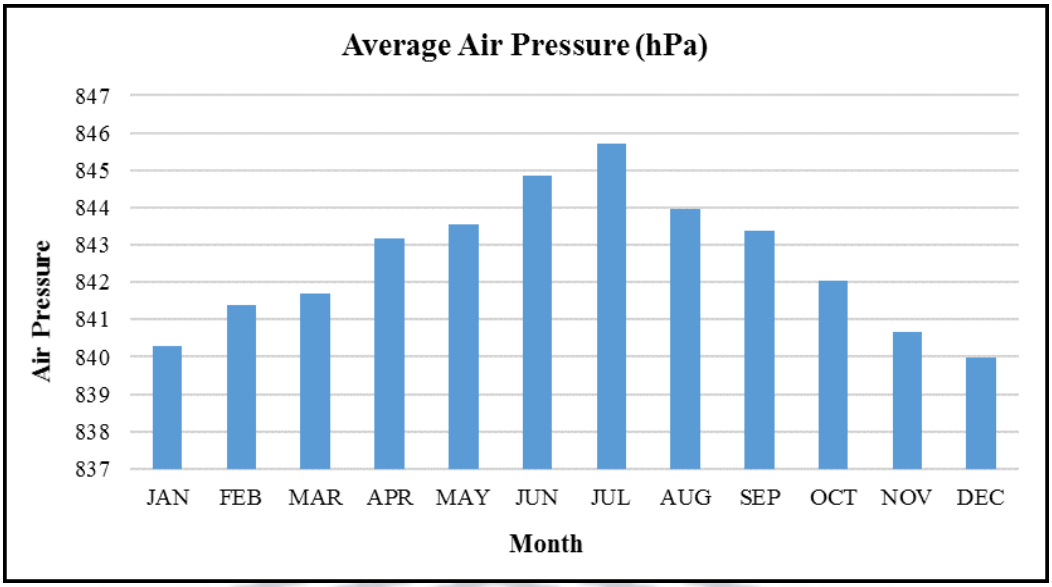

Figure 3.17: Summary of the average air pressure of the study area from 2003 to 2012

The distribution shape of the data plotted demonstrates minimal intervals between the values computed for each month. As the climate approaches winter time, the air pressure increases; but as the climate drifts towards summer time, the air pressure decreases.

3.6 Geology of the Study Area

The study area, Randfontein, and Krugersdorp lie in the outcrop area of several groups of rocks. The sources of tailing dams are the gold-bearing rocks of the Witwatersrand Supergroup, which consists of sediments deposited in an ancient basin (Gold One International Limited, 2013).

3.7 The Witwatersrand Supergroup

The Witwatersrand basin is situated on the Highveld and elevations above sea-level range from 1 340 m to 1 820 m (Whiteside, H. C. M., Glasspool, K. R., Hiemstra, S. A., Pretorius, D. A., Antrobus, 1976). In general, the topography is flat with gentle ridges from Johannesburg to Krugersdorp, long low hills along the West Wits Line and mountains at Heidelberg and around the northern crescent of the Vredefort Dome (Whiteside, Glasspool, Hiemstra, Pretorius, & Antrobus, 1976).

The Witwatersrand System is divided into upper division, which is subdivided into Kimberley-Elsburg Series and Main-Bird Series (Whiteside, H. C. M., Glasspool, K. R., Hiemstra, S. A., Pretorius, D. A., Antrobus, 1976); and lower division which is subdivided into Jeppestown Series, Government Reef Series ad Hospital Hill Series (McCarthy, 2006) (Figure 3.18). And the Supergroup is composed of a succession of shales, meta-quartzites and conglomerates (Phillips, 1994). SACA (1980) placed the age of the Witwatersrand Supergroup between 2300 million years and 2800 million years. The maximum thickness and description of each of subdivision is listed at Table 3.1.

Table 3.1: Formation into the Witwatersrand basin

System	Subdivision	Stage Unconformity	Max. thickness (m)	Description
Witwatersrand Upper Division	Kimberley-Elsburg Series	Elsburg Stage	1370	Quartzite, conglomerate
		Kimberley Stage	490	Quartzite, conglomerate, shale
	Main-Bird Series	Bird Reef Stage	810	Quartzite, conglomerate, lava
		Main Reef Stage	200	Quartzite, conglomerate
Witwatersrand Lower division	Jeppestown Series		1130	Shale, quartzite, lava
	Government Reef Series		1920	Quartzite, shale, conglomerate
	Hospital Hill Series		1490	Shale, quartzite, banded ironstone

(Source: Whiteside, Glasspool, Hiemstra, Pretorius & Antrobus, 1976)

Extensive major faulting took place along the strike of the beds, tangential to the West Rand Basin. These faults occur for a large part in the alternation zones of shale and quartzite of the Lower Witwatersrand but in places they affect the beds of the Upper Witwatersrand (Whiteside, Glasspool, Hiemstra, Pretorius & Antrobus, 1976). Two major faults (Witpoortjie to the north and Roodepoort to the south) bring up a segment of shale and quartzite belonging to the Jeppestown, Government Reef and Hospital Hill Series between the West Rand basin and the South Roodepoort and Durban Roodepoort Mines (Whiteside, Glasspool, Hiemstra, Pretorius & Antrobus, 1976). The gold-bearing conglomerate reefs of the Witwatersrand are mined in seven major goldfields, which are Evander, East Rand, Central Rand, West Rand, West Wits, Klerksdorp, and Welkom.

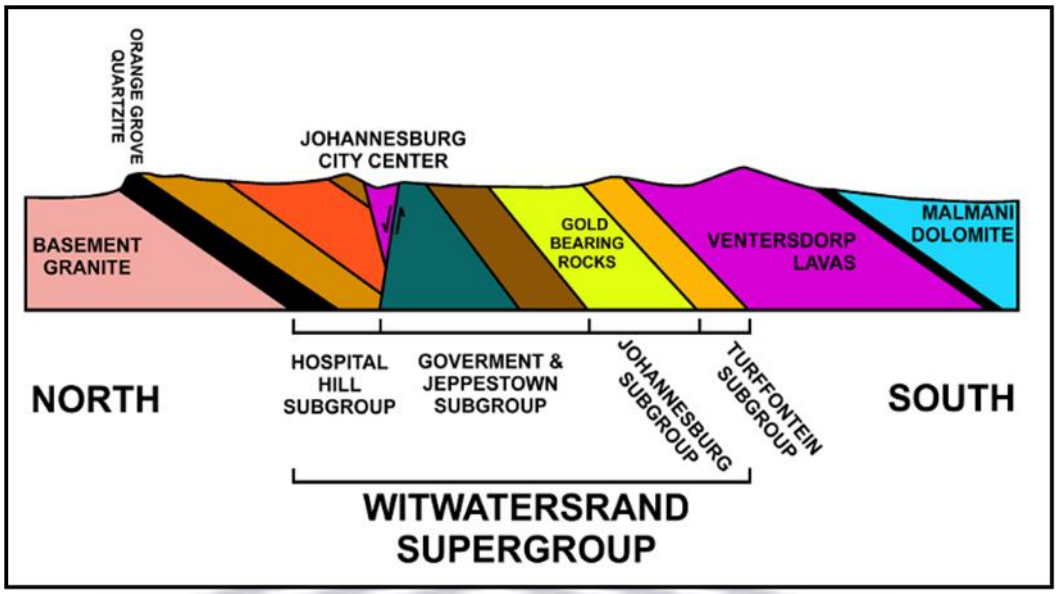

Figure 3.18: Witwatersrand Supergroup

The metamorphic history of the Witwatersrand Supergroup is important to gold mineralization (Phillips, 1994). It was recorded as a remarkable uniform metamorphic grade over most of the goldfields, with temperatures in the range of 300-350°C and pressures of 2.5-3.0 kb (Phillips, G.N., Law, J.D.M., Steven, 1997). The indicated geothermal gradient is about 35°C/km. In the main basin metamorphic grade increases towards the Vredefor structure, where coarse-grained amphibolite facies hornfels is developed in West Rand Group shales, and granulite facies rocks occur within the basement core of the structure (Bisschoff, 1982).

Gibson & Wallmach (1995) indicated that peak metamorphic conditions in the lower West Rand Group temperatures of 570-600°C and pressures of 4.5 kb imply a peak geothermal gradient of 40°C/km. They recognised a second metamorphic event characterised by the development of cordierite porphyroblasts associated with biotite, which overgrow the peak metamorphic assemblage of andalusite, staurolite and biotite. Stevens, Boer, and Gibson, 1997 suggested that in prograde metamorphism large quantities of fluid were released, particularly, from West Rand Group rocks.

3.8 West Rand Group

The West Rand Group (Hospital Hill, Government and Jeppestown Subgroups) comprises an alternating sequence of shales, quartzites, occasional conglomerate layers and a single lava band (Potgieter & Mendelsoha, 2001). Many of the quartzites are represented by shelf sand bodies (Eriksson, Turner & Vos, 1981). And the conglomerates are rare and distal, shales are iron-rich and eight magnetite-earing iron-formation layers are developed within the shale units, which contain siliceous beds and it true banded iron-formation (McCarthy, 2006). In the Johannesburg's area, the best-exposed portion of the Witwatersrand is the Hospital Hill Subgroup (Potgieter & Mendelsoha, 2001). The maximum elevation of the West Rand Basin is 1701 meters, while the minimum elevation is 1408 meters.

The Hospital Hill Subgroup consists primarily of shallow-marine orthoquartzites, more distal siltstones, outer-shelf shales and iron-formation (McCarthy, 2006). In addition, the rocks forming the Hospital Hill Subgroup have a direct influence on the topography of Johannesburg (Potgieter & Mendelsoha, 2001). The quartzite layers of the Orange Grove Quartzite Formation are very hard and resistant to weathering and erosion (Potgieter & Mendelsoha, 2001). As a result, they form the prominent ridge that extends from Bedfordview in the east to Krugersdorp in the west (Potgieter & Mendelsoha, 2001). The area to the north of the Bedfordview-Krugersdorp escarpment is underlain by basement rocks that weather easily, as well form low ground (Potgieter & Mendelsoha, 2001). And the layers of different sediment types are stacked one upon the other, which are described as following: sandy sediment at the base–which is quartzite; then, silt sediment–which is shale; and finally, iron-rich chemically precipitated sediment on the top–which is banded ironstone (Potgieter & Mendelsoha, 2001).

The Government Subgroup is the most lithologically diverse sequence of the West Rand Group, which contains rocks ranging from conglomerate to iron-formation, together with several diamictite horizons reflecting a wide diversity of depositional settings (McCarthy, 2006). The Government and Jeppestown Subgroups that overlie the Hospital Hill sediments are not completely exposed in the Johannesburg area (Potgieter & Mendelsoha, 2001). Although, the Government Subgroup is

partly exposed in eastern Johannesburg (Potgieter & Mendelsoha, 2001). These groups of rocks are probably the most diverse in the entire Witwatersrand Supergroup. And they consist of interlayered conglomerates, quartzites and shales (Potgieter & Mendelsoha, 2001).

Gold is sporadically mined from the conglomerate layers (Oelofse, 2002). The Government Subgroup was formed in response to a period of marked instability in the north area of the basin (Goldfarb et al., 2002). Faults developed caused topographic highs and alluvial fans built out into the basin formed conglomerate layers (Potgieter & Mendelsoha, 2001). On the other hand, the Jeppestown Subgroup includes a variety of rock types, ranging from conglomerate to iron-formation (Phillips, 1994).

3.9 Rock Type

The Witwatersrand Supergroup consists mainly of sedimentary rocks accumulated on the earth crust between 2800 and 2400 million years ago (Potgieter & Mendelsoha, 2001). They are formed on the eroded surface of the Basement rocks, and most of the Witwatersrand rocks are covered beneath younger rocks and appear at the surface over a limited area, only in the northern half of the basin (Potgieter & Mendelsoha, 2001).

As similarly discovered in the West Rand Group, the Witwatersrand Supergroup also comprises a 6000 meters thick pile of layers of different types of sedimentary rock, mainly shales and quartzites, but includes minor conglomerates or pebbly layers and some thin lava (Potgieter & Mendelsoha, 2001). The most remarkable aspect of the Witwatersrand Supergroup is the abnormal concentration of gold (Potgieter & Mendelsoha, 2001). And in some cases, uranium in the pebble layers or reefs. Pyrite is also one of the important constituents of the conglomerate (Potgieter & Mendelsoha, 2001).

The rocks of the Witwatersrand Supergroup are 2000 meters above sea level, but they were originally formed in a sea as horizontal layers along a coastline extending from northeast to southwest, with open sea to the southeast (Potgieter & Mendelsoha, 2001). As a result of the weight of the sedimentary rocks together with

the lavas by which they were subsequently covered, the region where they occurred sagged and the layers became tilted (Potgieter & Mendelsoha, 2001). This results in the present shape of the basin (Potgieter & Mendelsoha, 2001). Mineral resources in Witwatersrand Basin includes quartz phyllosilicates, pyrite and minor amounts of gold uranium, and other heavy minerals.

Two rock types are predominant in the Witwatersrand Supergroup, which are quartzite and shale. The quartzite is a rock composed of sand and bonded by heat, pressure and rock cement to form a hard resistant rock, while shale is formed from silt and mud, as well bonded, but forming a softer rock (Potgieter & Mendelsoha, 2001). Less common are the conglomerates, which consist of rounded pebbles in a sandy matrix and banded ironstones (Potgieter & Mendelsoha, 2001). They are rarely banded rocks that comprise alternating layers with large quantity of iron oxides or silica (Potgieter & Mendelsoha, 2001). The matrix consists predominantly of quartz of sand size, with varying amounts of pyrite and another sulphide (Whiteside, Glasspool, Hiemstra, Pretorius & Antrobus, 1976).

Heavy minerals are represented by chromite, zircon and leucoxene, and the valuable constituents are gold, uraninite, and minute traces of iridosmine and osmiridium. The phyllosilicates are present in the form of muscovite/sericite, pyrophyllite and chlorite. Carbon is notable in some of the conglomerates (Whiteside, Glasspool, Hiemstra, Pretorius & Antrobus, 1976). The pebbles vary in composition, size, and colour but consist mainly of vein quartz (Revuelta, 2018). Round grains of pyrite are often visible in the matrix, and sometimes are used as indicators for high gold concentrations (Revuelta, 2018).

3.10 Hydrogeology of the Study Area

There are seven main rivers systems that interact with the West Rand area, namely: the Skeerpoort River, Magalies River, Rietspruit, Crocodile River, Wonderfonteinspruit, Loopspruit and Leeuspruit. Wonderfonteinspruit is largely the surface water that links to the gold tailings in the study area.

3.10.1 Surface Water

In the study area, large quantity of surface water resource emanates from Mooi River, which is part of the Vaal River System. The Mooi River with its two main tributaries, known as the Wonderfonteinspruit (or, Mooirivierloop) and the Loopsupruit, has a relatively flat topography with elevations varying from 1520 meters in the north to about 1300 meter in the south-west (ILISO Consulting Pty Ltd, 2009). Mooi River originates from the Bovenste Oog in the Mathopestad area near Ventersdorp and flows into the Vaal River. And the Wonderfonteinspruit originates in the southern part of Krugersdorp (Mogale) on the Witwatersrand ridge, the catchment between the Vaal and Crocodile West Catchment. Then, the Wonderfonteinspruit flows through the municipal areas of Westonaria and Merafong into the Mooi River, upstream of Potchefstroom (ILISO Consulting Pty Ltd, 2009).

Mining in the lower part of the Wonderfonteinspruit has been in operation for approximately 50 years. Several mines and industrial activities, especially in the upper part of the catchment, disclosed evidence of damage on the water resources (ILISO Consulting Pty Ltd, 2009).

Figure 3.19: River net to Gold One mine

Figure 3.20: Robinson Lake

(Source: Pictures were taken at the study site)

Robinson Lake is situated between the Randfontein Golf Course and the suburb of Robin Park (Figure 3.20). The lake was a former recreational lake filled with water pumped from the Robinson Deep gold mine, later called Gold One tailings after the mine eased. According to the Municipality of Randfontein, the lake has a pH of 2.6 with a uranium concentration of 16 mg/l. Though, this is above 220 times of safe levels if compared with a concentration of 0.07 mg/l safe to drink water standard in South Africa. Due to this, the Robinson Lake was declared a radioactive area and prohibited to the public. The deduction was that the effect is caused by AMD. Robinson Lake is in the study area and considered for study purpose, where water samples are collected.

3.10.2 Groundwater

The Malmani dolomite of the Tansvaal sequence generates groundwater that moves rapidly in large volumes through large solution cavities in the dolomites (Stevens et al., 2014). And it is considered as the most important aquifer in South Africa. There are eight primary groundwater aquifers in Mogale City Local Municipality (MCLM). The dolomite in MCLM is regarded as a major aquifer that can supply large quantities of good quality groundwater (Stevens et al., 2014). And it is a vital water source for Gauteng Province (Stevens et al., 2014).

Figure 3.21: Gold One_2 tailing AMD

(Source: picture was taken on the study site)

AMD is one of the biggest groundwater-related problems facing the study area due to extensive mining activities, both historical and contemporary tailing dam reclamation (Figure 3.21). AMD from the West Rand Mining Basin began in 2002. The Krugersdorp Game Reserve lies closely downslope of AMD, with other potential receptors like the neighbouring smallholdings and the Cradle of Humankind World Heritage Site (Stevens et al., 2014).

3.11 Residential Distribution

The residence Amberfield complex (Figure 3.22) is located opposite of the Mogale Tailings, and West Village (Figure 3.23) is the other residents in the same area. Road 28 separates the residential area, include the tailings into northern and southern structures.

Figure 3.22: Amberfield Complex

Figure 3.23: West Village Residential area

(Source: Pictures were taken at the study site)

There are a few informal settlements closed to the Mogale tailings as well, where criminal activities happened due to illegal mining in the area.

Figure 3.24: Informal settlement

(Source: Pictures were taken at the study site)

CHAPTER FOUR

4. METHODOLOGY

4.1 Introduction

The methodology applied in this study involves five procedural stages that are crucial in realising the objectives emphasised in the section 1.5. These stages are diagrammatically represented in Figure 4.1 as field trip and sampling, mineralogical analysis, geochemical analysis, and prediction methods, (environmental impact) modelling development with each one having subprocess stages.

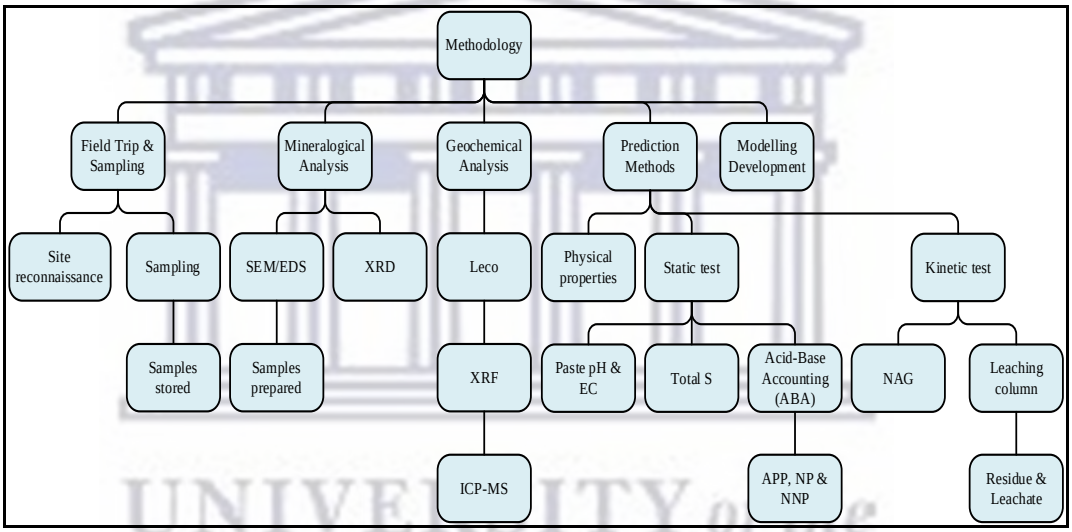

Figure 4.1: Methodology of the study

According to the diagram Figure 4.1, the first stage is 'field trip and sampling', which was implemented to carry out site inspection, sampling collection and samples storage. The second stage is 'mineralogical analysis', which involves three subprocess stages such as scanning electron microscopy/energy dispersive spectroscopy (SEM/EDS), x-ray powder diffraction (XRD) and samples preparation. 'Geochemical analysis' is the third stage with direct three subprocess stages, such as Leco, x-ray fluorescence (XRF) and inductively coupled plasma-mass spectrometry (ICP-MS). The next stage is 'prediction methods', which also involves subprocess stages such as the physical properties of the samples, static test and kinetic test, including paste pH and Electrical Conductivity (EC), total sulphur

(total S), acid-base accounting (ABA) and acid production potential (APP), neutralisation potential (NP), net neutralisation potential (NNP), net acid generation (NAG), leaching column, residue and leachate. The last stage of the methodology is 'modelling development' with no subprocess stages, which engages the demonstration of the environmental impact of the tailings across the affected areas.

4.2 Field Trip and Sampling

Appropriate investigation and complete collection of tailing and water samples were made possible due to the three field trips took to the study site.

4.2.1 Field Trip

The first field trip travelled was in February 2011 when six gold companies and sites were visited to determine the appropriate sites for required study samples. The six gold companies and sites visited are Savuka Mine of AngloGold Ashanti, Harmony Kusasalethu, Gold Fields, the Cradle of Humankind, Barberton Gold Waste Dump Station and Barberton Gold Mine. After the first visit, three gold tailing dams were selected for study, which are Mogale tailings (Mogale Gold Company) in Krugersdorp, Gold One_1 and Gold One_2 (Gold One Company) in Randfontein area. These three gold tailing dams were thoroughly discussed in Chapter 3. However, the criteria followed in selecting the three tailings are:

- Tailing must be located within the Western Basin area–where AMD have occurred in the past few years,
- Tailing must decant acid water–as discovered in Gold One_2 tailings, and
- Tailing must have a plan to re-operate in next five to ten years–as discovered with the three selected tailings.

During the inspection visit to the tailing sites, it was discovered that Gold One_2 has already begun operation and Mogale tailings have partially started re-treatment. Preceded study revealed that AMD problems may affect the Krugersdorp Game Reserve, including the residential area vicinity of the tailings. The tailings site images were presented in Chapter 3.

The second field trip was travelled between September and October 2012 to collect the soil, sediments, and tailings samples at the three gold tailings and their surrounding areas. Samples collected were appropriately given a conventional label pattern, as well carefully transported to the lab from Johannesburg to Cape Town.

In addition, the third field trip travelled was in December 2014 with the intention of collecting water samples from the tailings' surrounding areas in the summer season. Water samples were collected from Robinson Lake, Gold One_2 tailing site, Mogale tailings water treatment plant and the stream in the same area. The stream path is from Gold One_1 and Gold One_2 goes to Krugersdorp Game Reserve, with a path distance of approximately 5.5 kilometres and well planted vegetations.

Figure 4.2: Robinson Lake (raining season)

Figure 4.3: The river along the Mogale tailing

(Source: Pictures were taken at the study site)

A total of ninety-nine (99) tailing samples from eleven drilled holes were collected from the field trips, together with eight (8) sediments samples, thirteen (13) soil samples, only seventeen (17) water samples were collected from flowing lake and river.

4.2.2 Logging and Drilling

Sample location and number of the holes of the Gold One_1, Gold One_2 and Mogale tailings were appropriately identified at the site and carefully drilled to collect sufficient samples to deter access limitation to the tailings. In the process, two auger methods were applied, which are hand auger and drilling machine (Figure

4.4 and Figure 4.5). At the Mogale tailings, five holes were drilled by hand auger because the area was rough for a drilling machine branded AMS Power-Probe 9700-VTR (Figure 4.4). At the Gold One_1 and Gold One_2 tailings, drilling machine was used to drill the holes by adopting a direct push drilling method. The core sample was sealed in a plastic tube to avoid handling of the samples taken place.

Figure 4.4: Drilling machine

Figure 4.5: Hand auger

(Source: Pictures were taken at the study site)

Tailing samples collected and soil profile are based on the guidelines specified for soil and rock logging (Brink & Bruin, 2001) on the site and geochemical properties were also observed. Geological logging was executed for all eleven holes that were drilled for samples collection in the three gold tailings.

Figure 4.6: Tailing raw samples (before seized and milled)

The samples were taken from each vertical meter of the drilled hole. And thereafter, each sample was given a tag with logging information (Figure 4.6). On the site, the variety of lithological units and physical properties of the tailing sample are

properly observed. 10 meters deep holes were drilled in the area where the drilling machine could function perfectly (Figure 4.7), but in the area where the drilling machine could not operate, such area as hard-residual soil, close to 3 meters deep holes were drilled (Figure 4.8).

Figure 4.7: Drilling machine core sample

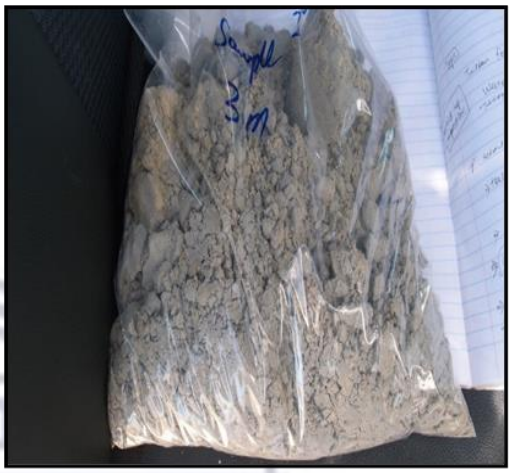

Figure 4.8: Hand augur sample

(Source: Pictures were taken at the study site)

In Gold One_1 tailing, three holes were drilled for samples collection labelled as T001, T002, and T003. Equal number of holes were drilled in Gold One_2 tailing, which are labelled as T005, T006, and T007. And five holes were drilled in Mogale tailings, which are labelled as T004, T008, T009, T010 and T011. The information of drilled holes was captured into Downhole Explorer for logging analysis. The software plotted all downhole data as scaled drill holes' log sheets with optional colour and pattern fills.

4.3 Samples Collection and Preparation

4.3.1 Tailing Samples

As earlier mentioned in Chapter 3, the three tailings are in areas not far from each other. More detailed map that indicates the three close locations of the three tailings are displayed in Figure 4.9, with latitude from 26.094906 S to 26.158580 S, and the longitude is from 27.681951 E to 27.774426 E. The GPS and UTM coordinates gave accurate locations of all the sites where the samples were collected. A total of

120 tailing samples were collected from 11 drilled holes, which were numbered from 001 to 120 tailing samples.

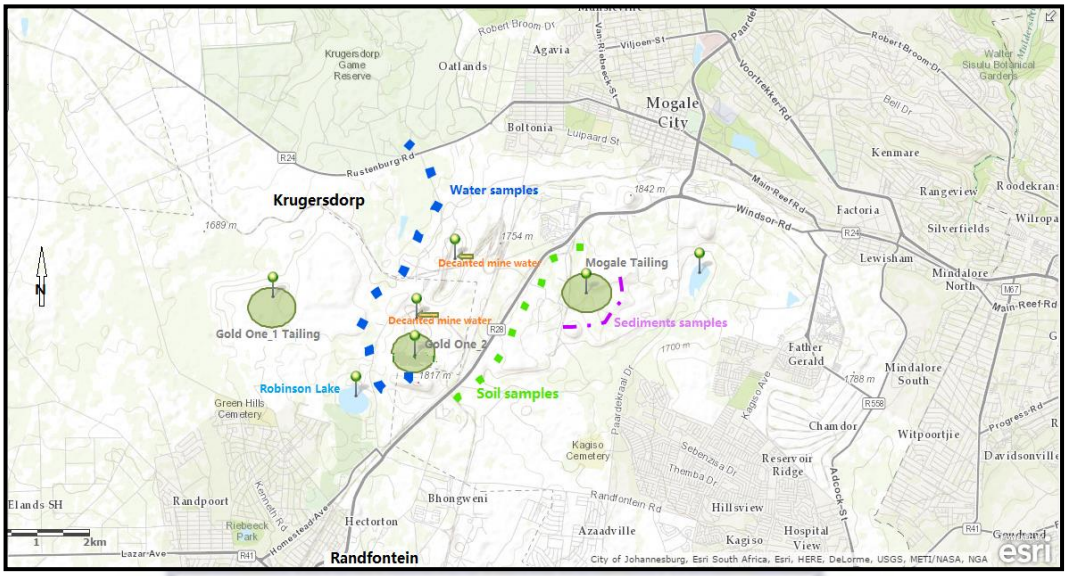

Figure 4.9: Samples collection map

(Source: Esri South Africa)

In addition, all the samples were dried at 40°C in covered watch glasses for 16 hours. The bulk tailings samples were pulverised to a fine powder and sieved through stainless steel sieves. Thereafter, the powdered samples were milled by Dickie and Stockler milling machine. The bulk tailings samples were reserved as raw materials for the leaching column test. Each powdered sample was stored in a paper bag, with appropriate sample label and weighed for different analysis. All the samples were stored in the dry room.

Mogale tailings with hole label T004 was drilled by using hand-augur (Figure 4.11) and the samples collected from the hole were labelled as MT038–046. Other holes drilled in Mogale tailings were labelled as T008, T009, T010 and T011 and executed by using drilling machine (Figure 4.12). The samples collected from these holes were labelled as MT001–037 and the holes were selected to drill from surface of the tailing dam and the slop of the tailing dams.

Figure 4.10: Using drilling machine to collect samples

Figure 4.11: Using hand augur to collect samples

(Source: Pictures were taken at the study site)

Similarly, in Gold One_1 tailing, holes drilled were labelled as T001, T002 and T003 with samples collected from these holes labelled as GT1–048 to 076. And holes labelled T005, T006 and T007 were drilled in Gold One_2 tailing, and samples collected from these holes were labelled as GT2–083 to 090. Moreover, the samples collected from the sediments to soil include water are discussed further in the subsequent subsections.

4.3.1.1 Sediments Samples

Seven sediment samples were collected from Wonderspruit river downstream, which is the only water source that is close to Mogale tailings. However, it was discovered that there was no flowing of water in the dry season. And the sediment samples were collected from 20-30 cm deep the ground. All the sediment samples were stored in the sealed plastic bag and labelled with location and number. The samples were dried at 40^{o}C for 16 hours and milled by Dickie and Stockler milling machine. Milled samples were stored in paper bags and labelled with sample numbers and weight. All the samples were stored in a dry storeroom.

4.3.1.2 Soil Samples

Thirteen soil samples were collected in the gold tailings located area, particularly in the area close to the residential along the road 28. All soil samples were selected within a 1 km distance and dug from 20-30 cm deep the ground. Samples were stored in the sealed plastic bag and transported back to the lab for preparation and analysis. All soil samples were milled and conserved in paper bag and labelled with sample numbers and weight.

4.3.1.3 Water Samples

Seventeen water samples were collected from Gold One_1 and Gold One_2 tailing areas. Collection of samples started from the tailings water pond and along the Robinson Lake to R24 Roodepoort. Also, samples were collected along the Skeerpoort River water for each kilometre distance taken as the river flows into Krugersdorp Game Reserve. The water samples were as well collected from Sibanye Gold treatment plant.

To ascertain samples' concentration levels, pH and EC test were taken and recorded on the site for all the water samples. Water samples were filtered and sent to the Council for Geoscience of South Africa (CGS) in Pretoria for analysis. For quantitative analysis by ICP-MS, the water samples were preserved by ultrapure nitric acid (HNO3), with no perseveration for anions test. All water samples were stored in a refrigerator before being transported.

4.4 Samples Analysis

Analysis of all samples is expected to demonstrate 'geological continuity', which implies features that control mineralization and 'value continuity', which implies a measure of neutralisation potential and variable spatial occurrence. The methods considered for samples analysis are mineralogical and geochemical analyses.

4.5 Mineralogical Analysis

The mineralogical analysis of the tailing samples involved the use of XRD test and SEM with EDS. The XRD analyses included standard qualitative analysis to

determine the minerals present in the tailing samples and to provide information on unit cell dimensions of the samples.

4.5.1 SEM/EDS

SEM is primarily used in providing a 3–dimensional image of the surface of a sample. This device is suitable in viewing large objects. The specimens are captured with a beam of electrons. This beam is scanned across to create the image of the surface of the samples, with exceptional depth of field. Furthermore, SEM enables the determination of modes of occurrence of the carbonate and sulphide minerals, including their textures, grain size, morphology and mineral association.

SEM/EDS analysis determines minerals, grain size and arrangement of mineral grains in the samples examined, as well to estimate their elemental composition (Marchant & Lawrence, 1991). The large depth of field attainable can produce an image of great visual depth with a 3–dimensional appearance. The samples are mounted on a stub of metal with adhesive, coated with carbon and then observed in the microscope.

Figure 4.12: SEM machines

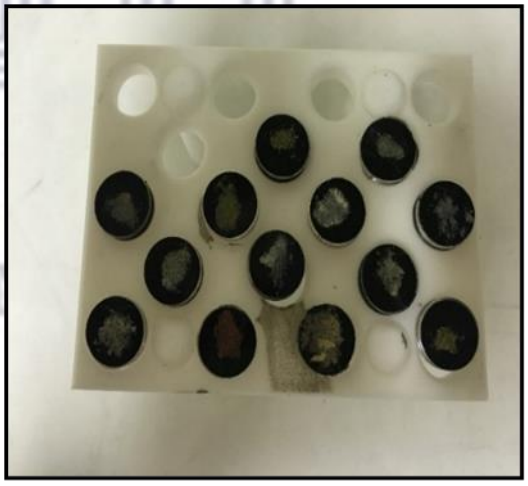

Figure 4.13: SEM/EDS samples preparation

(Source: Pictures were taken at the study site)

Preparation procedures of samples for SEM/EDS analysis are highlighted below:

- Clean the stubs by methanol and mark with number,

- Put carbon tables onto the stub,
- Take off the sticker from carbon tabs,
- Spread the sample onto the carbon tab,
- Air spray to clean the dust,
- All stubs on the stub holders,
- Carbon coating procedure for all prepared samples, such as turbo high vacuum pump for rapid pumping, then outgas the evaporating material and followed by coating stage, and
- Samples are ready for analysis.

The SEM/EDS analysis was executed by The Electron Microscope Unit of the Physics and Astronomy Department, University of the Western Cape, South Africa. The following equipment was utilised for samples preparation and analysis, which are EMITECH K950X carbon coating machine and Scanning Electron Microscope (Hitachi X650) equipped with Energy Dispersive Spectroscopy (EDS).

4.5.2 XRD Analysis

Before performing XRD analysis, forty tailing samples were selected from different drilled holes and layers of the holes. These samples were sent for XRD analysis at the Materials Research Department of iThemba Laboratory, South Africa. XRD analysis was executed with the use of x-ray beam to examine the powdered sample randomly packed into a cavity in a holder. In the process, the flat surface of the powdered sample was directly facing the x-ray beam for XRD analysis. Mineral phases were determined by comparison of the locations and intensities of the diffraction peak with those of mineral reference standards in a database (Marchant & Lawrence, 1991).

The XRD analysis methodology was executed by iThemba Lab. The process involved the use of analysis apparatus such as BRUKER AXS (manufactured in Germany) and D8 Advance as diffract-meter. The measurements ϑ-ϑ scan was in locked coupled mode, x-ray tube is Cu-K radiation (K_1 = 1.5406Å). And the detectors selected Position-Sensitive Detector Vantec-1. The data were evaluated and analysed by using ICDD, PDF database 1998 and data evaluation by EVA software from BRUKER.

Samples preparation procedure was provided by iThemba Labs as highlighted below:

- A 1.2 g of powder sample each was deposited in the centre of the sample holder, which consists of a 20 mm by 20 mm corning glass.
- Heap of powder was smoothly flattened into a disc shape of 15 mm diameter and 1 mm thickness using circular motion of a microscope glass slide until the zero levels for a correct sample height was achieved.
- The measurements were carried out for 5 days, and each sample is measured with the same parameters and preparation method.

4.5.3 Geochemical Characterisation

The milled tailing samples were transported to ACME Analytical Laboratories Ltd, Vancouver in Canada for geochemical analysis. ACMELabs described the method of major oxides by XRF analysis as a predetermined amount of sample is roasted to determine the loss on ignition (LOI). The roasted sample is then fused in a platinum-gold crucible with a commercial lithium tetraborate flux. Then, the molten material is cast in a platinum mould. Fused discs are analysed by XRF. Total carbon and Sulphur are determined by the Leco method. SiO_2, Al_2O_3, Fe_2O_3, CaO, MgO, Na_2O, K_2O, MnO, TiO2, P_2O_5, Cr_2O_3, Ba, Total Carbon and Total Sulphur are tested for the tailings' samples. The measurement unit for XRF analysis is wt. % oxides.

In addition, ACME Labs described the method of trace element by ICP-MS analysis as a prepared sample is mixed with $LiBO_2/Li_2B_4O_7$ flux. In the process, the crucibles are fused in a furnace and the cooled bead is dissolved in ACS grade nitric acid. Loss on ignition (LOI) is determined by igniting a sample split then measuring the weight loss. The trace elements Ba, Be, Co, Cs, Ga, Hf, Nb, Rb, Sn, Sr, Ta, Th, U, V, W, Zr, Y, La, Ce, Pr, Nd, Sm, Eu, Gd, Tb, Dy, Ho, Er, Tm, Yb, Lu, Mo, Cu, Pb, Zn, Ag, Ni, As, Au, Cd, Sb, Bi, Hg, Ti, Se are tested for the tailings samples. The measurement unit for ICP-MS analysis is ppm, except Au element is ppb.

4.6 Prediction Methods

According to the diagram given in Figure 4.1, prediction methods comprise three subprocesses which are physical properties of the samples analysed, static test (a combination of paste pH and EC, total S and acid-base accounting (ABA)– generates acid production potential (APP), neutralisation potential (NP) and net neutralisation potential (NNP)), and kinetic test (a combination of net acid generation (NAG) and leaching column test– generates residue and leachate). These subprocesses are discussed in the subsections below.

4.6.1 Samples Physical Properties

The sample collection sites were observed during the field trip, which included other elements like tailings oxidisation and leaching, tailing operation status, tailing protection, surrounding area pollution, etc. The physical properties of the samples collected were examined and recorded such as soil moisture, colour, smell and texture.

Figure 4.14: Paddock of the tailings

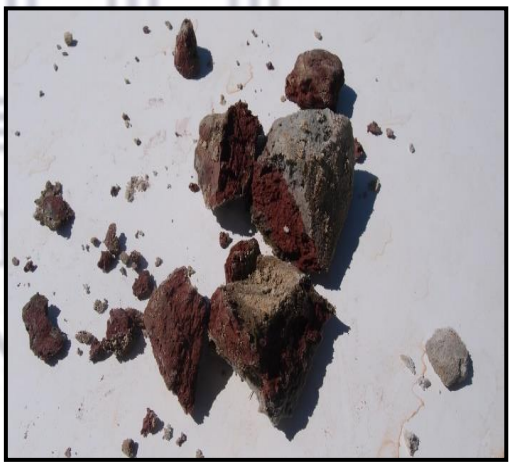

Figure 4.15: Tailing samples

(Source: Pictures were taken at the study site)

4.6.2 Static Test

Static test for this study includes paste pH & EC; Total S, and Acid-Base Accounting. Total Sulphur is measured by AcmeLab.

4.6.2.1 Total Sulphur

Total Sulphur stands for the sum parameter of all organic and inorganic sulphur compounds (Méndez-Ortiz et al., 2007). Total Sulphur is determined by sulphur/carbon analyser Leco. Total Sulphur analysis normally is required for the AP calculation (Price, 2009).

4.6.2.2 Paste pH and EC

The paste pH/EC is determined by equilibrating the sample in deionized water to water ration of 1:2 for approximately 12 hours at a solid state, and then measures the pH and EC. This indicates the characteristic acidity and salinity of the waste material when initially exposed in a waste emplacement area (INAP, 2002). The paste pH/EC test was done at the Chemistry Department of the University of the Western Cape. All samples were tested, and the procedures followed are given below.

- Placed 25 g of pulverised 75 µm sample into a beaker and added 50 g of distilled water and continually stir it,
- Allow the slurry to stand for 12 hours, and
- Measure the pH and EC directly on the slurry and recorded.

4.6.2.3 Acid-Base Accounting (ABA)

Several procedures have been developed to determine the acid-forming characteristics of mine waste materials. The most widely used assessment methods for AMD characterisation are ABA and NAG tests. These methods are referred to as static test procedures because each involves a single measurement in time (Ian Wark Rearch Instiute, 2002). The term APP is equivalent to maximum potential acidity (MPA). Acid neutralising capacity (ANC) is equivalent to NP and NAPP is the same as NNP, and denoted with a positive or negative prefix (Skousen et al., 2000). The standard guideline for defining strata as either acid-generating or alkaline is shown in Table 4.1.

Table 4.1: A general standard guideline for strata specification

	Acid Tons/1000 Tons	Undecided Tons/1000 Tons	Alkaline Tons/1000 Tons
ANC/NP	<10	10-21	>21
NAPP	<0	0-12	>12

- **Sulphur Species analysis**

Elemental sulphur (S) occurs naturally as an element, or as native sulphur, but most commonly occurs in combined forms as sulphide and sulphate minerals. Total Sulphur (S%) result is a laboratory analysis, which is the sulphur in all its forms of material. Sulphide–sulphur is the sulphur present in the material as a sulphide. Sulphate Sulphur is calculated as the difference between Total S and Sulphide S.

Sulphide S = Total S – Sulphate S

The use of the total sulphur to estimate the MAP is a conservative approach because some sulphur may occur in forms other than pyrite. For example, sulphate–sulphur and native sulphur are non-acid generating sulphur forms.

- **Maximum Potential Acidity (MPA)**

The MPA generated by a sample is determined by multiplying the sulphide–sulphur values in percentage by 30.6. This constitutes the reaction stoichiometry for the complete oxidation of pyrrhotite and pyrite by O_2 to Fe $(OH)_3$ and H_2SO_4. The calculation assumed that the measured sulphur content occurs as pyrite (FeS_2). And that pyrite reacts under oxidizing conditions to generate acid as shown in the reaction written below.

$FeS2 + 15/4\ O2 + 7/2\ H2O \rightarrow Fe\ (OH)\ 3 + 2H2SO4$ ……..…….. Equation 4.1

According to this reaction, the MPA of a sample containing 1% S as pyrite is 30.6 kg of H_2SO_4 per tonne of material (kg H_2SO_4/t). Hence, the MPA of a sample is calculated from the total sulphur content using the following formula.

MPA (kg H_2SO_4/t) = (Total S – Sulphate S) x 30.6

Note: MPA does not consider the effect of any acid consuming materials in the tailing materials.

- **Acid Neutralising Capacity (ANC)**

The acid formed from pyrite oxidation moderately react with acid-neutralising minerals contained within the sample. This inherent acid buffering is measured in terms of the ANC, and its result is usually expressed by carbonated (e.g. calcite and dolomite) and silicates. In addition, the ANC is commonly determined by a modified Sobek method (Marescotti, 2010). This method involves the addition of a known amount of standardised hydrochloric acid (HCl) to an accurate weighed sample, which allows the sample time to react with heating, then back-titrating the mixture with standardised sodium hydroxide (NaOH) to determine the amount of unreacted HCl. The amount of acid consumed by reaction with the sample is then calculated and expressed in the same units as the MAP, which is kg H_2SO_4/t.

Step 1: A "fizz rating" is introduced in determining the amount and concentration of acid to be used in the analysis. This is obtained by placing pulverised sample with an approximate weight of 0.50 g on a ceramic plate. One or two drops of 1:3 HCl, 8% concentration is then added to the sample. The presence of $CaCO_3$ is indicated by a bubbling or audible "fizz". A rating is then given to the scale of reaction presented in Table 4.2.

Table 4.2: Tabularised values of fizz rating computed in relation to HCl and NaOH

Reaction	Fizz Rating	HCl		NaOH
		Molarity (M)	Volume (ml)	Molarity (M)
No Reaction	0	0.5	4	0.1
Slight Reaction	1	0.5	8	0.1
Moderate Reaction	2	0.5	20	0.5
Strong Reaction	3	0.5	40	0.5
Very Strong Reaction	5	1.0	40	0.5
	5*	1.0	60	0.5

5* is used for very high ANC material (>400 kg H_2SO_4/t) e.g. limestone

Step 2: Deposited a weight of 2.00 g air-dried pulverised sample into a clean dry 250 ml Erlenmeyer flask or beaker. Carefully pipette the required amount of HCl into the beaker and add approximately 20 ml of distilled water. Also, prepare blanks by pipetting the same volume and concentration of acid into clean beakers containing no sample and add approximately 20 ml of distilled water. Blanks must be run for each volume and concentration of acid used for each fizz rating used.

Step 3: Place beakers covered by a watch glass in a hot plate and heat to 80 to 90℃, swirling the beaker occasionally for 1 to 2 hours until the reaction is complete. The reaction is completed when no gas evolution is evident, and the particles settle evenly over the bottle of the flask.

Step 4: Allow the beaker to cool at room temperature. Then add distilled water to give a total volume of approximately 125 ml, and then measure the pH of the mixture. If the pH falls within the range 0.8 to 1.5, then process with the titration. For all the fizz ratings, from 1 through to 5.0 if the pH is greater than 1.5, then there may be a need for more acid to be added to the sample, either that the total amount added is equivalent to the next highest fizz rating, or the test needs to be re-started on a new sub-sample using the next highest fizz rating. If the pH of the mixture is less than pH 0.8, then it indicates that too much acid may have been added, except when the test is being run at a fizz rating of 5.0. In such cases, it is recommended that the test should be repeated the test using the next lowest fizz rating.

Step 5: Titrate against standardised sodium hydroxide solution (using molarity of NaOH listed in Table 4.2) with constant mixing. Stop the titration near pH 5.0 and add 2 drops of 30% H2O2 to oxidise any dissolved ferrous ion. Continue titration to pH 7.0 and record volume of NaOH added. Titrate the blank using NaOH as indicated in the above table. Run duplicates on every fifth sample.

Step 6: Calculation of ANC

$$ANC = [Y \times \frac{M_{HCl}}{wt}] \times C \quad \text{.....Equation 4.2}$$

Where:

Y = (Volume of HCl added) – (Volume of NaOH titrated x B) ……...Equation 4.3

B = (Volume of HCl blank) / (Volume of NaOH titrated in blank) …..Equation 4.4

MHCl = Molarity of HCl

wt = Sample weight in grams

C = Conversion factor

C = 49.0 (to calculate kg H2SO4/t)

C = 5.0 (to calculate % CaCO3 equivalent)

- **Net Acid Producing Potential (NAPP)**

The ABA involves static laboratory procedures that evaluate the balance between acid generation processes (oxidation of sulphide minerals) and acid neutralising processes (dissolution of alkaline carbonates, displacement of exchangeable bases and weathering of silicates). The values arising from the ABA are MPA and ANC, respectively. The difference between the MPA and ANC is NAPP. In this context, a negative NAPP indicates that all acid produced is neutralised, while a positive NAPP indicates that material is net acid-producing.

- **ANC/MPA Ratio**

The ANC/MPA ratio is frequently used as a means of assessing the risk of acid generation from mine waste materials. It is another way of examining the acid-base account. A positive NAPP is equivalent to an ANC/MPA ration less than 1, while a negative NAPP is equivalent to an ANC/MPA ration greater than 1. A NAPP of zero is equivalent to an ANC/MPA ratio of 1. The purpose of the ANC/MPA ratio is to indicate the relative margin of safety within a material. Various ANC/MPA values are reported in the literature to demonstrate the safe values for prevention of acid generation. These values typically range from 1 to 3. As a rule, an ANC/MPA ration of 2 or more generally signifies that there is a high probability that the material will remain circum-neutral in pH.

4.7 Kinetic Test

Kinetic test procedures involve several measurements over time, which are used to assess a range of acidity issues including sulphide reactivity, oxidation kinetics, metal solubility and leaching behaviour of test material (Ian Wark Rearch Instiute, 2002). The kinetic test provides a better definition of AMD characteristics of samples as well resolves issues of uncertainty identified in AMD static test.

4.7.1 Net Acidity Generation (NAG)

Twenty-four (24) samples were assessed for NAG test. NAG test is performed to ascertain the gross level of acid generated in these samples. The experimental reagents are 15% H_2O_2, 0.1M NaOH, 0.5M NaOH, 4.5 and 7.0 pH indicator. However, before using H_2O_2 ensure that the pH is greater than 4.5. If it is less than

4.5, it is called a diluted NaOH solution–that is, 1 g NaOH with 100ml distilled water, until the pH is greater than 4.5. The experimental procedures are highlighted below:

- Weigh 2.5 g of sample and put in a 500 ml reagent bottle.
- Slowly add 250 ml of 15% H_2O_2 at room temperature (30% H_2O_2 is diluted with 1:1 distilled water).
- Cover the reagent bottle with glass and place it in a well-ventilated area for 24 hours; H_2O_2 will reacts with the sample.
- After the reaction, heat the sample evenly for 2 hours. Add appropriate distilled water to keep the sample solution stable and not burned.
- Let the sample cool at room temperature, add distilled water to make the total sample mixture 250 ml, test and record the pH value, record it as NAGpH.
- If the NAGpH value of the sample is greater than 2, titrate with 0.1M NaOH to pH 4.5, record the amount of titration solution, and continue titration to pH 7.0, record the amount of titration solution.
- If the NAGpH value of the sample is equal to 2, titrate with 0.5M NaOH to pH 4.5, record the amount of titrated solution, and continue titration to pH 7.0, record the amount of titrated solution.

4.7.2 Leaching Column Test

Leach column test is implemented to provide data on reaction rate and leachate chemistry (Ian Wark Rearch Instiute, 2002). A short-term kinetic column test was performed over three months on the tailing samples, which were drilled at a different depth from approximately 15 years old stagnant gold tailing dams, with wetting and drying cycles weekly. And the samples were collected for analysis to determine the acid generating potential. The leaching column test procedures are highlighted as follows:

- The free draining leach column operation is designed to achieve a weekly wet-dry cycle and a monthly leaching cycle.

- Materials requested are included: porcelain, 2100 ml capacity; filter paper-coarse; 500ml -1 L collection containers; 150w floodlight heat lamps; shelving; test solution which are distilled water.
- Columns: internal diameter 90mm, height 150mm, estimated sample mass is 500g to 1 kg. Place filter paper over the perforations at the base of the column and load the samples.
- Samples were stacked into columns according to their drilled depth to simulate conditions of the tailing dams. The height and mass of the material were recorded.
- Allowing easy access to the top and bottom shelves for watering and leachate collection; heat lamps are required to ensure that the columns dry-out between watering. Heat lamps are operated on a weekly cycle: day 1-5, switch heat lamps on during daylight hours which are 8-10 hours; day 6-7 switch heat lamps off. Switch heat lamps off at least 3 hours prior to water application to reduce surface evaporation effects.
- Weekly wetting and drying cycle were conducted by adding aerated deionized water (by sparging oxygen through a container of de-ionised water before use).
- The amount of wash water should aim to simulate rainfall in the area (WeatherSA data) and calculated based on the area of the stacked sample. The wash water is first flooded and then allowed to flow out of the columns freely and collected for analysis.
- 100 ml test solution is applied to the surface of the columns on weekly and monthly cycles: weekly apply test solution on Day 5, after heat lamp on phase; and in monthly apply test solution on Day 5 of Week 4 after heat lamp on phase.
- The solids can dry naturally.
- The washing and drying processes are repeated every week for over three months. At the end of the test period, a final washing process is conducted, and then the solid residue filtered and dried for analysis to complete the mass balance.

- Collect leachate on Day 1 (weekly cycle) of week 1 (monthly cycle) before heat lamp on phase. Record volume of leachate collected. Routine leachate analyses including pH, EC and record acidity.
- The collected leachate is filtered (<0.45µm) and preserved with acidified to pH<2 prior before is sent to the Chemistry Department of the University of the Western Cape for elemental analysis. pH and EC were measured using calibrated Metrohm Meters. Trace elements Si, Ca, Ce, Mg, Na, K, Pb, Nb, Y, Rb, Th, Cu, As, Zn, Mo, Co, Cr, Ni, Se, P, Cd, Li, Be, Zr, Ti, Sr and Fe were analysed by ICP-MS. The residues were sent to iThemba Laboratory for XRD mineralogical analysed.
- The residues from the leach column test are sent Scientific Services C.C in Cape Town to have geochemical analysis, elements include Ag, Al, As, Ca, Cd, Co, Cu, Fe, K, Mg, Mn, Mo, Na, Ni, Pb, S, U and Zn.
- The residues from the leach column test will be completed XRD mineralogical analysis.

4.8 Quality Assurance/Quality Control

Note that, individually, each test method has some limitations that affect its prediction reliability in acid-forming potential. In combination, these test methods result in better definition of acid-forming potential and highlight samples that require further investigation (Skousen et al., 2000).

CHAPTER FIVE

5. MINERALOGICAL CHARACTERISATION

5.1 Introduction

This chapter presents the mineralogical study of the tailing sample. In this chapter, XRD and SEM/EDS were approved to analyse the mineralogy of the selected tailing samples. As part of the analysis, the residue samples obtained from the leaching column test were also analysed as a comparison to the raw tailing samples. In addition, XRD analysed fifty-four tailing samples, while SEM/EDS analysed only eighteen tailing samples. Twenty-four residue samples obtained from the leaching column test were as well analysed by XRD to perform mineral phase change comparison.

5.2 Site Observations

According to the site study exercise discussed in the Chapter 3, three tailings were carefully observed within the study area. These three tailings, Mogale, Gold One_1 and Gold One_2, have been accumulating since 1950. The tailings contain sulphides during weathering and make them a major source of environmental contaminants in the area. Concise discussions on the site samples collected, observations of the samples collected and logging description of the samples collected from the three tailing dams are given in the subsections below.

5.2.1 Sample Description of Mogale Tailings

Previously in Chapter 3, a detailed description of Mogale tailings as one of the three tailings located within the study area were presented. In this subsection, comprehensive description of the samples collected at the Mogale tailings is presented in accordance with characterised analysis of the soil texture and wind limitations.

At Mogale tailings, five holes were drilled with the use of hand auger. And during the sample collection process, it was observed that the soil surface in the Mogale tailings is dry with loose fine sands. The eroded paths at the partially operated

tailings were detected due to the crushing effects of precipitation along the sides of the tailing dam. In this tailing area, wind is not heavy in the summer, evens so re-treatment operations are still dusty as well cause air pollution. Also, the initial deposit of the sampled tailing dams is a greyish colour. The tailings are finely grounded materials with large surface area that contains sulphides. In effect, sulphur compounds are smelt as tailings operation was ongoing.

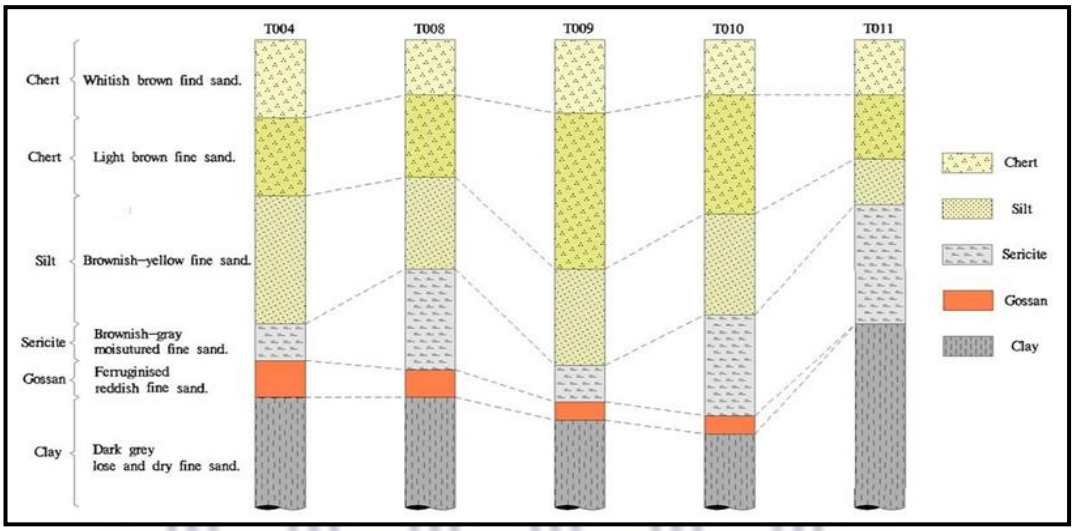

Figure 5.1: Mogale tailings downhole description

As displayed in the figure above, the surface of the tailings is a whitish brown fine-grained sand with a dry, loose material. As the augur goes deeper, its moisture content increases and becomes sticky fine-grained earth. The colour of the tailing material is altered by the different meters of depth. The deepest hole among the five holes is ten meters deep. According to the sample hole labels, as displayed in Figure 5.1, T004, T008 and T009 were drilled on surface in Mogale tailings from 7 – 8.3 meters deep. Tailings contents detected are ferruginous reddish colour, which are literally moisture sand. The sample hole labelled T010 was drilled from the south slope of the tailing dam by detecting ferruginous reddish sand from 8.2 – 8.6 meters deep. Similarly, sample hole T011 was drilled from east slope of the tailing dam but the ferruginous reddish colour layer not detected.

In addition to the above observations, the layers from the top to bottom demonstrate variation in sizes (Figure 5.1) of the sand types. In some cases, Gossan (ferruginised reddish fine sand) becomes smaller from one sample hole to another except in the

sample hole T011. But Clay (dark grey lose and dry fine sand) and Sericite (brownish-grey moisture fine sand) are deeper in size in T011. More so, Chert, with light brown fine sand, is deeper in size in both T009 and T010 than other three sample holes, while a similar sand type with whitish brown fine sand is almost equal in size across the five sample holes. The most varied among the sand types is Gossan, followed by Chert (light brown fine sand) and Sericite.

5.2.2 Sample Description of Gold One_1 Tailing

Gold One_1 is another tailing observed within the study area (Chapter 3), which is yet to be operated for re-treatment. The tailing includes two parts namely Rietfontein 162 and Randfontein 247. In the process of sample collection, some areas were difficult for drilling machines to access due to the height of the tailings (Chapter 4). Even so, two sample holes labelled T001 and T002 were drilled on the east surface of Rietfontein 162 and a sample hole labelled T003 was drilled from the east slope of tailing Rietfontein 162.

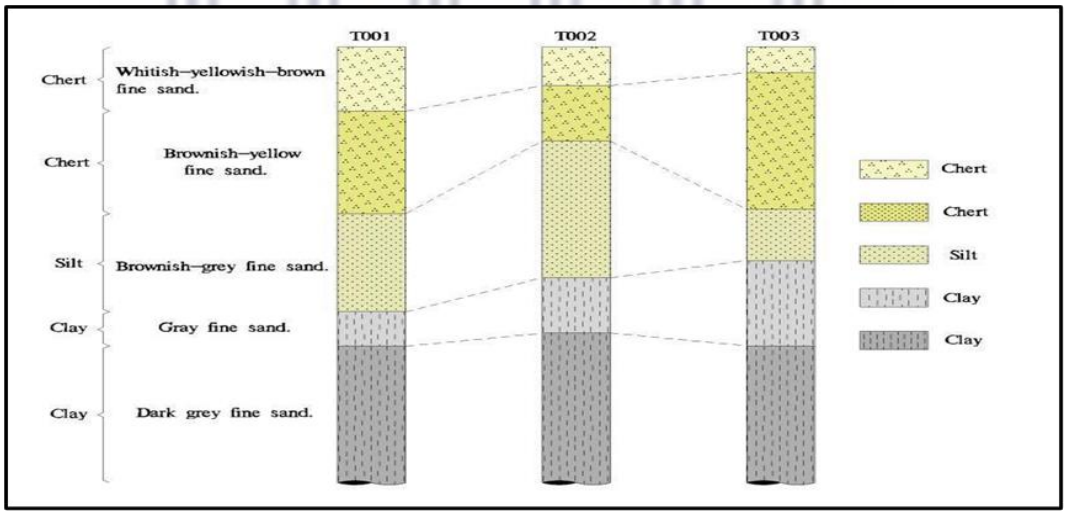

Figure 5.2: Gold_One 1tailing downhole description

Three holes were drilled by a drilling machine and reached a depth of 8-10 meters. The surface of the tailing is covered by whitish to yellowish loose fine sand. From the samples obtained, no ferruginous contents were observed. The tailings are finely grounded materials with large surface area, which contain sulphides.

From Figure 5.2, similar visual structure to Figure 5.1 is presented with observed variation in the five sand types sampled. Unlike in Figure 5.1, only three sample holes were sampled with the observation of two types of Chert and Clay, Silt expect Sericite and Gossan. Further observations show that Clay, with dark grey fine sand, was deeper in size in the three sample holes (T001, T002 and T003). In addition, Chert, a whitish–yellowish–brown fine sand, reduces in size as sampling approaches sample hole labelled T003 while Clay, with grey fine sand increases in size as sampling approaches sample hole labelled T003. Other sand types such as Chert (brownish–yellow fine sand) and Silt (brownish–grey fine sand) were not linearly increasing or reducing in size as sampling approaches sample labelled T003.

5.2.3 Sample Description of Gold One_2 Tailing

Gold One_2 tailing is the only fully operated tailing among the three observed tailings within the study area. During the sampling process, three holes were drilled as done in Gold One_1 tailing sampling, with the use of a drilling machine. Out of the three sample holes, only two of the sample holes was drilled up to two meters deep due to presence of hard rocks beneath the sands. The sample hole labelled T007 was only hole drilled up to a depth of 10 meters. The tailings samples collected are moisture greyish clay on its initial deposit, with no detection of ferruginous contents.

From Figure 5.3, three different types of Clay were detected as samples extracted from the three holes. Whitish–brownish fine sand and grey fine sand types of Clay sand are common to the three samples collected from the sample holes T005, T006 and T007, whereas a Clay sand with light brownish yellow was found in the sample hole labelled T006 and a Clay sand with brownish grey was found in the hole T007.

General deductions demonstrate that only Mogale tailings produced ferruginous sand, which contains iron (Fe) oxide (that is, a dark red colour sand layer). More so, it is observed that not every hole was dug to 10 meters depth before sand samples were collected, due to presence of rock beneath the sands.

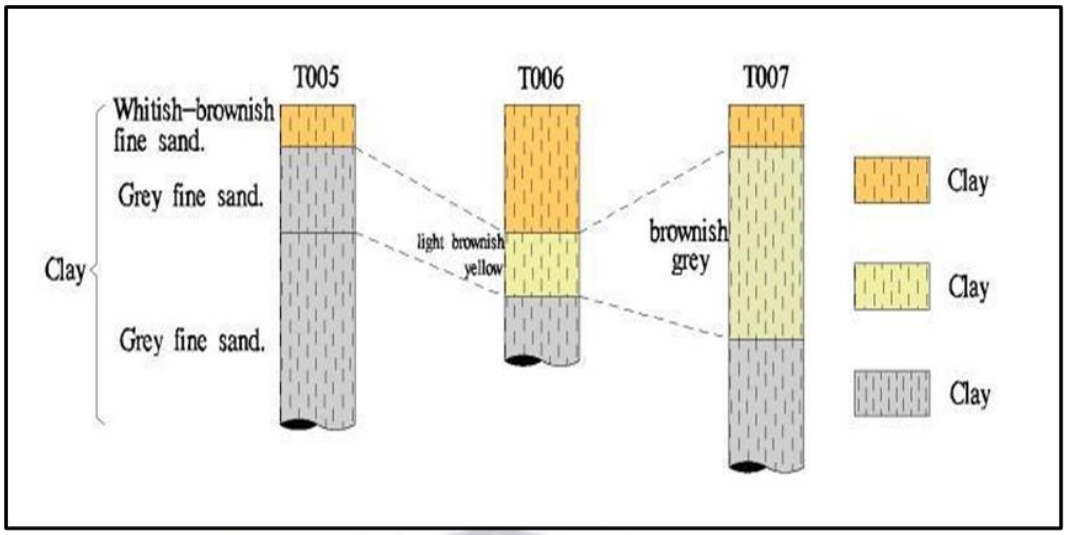

Figure 5.3: Gold One_2 tailing downhole description.

The size of each sand as dug out from the sample holes are either linear or nonlinear across the labelled samples. For instant, Clay sand is substantial in size across the three tailings than any other type of sand while Gossan sand is the smallest in size, which is found only in Mogale tailings.

5.3 Mineralogical Characteristics of the Tailings

The mineralogical characteristics of the three tailings were thoroughly evaluated to quantify the quantity (content) of the minerals in the tailing samples by using XRD test as well to determine the modes of existence of carbonate and sulphide minerals in the tailing samples, which includes their textures, grain size, morphology and mineral association through a deployment of SEM/EDS as precisely discussed in section 4.5.

The initiation of this process paved the way for the selection and preparation of the static and kinetic tests including the detailed interpretation of the results obtained through analysis. In the process, SEM produced a backscatter electron image, wherein an average atomic number of minerals determines the shade of grey. In that case, silicate minerals with a lower average number appear dark grey colour, while sulphide minerals with higher atomic numbers are lighter grey colour. Also, EDS measures the elemental composition of small areas of interest as well determine the mineral phases that are associated with different shades of grey in the SEM images.

On the other hand, XRD identifies and measures mineral phases from the peaks produced by scatter radiation in three-dimensional arrays of atoms exclusive to each mineral. The functionality of XRD is not limited to grain size only, but also used in distinguishing minerals such as pyrite and marcasite with similar composition but a different crystal structure. The XRD analysis of this study traditionally provided semi-quantitative data.

5.3.1 Tailing Samples SEM/EDS Analysis

In this subsection, the SEM/EDS analysis protocol is initiated to interpret the morphology of the samples evaluated. SEM/EDS analysis procedure was performed for 18 samples extracted from holes T004, T008, T009 and T010 in Mogale tailings including hole T003 in Gold One_1 tailing. The electron images and spectrum showed the constituent element and weight of percentage. Five samples collected from the hole T008 in Mogale tailings and four samples collected from the hole T003 in Gold One_1 tailing will be discussed based on the material morphology and element contents by using electron images and spectrum distribution. The electron images obtained display clear images closed to the sample surface as SEM/EDS used low acceleration voltage of 5kv and were consecutively captured on the same day.

5.3.1.1 Mogale Tailings Samples

The diagrams present in Figure 5.4, Figure 5.5, Figure 5.6 and Figure 5.7 represent the electron images of the sample 005 of the top layer of the sand sample collected from hole T008. The depth of SEM applied is 1 µm, 10 µm, 100 µm and 200 µm. The material morphology derived shows irregular shape and some of the iron cubic are less distributed.

In addition, SED/EDS analysis continues with further clarification on the sand sample layers as represented in Figure 5.8, Figure 5.9, Figure 5.10 and Figure 5.11. Just as executed in Figure 5.4, Figure 5.5, Figure 5.6 and Figure 5.7, electron images of the sample 007 of a deep length of 6 – 7 meters layer sample collected from hole T008 were evaluated.

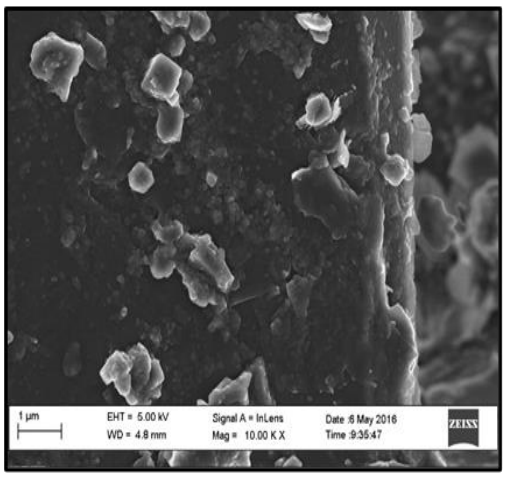

Figure 5.4: Sample 005 electron image under 1 µm

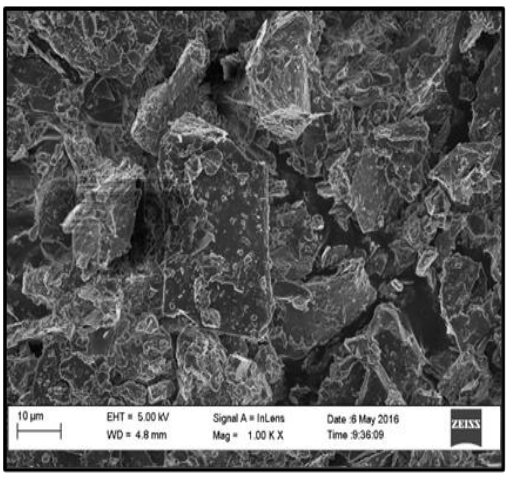

Figure 5.5: Sample 005 electron image under 10 µm

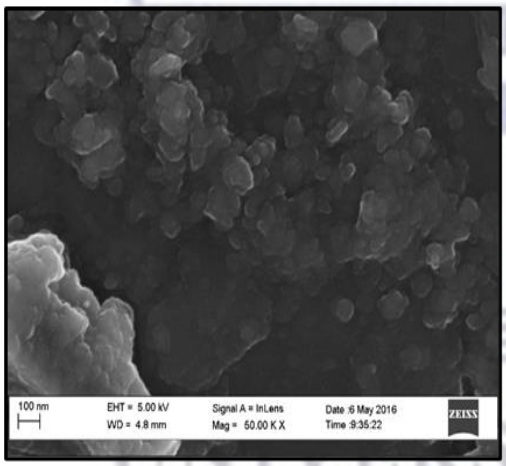

Figure 5.6: Sample 005 electron image under 100 µm

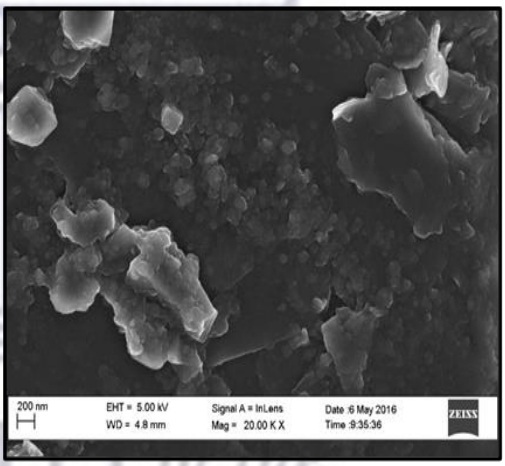

Figure 5.7: Sample 005 electron image under 200 µm

The morphological information obtained indicates that the material has irregular shape as demonstrated in sample 005 and aluminium (Al) is detected. In effect, iron cubic could not acquire the information from the images due to a low weight of percentage. Then, zinc (Zn) element was detected in the layer at a low quantity.

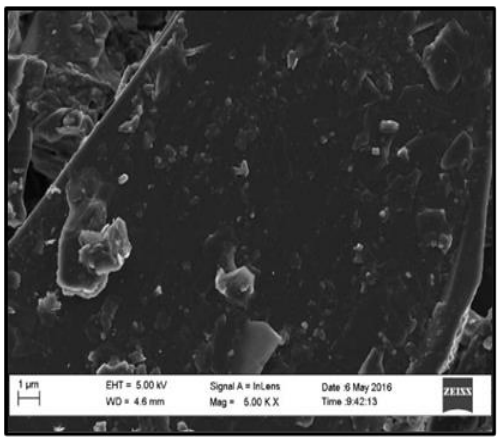

Figure 5.8: Sample 007 electron image under 1 µm

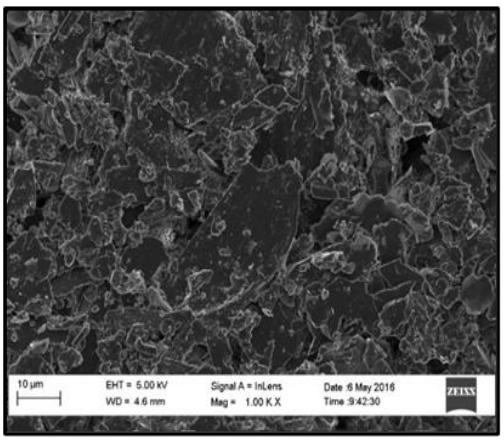

Figure 5.9: Sample 007 electron image under 10 µm

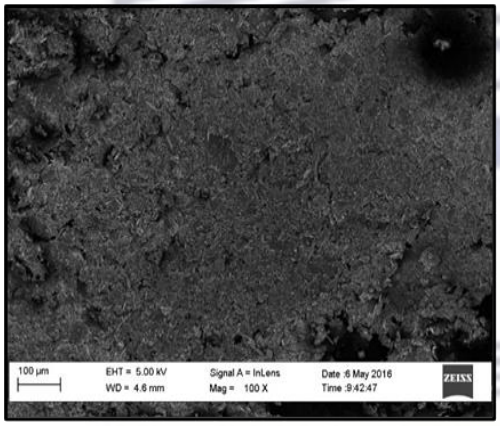

Figure 5.10: Sample 007 electron image under 100 µm

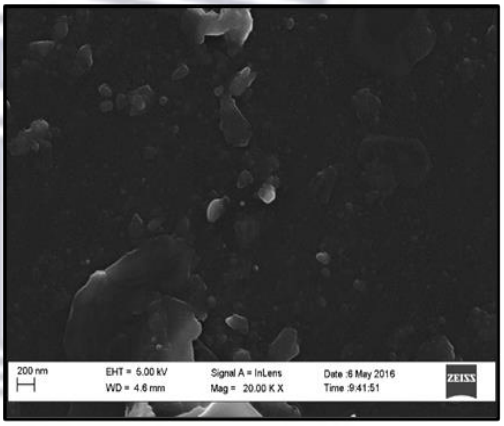

Figure 5.11: Sample 007 electron image under 200 µm

The next SEM/EDS evaluation process was executed to attain the right information about the electron images under the depth of 1 µm, 10 µm, 100 µm and 200 µm, and the morphological details of the material as displayed in Figure 5.12, Figure 5.13, Figure 5.14 and Figure 5.15. The diagrams display the electron images of the sample 007–1, a 7.4-meter layer sand sample extracted from the hole T008. Following the observation deduced, the morphological information shows a regular shape material and the iron cubic is well distributed. The iron (Fe) element detected in the material is high and rich at 18.04 wt%, with high aluminium (Al) content.

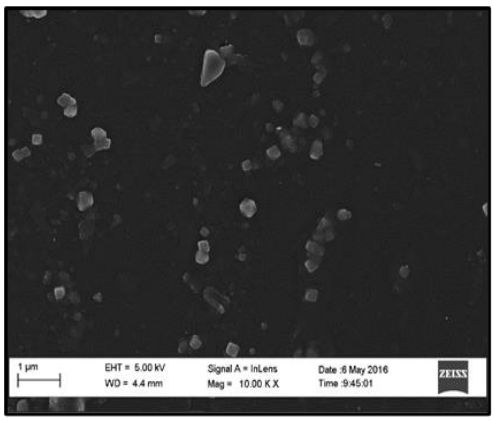

Figure 5.12: Sample 007–1 electron image under 1 µm

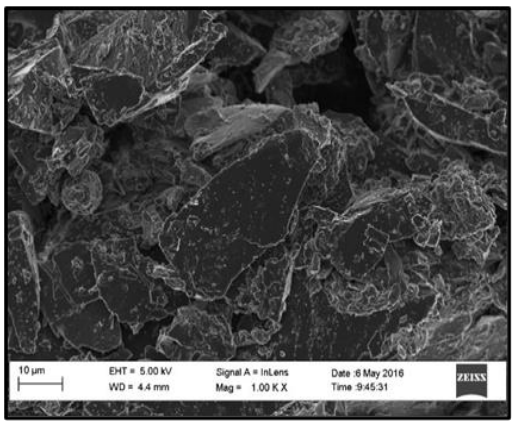

Figure 5.13: Sample 007–1 electron image under 10 µm

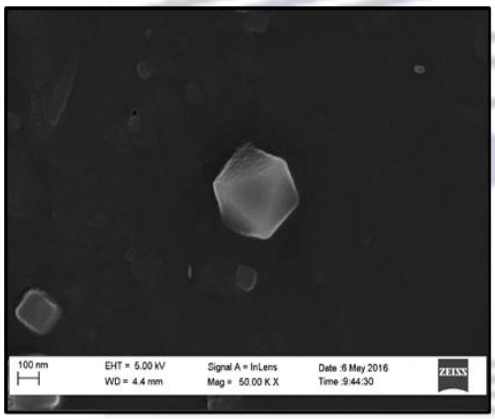

Figure 5.14: Sample 007–1 electron image under 100 µm

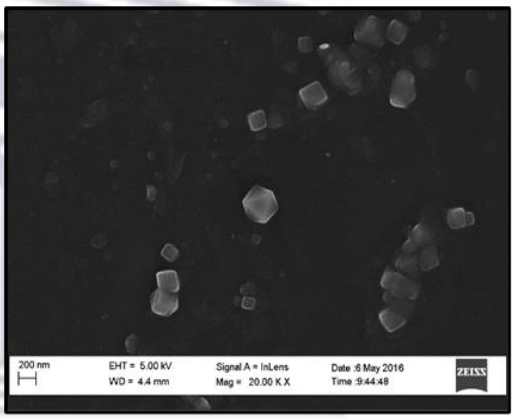

Figure 5.15: Sample 007–1 electron image under 200 µm

The electron images of sample 008–1, an 8.0-meter layer sample extracted from hole T008 are displayed in Figure 5.16, Figure 5.17, Figure 5.18 and Figure 5.19. According to the morphological report deduced, the material has irregular shape, but the iron cubic is well distributed. As a result, titanium (Ti) element was detected in the layer at a low quantity.

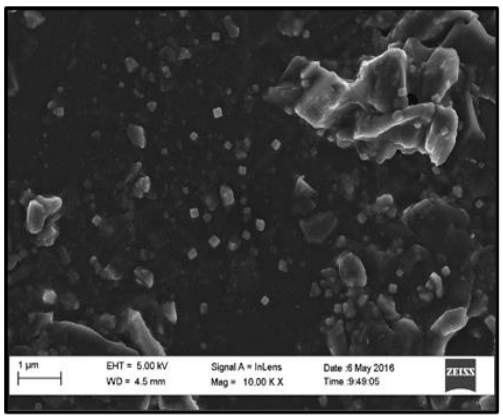

Figure 5.16: Sample 008–1 electron image under 1 µm

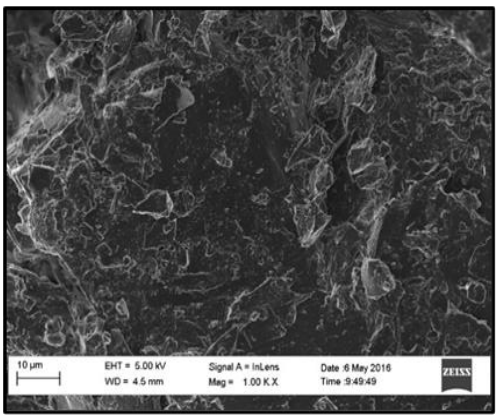

Figure 5.17: Sample 008–1 electron image under 10 µm

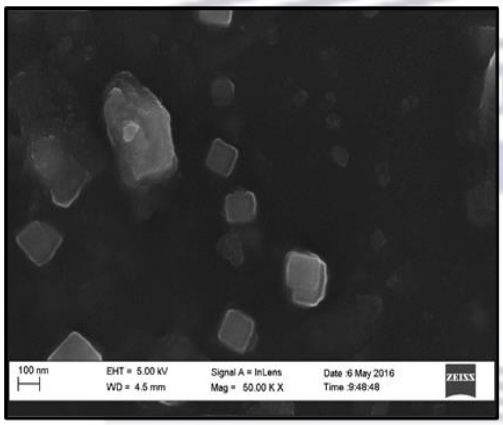

Figure 5.18: Sample 008–1 electron image under 100 µm

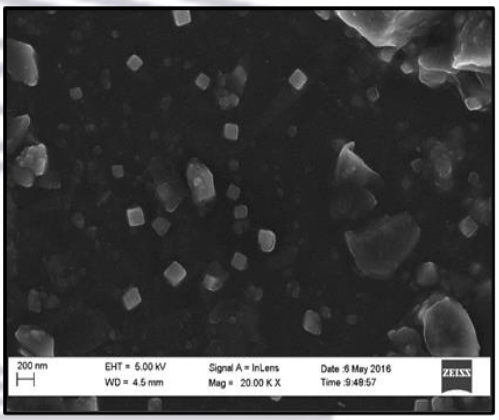

Figure 5.19: Sample 008–1 electron image under 200 µm

Figure 5.20, Figure 5.21, Figure 5.22 and Figure 5.23 show the electron images of sample 008–2, a 9.0-meter layer sample extracted from hole T008. The morphological information obtained shows that the material has irregular shape and unevenly distributed. Calcium (Ca) was detected in the layer, including other metal elements with low weight of percentage.

The overview of SEM/EDS analysis of all the samples extracted from hole T008 demonstrate that some samples such as samples 005, 007, 008–1 and 008–2 have irregular shape material, wherein the iron cubic is either less distributed or well distributed. But, in sample 007, the iron cubic was neither less distributed nor well distributed due to a low weight of percentage and sample 008–2 demonstrated an

unevenly distributed iron cubic. Only sample 007–1 exhibited regular shape material and the iron cubic was well distributed.

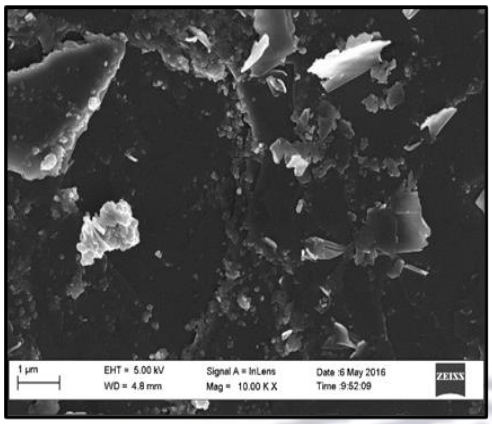

Figure 5.20: Sample 008–2 electron image under 1 µm

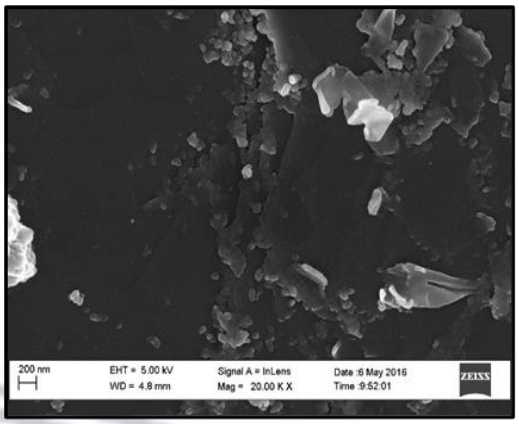

Figure 5.21: Sample 008–2 electron image under 10 µm

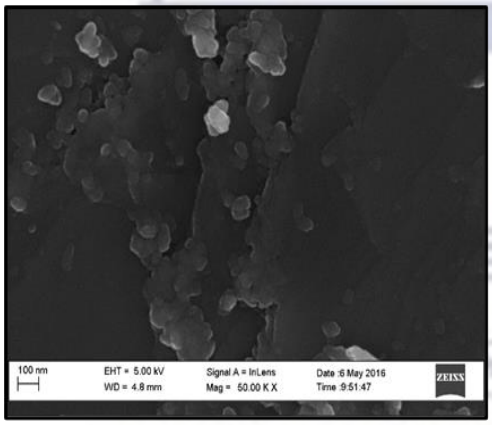

Figure 5.22: Sample 008–2 electron image under 100 µm

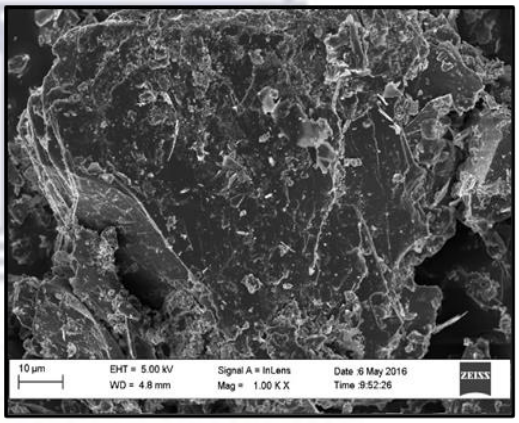

Figure 5.23: Sample 008–2 electron image under 200 µm

The electron images for each sample deduced that some metal element contents were detected in some samples in high or low quantity such as zinc (Zn) element detected in sample 007 at a low quantity, iron (Fe) and aluminium (Al) elements detected in sample 007–1 in high quantities, titanium (Ti) element detected in sample 008–1 at a low quantity and calcium (Ca) element with other metal elements were detected in the sample 008–2.

Spectrographic illustration of samples 005, 007, 007–1, 008–1 and 008–2 is sequentially presented in Figure 5.24, Figure 5.25, Figure 5.26, Figure 5.27 and

Figure 5.28 to validate the assessment performed with the use of the SEM/EDS. The spectrum demonstrates the weight of percentage and the distribution of elements detected in the samples spectrographically analysed. In this illustration, silicon (Si), aluminium (Al), iron (Fe) and sulphur (S) are major elements detected. And some elements as titanium (Ti), zinc (Zn), calcium (Ca) and sodium (Na) are found at a certain depth layer of the hole. In addition, the manganese (Mn) element was found within a depth range of 7 – 8 meters deep, whereas rich iron (Fe) and calcium (Ca) were found at 7 meters and 8 meters deep in the hole T008, respectively. Only sodium (Na) element was found at the top layer of the hole.

In sample 005 spectrum below (Figure 5.24), only nine elements were detected in the layers of the hole. Among the nine elements, only titanium (Ti) and iron (Fe) were metallic elements detected in low quantities in the various parts of the layers. Some other metallic elements detected are aluminium (Al), sodium (Na) and potassium (K), while silicon (Si), oxygen (O), carbon (C) and sulphur (S) elements are four non-metallic elements detected in high quantities in the sample more than any other elements.

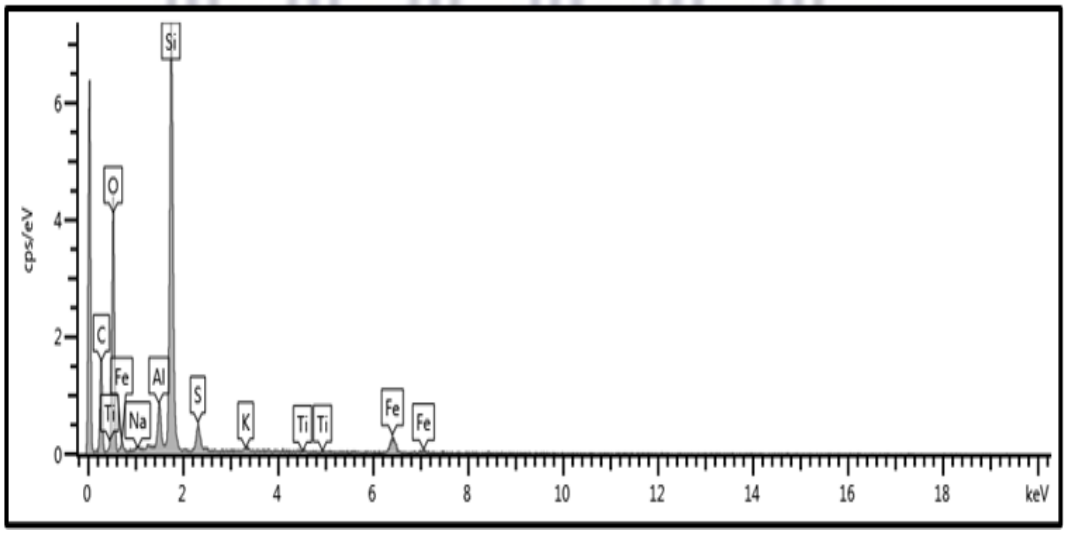

Figure 5.24: Sample 005 spectrum

Unlike sample 005 spectrum, 10 elements were detected from the sample 007 spectrum. As displayed in Figure 5.25, only three metallic elements are detected in the layers of the sample spectrographically analysed. These elements are manganese (Mn), iron (Fe) and zinc (Zn), which occurred in low quantities in the various parts

of the layers. In addition, presence of magnesium (Mg) is detected in the sample, along with aluminium (Al), which was detected in a high quantity unlike other metallic elements. In the sample, non-metallic elements like silicon (Si), oxygen (O) carbon (C) and sulphur (S) remain regular in the sample in high quantities.

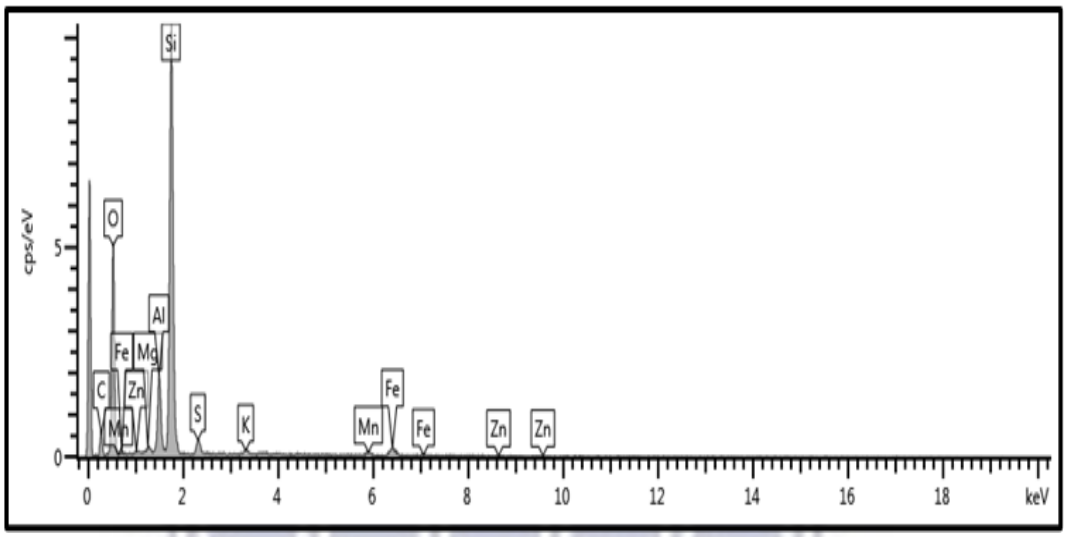

Figure 5.25: Sample 007 spectrum

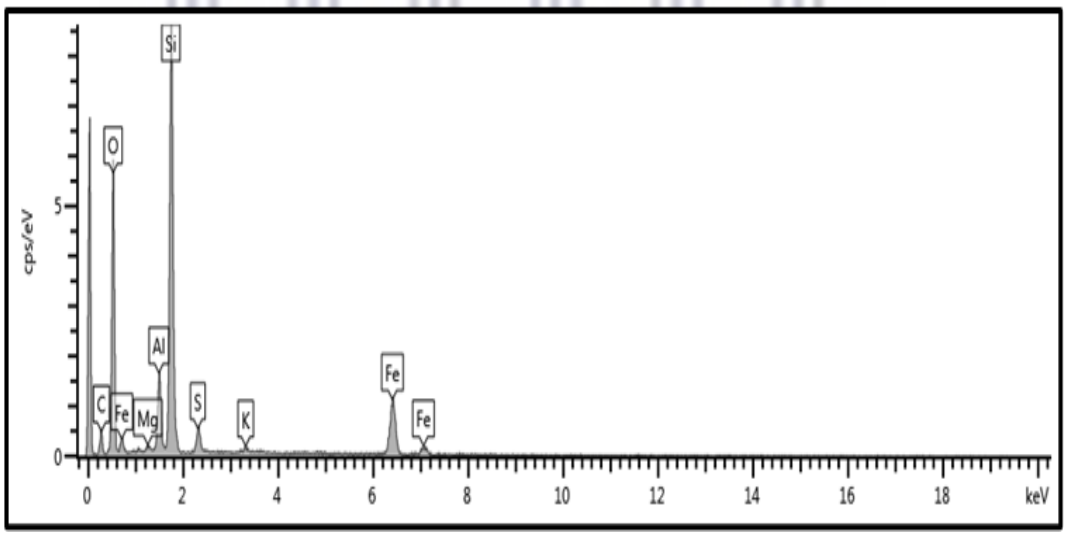

Figure 5.26: Sample 007–1 spectrum

In the sample 007–1 spectrum, as displayed in Figure 5.26, fewer number of elements (eight elements) were detected, which are the combination of metallic and non-metallic elements. Among the metallic elements detected, only iron (Fe) was detected in the various parts of the layers of the sample at a well distributed quantity.

And aluminium (Al), another metallic element was detected in a high quantity. On the other hand, non-metallic elements like carbon (C), oxygen (O), sulphur (S) and silicon (Si) continue to have regular occurrence in high quantities in the sample.

Spectrographic analysis of sample 008–1 spectrum, as presented in Figure 5.27, demonstrates that nine elements were detected. And only two metallic elements were detected in the various parts of the layers, which are titanium (Ti), in a low quantity and iron (Fe), at a well distributed quantity. This observation is similar to the spectrographic analysis performed for sample 005 spectrum in Figure 5.24, but the only newly detected element is magnesium (Mg) in a low quantity. Also, only aluminium (Al) among the metallic elements demonstrated a high quantity, while the four non-metallic elements are regular in the sample in high quantities. But only carbon (C), among the non-metallic elements, was detected in a low quantity.

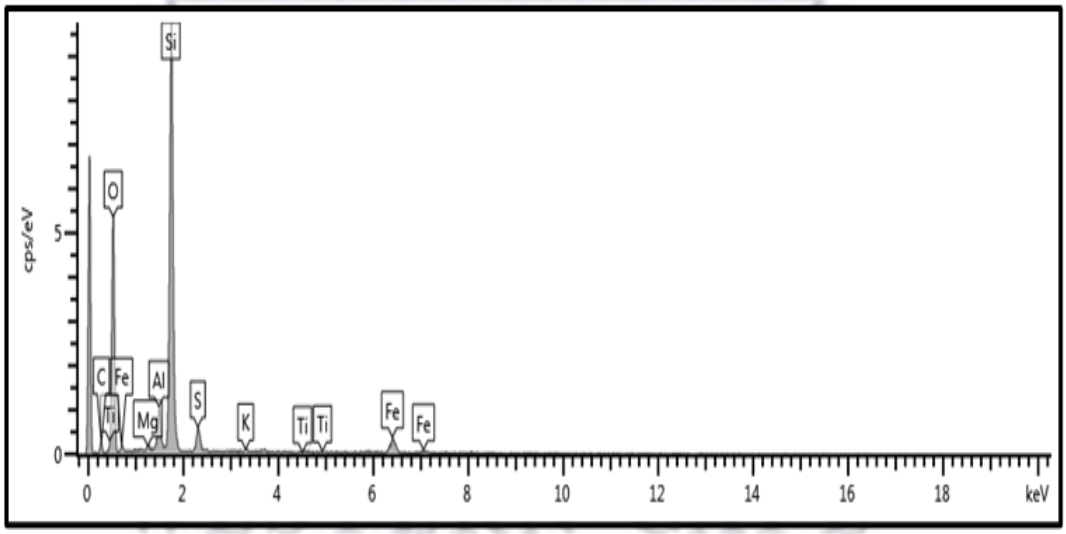

Figure 5.27: Sample 008–1 spectrum

The last of the sample spectrum analysed is presented below in Figure 5.28. Sample 008–2 spectrum produced 10 elements, which includes seven metallic elements and three non-metallic elements. Out of seven metallic elements detected in the sample, only manganese (Mn), calcium (Ca) and iron (Fe) were detected in low quantities in the various parts of the layers, while aluminium was detected in a high quantity more than other metallic elements. Non-metallic elements such as oxygen (O) and silicon (Si) are observed in high quantities in the layers more than carbon (C) and sulphur (S).

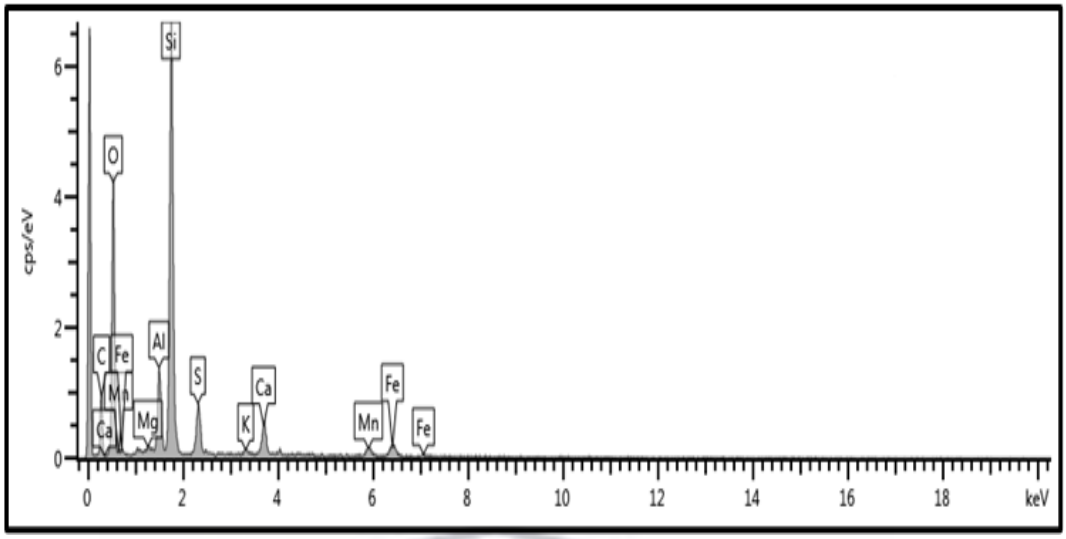

Figure 5.28: Sample 008–2 spectrum

From an overview understanding of the spectrographic analysis of the samples 005, 007, 007–1, 008–1 and 008–2 collected from the hole of T008, it is understood that non-metallic and metallic elements were detected in all the samples. Non-metallic elements like carbon (C), oxygen (O), sulphur (S) and silicon (S) were detected in all the samples at various quotients. Similarly, metallic elements like iron (Fe), aluminium (Al) and potassium (K) were detected in all the samples at various quotients, while other metallic elements such as titanium (Ti), sodium (Na), Manganese (Mn), Magnesium (Mg), zinc (Zn) and calcium (Ca) were detected in various quotients, but not in all the samples. Accordingly, aluminium (Al) was detected in a high quantity in four samples except in sample 005. And other metallic elements like titanium (Ti), zinc (Zn), manganese (Mn), magnesium (Mg) and calcium (Ca) were either detected in high or low content in some samples.

Other samples 020, 021, 021–1, 025 and 027–1 collected from the hole T010 drilled in Mogale tailings alongside holes T004, T008, T009 and T011. In comparison with samples collected from hole T008, the metallic elements detected in the layers of the samples collected from the hole T010 are small in content (quantity) such as copper (Cu), titanium (Ti) and arsenic (As). Regardless, silicon (Si), aluminium (Al) and iron (Fe) remain major constituents of the tailings. Among the five samples spectrographically analysed sample 027–1 demonstrated a high content of iron from the 7-8 meters hole drilled in the tailings.

5.3.1.2 Gold One_1Tailings Samples

The SEM/EDS analysis of the tailing samples collected from the hole T003 drilled in Gold One_1 tailing is presented in this subsection. Samples analysed on SEM/EDS are labelled 068, 069, 073 and 076. Analysis results indicate that the elements are fine structure with smaller particle size than the particle size of the elements analysed in the Mogale tailing.

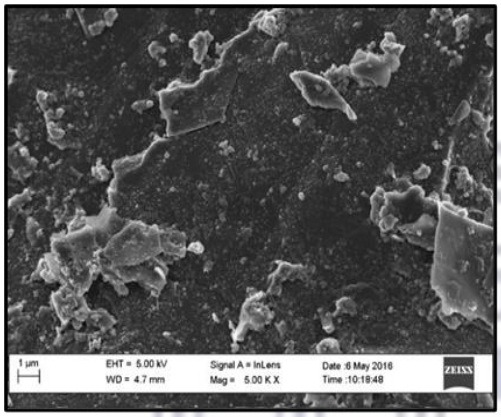

Figure 5.29: Sample 068 electron image under 1 µm

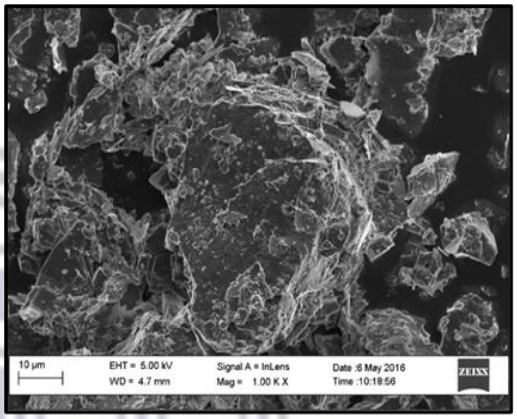

Figure 5.30: Sample 068 electron image under 10 µm

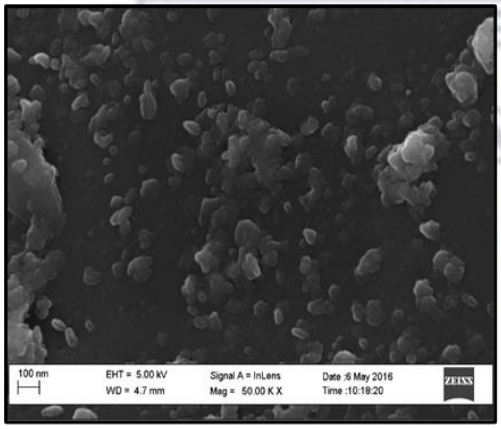

Figure 5.31: Sample 068 electron image under 100 µm

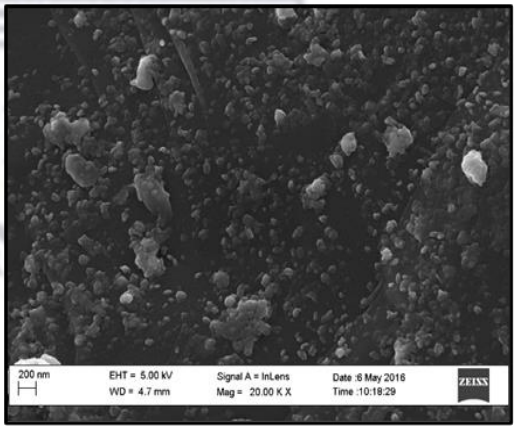

Figure 5.32: Sample 068 electron image under 200 µm

The electron images of the sample 068 examined under the SEM depth of 1 µm, 10 µm, 100 µm and 200 µm are showed in Figure 5.29, Figure 5.30, Figure 5.31 and Figure 5.32. Sample 068, the surface of the tailings, is highly rich in silicon (Si) and aluminium (Al). Also, other elements as sodium (Na), potassium (K) and calcium

(Ca) are detected in the sample, whereas iron (Fe) and cadmium (Cd) are detected in the top layers of the samples in small quantities. More so, sulphur (S) is detected in a high quantity than silicon in the top drilled layer of the hole.

In Figure 5.33, Figure 5.34, Figure 5.35 and Figure 5.36, the electron images of the sample 069 under 1 µm, 10 µm, 100 µm and 200 µm indicate that material morphology of the sample is irregular shape, with small size particles wildly distributed. And sulphur (S) is a principal element in this particular layer of the hole.

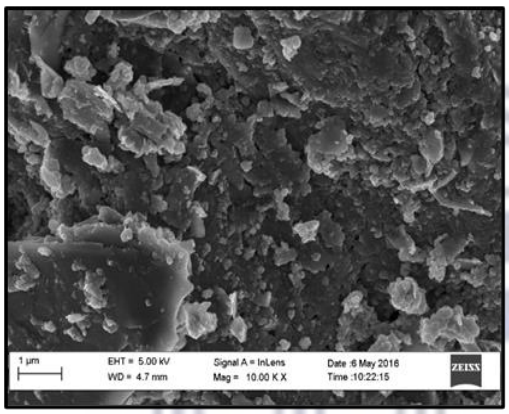

Figure 5.33: Sample 069 electron image under 1 µm

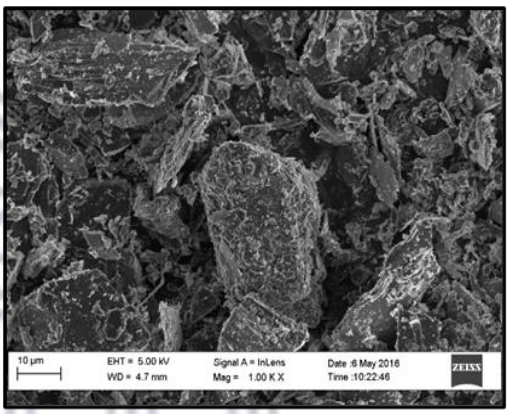

Figure 5.34: Sample 069 electron image under 10 µm

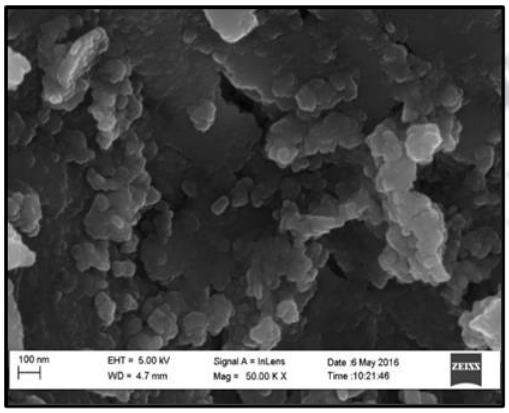

Figure 5.35: Sample 069 electron image under 100 µm

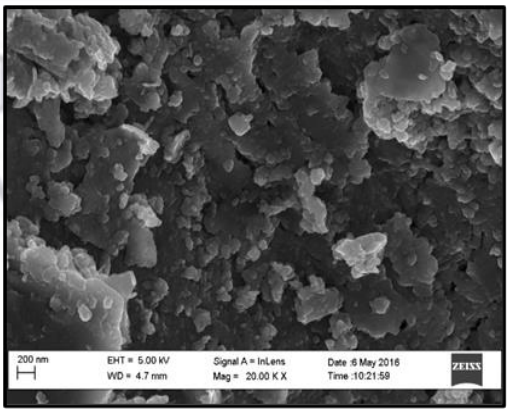

Figure 5.36: Sample 069 electron image under 200 µm

This is a morphological report of sample 073 examined under 1 µm, 10 µm, 100 µm and 200 µm as displayed in Figure 5.37, Figure 5.38, Figure 5.39 and Figure 5.40. Observation indicates that the material morphology is irregular shape, with no

iron (Fe) element. Silicon (Si) and aluminium (Al) are observed as the principal elements in high quantities.

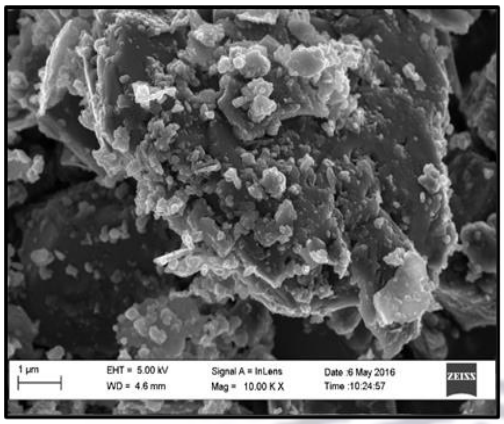

Figure 5.37: Sample 073 electron image under 1 µm

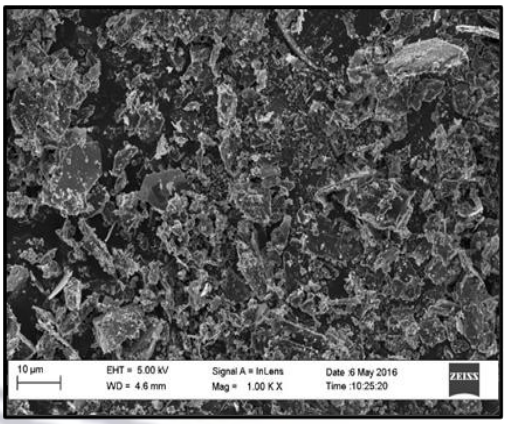

Figure 5.38: Sample 073 electron image under 10 µm

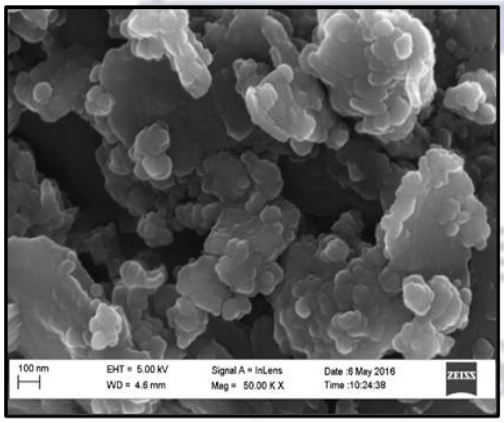

Figure 5.39: Sample 073 electron image under 100 µm

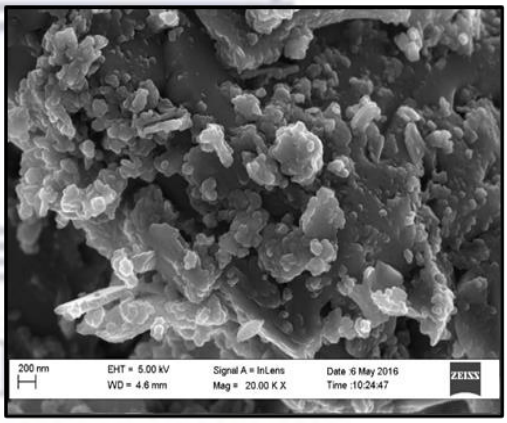

Figure 5.40: Sample 073 electron image under 200 µm

The electron images of the sample 076, as displayed in Figure 5.41, Figure 5.42, Figure 5.43 and Figure 5.44, indicate that material morphology is irregular shape. Other observations demonstrate that silicon (Si) is a highly predominant element in the sample, and aluminium (Al) is poorly distributed in the sample as well as other metallic cubic.

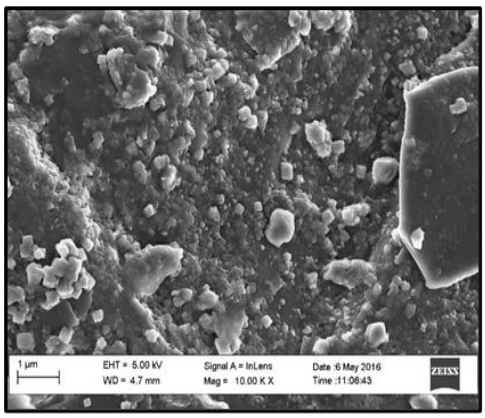

Figure 5.41: Sample 076 electron image under 1 µm

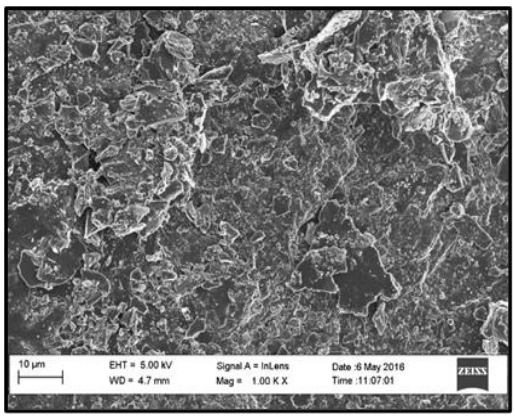

Figure 5.42: Sample 076 electron image under 10 µm

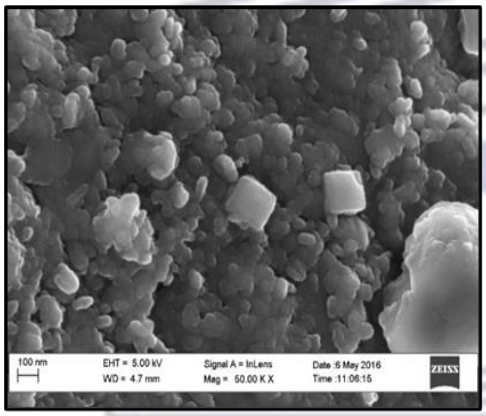

Figure 5.43: Sample 076 electron image under 100 µm

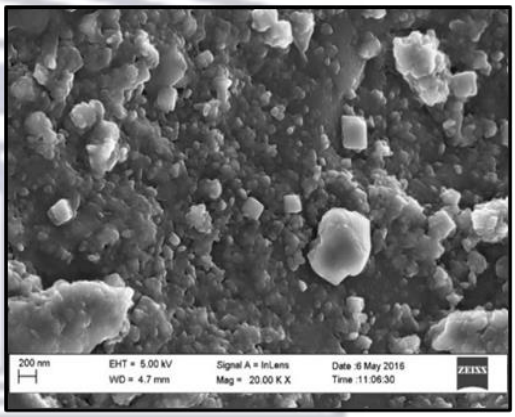

Figure 5.44: Sample 076 electron image under 200 µm

General deductions obtained show that samples 068, 069, 073 and 076 material morphologies reveal irregular shapes. Although, aluminium (Al) and silicon (Si) are considered as principal elements in high quantities in samples 068 and 073, but only aluminium out of the two elements that is poorly distributed in sample 076. Other metallic elements as sodium (Na), potassium (K) and calcium (Ca) are detected in sample 068, including iron (Fe) and cadmium (Cd) in small quantities. And sulphur (S), a non-metallic element, is detected in a high quantity in samples 068 and 069. The aforesaid deductions are validated with the use SEM/EDS to ascertain other elements distributed in the samples in high or low quantities.

The spectrum assessment process is initiated to further ascertain the distribution or quantities of other elements in the samples previously examined by the electron

images. Accordingly, Figure 5.45, Figure 5.46, Figure 5.47 and Figure 5.48 spectrographically illustrate the spectrum of the samples 068, 069, 073 and 076 to demonstrate distribution of different elements and the weight of percentage for each sample.

In Figure 5.45, spectrographic analysis of sample 068 demonstrates that only aluminium (Al) and potassium (K) among the metallic elements have high quantities. However, other metallic elements as iron (Fe), titanium (Ti) and calcium (Ca) are well distributed in the sample in low quantities. Non-metallic elements detected are concentrated in certain quantities in the sample 068. Only oxygen (O) and silicon (Si) are detected in high quantities. And a rare occurrence of metallic element like cadmium (Cd) in the sample.

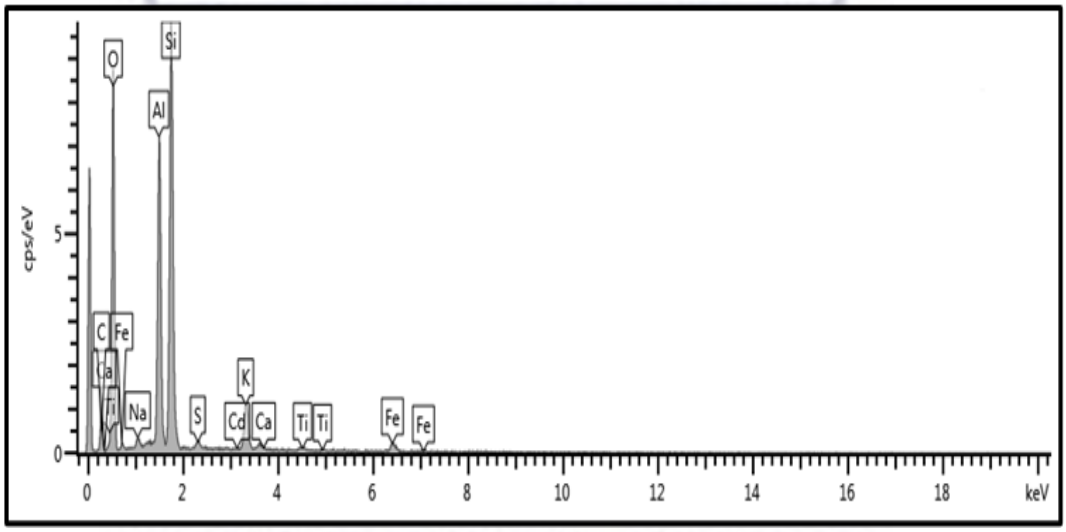

Figure 5.45: Sample 068 spectrum

The spectrographic display of elements detected in sample 069 (Figure 5.46) is similar to the results obtained in sample 068. The only difference is that new elements are detected, such elements as arsenic (As) and magnesium (Mg). According to the graph below, metallic elements like iron (Fe), calcium (Ca) and arsenic (As) are well distributed in the sample in low quantities.

Other metallic elements as sodium (Na), magnesium (Mg) and potassium (K) are concentrated within the sample in low quantities, only aluminium (Al) is highly concentrated in quantity. The regular four non-metallic elements are detected at a

concentrated level, wherein silicon (Si) and oxygen (O) are more concentrated than carbon (C) and sulphur (S) in the sample.

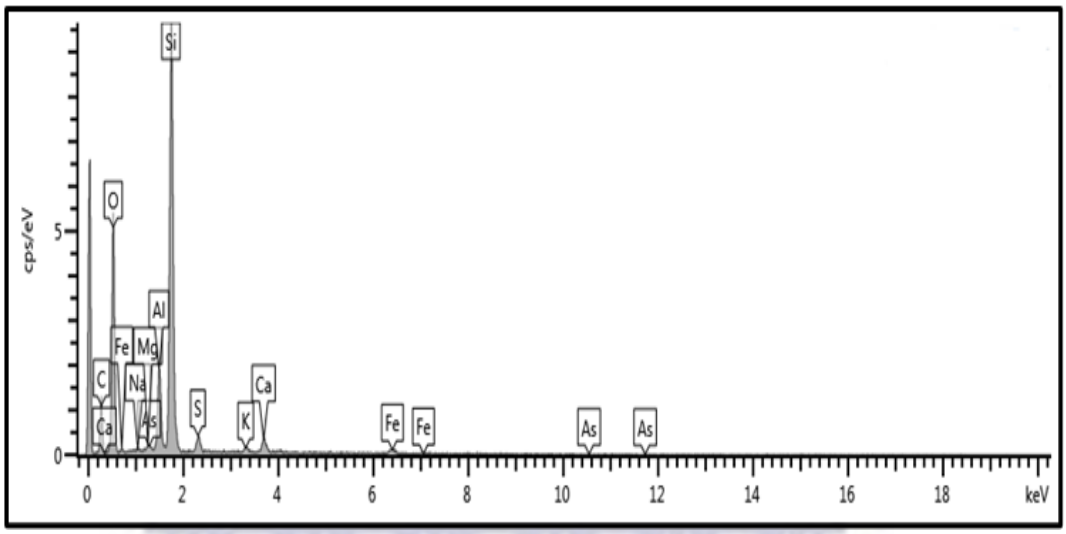

Figure 5.46: Sample 069 spectrum

In Figure 5.47, metallic elements as aluminium (Al) demonstrates high concentrated quantity, and others such as calcium (Ca) and iron (Fe) are well distributed in low quantities in the sample 073. But potassium (K) and magnesium (Mg) are concentrated in low quantities. Non-metallic as carbon (C), oxygen (O) and silicon (Si) are highly concentrated in the sample.

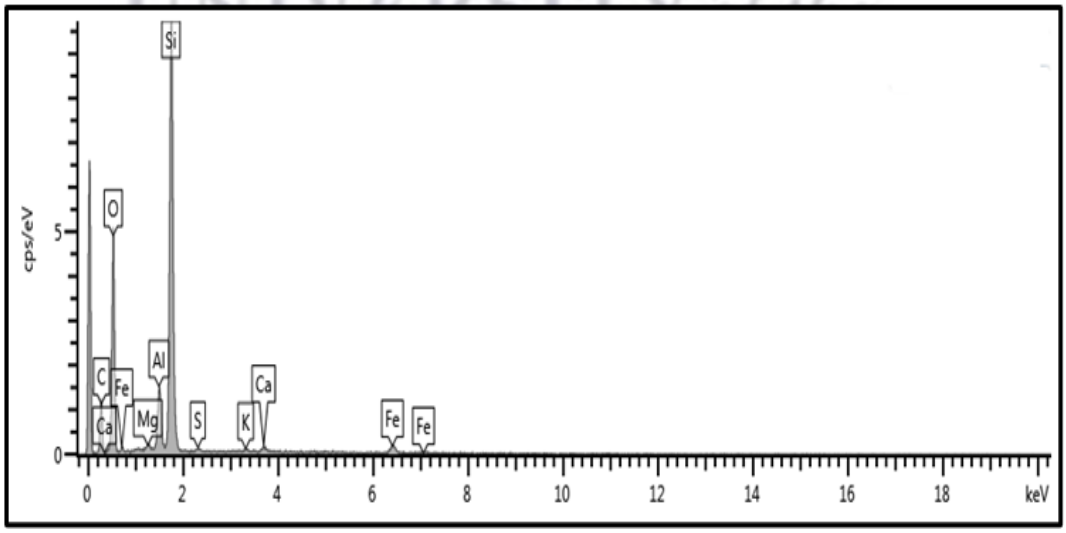

Figure 5.47: Sample 073 spectrum

Sample 076 low quantity distributions of metallic elements like calcium (Ca) and iron (Fe) are spectrographically presented in Figure 5.48, and aluminium (Al) is highly concentrated in the sample, but cadmium (Cd) and magnesium (Mg) are poorly concentrated in the sample. In addition, silicon (Si) and oxygen (O) are concentrated in high quantities more than carbon (C) and sulphur (S) in the sample.

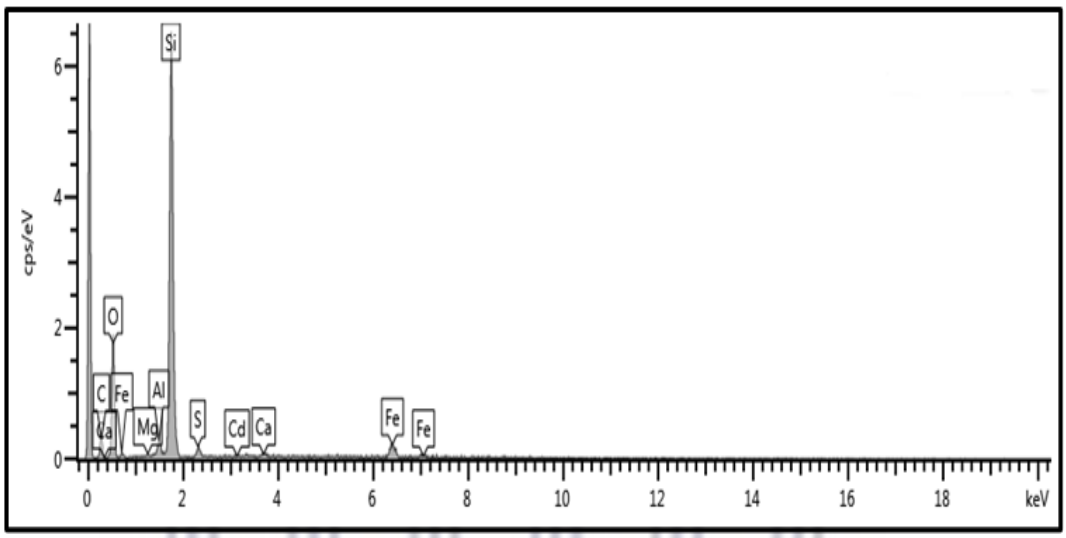

Figure 5.48: Sample 076 spectrum

The overview of the spectrographic evaluation validates the results obtained in the analysis of the electron images of each sample. Elements such as aluminium (Al), oxygen (O) and silicon (Si) are highly concentrated in all the samples (068, 069, 073 and 076) more than carbon (C) and sulphur (S). Iron (Fe) and calcium (Ca) are well distributed throughout the samples in low quantities, including titanium (Ti) and arsenic (As) which are irregular. Other metallic elements such as sodium (Na), magnesium (Mg), cadmium (Cd) and potassium (K) are in low concentrated quantities in some of the samples.

The three tables given below contain the tabularised summary of the constituent elements detected in the samples collected from the Mogale and Gold One_1 tailing holes evaluated. Across the three tables, elements such as oxygen (O), aluminium (Al), silicon (Si), sulphur (S) and potassium (K) are found in all samples evaluated.

Table 5.1: Summary of the constituent elements of Mogale tailing hole T008 samples

Sample	Element												Total
	O	Na	Al	Si	S	K	Ca	Ti	Fe	Mg	Mn	Zn	
005	51.95	0.35	3.55	34.24	3.02	0.38	-	0.24	6.27	-	-	-	**100**
007	48.6	-	6.28	37.05	1.97	0.62	-	-	3.32	0.44	1.37	0.35	**100**
007–1	44.57	-	5.24	29.1	2.21	0.45	-	-	18.04	0.38	-	-	**99.99**
008–1	51.68	-	3.29	35.03	2.95	0.3	-	0.16	6.09	0.5	-	-	**100**
008–2	51.46	-	5.28	28.05	4.4	0.48	3.84	-	3.64	0.27	2.58	-	**100**

Table 5.2: Summary of the constituent elements of Mogale tailing hole T010 samples

Sample	Element														Total
	O	Na	Al	Si	S	K	Ca	Ti	Fe	Mg	Cu	Ni	Zn	As	
020	52.31		9.74	33.76	0.56	0.74	-	0.25	1.94	-	-	0.21	0.5	-	**100.01**
021	52.07	0.25	5.5	37.49	0.56	0.42	-	0.65	2.39	-	0.44	-	-	0.23	**100**
021–1	53.22	0.75	5.7	36.35	0.9	0.86	-	-	1.5	-	0.58	-	-	-	**99.86**
025	52.46	0.23	8.28	34.78	1.23	0.38	-	0.41	1.62	0.21	0.4	-	-	-	**100**
027–1	48.63	0.37	6.4	32.11	2.64	0.68	0.26	-	8.47	0.45	-	-	-	-	**100.01**

Table 5.3: Summary of the constituent of Gold One _1 tailing hole T003 samples

Sample	Element										Total
	O	Na	Al	Si	S	K	Ca	Ti	Fe	Cd	
068	52.04	0.72	15.3	24.17	0.5	4.19	0.15	0.44	2.07	0.41	**100**
069	52.33	0.26	0.3	6.21	34.07	1.87	0.7	2.03	1.9	0.31	**99.98**
073	51.09	0.48	5.27	38.2	0.39	0.38	0.81	3.38	-	-	**100**
076	41.79	0.19	1.49	45.22	1.78	0.74	8.22	0.57	-	-	**100**

Some elements are highly or poorly concentrated, while others are highly or poorly distributed in accordance with the values presented. The total weight of percentage derived from elements concentration or distribution sum in sample 007–1 (Table 5.1), 021–1 (Table 5.2) and 069 (Table 5.3) are slightly lowered compared to the total weight of percentage derived in other samples. Samples collected from the Gold One_1 tailing has more titanium (Ti), while samples collected from Mogale tailing has more iron (Fe).

In Mogale tailing, examination of samples collected from hole T008 yielded more elements than samples collected from hole T010. Observation indicates that manganese (Mn) is detected in samples 005, 007–1 and 008–1 in Table 5.1. Equally, in Table 5.2, nickel (Ni) is detected only in sample 020, arsenic (As) is detected only in sample 021 and copper (Cu) is detected in three samples in T010. Also, in Table 5.3, cadmium (Cd) is detected only in samples 068 and 069, which collected from the surface of the Gold One _1 tailing.

5.3.2 Tailings Samples XRD Analysis

XRD analysis is performed semi-quantitatively in this subsection to determine the amount and phases of minerals present in the 52 samples collected from the holes T004, T008, T009, T010 and T011 drilled in Mogale tailings and holes T001, T002 and T003 of Gold One_1 tailing. According to the results deduced, it is observed that quartz is dominantly present, followed by other primary and secondary minerals. The results are discussed in the subsequent subsections.

5.3.2.1 Mogale Tailings Samples

The primary and secondary minerals detected in Mogale tailings based on the samples analysed are summarised in the Table 5.4 as sectionally presented in the Figure 5.49 below. The graph presents the spectrographic display of the XRD analysis of the minerals in the sample 005 according to their position and amount of detection in Mogale tailings. As illustrated in the table and the graph, it is observed that quartz (SiO_2) is well distributed in large quantity in the sample 005, followed by pyrophyllite ($Al_2Si_4O_{10}(OH)_2$) and pyrite (FeS_2). And other minerals are distributed in smaller quantities in the sample. However, the distribution shape

of the smaller minerals varies in sizes throughout all the samples. For instance, in Mogale tailing, some minerals depleted in size, and increased in size in some samples; such instance occurred particularly in gypsum ($CaSO_4 \cdot 2H_2O$).

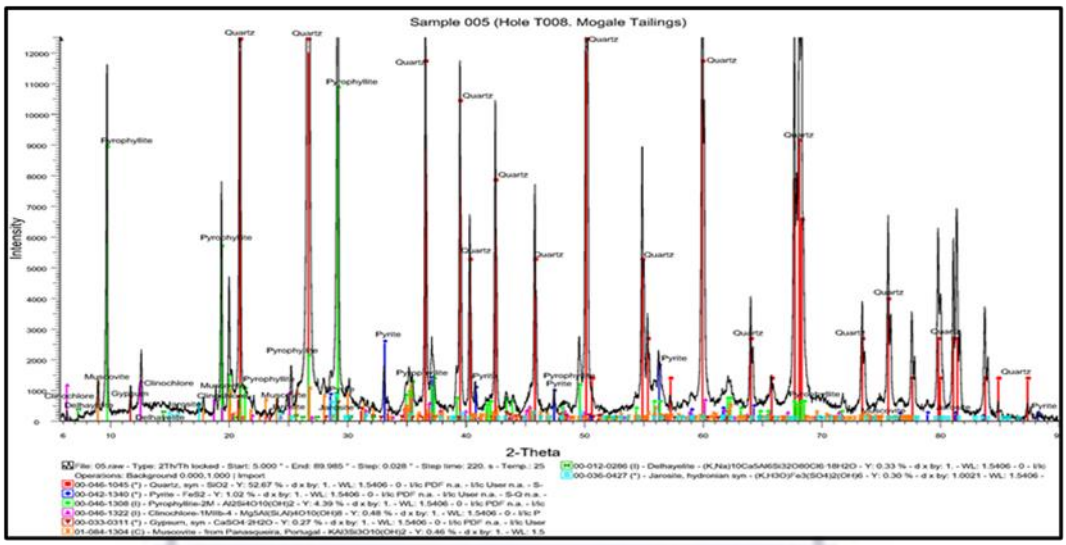

Figure 5.49: Sample 005 XRD analysed data (pyrite and jarosite observed)

In addition, the mineral muscovite ($KAl_3Si_3O_{10}(OH)_2$) is presented as one of the forms of phyllosillicates, together with mineral pyrophyllite ($Al_2Si_4O_{10}(OH)_2$). It is understood that the presence of delhayelite ($(Na, K)_{10}Ca_5Al_6Si_{32}O_{80}(Cl_2, F_2, SO_4)_3 \cdot 18(H_2O)$) is not officially observed yet in any mineralogical assessment of the Witwatersrand gold ore and tailings. This observation can be validated by the substantial amounts of K_2O, Na_2O and CaO from XRF analysis results obtained. More so, the mineral phases of Clinochlore ($Mg_5Al(Si, Al)_4O_{10}(OH)_8$) and Delhayelite ($(Na, K)_{10}Ca_5Al_6Si_{32}O_{80}(Cl_2, F_2, SO_4)_3 \cdot 18(H_2O)$) are presented in the graph.

The gold tailings located in Witwatersrand are constrained within a relatively narrow compositional range. The gold tailing is avowed to consist of 70–90% quartz, 10–30% phyllosilicates (mainly, Sericite), and 1–2% contain other minerals such as uraninite, chromite etc. (Yibas et al., 2010).

Numerical results of the XRD analysis of sample 001 are tabulated in the Table 5.4, along with other samples collected from all the holes drilled in the Mogale tailings.

Table 5.4: Mogale tailings samples XRD analysis results

Sample	Quartz	Pyrophyllite	Pyrite	Clinochlore	Gypsum	Muscovite	Delhayelite	Jarosite	Hematite
001	50	4.17	-	0.46	0.26	0.44	0.31	1.39	
002	52.51	4.38	-	0.48	0.27	0.46	0.33		
005	52.67	4.39	1.02	0.48	0.27	0.46	0.33	0.30	
007	52.67	4.39	1.02	0.48	1.68	0.46	0.33		
007-1	50.00	4.17	2.12	0.46	0.26	0.44	0.31		2.08
007-2	52.67	4.39	1.02	0.48	1.68	0.46	0.33		
008	52.67	4.39	1.02	0.48	1.68	0.46	0.33		
008-1	54.56	4.55	1.06	0.50	1.74	0.48	0.34		
008-2	54.56	4.55	1.06	0.50	1.74	0.48	0.34		
009	54.56	4.55	1.06	0.50	1.74	0.48	0.34		
010	54.56	4.55	1.06	0.50	1.74	0.48	0.34		
014	54.56	4.55	1.06	0.50	0.22	0.48	0.34		
015	54.56	4.55	1.06	0.50	0.22	0.48	0.34		
016	54.56	4.55	1.06	0.50	0.22	0.48	0.34		
017	50.00	4.17	2.12	0.46	0.26	0.44	0.31		2.08
017-1	54.56	4.55	1.06	0.50	0.22	0.48	0.34		
018-1	54.56	4.55	1.06	0.50	0.22	0.48	0.34		
019	54.56	4.55	1.06	0.50	0.22	0.48	0.34		
020	50.00	4.17	0.97	0.46	0.26	0.44	0.31	1.39	
021	54.56	4.55	1.06	0.50	0.22	0.48	0.34	0.66	
021-1	54.56	4.55	1.06	0.50	0.22	0.48	0.34	0.66	
022	54.56	4.55	1.06	0.50	0.22	0.48	0.34	0.66	

Table 5.4 continued.

Sample	Quartz	Pyrophyllite	Pyrite	Clinochlore	Gypsum	Muscovite	Delhayelite	Jarosite	Hematite
023-1	50.00	4.17	0.97	0.46	0.26	0.44	0.31		
025	54.56	4.55	1.06	0.50	0.22	0.48	0.34	0.66	
027	54.56	4.55	1.06	0.50	0.22	0.48	0.34	0.66	
027-1	50.00	4.17	2.12	0.46	0.26	0.44	0.31		2.08
029	54.56	4.55	1.06	0.50	0.22	0.48	0.34	0.44	
030	54.56	4.55	1.06	0.5	0.22	0.48	0.34	0.44	
032	54.56	4.55	1.06	0.5	0.22	0.48	0.34	0.44	
033	54.56	4.55	1.06	0.5	0.22	0.48	0.34	0.44	
034	50.00	4.17	0.95	0.25	0.26	0.44	0.31		
035	50.00	4.17	0.95	0.87	0.26	0.44	0.31		
036	50.00	4.17	0.95	0.87	0.26	0.44	0.31		
038	54.56	4.55	1.06	0.50	0.22	0.48	0.34	0.44	
038-1	54.56	4.55	1.06	0.50	0.22	0.48	0.34	0.44	
039-1	54.56	4.55	1.06	0.50	0.22	0.48	0.34	0.44	
042-1	54.56	4.55	1.06	0.50	0.22	0.48	0.34	0.44	
043	54.56	4.55	1.06	0.50	0.22	0.48	0.34	0.44	
044	50.00	4.17	2.12	0.46	0.26	0.44	0.31		2.08
047	55.13	4.60	1.07	0.51	0.22	0.48	0.34	0.44	

This sample and sample 002 were collected from the first two meters of the hole T008. In the two samples, as arrayed in Table 5.4, no pyrite (primary product) was detected, but jarosite (secondary product) ($KFe^{3+}3(SO_4)_2(OH)_6$) was detected in sample 002 and in some other samples. Primarily, the oxidation of sulphide minerals results in the production of secondary minerals such jarosite ($KFe^{3+}3(SO_4)_2(OH)_6$) and gypsum ($CaSO_4 \cdot 2H_2O$) (Rosner et al., 2001). However, jarosite ($KFe^{3+}3(SO_4)_2(OH)_6$) can easily be hydrolysed into iron hydroxide; and it is found in a low quantity in the top layers up to 6 meters but diminishes downward. Graphical illustration of the XRD analysis of sample 001 is given in the figure below (Figure 5.50).

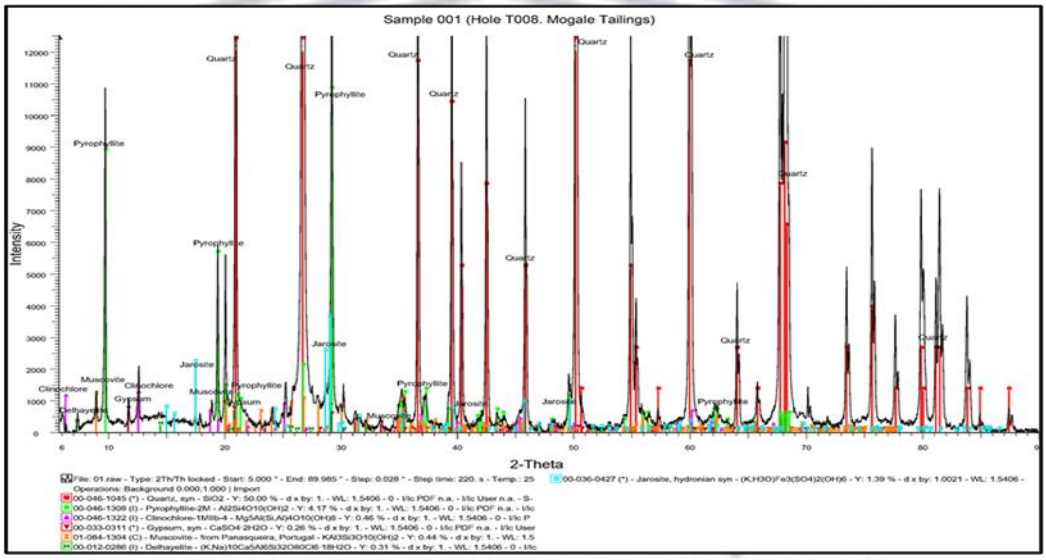

Figure 5.50: Sample 001 XRD analysed data (jarosite observed, but no pyrite)

More observations reveal that gypsum ($CaSO_4 \cdot 2H_2O$) is detected in all the samples collected from the Mogale tailings. The distribution shape of the value indicates variation in the quantity of gypsum mineral detected. This illustration specifies that the tailings contained buffer elements, but not adequate to neutralise potential acid generated by the tailings. This literally insinuates that no enough buffer elements to prevent oxidation. Most of the tailings samples in Witwatersrand have higher AP than NP.

Another mineral with a smaller quantity throughout the samples is hematite (Fe_2O_3). Hematite (Fe_2O_3) is detected in four holes at some certain depths, suchlike 7 meters

deep in hole T004, 8 meters deep in hole T008, 7 meters deep in hole T009 and 7 meters deep in hole T010. These are the drilling lengths of the layers where hematite was detected. And these layers are the exact position in the holes where ferruginous reddish fine sand was detected.

The graph below illustrates the detection of hematite and other mineral phases detected in the sample 007–1. From the graphical illustration, it is denoted that more quartz (SiO_2) mineral was detected in a high quantity, followed by pyrite (FeS_2) and pyrophyllite ($Al_2Si_4O_{10}(OH)_2$), whereas delhayelite ($(Na, K)_{10}Ca_5Al_6Si_{32}O_{80}(Cl_2, F_2, SO_4)3{\cdot}18(H_2O)$) and hematite ($Fe_2O_3$) were distributed in lowest quantities in sample 007–1 collected from hole T008 in Mogale tailings.

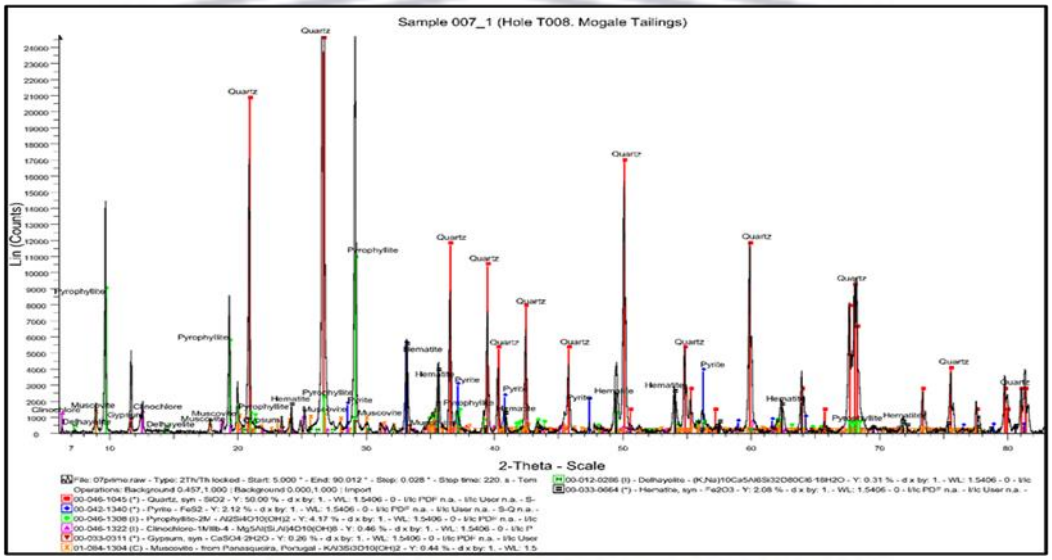

Figure 5.51: Sample 007–1 XRD analysed data (hematite observed)

In Figure 5.52, XRD analysis of the sample 017 is graphically presented to demonstrate the presence of minerals. The results derived in the sample 017 is graphically like the results obtained in the XRD analysis of the sample 007–1. Among the minerals detected, as tabulated in the Table 5.4, quartz (SiO_2) and pyrite (FeS_2) were detected at well distributed quantities in the sample, but delhayelite ($(Na, K)_{10}Ca_5Al_6Si_{32}O_{80}(Cl_2, F_2, SO_4)3{\cdot}18(H_2O)$) and hematite ($Fe_2O_3$) remain the two well distributed minerals with lowest quantities.

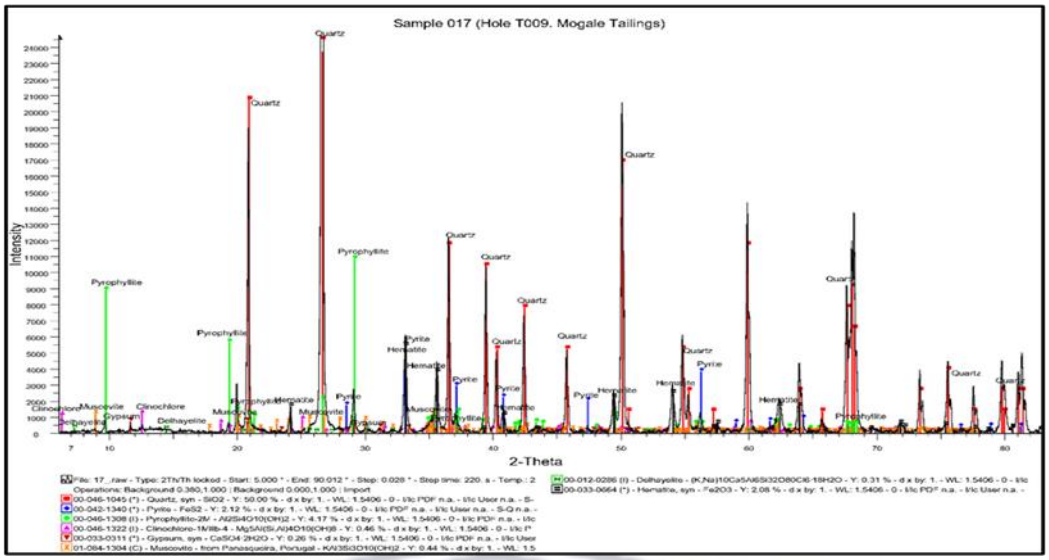

Figure 5.52: Sample 017 XRD analysed data (hematite observed)

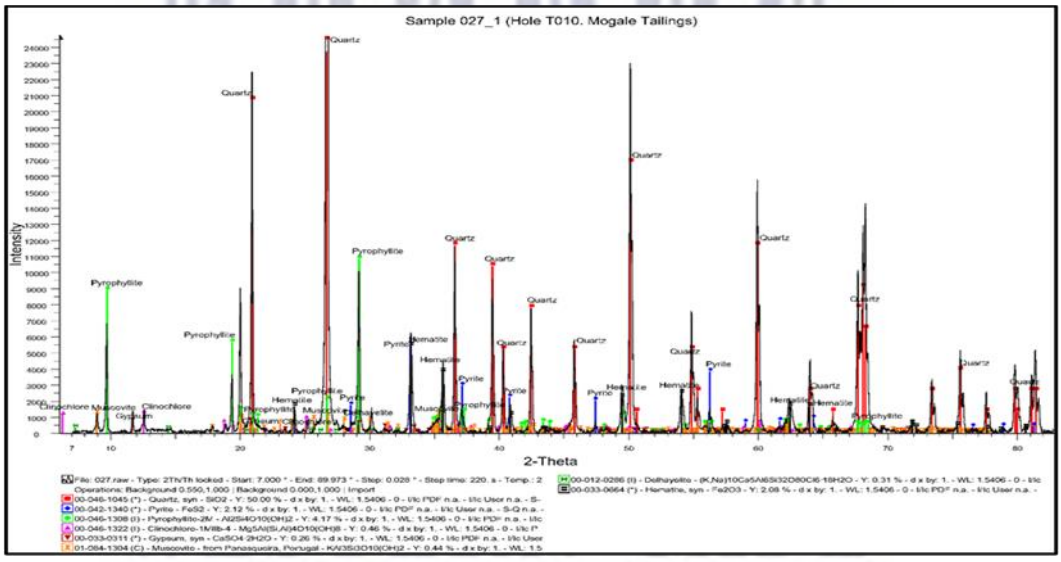

Figure 5.53: Sample 027–1 XRD analysed data (hematite observed)

Graphical illustration of XRD analysis of the sample 027–1 is presented in the Figure 5.53. From the spectrographic display, it is deduced that hematite (Fe_2O_3) is well distributed in the sample, but in lowest quantity. Also, quartz (SiO_2) is well distributed with high quantity compared to pyrite (FeS_2) and pyrophyllite ($Al_2Si_4O_{10}(OH)_2$) poorly distributed in this sample. Although, quartz (SiO_2) and pyrophyllite ($Al_2Si_4O_{10}(OH)_2$) minerals remain the principal mineral phases.

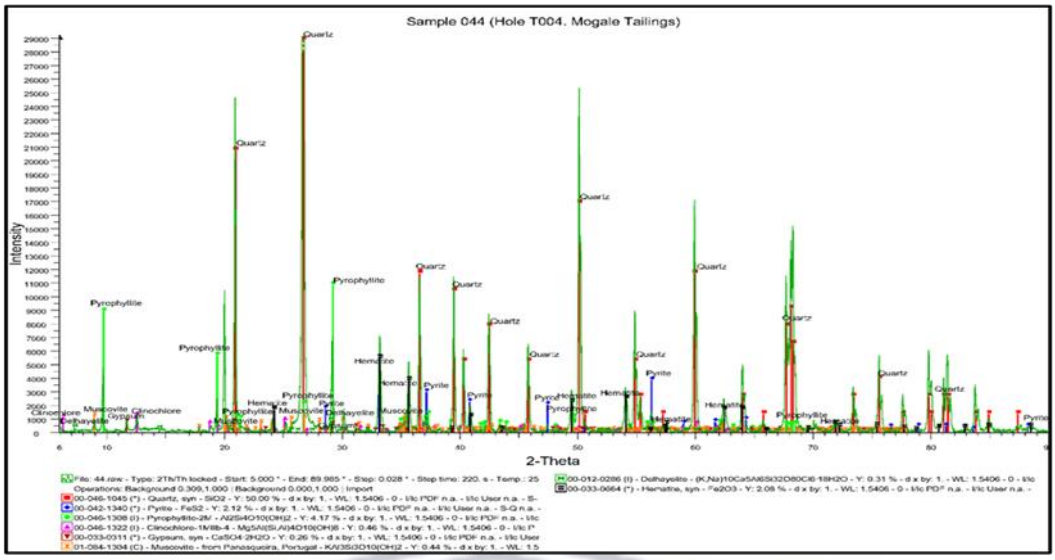

Figure 5.54: Sample 044 XRD analysed data (hematite observed)

XRD analysis of sample 044 is spectrographically presented in Figure 5.54 shows that quartz (SiO_2) is poorly distributed than pyrophyllite ($Al_2Si_4O_{10}(OH)_2$). Nonetheless, the mineral remains the principal mineral among other detected minerals in the sample 044. Unlike in sample 027–1, hematite (Fe_2O_3) is less distributed in the lowest quantity in the sample 044.

5.3.2.2 Gold One_1 Tailings Samples

The numerical data obtained from the XRD analysis of the samples collected from the Gold One_1 tailing is arrayed in the Table 5.5. Data demonstrates that quartz (SiO_2) is principally present in the samples, followed by pyrophyllite ($Al_2Si_4O_{10}(OH)_2$) as second most principal mineral phase, which is accompanied by other principal mineral phases such as Pyrite (FeS_2) and Clinochlore $(Mg,Fe)_6(Si, Al)_4O_{10}(OH)_8$). In addition, gypsum ($CaSO_4 \cdot 2H_2O$) is found in the tailings as the secondary mineral phase, followed by yoshiokaite (Ca (Al, Si)$_2O_4$) found at the tailing dam except the surface of hole T003.

Further observations reveal that values arrayed in the Table 5.5 demonstrate variations in the distribution of the mineral phases in the XRD analysed samples. In some samples, the quantities of the mineral phases are high while they are low in some other samples. Also, in some cases, pyrophyllite ($Al_2Si_4O_{10}(OH)_2$) observed to be less than one in samples 058, 073 and 093, and gypsum

($CaSO_4 \cdot 2H_2O$) are greater than one in samples 068 and 069. More so, yoshiokaite ($Ca\ (Al, Si)_2O_4$) is not detected in samples 068 and 069.

Table 5.5: Gold One_1 tailing samples XRD analysis results.

Sample	Quartz	Pyrophyllite	Pyrite	Clinochlore	Gypsum	Yoshiokaite
049	52.13	2.71	0.13	0.18	0.49	0.09
052	46.75	2.43	0.12	0.16	0.44	0.08
055	46.68	2.43	0.12	0.16	0.44	0.08
058	46.68	0.91	0.12	0.27	0.44	0.08
061	49.28	1.18	0.5	0.28	0.34	0.13
064	41.67	1	0.42	0.24	0.27	0.15
067	41.67	1	0.42	0.37	0.27	0.37
068	63.65	5.87	0.64	0.37	1.77	
069	41.67	3.84	0.42	0.24	1.16	
073	41.75	0.81	0.42	0.24	0.39	0.08
076	46.68	0.91	0.47	0.27	0.44	0.08

From the graph below, quartz (SiO_2) is principally distributed in a high quantity in the sample 068 collected from hole T003 in Gold One_1 tailing. Pyrite (FeS_2) is less distributed than pyrophyllite ($Al_2Si_4O_{10}(OH)_2$) in the sample. And gypsum ($CaSO_4 \cdot 2H_2O$) is poorly distributed in a small quantity, including Clinochlore ($(Mg,Fe)_6(Si, Al)_4O_{10}(OH)_8$) in the sample.

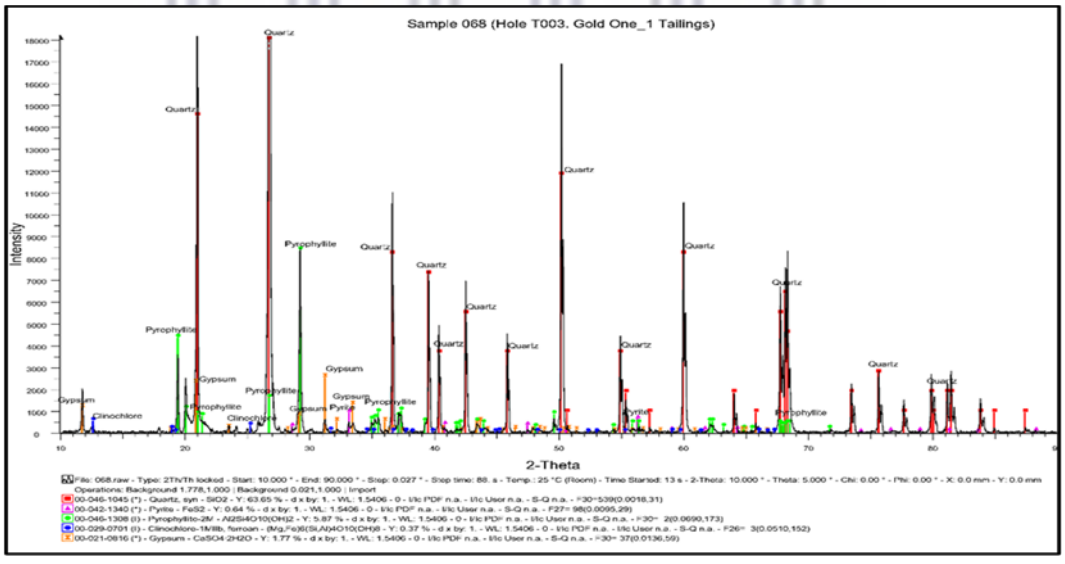

Figure 5.55: Sample 068 XRD analysed data

XRD analysis of the sample 069 collected from hole T003 is graphically demonstrated in the Figure 5.56. Observations deduced in this sample is like the results obtained in sample 068. Quartz (SiO_2) remains the principal mineral phase in a high quantity in the sample. Pyrophyllite ($Al_2Si_4O_{10}(OH)_2$) is observed to be

well distributed than pyrite (FeS_2) in a high quantity. In addition, gypsum ($CaSO_4 \cdot 2H_2O$) and clinochlore $(Mg,Fe)_6(Si, Al)4O_{10}(OH)_8$) are poorly distributed in small quantities in the sample 069.

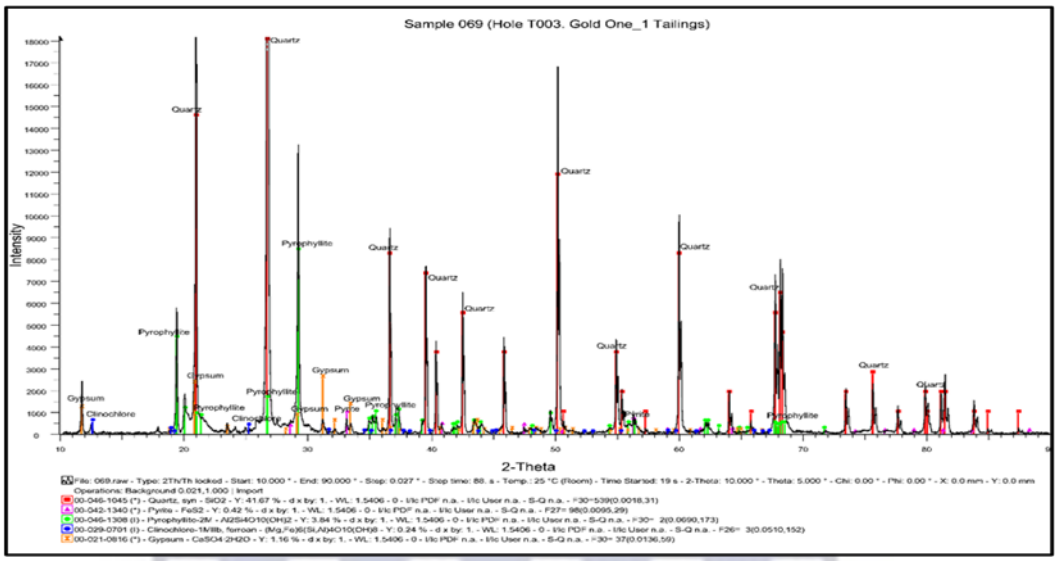

Figure 5.56: Sample 069 XRD analysed data

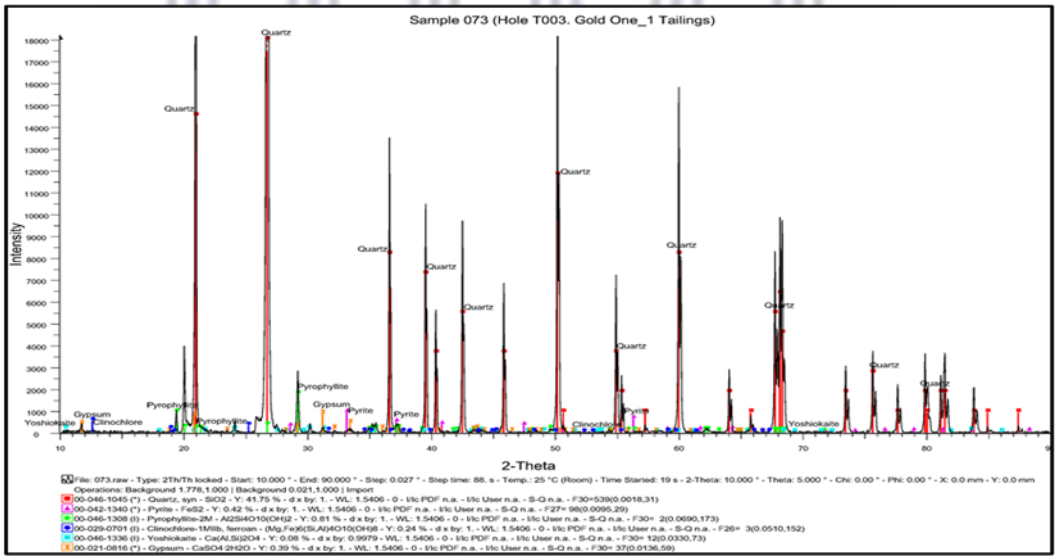

Figure 5.57: Sample 073 XRD analysed data

In Figure 5.57, XRD analysis of sample 073 revealed a well distributed quantity of quartz (SiO_2). In this sample, pyrophyllite ($Al_2Si_4O_{10}(OH)_2$) was detected in more quantity than pyrite (FeS_2), as they both are poorly distributed. Gypsum ($CaSO_4 \cdot 2H_2O$) was detected in a slightly more quantity than clinochlore

$(Mg,Fe)_6(Si, Al)_4O_{10}(OH)_8$), but they both are poorly distributed. Another mineral phase detected in the sample was yoshiokaite ($Ca(Al,Si)_2O_4$), with a smallest quantity.

The graphical presentation of the XRD analysis results of sample 076 is given in Figure 5.58. The results obtained in this sample indicate slight improvement in the quantity of all the mineral phases compared to samples 069 and 073. Mineral phases like quartz (SiO_2), pyrophyllite ($Al_2Si_4O_{10}(OH)_2$), pyrite (FeS_2), clinochlore $(Mg,Fe)_6(Si, Al)_4O_{10}(OH)_8$) and gypsum ($CaSO_4 \cdot 2H_2O$) are all improved in quantity level except yoshiokaite ($Ca(Al,Si)_2O_4$). Graphical observations indicate that quartz remains the principal mineral phase in a well distributed quantity more than any other mineral phase.

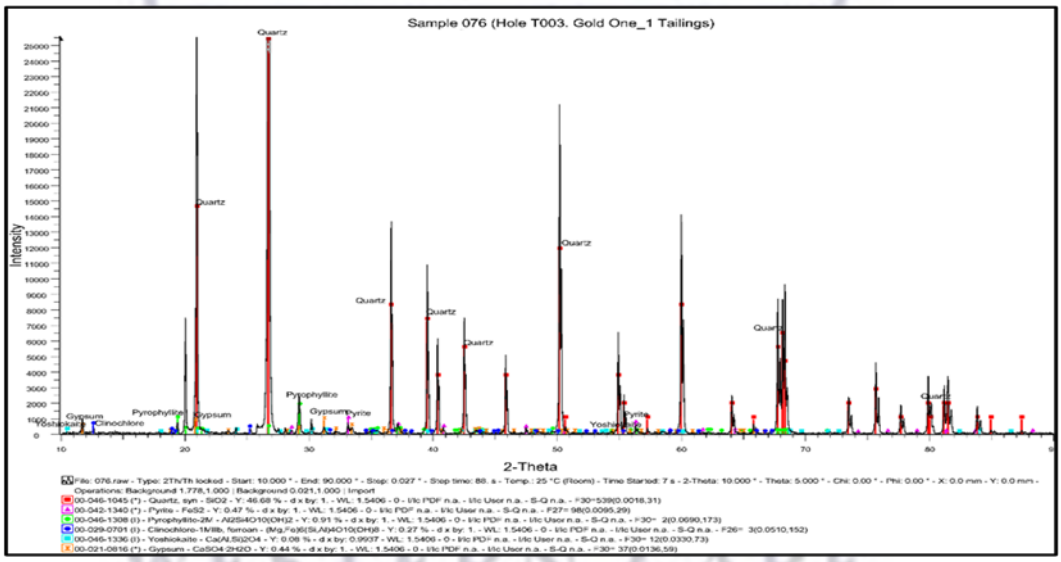

Figure 5.58: Sample 076 XRD analysed data

Pyrite (FeS_2) and gypsum ($CaSO_4 \cdot 2H_2O$) are sparsely distributed in quantities, followed by clinochlore $(Mg,Fe)_6(Si,Al)_4O_{10}(OH)_8$) and yoshiokaite ($Ca(Al,Si)_2O_4$).

5.4 Conclusion

The SEM/EDS and XRD analysis results for two gold tailing dams indicate that the tailings are primarily constituted by gangue of the exploited mineralisation, which are determined as quartz (SiO_2), phyllosilicates ($Al_2Si_4O_{10}(OH)_2$) and pyrite (FeS_2). On the other hand, quartz (SiO_2) and Phyllosilicates ($Al_2Si_4O_{10}(OH)_2$)

predominated in the tailings, while some small quantity of clinochlore $(Mg,Fe)_6(Si, Al)_4O_{10}(OH)_8$), jarosite ($KFe^{3+}3(SO_4)_2(OH)_6$) and hematite ($Fe_2O_3$) demonstrate regular presence of Fe. As regards the white surface blooms, they are formed mostly of magnesium sulphate with different hydration states. The morphology of these mineral precipitates reveals impacts of a cycle of washing and subsequent dehydration. To that effect, these specific phases present great mobility in the environment as well contribute to the transport of metals from the tailings into the surrounding soil.

CHAPTER SIX

6. GEOCHEMICAL CHARACTERISATION

6.1 Introduction

This chapter discusses geochemical characterisation of the ninety-three tailing samples as analysed by ACME Analytical Laboratories (Vancouver) Limited. Major oxides elements analysis was done using $Li_2B_4O_7/LiBO_2$ fusion, XRF; Total Carbon (T/C) and Total Sulphur (T/S) analyses were done by Leco; and Trace Elements analysis was done using $LiBO_2/Li_2B_4O_7$/fusion, ICP-MS. In this study, the samples collected from the Mogale tailings and Gold One_1 tailing will be used predominantly for geochemical characterisation and comparison. The major objectives of this chapter are to:

- Identify the distribution pattern and abundance characteristics of the trace elements,
- Evaluate the geochemical composition to determine the extent of oxidation and acid products transportation between different layers of the tailing dams, and
- Classify the acid generation trend of the tailing dams.

The results of analysis of the major oxides elements and trace elements of the samples from the Mogale tailings demonstrate in this chapter are extracted from the article titled "Distribution patterns of contaminants in the Gold Tailing Dam: case study from South Africa" published on Environ Earth Sci. 75:1365."

6.2 Major Oxides Elements Concentration in the Three Tailings

Major oxides elements such as SiO_2, Al_2O_3, Fe_2O_3, CaO, MgO, Na_2O, K_2O, MnO, TiO_2, P_2O_5 and Cr_2O_3 were tested to get the weight of percentage of metal elements oxidation. From these oxides' elements, Total Sulphur and Total Carbon are tested, but Total Sulphur is used to calculate the sulphide sulphur. There are many trace elements that are associated with main element of gold. These trace elements are harmful. In addition, the trace elements contain in the tailing dams are released into

the atmosphere, soil and aquatic environment; thus, the effect led to environmental contamination in the affected areas. In this study, forty-five trace elements are tested for in each sample, but only the samples with high abundance content will be the focal point in this chapter. These trace elements are Ba, Co, Cs, Th, U, Zr, Mo, Cu, Pb, Zn, Ni, As, Au, Sb, Bi, and Hg. Other trace elements to be discussed are Se, Cd, Be, V, Y, La, Pr, Sm, Ga, Hf, Nb, Rb, Sn, Ta, W, Eu, Gd, Tb, and Dy, including Ho, Er, Tm, Yb, Lu, Ag, Sr, Ce, Nd and Ti. Also, those with minimal content will only be discussed in other studies, if there are related studies in the future.

Table 6.1: Summary of major oxides elements concentration in the three tailings

Major Element	Mogale Tailings (wt%)	Gold One_1 Tailings (wt%)	Gold One_2 Tailings (wt%)
SiO_2	84.34	86.36	84.03
Al_2O_3	6.45	5.47	7.36
Fe_2O_3	3.03	2.88	3.13
CaO	0.52	0.53	0.13
MgO	0.40	0.34	0.46
Na_2O	0.09	0.04	0.06
K_2O	0.34	0.21	0.28
MnO	0.06	0.02	0.02
TiO_2	0.24	0.28	0.32
P_2O_5	0.03	0.02	0.02
Cr_2O_3	0.04	0.06	0.05
Ba	0.01	0.01	0.01
LOI	3.44	3.27	3.71
Total	99.00	99.47	99.58

Summary results of major oxides elements concentration of the three gold tailings derived from the XRF analysis of the ninety-three (93) samples are tabularised in Table 6.1. Observation shows that among all the major oxides elements components arrayed in the table, only SiO_2 is detected in large measure in the three tailings samples. Therefore, SiO_2 is the main component in the three tailings samples. In addition, SiO_2 exhibited 86.36% largest proportion in the Gold One_1 tailing more than other two tailings with 84.34% (Mogale tailings) and 84.03% (Gold One_2 tailings), respectively. Although, some other observations indicate that Al_2O_3 exhibited 6.45% proportion in Mogale tailings, 5.47% proportion in Gold One_1 Tailings and 7.36% proportion in Gold One_2 Tailing, respectively as the only close quantities to SiO_2, followed by Fe_2O_3 with 3.03% proportion in Mogale tailings, 2.88% proportion in Gold One_1 tailing and 3.13% proportion in Gold One_2 Tailings.

Other elements in the table only exhibited minimal proportions except the loss of ignition (LOI), which demonstrated the total content of organic matter and volatile elements. Elements affected by LOI are CO_2, H_2O, C, Cl, F, S and cyanide–which is unstable and decomposes rapidly when exposed to sunlight and atmosphere (Changul et al., 2010). It is improbable that tailings may contain any significant concentrations of organic material as the content of kerogen is generally low in the gold ore (Revuelta, 2018). Each detected component has close percentage and content proportions in the three tailing dams. In this case, Mogale tailings' samples are used for the geochemical analysis in this chapter.

6.3 Layer Identification

The tailings dam comprises of four distinct layers, namely: oxidised layer, transition layer, reddish layer and un–oxidised layer. Oxidised layer is identified as the first or topmost layer in the tailings, with a light yellow to yellowish brown colour (Figure 6.1). Transition layer is identified as the second layer directly underlain the top layer in the tailings, with a brownish grey colour (Figure 6.2). The third layer in the tailings is identified as 'reddish layer', with a reddish colour. This layer represents the soil collected from the ferruginous zone (least altered zone) of the tailing hole (Figure 6.3), except in the hole T011. The last or fourth layer is classified as 'un–oxidised layer', with a grey colour (Figure 6.4). This layer is located at the base of the hole, from 9-10 meters as the bottled layer and it contains more moisture.

The aforesaid horizons encompass varying proportions of quartz, muscovite, pyrophyllite, gypsum, jarosite, delhayelite, hematite, pyrite and clinochlore based on the XRD results demonstrated in Chapter 5.

Figure 6.1: Topmost layer (oxidized layer) samples of the Mogale tailings

Figure 6.2: The 2nd layer (transition layer) samples of the Mogale tailings

Figure 6.3: The 3rd layer (reddish layer) samples of the Mogale tailings

Figure 6.4: The 4th layer (un–oxidised layer) samples of the Mogale tailings

Spatially, mineral contents such as quartz, jarosite and gypsum are higher in the two upper horizons (upper and lower oxidized zone), while pyrophilite, pyrite, hematite and muscovite contents dominate in the two lower horizons (lower and upper least altered zone). In this study, the spatial distribution of these minerals conform to the minerals usually found in ores and tailing dams of the Witwatersrand basin (Rösner & Van Schalkwyk, 2000).

6.4 Summary of Geochemical Data

The weight of percentage of major oxides, with the trace elements' contents, loss of ignition (LOI), total carbon (TOT/C) and total sulphur (TOT/S) derived from the analysis of the samples of each horizon in the Mogale tailings' dam are tabularly presented in the Table 6.2. Based on the geometric mean, as indicated under the 'entire analysed data' and the four layers (oxidised layer, transition layer, reddish layer and un–oxidised layer), it is understood that elements such as SiO_2, Al_2O_3 and Fe_2O_3 exhibited high geometric mean among other major oxides except LOI, with close weight of percentage values to Al_2O_3 and Fe_2O_3.

In the 'entire analysed data', the geometric mean values derived for SiO_2, Al_2O_3 and Fe_2O_3 are 84.24%, 6.25% and 2.64%. The sum of the geometric mean values of the three oxide elements plus geometric mean value of LOI (3.28%) represent more than 95.00% of the bulk composition of the samples (Rösner & Van Schalkwyk, 2000), while the geometric mean values of other major oxides were derived in minimal quantities. On the other hand, trace elements such as U, Au, Ni, As, Cu and Zn have maximum values of 655.5ppm, 1417.7ppm, 274.1ppm, 471.4ppm, 308.8ppm and 817ppm, respectively. Among these six trace elements mentioned, only Au (189.19ppm) and As (105.28ppm) have huge geometric mean values above 100ppm.

More so, these elemental contents were found in four different layers in various quantified quantities as tabularly displayed in the Table 6.2. These layers were abstracted from the Mogale tailings and they all exhibited variations in the elemental contents.

Among all the major oxides in the 'oxidised layer (topmost layer)' as arrayed in the table above, Na_2O (0.06%), MnO (0.01%), P_2O_5 (0.02%) and Cr_2O_3 (0.04%) exhibited marginal geometric mean values smaller to the values CaO (0.34%), MgO (0.25%), K_2O (0.33%) and TiO_2 (0.23%). And only SiO_2 exhibited highest geometric mean value of 87.32% compared to LOI (2.82%), Al_2O_3 (5.43%) and Fe_2O_3 (1.75%). Basically, it can be simplified further that more contents of SiO_2.

Table 6.2: Mogale tailings' samples geochemical analysis results

Variables	Entire Analysed Data					Oxidised layer		Transition layer		Reddish layer		Un–oxidised layer	
	Min	Max	G. Mean	A. Mean	Std. D	Std. D	G. Mean	Std. D	G. Mean	Std. D	G. Mean	Std. D	G. Mean
Major Oxides (% wt)													
LOI	1.72	7.26	3.28	3.44	1.12	0.92	2.82	1.06	3.37	0.65	4.00	1.27	3.36
SiO2	70.70	90.30	84.24	84.34	4.11	2.17	87.32	2.57	84.48	4.09	76.39	3.81	84.09
Al2O3	3.06	9.85	6.25	6.45	1.60	1.32	5.43	1.64	6.35	1.75	6.56	1.63	6.57
Fe2O3	0.86	9.31	2.64	3.03	1.93	0.66	1.75	0.59	2.64	0.22	9.03	0.79	2.60
CaO	0.06	2.75	0.43	0.52	0.44	0.25	0.34	0.18	0.41	0.53	0.74	0.57	0.44
MgO	0.09	0.86	0.35	0.40	0.18	0.19	0.25	0.22	0.41	0.10	0.45	0.16	0.37
Na2O	0.02	0.28	0.07	0.09	0.06	0.06	0.06	0.07	0.07	0.04	0.09	0.06	0.08
K2O	0.17	0.65	0.32	0.34	0.10	0.08	0.33	0.11	0.33	0.15	0.33	0.11	0.31
MnO	0.01	0.65	0.02	0.06	0.14	0.01	0.01	0.01	0.01	0.21	0.06	0.18	0.03
TiO2	0.18	0.35	0.24	0.24	0.04	0.03	0.23	0.04	0.25	0.03	0.24	0.04	0.24
P2O5	0.01	0.05	0.02	0.03	0.01	0.01	0.02	0.01	0.02	0.01	0.03	0.01	0.03
Cr2O3	0.03	0.08	0.04	0.04	0.01	0.02	0.04	0.01	0.04	0.01	0.04	0.01	0.04
Leco A. (%wt)													
TOT/C	0.01	0.22	0.05	0.07	0.05	0.06	0.04	0.04	0.05	0.10	0.10	0.05	0.05
TOT/S	0.26	2.19	1.00	1.14	0.51	0.29	0.48	0.38	1.13	0.18	1.52	0.46	1.23
Trace elements (ppm)													
Ba	29.00	264.00	58.59	67.02	45.96	13.97	52.25	18.02	52.08	58.84	73.51	60.91	63.59
Co	0.90	125.90	23.99	38.06	29.36	8.85	4.71	17.19	27.09	16.36	105.74	20.11	37.70
Cs	0.30	3.00	1.04	1.13	0.52	0.28	0.87	0.34	0.98	0.97	1.37	0.56	1.12
Th	3.60	54.10	8.61	10.08	8.07	1.15	4.89	2.95	8.71	5.76	10.43	10.80	10.84
U	4.00	655.50	25.53	45.48	90.46	2.42	6.88	173.47	34.71	10.95	38.62	21.54	37.40
Zr	92.70	233.80	122.80	125.14	26.69	15.61	112.26	34.49	121.05	15.65	152.81	24.65	124.41
Mo	1.20	6.40	3.57	3.86	1.39	1.40	3.74	1.45	3.31	1.38	4.45	1.38	3.50
Cu	3.80	308.80	35.43	51.29	58.70	11.11	13.20	69.87	36.24	19.53	65.05	65.37	50.47
Pb	15.40	150.20	42.91	49.66	29.26	29.11	46.70	14.84	41.69	31.42	52.67	35.54	40.41

Table 6.2 continues.

Variables	Entire Analysed Data					Oxidised layer		Transition layer		Reddish layer		Un–oxidised layer	
	Min	Max	G. Mean	A. Mean	Std. D	Std. D	G. Mean	Std. D	G. Mean	Std. D	G. Mean	Std. D	G. Mean
Trace elements (ppm)													
Zn	4.00	817.00	73.02	129.31	143.5	27.06	19.69	213.33	88.87	77.83	142.55	118.98	108.88
Ni	3.80	274.10	69.31	99.79	71.17	32.06	19.85	69.23	77.44	48.54	164.88	66.31	101.83
As	15.30	471.40	105.28	123.12	75.47	55.36	61.63	24.28	97.99	64.75	167.39	91.29	130.68
Au	58.10	1417.50	189.19	248.43	227.93	156.27	154.60	123.36	226.48	501.67	625.72	117.23	152.87
Sb	0.40	2.30	0.73	0.79	0.38	0.21	0.55	0.13	0.66	0.30	1.86	0.20	0.75
Bi	0.70	3.60	1.43	1.55	0.63	0.62	1.27	0.31	1.38	0.61	2.65	0.60	1.39
Hg	0.05	2.51	0.21	0.35	0.47	0.57	0.24	0.66	0.21	0.07	0.13	0.31	0.21

were found in the layer than any other major oxides. In addition, more contents of TOT/S were found in 'oxidised layer' than TOT/C. Also, the trace elements with highest and lowest contents were determined in the topmost layer. Observation shows that trace elements such as Cs, Sb and Hg exhibited insignificant geometric mean values of 0.87ppm, 0.55ppm and 0.24ppm compared to Ba, Zr, Cu, Pb, Zn, Ni, As and Au with improved geometric mean values. And among these trace elements, only Zr (112.26ppm) and Au (154.6ppm) demonstrated geometrical mean values above 100ppm in this layer.

In the 'transition layer', SiO_2 remains the major oxide with the highest content of 84.48% among the major oxides and Na_2O (0.07%), MnO (0.01%), P_2O_5 (0.02%) and Cr_2O_3 (0.04%) remain major oxides with marginal quantities. Other observations show that geometric mean value of SiO_2 in this layer decreased by 2.84% than the value obtained in the 'oxidised layer', only MnO, P_2O_5 and Cr_2O_3 were found at equal quantities. Thus, the geometric mean values of the remaining major oxides slightly increased in the layer. Further observations deduced demonstrate that the content of TOT/S is higher than TOT/C, but the geometric mean values are more than the values obtained in the 'oxidised layer'. And the geometric mean values of the trace elements generated in this layer exhibit undulatory distribution shape as demonstrated in the topmost layer. Trace elements such as Co (27.09ppm), U (34.17ppm), Zr (121.05ppm), Cu (36.24ppm), Zn (88.87ppm), Ni (77.44ppm), As (97.99ppm) and Au (226.48ppm) are measured in high contents in the 'transition layer' than the quantity measured in 'oxidised layer'. From the illustration, Zr and Au remain the only two trace elements with geometric mean values above 100ppm in this layer.

The third layer called 'reddish layer' produced the lowest value of SiO_2 (76.39%), which is largely decreased by 8.09% more than the value displayed in the 'transition layer'. Similar observations were deduced for major oxides elements such as Fe_2O_3 (9.03%), Al_2O_3 (6.56%) and LOI (4.00%) with improved geometric mean values. This is because SiO2 decreases in quantity/content down the first three layers, while other major oxides elements either increases in quantity, or remain unvaried in quantity across the first three layers (Table 6.2). As noted in both 'oxidised layer' and 'transition layer', TOT/S (1.15%) continues to improve in content level across the first three layers more than TOT/C. On the other hand, contents of the trace elements produced in the

'reddish layer' are progressively increased more than in the first two layers. It is observed that only six trace elements such as Co (105.74ppm), Zr (152.81ppm), Zn (142.55ppm), Ni (164.88ppm), As (167.39ppm) and Au (625.72ppm) exhibited geometric mean values greater than 100ppm in 'reddish layer'. This denotes that there are numerous trace elements discovered in reddish layer that exhibit improved quantity more than as observed in the first two layers.

Un–oxidised layer is the last layer with 84.09% and 6.57% contents of $SiO_2$and Al_2O_3, which are higher than the quantity attained in the 'reddish layer'. SiO_2 is largely increased by 7.70% and Al_2O_3 is slightly increased by 0.01% more than the values displayed in the 'reddish layer'. Other major oxides elements are either decreased in quantities or remain unvaried in quantities in this layer. Contents of TOT/S and TOT/C exhibited in the last layer declined. Despite the decline, quantity of TOT/S found in the layer is more than TOT/C. Similar to 'reddish layer', only five trace elements exhibited geometric mean values greater than 100ppm in the 'un–oxidised layer', such elements as Zr (124.41ppm), Zn (108.88ppm), Ni (101.83ppm), As (130.68ppm) and Au (152.87ppm).

General observations deduced from the exploration of major oxides elements to TOT/C, TOT/S and trace elements indicate that quantities of some elements are either increase or decrease across the four layers. Though, there are some elements with unvaried quantities throughout the four layers. In essence, this illustration indicates that quantity/content variations of elements exist in the four layers. Therefore, only 'oxidised layer' contained highest content of SiO_2, followed by 'transition layer' and 'un–oxidised layer', while 'reddish layer' produced the lowest content of SiO_2. In the case of the TOT/C and TOT/S, highest content of TOT/C was geometrically observed in the 'reddish layer', followed by an equal quantity in both 'transition layer' and 'un–oxidised layer' and lowest quantity was found in 'oxidised layer'. These quantities are very minimum compared to the proportions of TOT/S found in the four layers. In contrast, highest content of TOT/S was found in the 'reddish layer', followed by 'un–oxidised layer' and 'transition layer', whereas lowest quantity of TOT/S was observed in the first layer. Among the four layers, only 'reddish layer' contained the largest content of trace elements. Observably, Au and Zr were found in largest quantities across the four layers; that is, trace elements with quantities above 100ppm throughout the

four layers. And ‘reddish layer’ is identified as a ferruginous layer (rick red layer) due to the presence of hematite.

6.5 Multivariate Statistics

Hierarchical Cluster Analysis (HCA) dendrogram displayed in Figure 6.5 illustrates the classification of these samples into two clusters as ‘cluster 1’ and ‘cluster 2’. Then, the two clusters were grouped into two sub-clusters each as ‘sub–cluster 1a’ and ‘sub–cluster 1b’ for cluster 1 and ‘sub–cluster 2a’ and ‘sub–cluster 2b’ for cluster 2. The HCA of SiO_2 as cluster 1, with sub–cluster 1a and sub–cluster 1b accounted for 88.2% of the original grouped cases correctly classified, and the HCA of Al_2O_3 as cluster 2, with sub–cluster 2a and sub–cluster 2b accounted 49% of original grouped cases correctly.

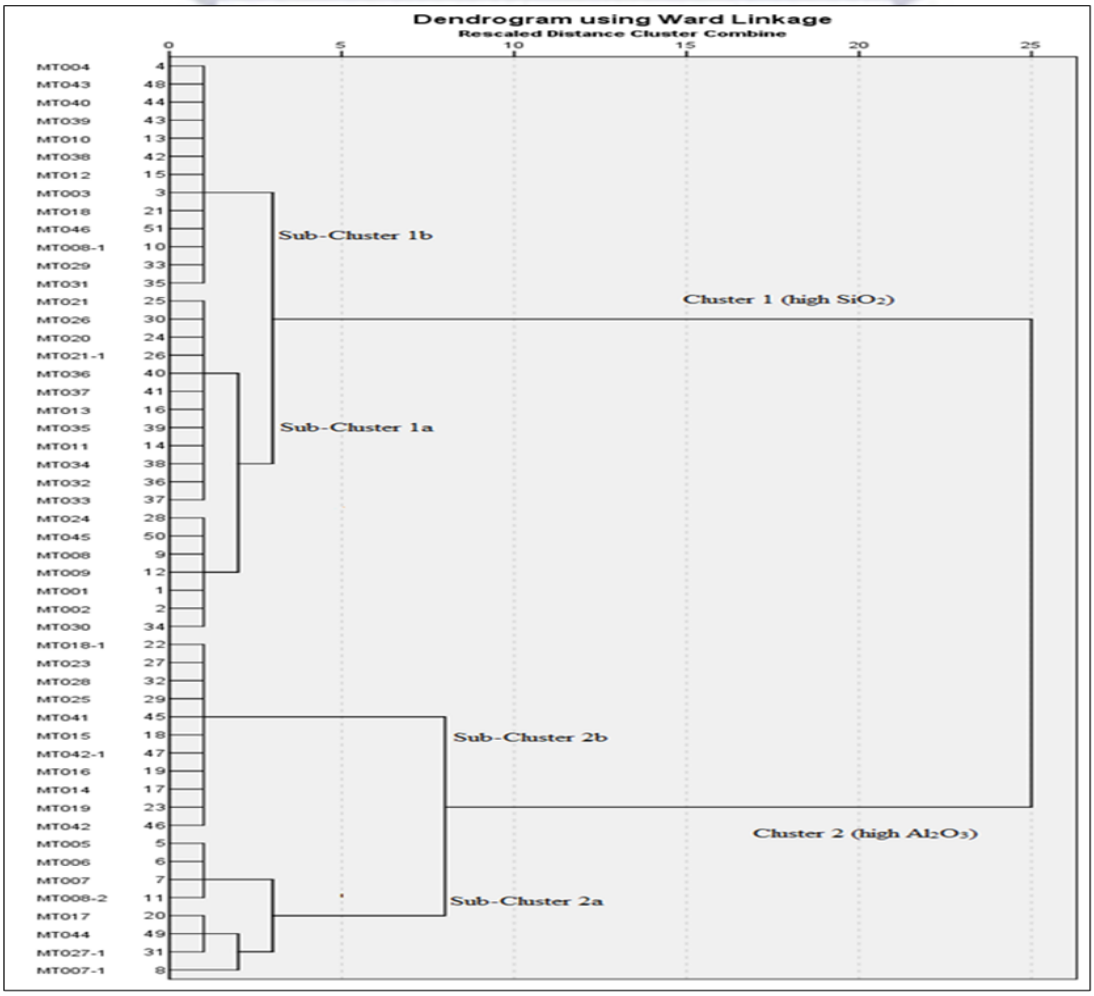

Figure 6.5: Dendrogram showing the results of HCA classified

The establishment of the sub–clusters indicate presence of a generic composition in the two clusters. The composition structure of these clusters demonstrates that samples in cluster 1 are rich in SiO_2, but depleted in Al_2O_3 and in contrast, samples in cluster 2 are rich in Al_2O_3, but depleted in SiO_2.

The canonical discriminant function approach was adopted to classify the sub–clusters using variables (Table 6.3). Therefore, the two major elements used for this analysis are SiO2 and Al2O3. These two major elements were considered because they largely defined the cluster analysis. In the process, the illustration of the two functions yielded four trends. As diagrammatically illustrated in Figure 6.6, function 1 axis demonstrated increase in SiO2 (quartz) and decrease in carbonates, with positive and negative correlation. Also, function 2 axis demonstrated increase in Al_2O_3 (clay) and decrease in sulphides (chalcophile) and ferruginised content, with positive and negative correlation.

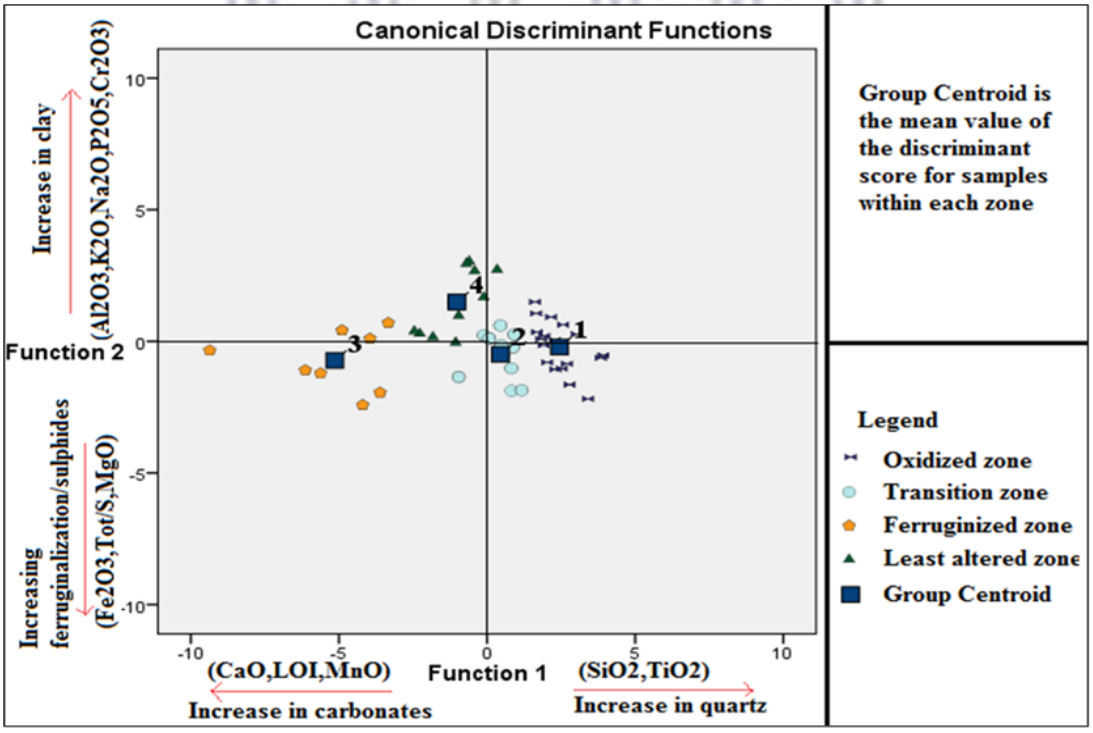

Figure 6.6: Canonical Discriminant Function analysis of Mogale tailings samples

The discriminant analysis reveals a more deterministic distribution of elements within the tailings (structure matrix) (Table 6.3). The group centroid demonstrates the actual characterisation of a sub-cluster group. And the significant concentrations of LOI,

Fe_2O_3, CaO, MnO, TOT/S and TOT/C, with very low concentration of SiO_2 were categorised in sub–cluster 2a, while elements with high values of Fe_2O_3,, Au and heavy metals that are sulphide–related were categorised in sub–cluster 2b. In that case, this confirms the petrography and mineralogical results that characterised the ferruginised zone (reddish layer).

Conversely, sub–cluster 1a is characterised by the presence of high content SiO_2 and lower enrichment in chalcophile elements. In this case, SiO_2 is not positively associated with other elements. And sub–cluster 1b is characterised by a group of cases of cluster depleted in other heavy metals but demonstrated high values in SiO_2 (compared to sub–clusters 2a and 2b). The first few layers for each hole drilled characterised sub–cluster 1a, which accounted for high quartz content.

Table 6.3: Structure matrix defining the summary of the clusters

Standardised Canonical Discriminant Function Coefficients		
Variables	**Function**	
	1	**2**
SiO2	1.106	.336
Al2O3	.264	1.125

Structure Matrix		
Variables	**Function**	
	1	**2**
SiO2	.974*	-.228
CaOb	-.434*	-.026
LOIb	-.398*	-.019
MnOb	-.357*	.033
TiO2b	.122*	.054
Al2O3	.291	.957*
K2Ob	-.208	.665*
Fe2O3b	-.300	-.570*
Na2Ob	-.071	.565*
TOT/Sb	-.334	-.403*
P2O5b	-.286	.387*
MgOb	-.048	-.341*
Cr2O3b	.078	.114*

*100% of original grouped cases correctly classified; Pooled within-groups correlations between discriminating variables and standardised canonical discriminant function; and Variables ordered by absolute size of correlation within function. (From the table: * = Largest absolute correlation between each variable and any discriminant function; b = This variable not used in the analysis).*

The knowledge of the relationship between samples makes it necessary to determine the factors that define the compositional pattern of elements within the tailings. Factor analysis was performed on twenty-seven variables (elements), from which seven factors were abstracted based on the nature of the analysis. Table 6.4 presents the factor analysis for layers using extraction methods, such as:

- Extraction Method (Principal Component Analysis (PCA)), and

- Rotation Method (Varimax with Kaiser Normalisation).

In Table 6.4, factor 1 presents carbonates, factor 2 presents ferruginised zone, factor 3 presents sulphides, factor 4 presents clay zone, factors 5 and 6 present refractory materials, and factor 7 presents chalcophile. Numerical results deduced illustrate that significant positive scores for MnO, Th, CaO, As, Pb, Bi, TOT/C and LOI were generated in factor 1, but a negative value was computed for SiO_2. Thus, the group of elements with positive values is called carbonates group, such as additives and dolomite. In factor 2, significant positive values for TOT/C, Sb, Fe_2O_3, Au, Bi and Co were generated, but a negative value was computed for SiO_2 as observed in factor 1. This particular factor is Fe/Au rich group. Factor 3 demonstrates significant positive values for Co, Ni, Zn, MgO, LOI and TOT/S, but a negative value for SiO_2 as observed in factors 1 and 2. This factor is called the sulphide group.

Table 6.4: Rotated component matrix Factor Analysis

Rotated Component Matrixa							
Variables	**Component**						
	1	**2**	**3**	**4**	**5**	**6**	**7**
MnO	.896						
Th	.892						
CaO	.888						
As	.884						
Pb	.812						
TOT/C	.545	.407					
Sb		.898					
Fe2O3		.863					
Au		.843					
Bi	.597	.621					
Co		.617	.576				
SiO2	-.440	-.544	-.457	-.487			
Ni			.822				
Zn			.820				
MgO			.766				
LOI	.535		.601				
TOT/S			.579				.410
K2O				.910			
Al2O3				.889			
Na2O				.887			
P2O5				.625			.496
Zr					.905		
TiO2				.433	.582		-.488
Cr2O3						.797	
Mo						.703	
U						-.521	
Cu							.820
% V	**20.31**	**14.33**	**14.19**	**14.01**	**7.566**	**6.663**	**6.473**

Additionally, factor 4 produced significant positive values for K_2O, Al_2O_3, Na_2O, P_2O_5, TiO_2, but a negative value for SiO_2 was produced. This factor is identified as clay group. Only factor 4 produced value for Al_2O_3, negative values were produced for SiO_2 in the table. Factor 5 equally produced significant positive values for Zr and TiO_2. This factor is characterised as titanium refractory group. Also, factor 6 produced significant positive value for Cr_2O_3 and Mo, but negative value for U. This factor is classified as refractory group. Factor 7 produced significant positive values for TOT/S, Cu and P_2O_5, but negative value for TiO_2. This indicates that some certain sulphides show negative relationship to the titanium refractory group. The state of the tailing dam samples peculiar to a specific layer within the tailings indicates that a certain part of the tailing has been oxidised and undergoing oxidation.

6.6 Geochemical Mass Balance (GMB) Results

The geochemical mass balance (GMB) is applied to determine the weathering processes in rock materials. This process can be executed in various ways, where ISOCON method of mass balance is widely apply as part of the process (Mukherjee & Gupta, 2008).

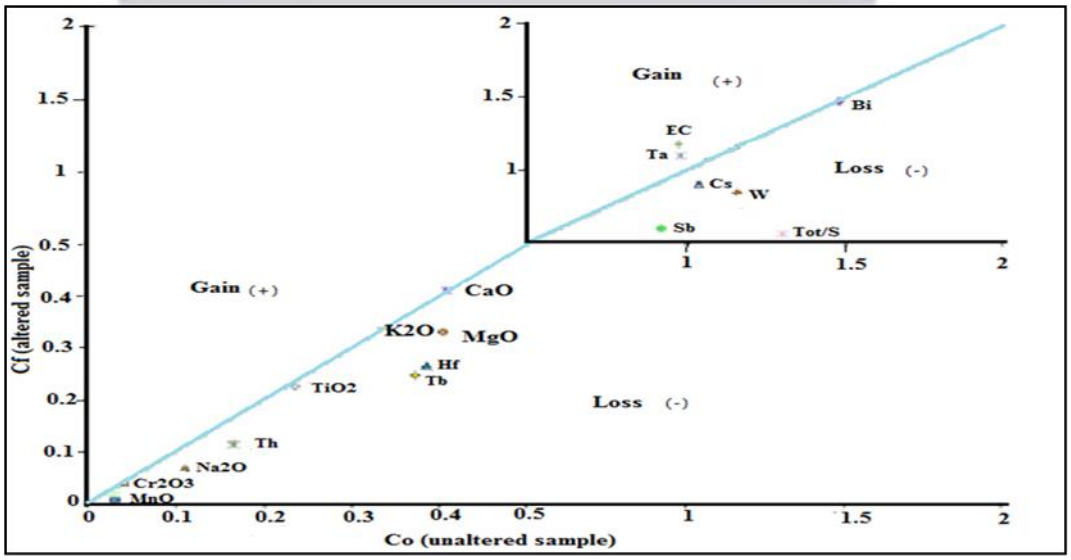

Figure 6.7: ISOCON diagram for layer 1 showing the elements gain and loss with respect to ΔCi

The average values of all major oxides and elements found in each layer as described by the petrography were used to calculate the mass balance in regard to the least altered samples (Figure 6.7). The bottommost samples are assumed to be the least altered samples. This is due to its simplicity in terms of flexibility and its graphical approach (Mukherjee & Gupta, 2008).

Application of GMB discloses variations in gain or enrichment and loss of constituents extant. The framework of the tailings is reflected through the existence of the major oxides and using observable variations to attain useful information based on the processes that occurred within the tailings.

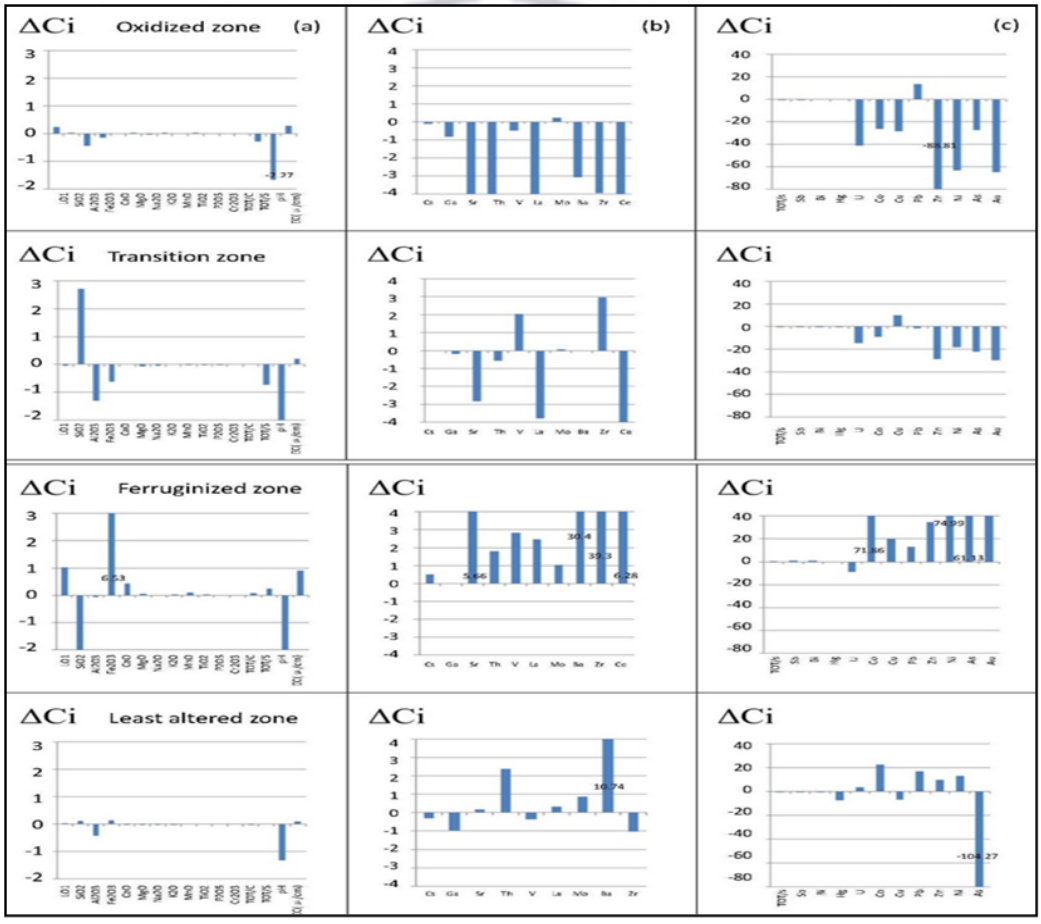

Figure 6.8: Histogram illustrating elemental loss and gain of tailings samples from each identified layer

(a) Major elements. (b) Trace elements group I. (c) Trace elements group II (sulphide related).

Figure 6.8 presents the mass balance results of major elements (%wt) and trace elements (ppm). Trace elements are grouped into two, which are 'trace element

group I' and 'trace element group II (sulphide related)'. In the graphs below, layer 1 gained 2–3 wt% of SiO2, with a loss of 1–2 wt% of Al2O3 and TiO2. These three elements are grouped under 'major elements'.

In view of 'trace elements', loss or dispersion of elements ranges from 0 to 8 ppm for Sb, Sr, V, Mo to about 80 ppm loss for Ba, Pb, As, Co, Cu, U, Au, Ni and Zn, in increasing order. In addition, further down the hole, layer 2 (transition zone) exhibits a low gain in SiO_2 and a great reduced loss of Ba, Zr, Pb, As, Co, Cu, U, Au, Ni and Zn, also in increasing order. Similar observation demonstrates that pronounced gains in trace elements occur in layer 3 (ferruginized zone), from 4 ppm gain for Sb, Sr, V, Mo to about 80 ppm for Ba, Zr, Pb, As, Co, Cu, U, Au, Ni and Zn, in increasing order. On the other hand, layer 4 (least altered zone) exhibits very low gain or loss of major elements and trace elements, except for As and V.

Other observation deduced reveals that a great percentage of loss in oxidised zone is exhibited by total sulphur. Therefore, the decreasing order is observed in the order of layer 1, layer 2, layer 4 and layer 3. The trends in the mass balance validate results from statistical summary, hierarchical clustering and factor analysis.

6.7 GIS Inverse Distance Weighed (IDW) Analysis Results

In relation to the factor analysis and GMB results, elements from similar origin are determined and grouped as factors and layers based on weathering. Generally, SiO_2 observably demonstrated a significant negative correlation with each factor. Therefore, the enrichment of silica indicates the depletion or weathering of surface; that is, loss of other elements. In this analysis, only six layers were used, which are upper and lower oxidised layers, transition layer, ferruginised layer, upper and lower un–oxidised layers. With the use of IDW analysis, a spatial distribution of elements with similar trend down depth was observed (Setianto & Triandini, 2015).

It is evident that elements in each factor demonstrate a peculiar trend. Among these elements, SiO_2 and Al_2O_3 were selected due to the inverse relationship observed in the results attained from the cluster analysis and factor analysis. As previously explicated in section 6.5, SiO_2 was negatively correlated to most of the factors identified as computed in factor analysis. Factors identified are clay group (Al_2O_3),

sulphides (TOT/S), carbonates (CaO), and Au/Fe rich group (Au). Uranium was selected based on the GMB; although, the element exhibited no significant relationship with the factors mentioned above. But the element is highly mobile. Also, the variation pattern of SiO_2 can also serve as a basis for the four factors.

Table 6.5: Percentiles values of elements used in IDW analysis as intervals for the map display.

Percentiles	SiO2 (wt%)	Al2O3 (wt%)	Fe2O3 (wt%)	CaO (wt%)	TOT/S (wt%)	U (ppm)	Au (ppb)
25%	82.30	5.33	1.97	0.30	0.83	10.0	106.0
50%	85.10	6.28	2.59	0.40	1.09	32.4	186.7
75%	87.20	7.51	3.40	0.54	1.53	43.1	322.0
Minimum (0%)	70.70	3.06	0.86	0.06	0.26	4.0	58.1
Maximum (100%)	90.30	9.85	9.31	2.75	2.19	655.5	1417.5

For each element, the quartile values of the element in the entire dataset were used to demonstrate an unbiased distribution pattern. The quantile values computed for the elements are presented in Table 6.5. The first row to the fourth row represents range of values from the minimum, 25%, 50% and 75% percentiles to the maximum values for individual element.

6.7.1 Distribution of SiO_2 and Al_2O_3 in Layers Down Depth

The distribution of SiO_2 and Al2O3 in the layers down depth is illustrated according to concentration level of these two elements in the six layers mentioned earlier in section 6.7. The patterns obtained are graphically illustrated in Figure 6.9 and Figure 6.10. In the graphs, upper and lower oxidised layers exhibited high concentration of SiO_2 and low concentration of Al_2O_3. Although, lower oxidised layer contained more of SiO_2 than upper oxidised layer.

In the southern part of the tailings dam, upper oxidised layer exhibited high concentration of SiO_2. Thus, it can be stated that the area containing the highest content of SiO_2 and lowest content of Al_2O_3 increases in a south-north trend, from first meter to second meter of the tailings dam. The SiO_2 and Al_2O_3 contents decrease and increase, respectively, as it proceeds into the transition layer, ferruginised layer and unoxidized layers. The ferruginised layer exhibited lowest values of SiO_2 and highest values of Al_2O_3. Contrariwise, the transition layer contained more and less contents of SiO_2 and Al_2O_3 than in the ferruginised layer.

The lower un–oxidised (least altered zone) layer contains the highest contents of Al_2O_3. The upper and lower unoxidized layers show similar distribution pattern of elements.

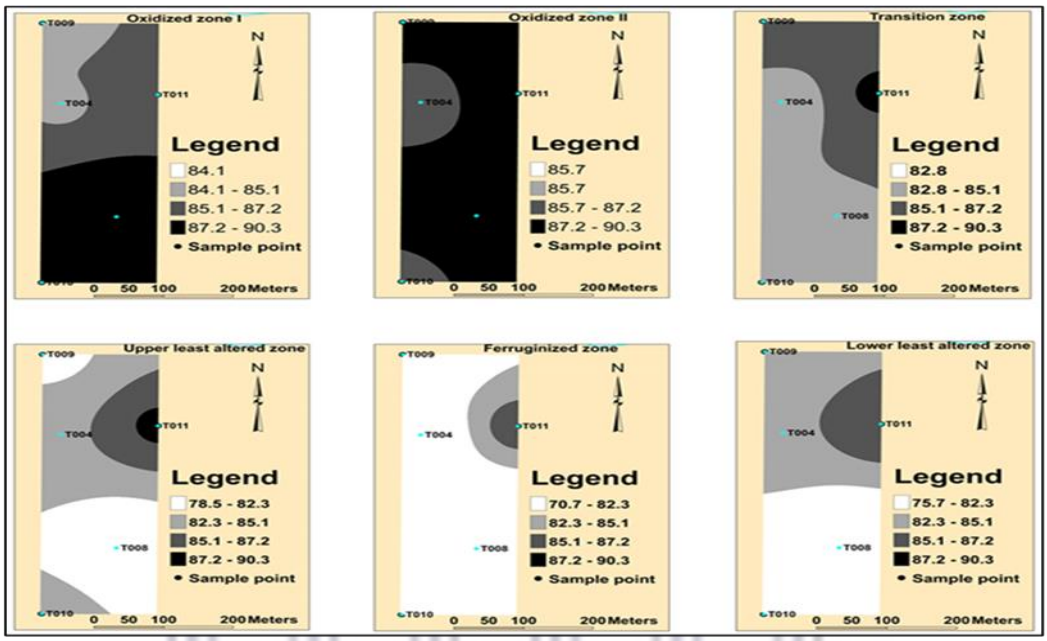

Figure 6.9: Downhole distribution pattern of SiO2 using inverse weighted analysis

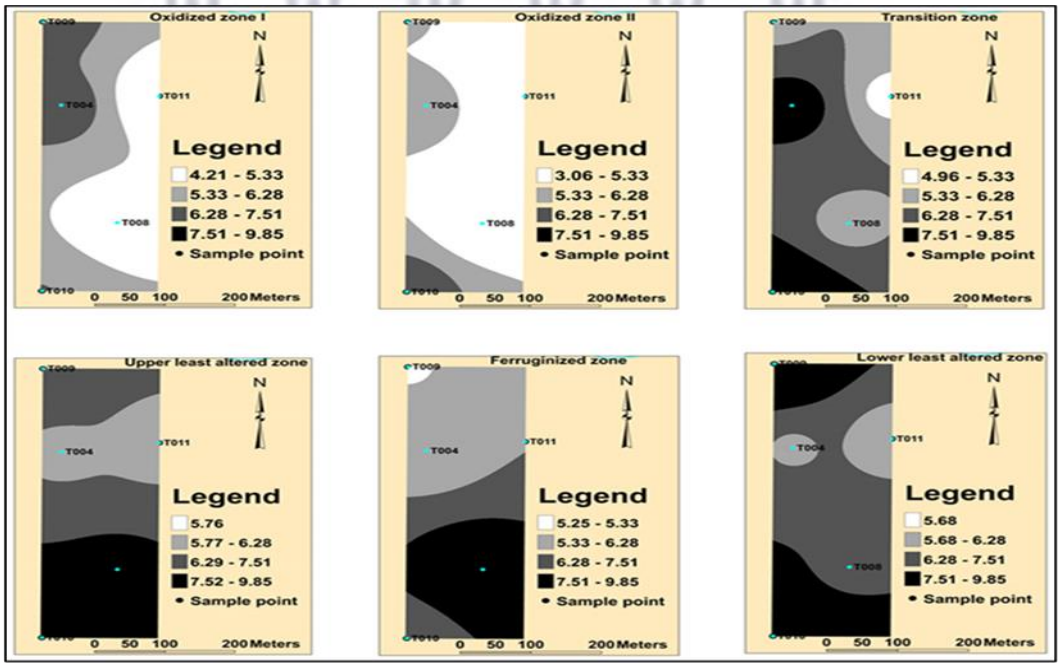

Figure 6.10: Downhole distribution pattern of Al2O3 using inverse weighted analysis

The overall distribution of SiO_2 and Al_2O_3 depict a decreasing and increasing trend down depth to the lower un–oxidised layer, respectively. In addition, the first two meters show the highest and lowest concentration in SiO_2 and Al_2O_3, respectively. This conforms to the multivariate statistical analysis.

6.7.2 Distribution of Total Sulphur (Sulphide–Group Trend)

The distribution of total sulphur (sulphide–group trend) in the layer down depth is illustrated in Figure 6.11. It is observed that the total sulphur content in the upper oxidised zone is smaller than the lower oxidised zone, despite having higher contents of SiO_2 in the lower oxidised zone. The total sulphur concentration detected in this zone demonstrates a significant trend down depth that depicts leaching pattern of sulphides as graphically depicted below.

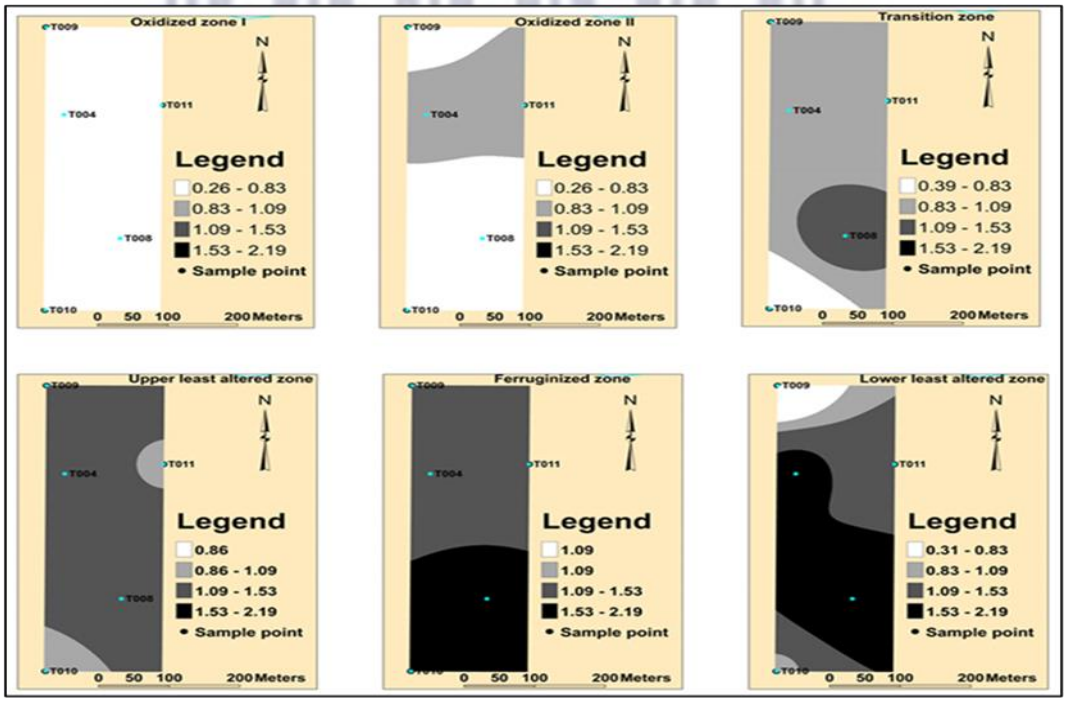

Figure 6.11: Downhole distribution pattern of TOT/S using inverse weighted analysis

At the upper oxidised layer, TOT/S concentration in depth fall within R1, which indicates a highly depleted surface. This indicates that the total area of tailings where this soil layer is collected contains lowest concentration of R1. At the lower oxidised layer, through the northwest to northeast of the tailing dam, the concentration of TOT/S increases and falls within R2, while other part of the

tailings dam still contains values/contents from R1 concentration range. Also, at the transition layer, the concentration of TOT/S reduces largely to R2 concentration range.

In the upper un–oxidised layer, the content of the total sulphur increases where larger area of the tailings dam falls within R3. In the ferruginised layer, the concentration of TOT/S increases in R3 and R4 at the northern and southern parts of the layer, respectively. In the lower un–oxidised layer, the concentration of TOT/S increases towards R4 through west to southeast of the tailings dam and decreases northward and southward. Therefore, this generally describes the distribution pattern of sulphides in the tailings.

6.7.3 Distribution Pattern of CaO (Carbonates)

The distribution pattern of the percentile values of CaO (carbonates) are graphically depicted in Figure 6.12. The percentile values are categorised as 0.06–0.30% within R1, 0.3–0.4% within R2, 0.4–0.54% within R3 and 0.54–2.75% within R4 in the upper oxidised zone. The presence of the CaO in this zone represents the carbonates group. In the upper oxidised zone, the northern part of the tailings contains high content of CaO in R4. And this could be attributed to precipitation of secondary minerals such as gypsum. The concentration of CaO in this layer decreases from north to south. On the other hand, CaO decreases in the lower oxidised zone but the larger area of the tailing dam contains concentration of CaO in R2.

In the transition layer, highest concentration of values within R4 are encompassed within the northeast area of the dam (around sample hole T011) and drifted towards the southeast of the tailing dam in upper un–oxidised layer. Also, the ferruginised layer exhibited content enrichment in R4 through its depth. This indicates that all boreholes contained highest content of CaO in R4, except borehole T011 without ferruginised layer.

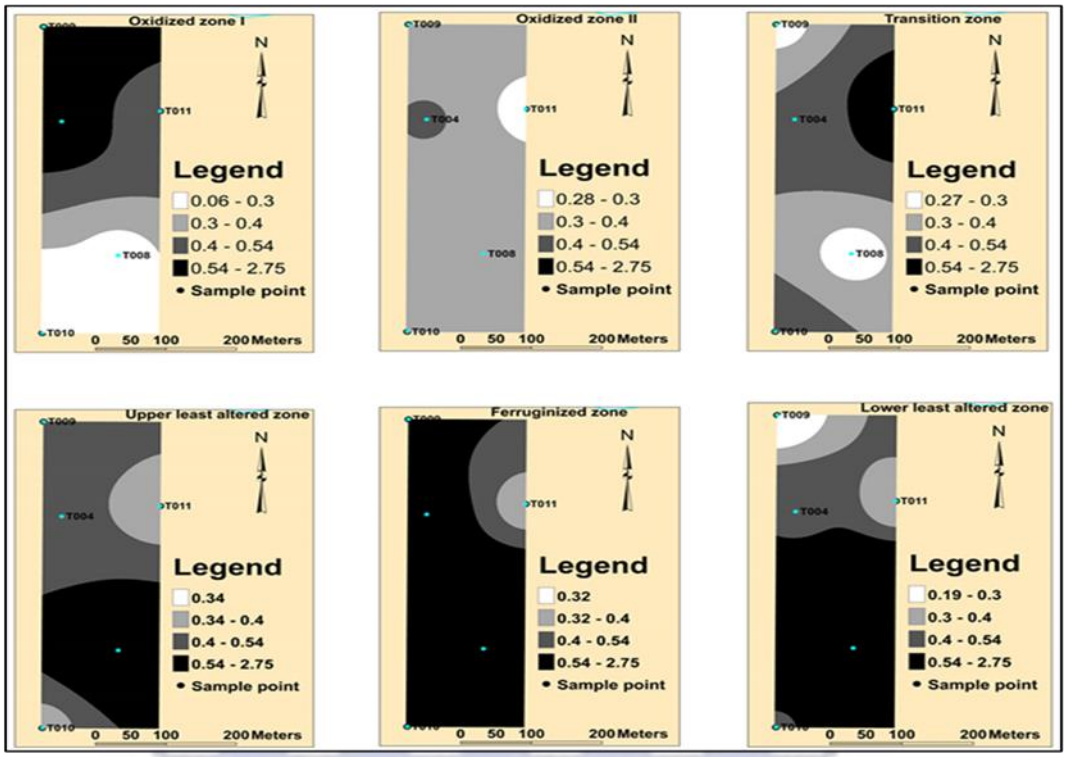

Figure 6.12: Downhole distribution pattern of CaO using inverse weighted analysis

The last two zones in the graph are upper and lower un–oxidised zones (upper and lower least altered zones). The chart shows that lower un–oxidised zone contains highest content of CaO within R4 in the south of the tailings, but decreases towards northern part as the unaltered tailings contained an elevated value of CaO. In that case, this insinuates that the initial tailings deposited contained carbonates, which could be attributed to addition of additives such as lime to increase the tailings neutralisation potential.

6.7.4 Distribution Pattern of Uranium (U)

Distribution pattern of uranium (U) percentile values are explicitly illustrated in Figure 6.13. Uranium (U) demonstrated similar distribution trend like TOT/S (Figure 6.11), and it emerges that both elements undergone the same leaching trend. In the graph, the upper oxidised layer exhibited complete depleted layer of U with minimum concentration values within R1. In the lower oxidised depth, the concentration of U increases towards R2 in a small portion of the layer, from the

upper northwest to northeast while other part remains R1. This demonstrates that U is leached in the oxidised layers.

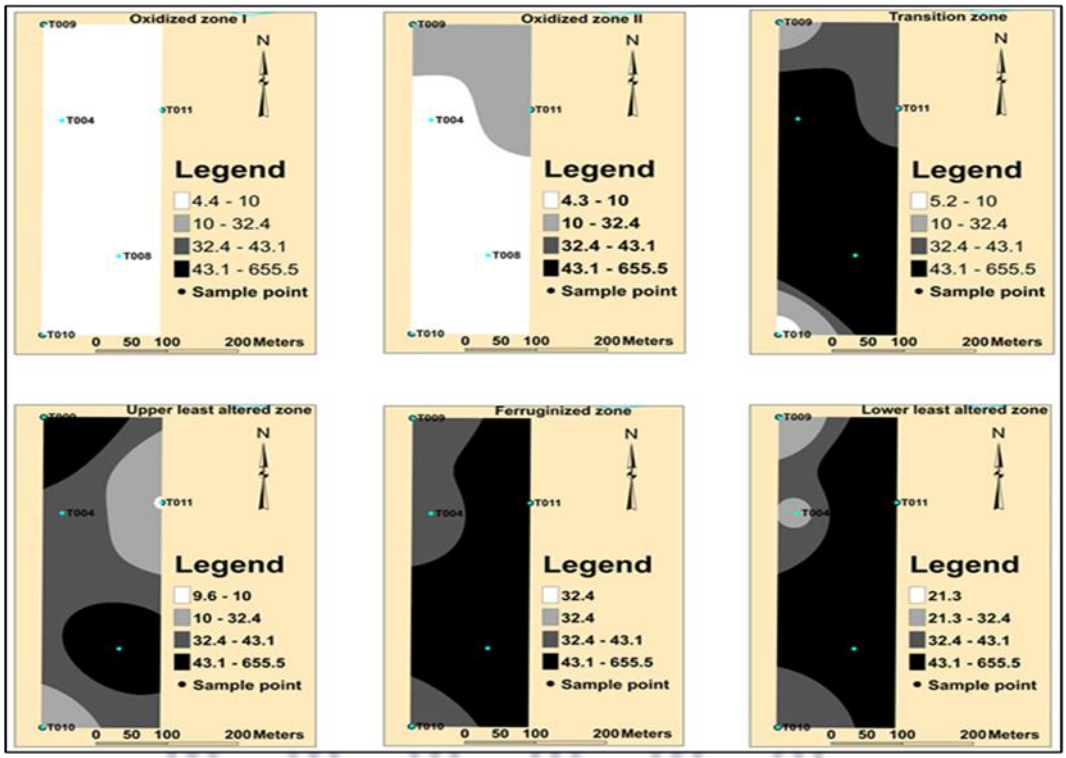

Figure 6.13: Downhole distribution pattern of U using inverse weighted analysis

In the transition layer, a sharp increase in U was observed, with larger and central parts of the layer containing R4. Unlike transition layer, area covered within R4 in the upper un–oxidised layer diminishes towards southwest of the tailings. On the other hand, concentration of U observed in the ferruginised layer was between R3 and R4. In this case, the layer is dominated by R4 and R3 was observed in northwest and southwest. And in the lower un–oxidised layer, area contained within R4 increases and forms a similar distribution pattern as illustrated in ferruginised layer. Although, proportion of R4 in this layer is lesser, and it contains lower contents in northwest and southwest.

6.7.5 Distribution Pattern of Gold (Au)

Distribution pattern of Gold (Au) is illustrated in Figure 6.14 from oxidised zones to transition zone and extended to ferruginised zone and un–oxidised zones. Au associates with elements such as sulphides, CaO and Fe2O3. More so, Au

demonstrated no specific distribution trend like TOT/S. And the element exhibited no association in factor analysis. In the graph, upper oxidised layer exhibited a decreasing trend of Au from the northwest R4 to the southwest R1. This effect could be due to leaching impact in the areas with lower concentration. In the lower oxidised layer, a shift was noted as the concentration of Au within R3 drifted towards the southeast of the layer.

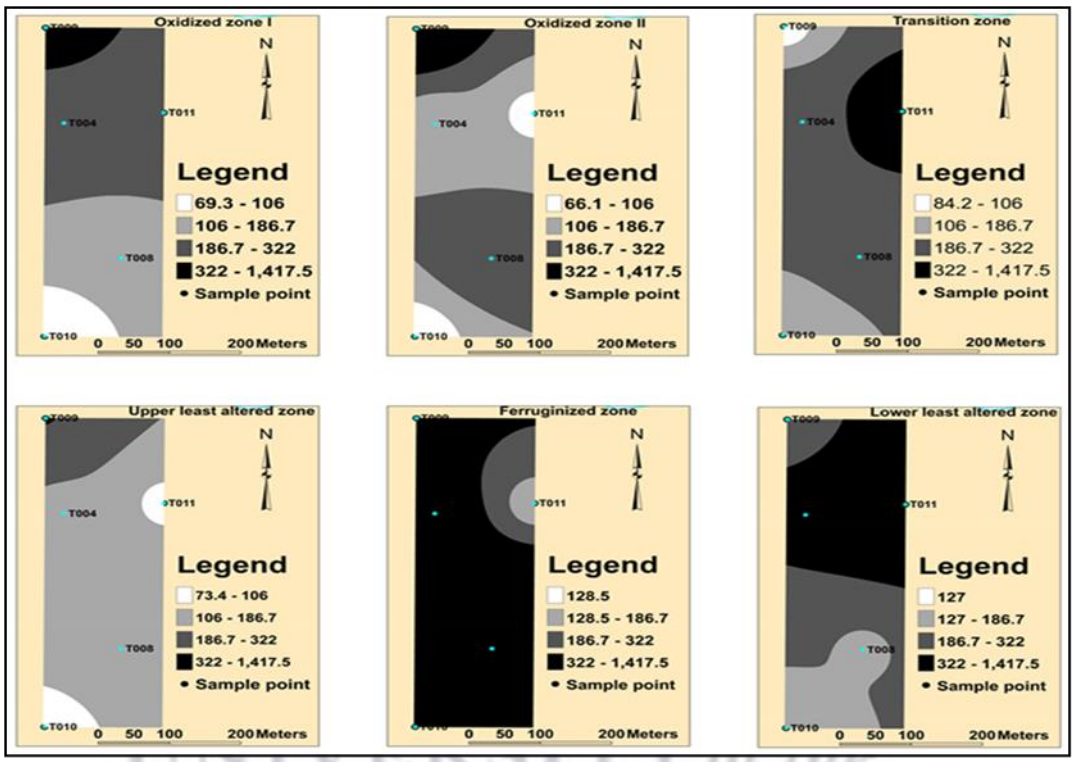

Figure 6.14: Downhole distribution pattern of Au using inverse weighted analysis

In the transition layer, a larger area containing R3 was noted with an increase in Au concentration. Interestingly, upper un-oxidised layer exhibited an extremely low content of Au than any other layer, with larger area containing R2. On the other hand, the ferruginised exhibited a high enrichment of Au (R4). This finding is in conformity with the multivariate analysis and GMB in revealing the enrichment of the ferruginised layer in Au. Also, lower un-oxidised layer exhibited enrichment in Au, wherein R4 is contained in the northern part and diminished towards R3 and R2 southward. Therefore, lower un-oxidised layer demonstrated high concentration of Au compared to other layers, except ferruginised layer.

6.8 The Geochemical Mass Balance (GMB) Prediction Model

The GMB prediction model was used to predict the rate of AMD generated over the period of the tailing dam existence. The formula used was Alteration rate = Σ^{i}_{n} $\Delta Ci/T$.

where:

ΔCi = loss or gain in concentration for element I,

T = estimated time in years (e.g., 50 years in which the tailing dam has been abandoned),

n = number of elements analysed for,

i = element analysed for, and

Σin = summation of the alteration rate of n elements used in the study.

Table 6.6: Rate of AMD generated in relation to time

Analysis	Layer 1	Layer 2	Layer 3	Layer 4
Cal. Rate (kg/ton)	-6.321	-2.195	13.872	-1.228
Max ΔCi	-6.610	-2.467	-0.293	-2.976
Min ΔCi	0.289	0.272	14.165	1.748
Av. Rate kg/tonne/year)	-0.122	-0.042	0.267	-0.024

Afterwards, the average of the alteration rate is computed to obtain the predicted rate of depletion or enrichment in layers. According to the values presented in Table 6.6, 0.122% and 0.042% of elements in layers 1and 2 are loss yearly, respectively. In contrast, layer 3 shows a noticeable enrichment, which indicates that certain portion of elements leached from layer 1 and 2 are trapped within the layer 3. Therefore, this could insinuate that 0.164% (±0.02%) of the tailing dam is leached yearly.

6.9 Conclusion

Minerals identified in this study conform to those commonly found in ores and tailing dams of the Witwatersrand basin (Tutu et al., 2008). Heavy metals and metalloids distribution as well as concentration in seepage and pore waters principally depend on the deposit geology (Heikkinen et al., 2009). The level of quantity of heavy metal pollution around mines is subjected to the degree of mineralisation and geochemical characteristics of the tailings (Navarro et al., 2008).

The most prominent major oxides contained in the Mogale tailings are SiO_2, Al_2O_3, Fe_2O_3 and volatiles (LOI).

Close to 0.2 % weight of total carbon content is indicative of a significant content of organic matter in the mine tailings (Rösner & Van Schalkwyk, 2000). The presence of total sulphur ranges from 0.26–2.19%, and this points to a significant potential acid generating capacity of the tailings dam (Nengovhela et al., 2006). Low total sulphur in the uppermost layer suggests an extensive depletion in sulphides in the horizon.

The overall low pH recorded in the tailing samples points to an acidic environment, which is advantageous in generating of AMD (Navarro et al., 2008). Tailing dams in Witwatersrand basin often contain elevated levels of radioactive and chemo-toxic heavy metals (Durand, 2012) (Table 6.2). The contents of U, Hg, As, Co, Cu, Pb, Zn, and Ni in Table 6.2 are significantly higher than permissible in mine waste (Hobbs & Cobbing, 2007). The enrichment of chalcophile elements, gold and uranium in layer 3 may be due to changing redox conditions down depth (Winde et al., 2004). The high contents of Au and U in the layer 3 can become a resource of economic attraction, which could incur profit in reprocessing the tailing dam and facilitate reclamation of the site (Akcil & Koldas, 2006).

Elemental associations and inter–relationship patterns of identified elements were determined by multivariate statistical analysis tools to evaluate the distribution pattern of the potential leachable heavy metals' loads and the risk of heavy metals' loads present in the tailings dam (Guagliardi et al., 2012). This analysis involved both the cluster and factor analyses.

Two main clusters were observed and sub–divided into two sub–clusters each, which yielded four clusters for samples clarity. Samples in cluster 1 are commonly defined by high content in SiO_2, while those in cluster 2 are low in SiO_2, but enriched in Al_2O_3. The relative abundance of SiO_2 for the cluster was defined as follows: sub–cluster 1>sub–cluster 1b>sub–cluster 2b>sub–cluster 2a (as defined by the discriminant analysis). Samples that are classified in cluster 1 are mainly found in the first 3 meters of the tailings. Further Canonical discriminant analysis highlights the major variables that defines the structure or composition of each sub–

clusters. The variables were highlighted by factors that are responsible for the compositional pattern of the tailings dam using factor analysis.

The factor analysis revealed the source of the major constituents in the tailing dam. For example, factor 1 exhibited positive score for CaO and revealed the presence of silicate minerals as well disclosed other additives during mineral processing. The positive score for CaO revealed the presence of additives products during mineral processing, such as CaSO4. These additives, mostly lime, are added to buffer acid generating potential of the sulphide minerals before disposing the mine tailings (Hobbs & Cobbing, 2007). Factor 2 with positive scores for Fe_2O_3, Sb and Au showed the presence of Au enrichment in certain layers and its association with Sb and Fe_2O_3. Factor 3 with positive score for total sulphur underpins the influence of sulphides on the distribution of chalcophile elements. Factor 4 with positive score for Al_2O_3 underpinned the enrichment of clays with depth. Factor 5 with positive scores for Zr and TiO_2 is associated with the presence of refractory titanium-rich minerals in ore (Hobbs & Cobbing, 2007). Factor 6 with positive score for Cr_2O_3 revealed the presence of Cr in slight quantity. Factor 7 with positive scores for TOT/S, Cu and P_2O_5 demonstrated that possible source of the sulphide of Cu differs from other sulphides.

The IDW interpolation analysis reflects the distribution pattern of elements down depth, and their relative behaviour based on the factor analysis (A. Parbhakar-Fox et al., 2013), which complement the statistical results. Essentiality of knowledge of the elemental distribution pattern assisted in understanding general trend of mobile and non-mobile elements and species in tailing dam sampled. The high concentration of SiO_2 accompanied with low concentration of Al_2O_3 and TOT/S in the first two meter depicts depletion in layer 1, as well confirms the distribution pattern of elements.

Sulphides and uranium demonstrate a distinct depletion trend, which indicates surface exposure to extensive leaching that has indicated the high mobility. The high presence of CaO in the first meter could be due to carbonates formed from neutralisation process and deposited as salts. There is enrichment of sulphides, carbonates and Al_2O_3 coupled with low SiO_2 at the ferruginised layer. This layer is

probably a sink for elements emanating from the upper layers. This could be because of the transportation of elements downwards, which often leads to retention of these elements by precipitation of secondary minerals, such as hematite and/or pH-controlled sorption processes (Dold & Fontboté, 2002). This could be due to increase in clay, which leads to decrease in porosity.

From the IDW interpolation, it can be suggested that tailings can be economically viable if assessed for U and Au, as well viable for reclamation. This implies that, the tailing dam could be said to be uraniferous-gold tailings. The geochemical mass balance results show a variable loss and gain in the contents of major oxides and trace elements in each horizon and down depth (illustrated in Figure 6.7 and Figure 6.8). The results further show that major oxides and trace elements loss is highest in the topmost layer, where the weathering is most intense and decreases down depth. This implies a change in the redox conditions with depth, from an upper oxidised zone with reddish colour through a brownish zone to a greyish basal zone.

Since Mogale tailing was built in 1952 and given a period of 2 years of depositional time, it was assumed that any prominent oxidation process starts 60 years ago. Table 6.4 demonstrated that layer 1 is the most leached surface, with about 0.122% of the layer leached yearly. Layer 3 exhibited high presence of clayey materials and extreme low value in SiO_2 as compared to other layers. This increases its retention capacity leading elements deposition. Elements leached downward are trapped within the third layer. This accounted for the highly moisturised layer 4, since leachates cannot drain out easily.

Ultimately, a large proportion of the tailings have been leached. The AMD leachates have been transported away along pathways of the slope of the dam. It should be noted that the steepness of the tailing determines the efficiency of the transport of AMD leachates.

CHAPTER SEVEN

7. PREDICTION TEST

7.1 Introduction

This chapter presents analysis results of the static and kinetic tests performed to predict the potential acid generation of samples. The results are supported with the mineralogical and geochemical analyses to develop a conceptual modelling for gold tailings AMD prediction. The lab prediction tests include Paste pH and EC, Acid-Base Accounting and leach column test. The tests and results are respectively described in the subsequent sections.

7.2 Paste pH and EC

Paste pH and EC were prefaced earlier in Chapter 4, which is said to be determined through sample equilibrate in deionised water ration procedure. In this section, paste pH is used to measure the natural pH of the sample after adding water. And paste pH and EC values are measures of the natural acid-base properties of the sample. Paste pH normally is performed before ABA to generate information on existed acidity of the samples.

Fifty-One and Twenty-Eight raw samples collected from the Mogale and Gold One_1 tailings were tested to generate the paste pH and EC values for different layers' samples. Table 7.1 shows paste pH and EC values for different layer's sample collected from Mogale tailings. The paste pH and EC values were arrayed according to sample holes' labels, from the top layer to the bottom layer. Holes tested are T004, T008, T009, T010 and T011. Graphical illustrations of the paste pH and EC values derived for samples collected from the five holes are given in Figure 7.1 and Figure 7.2.

According to Figure 7.1, the distribution of pH values across the five holes varied. Some holes contained higher pH values, such holes as T008, T009 and T011. In the hole T004, observation shows that paste pH values are obtained from the top layer

Table 7.1: Paste pH and EC value for Mogale tailings samples

Hole T004	038	039	040	041	042	042-1	043	044	045	046		
pH	4.41	3.32	3.84	3.9	3.61	2.96	3.64	3.79	3.93	4.63		
EC	0.84	1.71	0.87	1.02	1.23	1.63	1.53	1.13	1.2	0.95		
Hole T008	001	002	003	004	005	006	007	007-1	008	008-1	008-2	009
pH	4.33	3.49	2.99	3.45	2.91	3.27	6.66	6.82	6.22	4.96	6.28	5.29
EC	0.57	0.74	3.99	2.17	2.83	3.44	0.61	1.67	0.89	1.05	0.87	1.03
Hole T009	010	011	012	013	014	015	016	017	018	018-1	019	
pH	3.52	3.37	3.88	4.41	4.69	3.63	3.01	2.86	4.43	3.55	7.92	
EC	1.19	1.44	1.22	0.76	0.88	2.1	1.7	2.35	1.1	1.5	1.18	
Hole T010	020	021	021-1	023	024	025	026	027-1	028			
pH	4.73	3.12	3.73	4.1	3.97	4.4	3.57	2.88	4.74			
EC	0.46	0.63	0.43	0.7	0.78	0.95	0.71	2.34	1.13			
Hole T011	029	030	031	032	033	034	035	036	037			
pH	2.99	6.31	7.48	8.02	5.68	2.61	6.35	6.02	8.69			
EC	3.24	0.91	0.84	0.61	0.6	1.07	0.6	0.59	0.57			

to 9 meters depth of the tailings. For hole T004, the paste pH values are arrayed from 2.96 to 4.63. Similarly, hole T008 contained paste pH values from 2.91 to 4.33, which were observed from the top tailings to 6 meters depth and 6.22 to 6.82 paste pH values were observed from 7 meters layer as illustrated in the graph below. Also, a paste pH value of 4.96 was observed in the ferruginised layer, which is close to the unoxidized layers of the hole with paste pH values of 6.28 and 5.29, respectively (Table 7.1). The paste pH structure observed in hole T009 is similar to the paste pH structure in hole T004. In hole T009, paste pH values from 2.86 to 4.69 were observed from the top tailings to 9 meters deep. And a high paste pH value of 7.92 is observed at 10 meters layer.

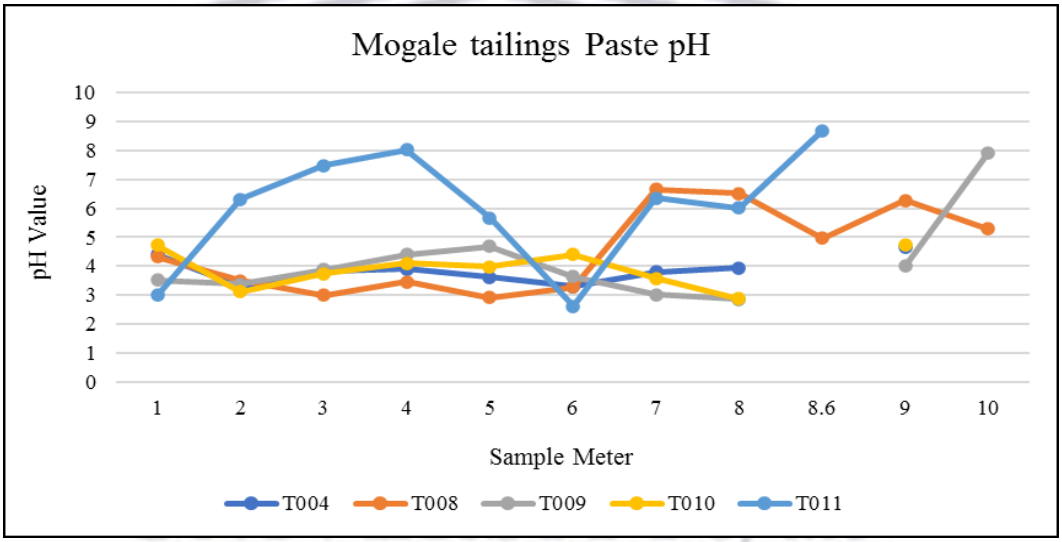

Figure 7.1: Paste pH results for Mogale tailings samples

Hole T010 is drilled up to 9 meters deep, where paste pH values from 2.88 to 4.47 are all acidic. Among the top tailings soil, only hole T011 demonstrated lower paste pH values of 2.99. The downward layers of the dam exhibited high pH value except at the 6 meters layer, where paste pH value is 2.61. The deductions gather from illustration indicate that samples collected from Mogale tailings are acidic.

Figure 7.2 illustrates the values observed from the paste EC test performed on the samples collected from the five holes as similarly done in the paste pH test. The EC test results demonstrate changes and trends observed in the values derived across the different sample layers collected from Mogale tailings. The paste pH values

discussed earlier offer a basic assessment of acidity and alkalinity of the samples. Generally, if the paste pH<5, the sample is likely to produce acid.

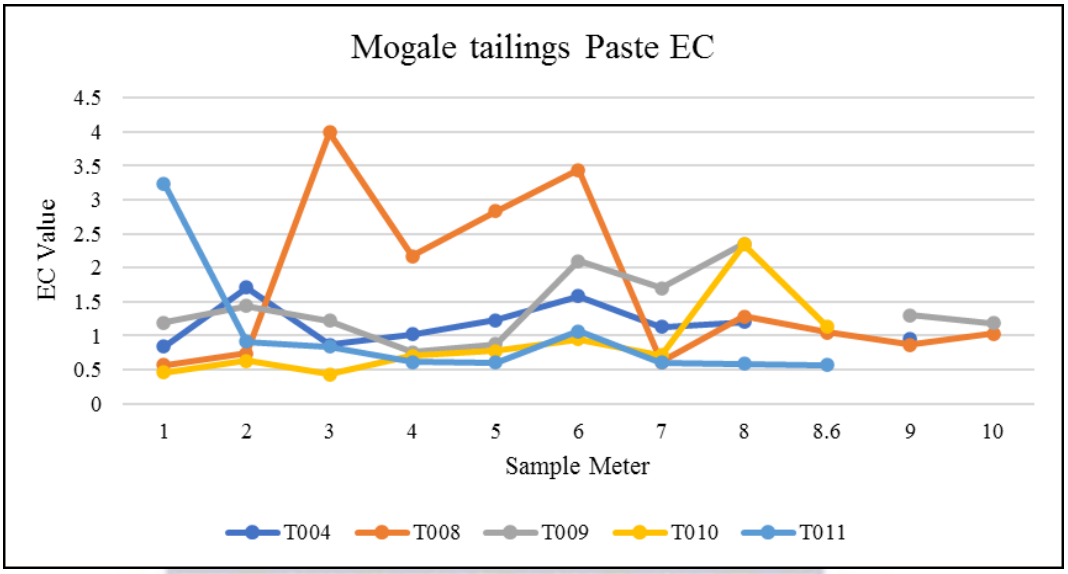

Figure 7.2: EC value for Mogale tailings samples

In Figure 7.2, highest value of paste EC (3.99) is observed in hole T008, at 3 meters away from the top layer, followed by paste EC value of 3.44 at 6 meters away from the top layer in the same hole. Hole T011 also contained a paste EC value above 3.00 at the top layer sample and the top layer of the tailing dams are oxidised with acidity concentration. Essentially, the paste pH and EC values of the samples from Mogale tailings shows that under the same conditions, the acidity of different samples can be characterised as the acidity or alkalinity.

In Gold One_1 tailings, only three holes were tested for paste pH and EC unlike in Mogale tailings. In this case, hole T001 and hole T003 contained predominantly higher paste pH values across the tested layers within some certain lengths (in meters) as indicated in Figure 7.3.

Table 7.2 presents an array of paste pH and EC results for the samples collected from borehole T001, T002 and T003 of Gold One_1 Tailings. The distribution of the values across the tested samples of layers collected from different holes in Gold One_1 varied.

Table 7.2: Paste pH and EC value for Gold One_1 tailings samples

Hole T001	048	049	050	052	053	054	055	056	057	058
pH	5.16	2.92	3.89	5.71	4.38	7.64	8.32	8.4	8.3	8.29
EC	0.21	1.01	0.99	1.14	0.94	0.54	0.56	0.53	0.53	0.53
Hole T002	059	060	061	062	063	064	065	066	067	
pH	3.97	3.18	3.93	3.84	3.69	4.13	3.97	8.11	8.23	
EC	0.53	1.27	0.82	0.89	0.89	1.28	1.09	0.56	0.69	
Hole T003	068	069	070	071	072	073	074	075	076	
pH	7.44	8.14	8.08	8.2	8.4	8.05	3.82	4.86	4.59	
EC	0.72	0.79	0.72	0.6	0.73	0.85	0.63	0.63	0.71	

In ascending order, by observing Figure 7.3, paste pH values obtained by testing samples of layers collected from hole T001 are from 2.92 to 5.71 within a length of 0.2 meter and 5 meters. Additional deductions indicate that paste pH values from 7.64 to 8.4 were observed within 6 meters and 10 meters. Similar to hole T001, paste pH values obtained in hole T002 exhibited acidity concentration, from 3.18 to 4.13 within 0.2 meter and 6 meters. From 7 meters downward, paste pH values of 8.11 and 8.23 were observed. In hole T003, samples tested contained higher pH values (7.44 to 8.40) from the top layer to 5 meters as illustrated in the graph. Lower paste pH values (3.82 to 4.86) were observed from 6 meters to 8 meters deep, which indicates acidic concentration level.

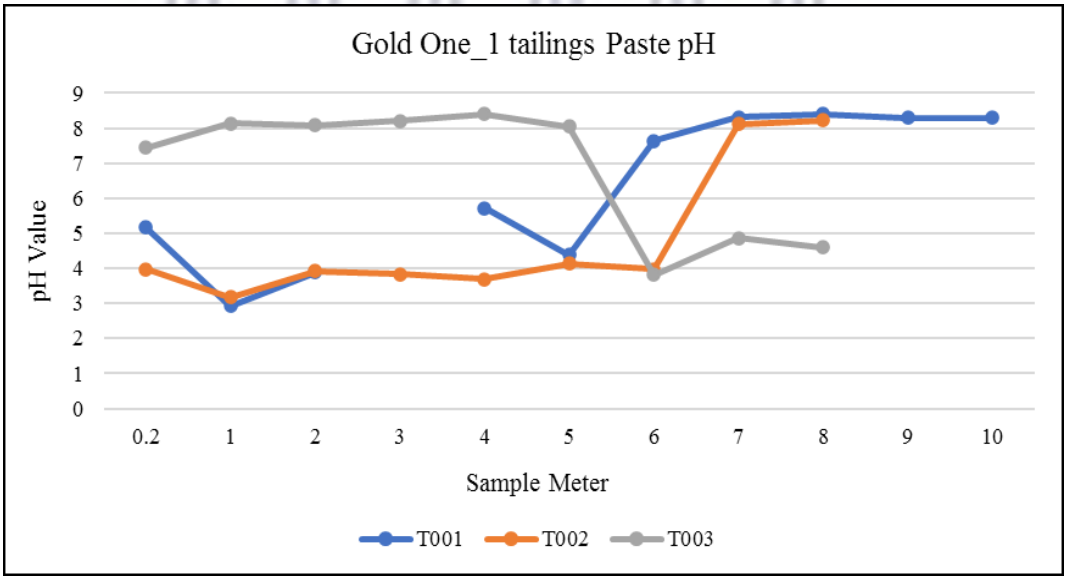

Figure 7.3: Paste pH results for Gold One_1 tailings samples

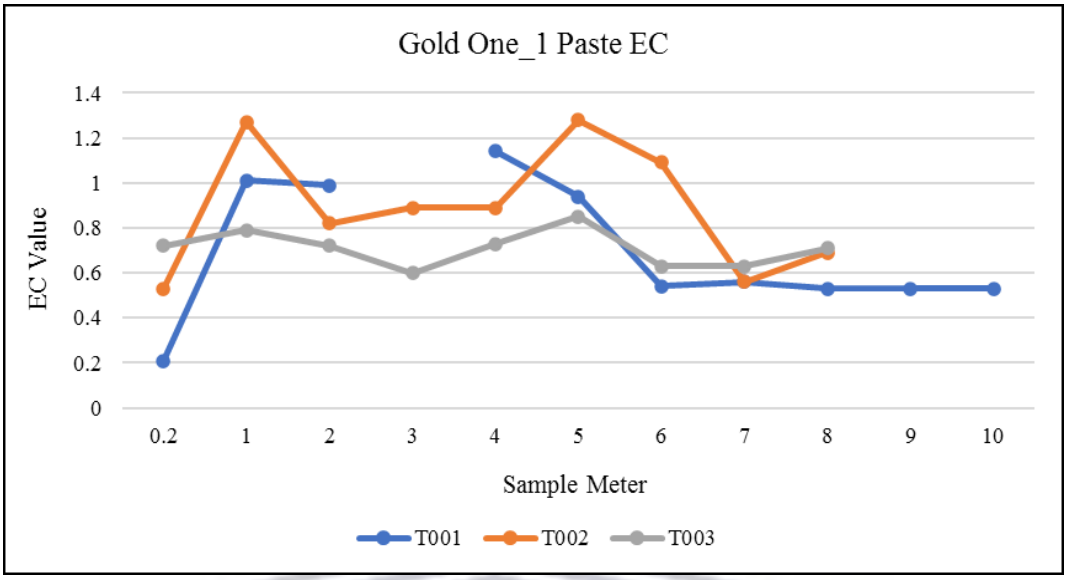

Figure 7.4: EC value for Gold One_1 tailings samples

In Figure 7.4, the graphical illustration of EC values across the three holes tested shows changes and trends of EC values at different layers of Gold One_1 tailings in line with changes and trends demonstrated by pH values in Figure 7.3. Higher values of paste EC is observed in hole T002, with 1.27 and 1.28 detected at one meter and 5 meters. Hole T001 yielded the lowest paste EC value of 0.21 at the top layer.

7.3 Acid-Base Accounting (ABA)

A concise description of ABA was earlier presented in Chapter 2 as a "measure of the total sulphur and total carbon contents in a sample (Dold, 2005)." Explicably, Stewart (2005) mentioned that ABA encompasses an acid-neutralising capacity from an utmost potential acidity of a sample. In this section, ABA is applied in accordance with the aforesaid descriptions. The approach is applied to analyse the topsoil samples by measuring the total acidity and alkalinity of the samples (Sobek et al., 1978). In the process, MPA (calculated by total sulphur) is considered as the actual potential acidity generation if sulphur containing in the rock is in form of sulphide pyrite. However, the total sulphur in the actual sample contains not only pyrite, but also other forms of sulphide, sulphate, and organic sulphur. The results calculated could be higher than ability of the actual potential acidity. The acid generation capacity is determined by the neutralisation of the acid by the alkaline

substances during the acid generation process of the minerals. The net acid production potential (NAPP) is the result of the remaining acidity after the reaction of the acidic and alkaline substances.

MPA (kgH2SO4/t) = (TOT/S - Sulphate S) = % Sulphide * 30.6 ..... Equation 7.1

NAPP = MPA – ANC .....…… Equation 7.2

In the Equation 7.1, 30.6 is a stoichiometric factor based on the chemical reaction formula of pyrite oxidation to produce acid. A negative value of NAPP indicates that the alkaline substance of the sample has a greater ability to neutralise acid than the ability to produce acid; therefore, it will not produce acidic substance emissions. Alternatively, a positive value of NAPP indicates that the sample has net acid production potential; therefore, it will produce acidic substance emissions. The units of MPA, ANC and NAPP is kgH_2SO_4/t.

7.3.1 Acid Neutralisation Capacity (ANC)

Laboratory experiment was performed to determine the ANC of the samples analysed. In this process, 14 samples collected from Mogale tailings were analysed together with 10 samples collected from Gold One_1 tailing. Two titrants were used for titration process in this experiment, which are 0.1M NaOH and 0.5M NaOH preparations. Further discussion on the titration process is given below.

- **0.1M NaOH standard titrant**

Weigh 110g NaOH and dissolve in 100ml carbon dioxide–free distil water and shake well. Then, pour the mixture into a polyethylene container and place it in a sealed container until the solution is reached. Use a plastic tube to measure the supernatant (as indicated in Table 7.3) and dilute up to 1000ml with carbon dioxide–free distil water. Then, shake thoroughly.

Table 7.3: Titration regulation for NaOH solution

Concentration of NaOH standard titrant [c(NaOH)]/(mol/L)	Volume of NaOH solution (V/mL)
1	54
0.5	27
0.1	5.4

Weigh potassium hydrogen phthalate (see the Table 7.4 standard weight), which was dried to constant weight in an electric oven at 105℃–110℃ (as indicated in Table 7.4). Add carbon dioxide–free distil water and dissolve it with two drops of phenolphthalein indicator solution (10 g/L). Titrate with the prepared NaOH until the solution displays pink and keep it for 30 seconds. And the blank test is done at the same time.

Table 7.4: Titration regulation for NaOH solution with the mixture Potassium Hydrogen Phthalate and Carbon Dioxide–Free Water

Concentration of NaOH standard titrant [c(NaOH)]/(mol/L)	Potassium Hydrogen Phthalate m/g	Carbon Dioxide–Free Water V/mL
1	7.5	80
0.5	3.6	80
0.1	0.75	50

Concentration of NaOH standard titrant [c(NaOH)] (mol/L),

$$c(\text{NaOH}) = \frac{m \times 1000}{(V_1 - V_2)M} \quad \text{..... Equation 7.3}$$

Where:

m = mass of potassium hydrogen phthalate (g),

V_1 = volume of NaOH solution (mL),

V_2 = volume of NaOH solution in the black test (mL), and

M = value of molar mass of potassium hydrogen phthalate (g/mol) [$M(KHC_8H_4O_4)$ = 204.22].

- **0.5M HCl standard titrant**

Measure HCl (as indicated in Table 7.5), pour it into 1000ml distil water. Then, shake thoroughly.

Table 7.5: Titration regulation for HCl solution

Concentration of HCl standard titrant [c(HCl)]/(mol/L)	Volume of HCl solution V/mL
1	90
0.5	45
0.1	9

Weigh the reagent anhydrous sodium carbonate, which was burned to constant weight in a high temperature furnace at 270℃–300℃ (as indicated in Table 7.6).

And then, dissolved it in 50ml of distil water and add 10 drops of bromocresol green-methyl red indicator solution. Titrate with the prepared HCl solution until the solution turns from green to dark red. Boil for 2 minutes and continue to titrate after cooling until the solution turns dark red again. Do a blank test at the same time.

Table 7.6: Titration regulation for HCl solution with Anhydrous Sodium Carbonate

Concentration of HCl standard titrant [c(HCl)]/(mol/L)	**Anhydrous sodium carbonate m/g**
1	1.9
0.5	0.95
0.1	0.2

Concentration of HCl standard titrant [c(HCl)] (mol/L),

$$c(HCl)=\frac{m \times 1000}{(V_1 - V_2)M}$$ ..... Equation 7.4

Where:

m = mass of anhydrous sodium carbonate (g),

V_1 = volume of HCl solution (mL),

V_2 = volume of HCl solution in the black test (mL), and

M = the value of molar mass of anhydrous sodium carbonate (g/mol [M ($\frac{1}{2}Na_2CO_3$) = 52.994].

ANC is the key calculation for ABA. The method of Sobek et al. (1978) is the earliest systematic acid-base calculation method.

$$ANC = (Y \times \frac{M_{HCl}}{wt}) \times C$$ ..... Equation 7.5

ANC test results for the samples collected from Mogale and Gold One_1 tailings are arrayed in Table 7.7. In the table, the negative values of ANC are due to the acid waste generated in the samples during acid-base titration process. In the process, NaOH is consumed, which lower the values computed for ANC.

Table 7.7: ANC test results

Sample	HCl	HCl	pH	NaOH	pH5.0	pH7.0	NaOH titrated	C	ANC (kgH2SO4/t)
038	0.5	8	1.34	0.1	41.46	0.53	41.99	49.0	3.3565
038-1	0.5	8	1.45	0.1	44.19	0.57	44.76	49.0	-2.891
038-2	0.5	8	1.44	0.1	44.49	0.72	45.21	49.0	-3.908
039	0.5	8	1.48	0.1	42.62	0.83	43.45	49.0	0.061
039-1	0.5	8	1.47	0.1	57.29	2.42	59.71	49.0	-36.591
040	0.5	8	1.37	0.1	50.74	1.22	51.96	49.0	-19.122
041	0.5	8	1.43	0.1	49.16	1.75	50.91	49.0	-16.746
042	0.5	8	1.34	0.1	47.57	1.69	49.26	49.0	-13.034
042-1	0.5	8	1.23	0.1	64.17	2.48	66.65	49.0	-52.234
043	0.5	8	1.24	0.1	48.46	1.40	49.86	49.0	-14.382
044	0.5	8	1.05	0.1	50.88	2.01	52.89	49.0	-21.217
045	0.5	8	1.38	0.1	55.12	1.79	56.91	49.0	-30.270
046	0.5	8	1.40	0.1	50.55	1.43	51.98	49.0	-19.159
047	0.5	8	1.40	0.1	49.68	1.35	51.03	49.0	-17.028
048	0.5	8	1.26	0.1	47.19	0.90	48.09	49.0	-10.400
049	0.5	8	1.25	0.1	47.12	1.39	48.51	49.0	-11.344
050	0.5	8	1.24	0.1	47.10	1.97	49.07	49.0	-12.605
052	0.5	8	1.27	0.1	45.07	1.42	46.49	49.0	-6.787
053	0.5	8	1.29	0.1	45.15	2.66	47.81	49.0	-9.763
054	0.5	8	1.15	0.1	40.15	1.04	41.19	49.0	5.157
055	0.5	8	1.24	0.1	39.59	1.89	41.48	49.0	4.508
056	0.5	8	1.13	0.1	40.11	2.29	42.40	49.0	2.426
057	0.5	8	1.10	0.1	39.7	1.30	41.00	49.0	5.586
058	0.5	8	1.14	0.1	46.94	1.29	48.23	49.0	-10.707

7.3.2 Maximum Potential Acid (MPA)

A concise description of MPA was presented in Chapter 4. MPA is calculated by Total Sulphur (Total/S) weight percentage of each sample received by XRF analysis and Sulphate–Sulphur as the process depends sulphide–sulphur, which is measured by Scientific Service C.C in Cape Town. The results computed for Sulphate and Sulphide of Mogale tailings samples are tabularised in Table 7.8. The three negative values in the last column of the table indicates that the corresponding samples were collected from 3-5 meters of borehole.

Table 7.8: Mogale tailings sulphate and sulphide calculation

Sample	Sulphate in 1ml (ppm)	Sulphate * V/g (45/2) ppm	% Sulphate	% Total Sulphur by XRF	% Sulphide
038	117.303	2932.575	0.2932575	0.44	0.15
039	182.3905	4559.7625	0.4559763	1.03	0.57
040	666.6965	16667.4125	1.6667413	1.02	-0.65
041	604.8205	15120.5125	1.5120513	1.08	-0.43
042	527.684	13192.1	1.31921	1.29	-0.03
042-1	327.143	8178.575	0.8178575	1.49	0.67
043	136.0715	3401.7875	0.3401788	1.2	0.86
044	496.3775	12409.4375	1.2409438	1.34	0.10
045	395.1325	9878.3125	0.9878313	1.58	0.59
046	290.719	7267.975	0.7267975	1.72	0.99

Table 7.9: Gold One_1 tailing sulphate and sulphide calculation

Sample	Sulphate in 1ml (ppm)	Sulphate * V/g (45/2) ppm	% Sulphate	% Total Sulphur by XRF	% Sulphide
048	3.76	84.54	0.01	0.01	0.00
049	78.58	1768.16	0.18	1.19	1.01
050	382.88	8614.87	0.86	2.04	1.18
052	161.59	3635.74	0.36	1.03	0.67
053	254.48	5725.70	0.57	1.41	0.84
054	69.52	1564.11	0.16	0.78	0.62
055	63.39	1426.18	0.14	0.83	0.69
056	89.29	2008.96	0.20	0.78	0.58
057	113.51	2553.94	0.26	0.92	0.66
058	20.78	467.47	0.05	0.81	0.76

Similar approach is applied to compute % Sulphide of the samples collected from Gold One_1 tailing. The results gathered are tabularised in Table 7.9. In this case, the values computed for % Sulphide are positive.

The % Sulphide results computed collected from both Mogale and Gold One_1 tailing were pooled to compute MPA results for each tailing sample. MPA values obtained are arrayed in Table 7.10. MPA is calculated by multiplying % Sulphide

of each sample by a constant factor (30.6) as illustrated in Equation 7.1. In the table, sample 048 yielded zero MPA, while samples 0.40, 041 and 042 still yielded negative MPA values. Further observation indicates that samples 044 and 0.38 yielded the lowest positive MPA values. Samples 046, 049 and 050 yielded MPA values >30. The results provided in the table below are prepared for NAPP calculation and prediction of acid production.

Table 7.10: Mogale and Gold One_1 tailings MPA calculation results

Sample	Sulphide	Factor	MPA = % Sulphide * 30.6
038	0.15	30.6	4.59
039	0.57	30.6	17.442
040	-0.65	30.6	-19.89
041	-0.43	30.6	-13.158
042	-0.03	30.6	-0.918
042-1	0.67	30.6	20.502
043	0.86	30.6	26.316
044	0.10	30.6	3.06
045	0.59	30.6	18.054
046	0.99	30.6	30.294
048	0.00	30.6	0.00
049	1.01	30.6	30.906
050	1.18	30.6	36.108
052	0.67	30.6	20.502
053	0.84	30.6	25.704
054	0.62	30.6	18.972
055	0.69	30.6	21.114
056	0.58	30.6	17.748
057	0.66	30.6	20.196
058	0.76	30.6	23.256

7.3.3 Net Acidic Production Potential (NAPP) Results

By subtracting ANC from MPA we obtained NAPP as illustrated in Equation 7.2. Basically, it means that the difference between MPA and ANC produces NAPP. ANC values in the table are results derived from lab experiments performed on the tailings' samples (Table 7.7). The NAPP values obtained after subtracting ANC from MPA for the samples collected from Mogale and Gold One_1 tailing is arrayed in Table 7.11 and Table 7.12.

In Table 7.11, it is observed that sample 040, collected from 3 meters depth of borehole in Mogale tailing, yielded a negative NAPP value (-0.768 kgH_2SO_4/t), while other samples yielded positive NAPP values. Among the samples with positive NAPP values, only sample 042_1 yielded highest NAPP values (72.736 kgH_2SO_4/t). This result indicates that this particular tailing sample is most possibly

to produce acid. And from 5.4 meters downward the borehole, NAPP value is also positive and high.

Table 7.11: NPAA results of Mogale tailings samples.

Sample Number	MPA	ANC	NAPP
MT038	4.59	3.3565	1.2335
MT039	17.442	0.061	17.381
MT040	-19.89	-19.122	-0.768
MT041	-13.158	-16.746	3.588
MT042	-0.918	-13.034	12.116
MT042-1	20.502	-52.234	72.736
MT043	26.316	-14.382	40.698
MT044	3.06	-21.217	24.277
MT045	18.054	-30.27	48.324
MT046	30.294	-19.159	49.453

In Table 7.12, observation indicates that none of the Gold One_1 tailing samples analysed yield negative NAPP value. They are all positive values. From the structure of the NAPP values arrayed in the table below, it is observed that NAPP values of top layers' samples is higher than the deep and bottom layers' samples. The highest NAPP value is 48.713 kgH_2SO_4/t. This particular sample is highly possible to produce acid from 1-2 meters of tailing dam.

Table 7.12: NPAA results of Gold One_1 tailing samples.

Sample Number	MPA	ANC	NAPP
GT1-048	0	-10.4	10.4
GT1-049	30.906	-11.344	42.25
GT1-050	36.108	-12.605	48.713
GT1-052	20.502	-6.787	27.289
GT1-053	25.704	-9.763	35.467
GT1-054	18.972	5.157	13.815
GT1-055	21.114	4.508	16.606
GT1-056	17.748	2.426	15.322
GT1-057	20.196	5.586	14.61
GT1-058	23.256	-10.707	33.963

Further findings demonstrate that positive value of NAPP value indicates the sample or layer of the tailings has potential capacity for acid production, the larger the value, the greater the acid generation capacity. If the value of NAPP is negative, the potential for acid generation is low; the greater the absolute value, the lesser the acidic waste produced. For instance, tailing sample 040 with negative value of NAPP and a small absolute value of 0.768 and paste pH 3.84. This indicates that the tailing sample has the potential for low acid generation as well contribute to high acidic waste production due to its small absolute value. As the process

progresses, further laboratory test experiment was performed to attain better estimates and measurements of the acid generation potential of the tailing samples. Therefore, leaching test was performed to improve the estimates and measurements of acid generation potential of the tailing samples.

7.3.4 ANC/MPA Ratio

When ratio of ANC/MPA is less than 1, then ANC/MPA is equivalent to a positive NAPP. And when ratio of ANC/MPA greater than 1, then ANC/MPA is equivalent to a negative NAPP. A numerical understanding of the above illustration is presented in the Table 7.13, where the results of ANC/MPA ratios are tabulated in corresponding to each tailing samples. The values arranged under ANC/MPA ratio are compared to the values arranged under NAPP. Another simple approach is by using tailing samples' borehole meters to analyse the acidic generation potential. For instance, sample 048 was collected from Gold One_1 tailing surface, 0.2-meter depth, yielded zero MPA and unattainable ANC/MPA ratio.

Table 7.13: Ratio of ANC/MPA of the samples from Mogale and Gold One_1 tailing

Sample	Meter	MPA	ANC	ANC/MPA Ratio	NAPP
038	1	4.59	3.3565	0.731	1.2335
039	2	17.442	0.061	0.003	17.381
040	3	-19.89	-19.122	0.961	-0.768
041	4	-13.158	-16.746	1.273	3.588
042	5	-0.918	-13.034	14.198	12.116
042-1	5.4	20.502	-52.234	-2.548	72.736
043	6	26.316	-14.382	-0.547	40.698
044	7	3.06	-21.217	-6.934	24.277
045	8	18.054	-30.27	-1.677	48.324
046	9	30.294	-19.159	-0.632	49.453
048	0.2	0.00	-10.4	–	10.4
049	1	30.906	-11.344	-0.367	42.25
050	2	36.108	-12.605	-0.349	48.713
052	4	20.502	-6.787	-0.331	27.289
053	5	25.704	-9.763	-0.380	35.467
054	6	18.972	5.157	0.272	13.815
055	7	21.114	4.508	0.214	16.606
056	8	17.748	2.426	0.137	15.322
057	9	20.196	5.586	0.277	14.61
058	10	23.256	-10.707	-0.460	33.963

7.3.5 Single Addition Net Acid Generation (NAG) Test

Most of the single addition net acid generation (NAG) test are applied for samples with total sulphide sulphur contents less than about 1.5% and with low

concentrations of metals such as copper, which can catalyse the decomposition of hydrogen peroxide. The NAGpH is >2, therefore, titrate with 0.1 M NaOH.

Figure 7.5: NAG test sample

Figure 7.6: NAG test solution

Table 7.14: Results of NAG test

Sample	VNaOH（mL） pH4.5	VNaOH（mL） pH7.0	NAGpH	NAPP	NAG/NAPP Ratio
038	1.1	4.49	3.13	1.2335	253.75
039	7.51	1.56	2.54	17.381	14.61
040	6.79	2.9	3.57	-0.768	-464.84
041	2.35	5.93	3.86	3.588	107.58
042	5.71	2.52	3.28	12.116	27.07
042-1	10.14	2.93	2.54	72.736	3.49
043	5.43	3.72	3.27	40.698	8.03
044	9.7	2.39	2.53	24.277	10.42
045	9.77	3.36	3.55	48.324	7.35
046	12.3	2.46	2.34	49.453	4.73
048	5.75	2.01	3.47	10.4	33.37
049	4.38	7.06	3.72	42.25	8.80
050	10.46	1.7	2.39	48.713	4.91
052	6.16	2.39	3.44	27.289	12.61
053	9.48	2.48	2.51	35.467	7.08
054	4.33	1.04	2.75	13.815	19.91
055	5.04	1.33	2.63	16.606	15.84
056	4.86	1.35	3.37	15.322	21.99
057	4.1	1.27	2.79	14.61	19.10
058	6.77	1.97	3.05	33.963	8.98

NAG test results are showed in Table 7.14. Titration to pH 4.5 and 7.0 is recommended to assist with the interpretation of results. Titration to pH 4.5 accounts for acidity due to Fe, Al and most of the hydrogen ion. Any additional

acidity accounted for in titration between pH 4.5 and pH 7 is usually indicative of soluble metals such as Cu and Zn.

Acid forming potential of a sample is classified into non-acid forming (NAF), potentially acid forming (PAF) and uncertain (UC) on the basis of the S, ANC, NAPP and NAG test results. Figure 7.7 shows the classification structure of the plot typically used for the presentation of geochemical data. Marked on this plot are the quadrants representing the NAF, PAF, and UC classification.

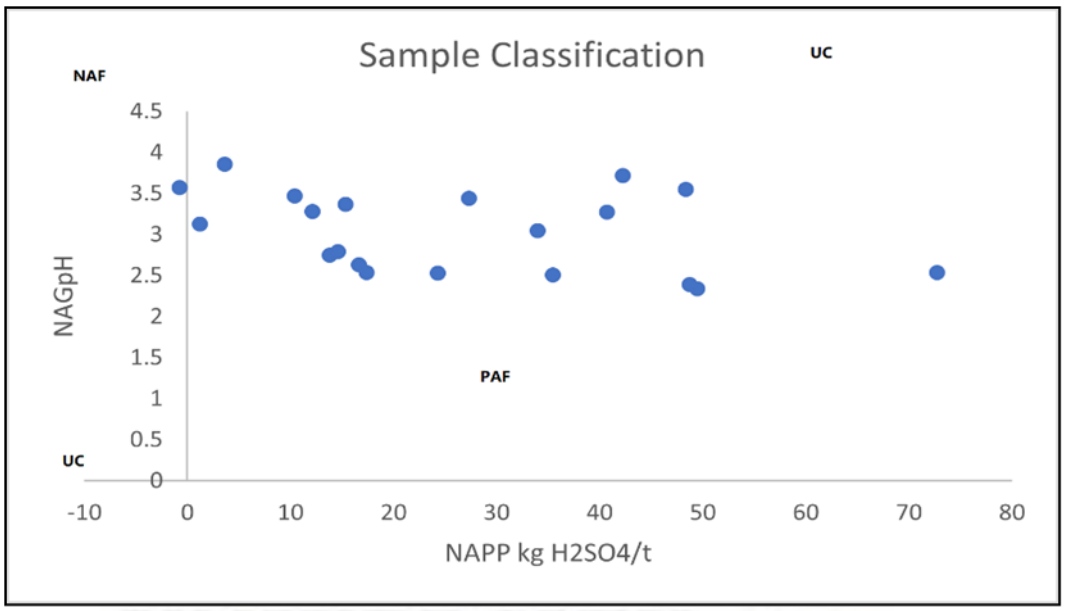

Figure 7.7: Tailing samples' acid forming classification

A sample classified as non-acid forming may, or may not, has a significant sulphur content but the availability of ANC within the sample is more than sufficient to neutralise all the acid that could be theoretically produced by any contained sulphide minerals. In that case, a sample is usually defined as NAF, when it has a negative NAPP value and final NAGpH = 5. On the other hand, a sample classified as potential acid forming always has a significant sulphur content, the acid generating potential of which exceeds the inherent acid neutralising capacity of the material. Therefore, a sample is usually defined as PAF, when it has a positive NAPP and a final NAGpH<4.5. Also, an uncertain classification is used when there is an apparent conflict between the NAPP and NAG results. Uncertain samples require more detailed investigation to determine the acid potential. The samples

from Mogale tailings and Gold One_1 tailing exhibited potentially acid forming as PAF classification, NAPP is positive and NAGpH<4.5.

7.4 Leach Column Test

Leaching column test is the kinetic test for the tailings samples to explore and modify the process of acid generation. Recall, a total of 23 samples were analysed, where 13 samples were collected from hole T004 in Mogale tailings and 10 samples were collected from Gold One_1 tailing. These samples were leached for 4 months, 84 days and the residues and leachates are analysed by ICP-MS and XRD. The mineralogical and geochemical results are compared with the raw tailings samples, and to simulate the process of acid-producing as well to study the migration and transformation of pollutants.

7.4.1 Objectives of the Test

The objective of the leaching column test is to accelerate the acid–base reaction of the sample, including the oxidation of pyrite to produce acid, the oxidative hydrolysis of iron, and the neutralizing effect of alkaline substances on the acid production. The leaching column test can fully carry out the acid–base reaction in a limited time (lab) and can obtain more information about the acid generation process. At the same time, the leaching column test results can compare with the ABA results.

7.4.1.1 Leach Column Test Preparation

Leaching column test samples from Mogale tailing are 038, 038_1, 038_2, 039, 040, 041, 042, 042_1, 043, 044, 045, 046 and 047 and samples from Gold One_1 tailing for leaching column are 048, 049, 050, 052, 053, 054, 055, 056, 057 and 058. Paste pH and EC, together with ABA results have shown that there are potential acid generation for the Mogale tailings and Gold One_1 tailing. The final acid generation prediction will be concluded for the case study gold tailing dams.

Figure 7.8: Tailing samples

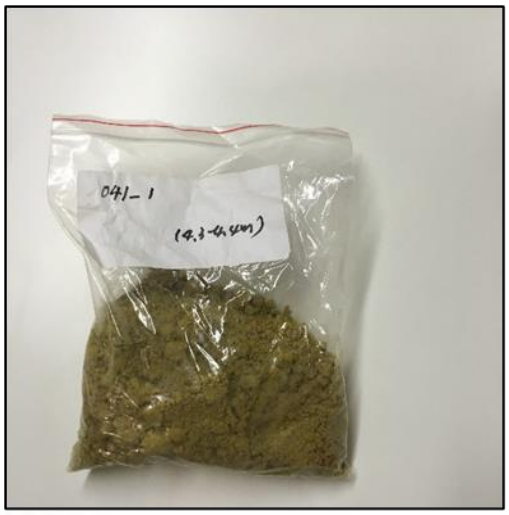

Figure 7.9: Tailing samples

Figure 7.10: Leach column test heat lamp on

Figure 7.11: Leach column test heat lamp off

Above mentioned samples are raw tailing samples and weighted for the test. The leach column test operation is designed to achieve a weekly wet-dry cycle and a monthly leaching cycle. Heat lamps are used to dry the sample between test solutions applications. The sample is wetted by applying the test solution-distilled water to the surface and leachate was collected at the base of the funnel. Therefore, the test solution was applied weekly and leachates were collected monthly. The conventional free drainage leach column set-up is designed to suspend the columns over a collection vessel allowing leachate to freely drain through the tailing samples. Heat lamps are installed above the leach columns to maintain a surface temperature

of 30–35℃. The total leach column test is 75 days, over three months. Figure 7.10 and Figure 7.11 shows the leaching column test lab set-up.

Figure 7.12: Leachate collected from each of samples

Samples collection during the leach column experiments includes three parts:

i. Collect leachate from the filtrate and measure its pH and EC value,
ii. The leachate is preserved and sent to ICP-MS for analysis of the chemistry of the solution, including constant K, Na, Ca, Mg, Fe, Mn, Al, Si and trace element content, and
iii. The residues from leaching column are tested by XRD to analyse mineral composition.

7.4.1.2 pH & EC Measurement

The pH and EC value of the leachate collected from each of the column test samples were measured for each of the free drainage cycles. The values derived from the measurement of the leaching cycle of pH and EC, together with the average pH and EC values of three months column test are presented in the Table 7.15. The distribution of the values demonstrate variation across 23 samples.

In the first cycle, the samples with low pH values are considerably acidic except samples 054, 055, 056 and 057, which were collected from the Gold One_1 tailing

within 6 meters to 9 meters deep of a borehole. The 10 meters depth sample from the same borehole exhibits a low pH value and an extremely high EC value. Observation indicates that leachate pH values increase from the second leaching cycle to third leaching cycle across the twenty-three samples, while the EC value is gradually decreased. This is caused by diluting certain amount of the tailings sample.

Table 7.15: Leachate pH and EC value for each cycle of the test

Sample	Meter	First Cycle		Second Cycle		Third Cycle		Average pH	Average EC
		pH	EC	pH	EC	pH	EC		
038	1m	4.868	112.33	5.365	84.45	6.547	30.50	5.593	75.76
038-1	1.2m	3.196	206.85	6.263	38.98	7.457	23.40	5.638	89.74
038-2	1.5m	3.714	177.60	6.233	35.58	6.635	25.30	5.527	79.49
039	2m	2.478	247.30	2.909	222.88	3.527	208.90	2.971	226.36
040	3m	2.148	265.98	2.419	250.55	2.875	247.70	2.481	254.74
041	4m	2.355	254.13	2.333	255.40	2.454	248.60	2.381	252.71
042	5m	2.611	239.77	2.250	260.08	2.678	259.30	2.513	253.05
042-1	5.4m	2.375	253.15	2.248	260.25	2.609	263.40	2.411	258.93
043	6m	2.053	271.25	2.252	259.93	2.816	251.20	2.374	260.79
044	7m	2.078	269.83	2.328	255.73	2.824	250.70	2.410	258.75
045	8m	2.075	269.83	2.265	259.23	2.724	256.80	2.355	261.95
046	9m	2.023	272.87	2.130	267.10	2.667	260.00	2.273	266.66
047	10m	2.107	268.15	2.334	255.35	2.929	244.50	2.457	256.00
048	0.2m	3.482	190.78	5.410	83.00	5.888	69.40	4.927	114.39
049	1m	3.027	216.30	4.199	150.23	4.551	148.60	3.926	171.71
050	2m	2.480	247.13	3.156	209.00	3.472	212.40	3.036	222.84
052	4m	2.226	261.53	2.514	245.20	2.969	242.10	2.570	249.61
053	5m	2.283	258.20	2.691	234.93	3.186	229.30	2.720	240.81
054	6m	6.518	26.83	7.355	27.68	7.401	20.20	7.091	24.90
055	7m	6.772	12.87	7.396	30.05	7.609	32.40	7.259	25.11
056	8m	6.688	30.70	7.530	35.15	7.714	38.60	7.311	34.82
057	9m	6.751	9.67	7.528	37.55	7.704	38.00	7.328	28.41
058	10m	2.242	261.80	2.682	235.73	3.340	220.10	2.754	239.21

7.4.1.3 Leachate Chemical Composition Analysis

More water leached to the samples, the drainage is washed out of the sample and pH value is increased. In the second cycle, leachate collected from some of the samples exhibited neutral and alkaline, such as the top layer of the Mogale tailings (samples 038, 038_1 and 038_2). And the top layer of the Gold One_1 tailing (sample 048) exhibits pH changes from acid to alkaline.

Some chemical elements were discovered from the analysis of the leachate by ICP-MS. Although, elements such as Nb, Y, Rb, Mo, Cd, Li, Be, Zr and Sr are not listed

Table 7.16: Mogale tailings samples leachate analysis (first collection for first cycle)

Sample	Element																		
	Ca	Si	Ce	Mg	Na	K	Th	Cu	As	Zn	Co	Cr	Ni	Se	P	Pb	Mn	Ti	Fe
038	34.73	0.44	0.02	3.54	-9.58	-3.15	-0.01	0.01	-0.12	0.00	-0.00	-0.05	-0.05	-0.15	-0.11	-0.03	0.12	-0.01	1.75
038-1	-	-	-	-	-	-	-	-	-	-	-	-	-	-	-	-	-	-	-
038-2	-	-	-	-	-	-	-	-	-	-	-	-	-	-	-	-	-	-	-
039	-	-	-	-	-	-	-	-	-	-	-	-	-	-	-	-	-	-	-
040	53.92	0.55	0.01	90.87	-12.78	-2.33	0.49	2.65	4.00	3.77	0.89	2.20	4.10	0.47	1.93	-0.01	1.54	0.06	-
041	45.32	2.71	0.16	35.82	33.78	-4.35	0.31	4.13	0.94	20.85	4.43	0.49	9.57	-0.03	1.46	0.01	1.01	0.02	-
042	62.98	1.55	0.53	109.34	2.59	9.75	0.11	2.55	0.19	23.02	5.52	0.98	18.77	-0.06	0.80	0.04	24.67	0.08	-
042-1	-	-	-	-	-	-	-	-	-	-	-	-	-	-	-	-	-	-	-
043	45.89	0.92	1.08	-	-5.98	5.80	0.07	5.06	12.54	16.81	8.55	2.41	23.76	0.31	7.10	0.08	28.76	1.19	-
044	64.60	1.38	0.81	-	10.86	-6.13	-0.17	6.05	4.09	12.95	4.05	1.44	11.61	0.15	3.35	0.06	16.34	0.08	-
045	34.33	1.42	0.59	96.08	-4.36	-7.41	1.10	2.64	7.86	5.61	1.10	0.60	5.52	0.29	1.99	-0.04	4.77	0.03	-
046	52.66	0.48	0.34	67.85	-1.87	7.13	-0.00	2.07	4.39	5.77	1.64	0.67	5.45	-0.14	1.53	0.01	4.79	0.03	-
047	75.33	1.60	1.13	-	-15.38	10.64	1.39	3.55	8.74	13.06	2.27	1.27	12.63	0.46	3.62	-0.02	17.08	0.11	-

Table 7.17: Gold One_1 tailing samples leachate analysis (first collection for first cycle)

Sample	Element																		
	Ca	Si	Ce	Mg	Na	K	Th	Cu	As	Zn	Co	Cr	Ni	Se	P	Pb	Mn	Ti	Fe
048	-	5.87	0.25	-	-3.76	53.27	2.30	5.27	72.66	2.57	2.25	10.75	9.77	3.59	13.58	0.08	5.41	1.09	-
049	61.32	0.29	0.46	13.01	-9.11	-0.23	0.69	2.84	2.38	8.05	3.40	1.97	7.63	0.50	0.78	-0.02	2.29	0.04	-
050	106.03	0.27	0.14	48.08	-1.99	1.19	0.29	1.75	2.86	5.45	3.00	3.16	7.50	0.70	1.02	0.01	6.13	0.06	-
052	53.07	0.08	0.15	65.70	-0.14	1.78	0.23	1.97	0.03	9.41	4.36	2.86	7.56	0.33	0.03	0.02	15.24	0.00	-
053	26.42	0.04	0.01	20.92	-9.47	-6.96	0.10	0.42	0.06	2.55	0.49	0.54	1.20	0.07	-0.01	-0.01	3.76	0.00	73.17
054	60.57	0.14	-0.00	4.63	1.96	12.30	0.03	0.01	-0.09	0.00	-0.00	-0.04	-0.03	-0.07	-0.05	0.02	-0.01	-0.00	0.46
055	70.57	0.47	0.01	3.61	-7.77	8.77	0.05	0.01	-0.07	-0.05	-0.00	-0.09	-0.07	-0.02	-0.09	-0.00	-0.03	-0.01	-0.14
056	70.81	0.24	0.00	7.59	-6.64	17.26	0.04	0.01	-0.03	0.08	0.04	-0.05	0.08	-0.13	-0.07	0.01	0.32	0.00	-0.11
057	60.71	0.25	0.00	4.41	1.43	-0.61	0.01	0.00	0.00	-0.01	-0.01	-0.05	-0.05	-0.07	-0.08	0.02	-0.02	-0.00	0.07
058	43.40	0.17	0.10	17.95	-9.52	-7.23	0.33	1.06	0.31	3.33	0.84	0.42	1.53	0.00	0.29	-0.02	1.36	0.01	-

as well not discuss in this study because of micro contents. The chemical composition analysis results derived are presented in Table 7.16 and Table 7.17 (first collection for first cycle), Table 7.18 and Table 7.19 (second collection for first cycle), Table 7.20 and Table 7.21 (last collection for first cycle), Table 7.22 and Table 7.23 (first collection for second cycle), Table 7.24 and Table 7.25 (last collection for second cycle), Table 7.26 and Table 7.27 (first collection for third cycle), Table 7.28 and Table 7.29 (last collection for third cycle) in Mogale and Gold One_1 tailings. These results indicate change in the whole leachate process. The unit for the analytical element is ppm.

The leachate from each sample and time of collection are recorded with the pH and EC and the colour of the changes was also recorded. The colour of each collection time was changed from dark brown or red to the yellow or light brown, with more drainage of water leaching. In Table 7.16, the results of the leachate analysis of the first collection for the first cycle across 13 samples collected from Mogale tailing show that samples 038_1, 038_2, 039 and 042_1 have error across all the elements, except samples 043, 044, 047 have error of Mg analysis, while only sample 038 has no element analysis error of Fe. On the other hand, among 10 samples collected in Gold One_1 as displayed in Table 7.17, samples 049, 050, 052 and 058 have element analysis error of Fe, only samples 048 has elements analysis error of Ca, Fe and Mg.

In Table 7.18, the results of the leachate analysis of the second collection for the first cycle across 13 samples collected from Mogale tailing demonstrate that samples 039, 040, 042, 044, 045, 046 and 047 have element analysis error of Mg, Th and Fe. Only sample 041 demonstrates element analysis error of Th and Fe. In Gold One_1 tailings, as shown in Table 7.19, samples 052 and 053 have element analysis error of Fe, only sample 058 have element analysis error of Th and Fe.

In Table 7.20, the results of the leachate analysis of the last collection for the first cycle indicate that samples 040, 043 and 044 collected from Mogale tailings show element analysis error of Mg, Th and Fe. Other samples as 042-1 and 046 only show element analysis error of Fe, while sample 047 exhibits element analysis error of Th and Fe. In Table 7.21, the results of the leachate analysis of the last collection

Table 7.18: Mogale tailing samples leachate analysis (second collection for first cycle)

Sample	Element																		
	Ca	Si	Ce	Mg	Na	K	Th	Cu	As	Zn	Co	Cr	Ni	Se	P	Pb	Mn	Ti	Fe
038	104.76	-288.91	-0.01	15.81	-5.22	31.86	-0.01	0.03	0.05	0.06	0.05	0.01	-4.91	0.35	0.04	0.08	0.08	-0.01	0.71
038-1	78.27	-299.59	0.06	13.80	-0.66	40.30	0.15	0.06	-0.39	0.23	0.03	0.27	-4.97	0.41	-0.05	-0.04	0.87	-0.02	7.47
038-2	67.08	-299.37	0.02	4.62	-1.62	44.70	0.08	0.03	-0.08	0.17	0.02	0.11	-5.11	0.44	-0.02	-0.04	0.34	-0.01	2.65
039	82.15	-297.86	0.08	-	-7.31	44.05	-	1.14	1.47	2.49	-0.88	4.47	0.13	2.25	3.19	0.03	3.24	0.01	-
040	97.22	-218.13	0.16	-	-0.16	37.99	-	5.49	8.32	10.68	-1.74	7.07	8.23	3.55	3.03	-0.05	4.24	0.03	-
041	94.77	-202.43	0.81	79.81	-1.58	39.84	-	9.02	2.57	45.54	5.10	1.68	22.53	1.27	4.89	0.03	2.53	0.05	-
042	98.73	-0.67	2.82	-	-0.82	40.66	-	10.68	33.44	32.66	-3.55	4.83	31.65	3.02	6.66	0.03	27.20	0.20	-
042-1	7.88	-297.74	0.10	8.42	-9.43	14.35	0.55	0.21	0.08	1.80	0.53	0.09	-3.44	0.34	-0.12	-0.03	2.16	0.05	36.40
043	13.66	-72.80	0.19	25.27	-6.88	8.75	1.13	0.67	0.06	8.22	1.30	0.31	6.18	0.69	0.38	-0.01	5.43	0.20	87.90
044	81.64	-61.29	1.26	-	10.52	36.98	-	6.57	3.08	15.14	-0.85	1.99	12.96	1.73	4.73	-0.03	19.07	0.02	-
045	105.36	-254.30	2.14	-	-1.54	45.24	-	8.05	36.78	24.52	-3.83	3.44	16.91	2.72	5.86	0.02	18.56	0.08	-
046	88.45	-75.27	1.43	-	-6.37	21.23	-	5.60	11.53	20.91	0.23	3.33	29.94	2.69	4.78	-0.06	35.17	0.30	-
047	103.64	-225.11	1.34	-	-8.51	38.12	-	3.85	7.14	17.13	-1.92	2.04	12.88	1.75	2.56	-0.03	21.18	0.01	-

Table 7.19: Gold One_1 tailing samples leachate analysis (second collection for first cycle)

Sample	Element																		
	Ca	Si	Ce	Mg	Na	K	Th	Cu	As	Zn	Co	Cr	Ni	Se	P	Pb	Mn	Ti	Fe
048	33.66	-217.46	0.07	0.40	-4.36	7.30	0.01	0.02	-0.26	0.08	0.01	0.03	-3.61	0.37	0.11	0.08	0.01	-0.01	0.51
049	77.23	-241.88	0.11	2.11	-6.28	24.53	0.07	0.75	-0.01	1.50	0.73	0.12	-1.94	0.17	0.15	0.09	0.45	-0.01	2.62
050	87.54	-146.23	0.05	4.87	9.27	52.01	0.72	0.23	-0.04	0.64	0.42	0.49	-0.15	0.24	0.03	0.04	0.78	-0.01	57.85
052	72.82	- 123.39	0.36	97.24	-1.97	20.06	5.34	2.92	0.06	15.80	8.14	6.08	11.18	3.83	0.16	-0.00	24.76	-0.01	-
053	77.85	-250.26	0.17	46.01	-4.37	38.11	3.17	1.00	-0.13	8.05	1.51	2.54	-0.09	1.72	0.07	-0.05	10.58	-0.01	-
054	93.69	-58.44	0.04	4.53	-7.40	22.52	-0.02	0.03	-0.26	0.06	0.02	-0.01	-0.16	0.30	0.23	0.20	0.02	-0.01	-0.01
055	76.29	-276.20	-0.02	2.84	-4.45	40.88	-0.06	0.00	-0.09	0.08	0.02	-0.05	-4.78	0.12	0.37	0.02	0.01	-0.02	0.24
056	55.08	-192.60	-0.01	3.50	-8.98	41.37	0.01	0.04	-0.05	0.10	0.04	-0.05	-2.52	0.20	0.01	-0.02	0.22	-0.01	-0.23
057	75.90	-171.71	0.02	1.47	-5.04	30.08	0.01	0.01	-0.04	0.05	0.01	-0.05	-1.84	0.13	0.02	-0.05	0.01	-0.01	-0.18
058	96.66	-251.40	0.77	81.13	-1.95	31.10	-	4.49	2.07	19.23	-0.79	3.40	5.07	1.79	2.71	0.02	7.32	-0.00	-

Table 7.20: Mogale tailing samples leachate analysis (last collection for first cycle)

Sample	Element																		
	Ca	Si	Ce	Mg	Na	K	Th	Cu	As	Zn	Co	Cr	Ni	Se	P	Pb	Mn	Ti	Fe
038	119.33	-1.39	0.11	9.79	5.19	37.25	-0.06	-0.01	0.22	0.10	0.06	-0.08	-0.01	-0.08	0.07	0.13	0.23	-0.00	-0.19
038-1	19.94	-1.96	0.01	0.82	2.26	24.04	-0.04	0.00	-0.19	0.14	-0.03	-0.05	-0.09	-0.12	-0.26	-0.09	0.02	0.01	1.70
038-2	58.46	-0.93	-0.06	0.81	1.69	13.37	0.12	-0.02	-0.14	0.09	-0.00	-0.06	-0.05	-0.01	0.20	0.08	0.02	0.09	2.23
039	18.32	-2.18	-0.04	1.60	0.04	-1.21	0.08	0.02	0.02	0.17	0.04	-0.09	-0.07	-0.05	0.31	0.06	0.03	0.01	3.33
040	102.23	1.91	0.05	-	-4.22	34.41	-	3.11	1.58	6.07	-0.84	3.57	4.72	1.39	1.24	0.05	2.79	0.01	-
041	94.61	-1.55	0.13	5.53	8.23	18.64	0.31	0.49	-0.21	2.65	0.72	0.01	1.04	-0.28	-0.03	0.11	0.19	0.01	19.13
042	101.04	-2.53	0.20	35.57	-25.31	37.26	0.87	0.85	-0.24	11.21	2.00	0.20	4.98	-0.12	0.40	-0.04	7.42	0.04	46.91
042-1	96.59	-0.93	0.31	54.21	4.67	38.98	3.01	1.19	0.03	11.93	3.14	0.38	7.44	0.40	0.34	-0.07	12.94	0.01	-
043	91.38	14.09	1.26	-	3.98	16.15	-	5.18	6.22	19.18	-0.13	3.00	19.71	2.21	3.95	-0.03	32.52	0.25	-
044	111.17	13.12	0.92	-	-3.00	35.88	-	6.70	3.15	16.29	0.03	1.88	11.40	1.18	4.02	-0.07	20.46	0.03	-
045	106.74	0.86	0.27	44.55	22.42	35.11	6.87	1.41	3.04	3.43	-0.55	0.48	2.84	-0.00	0.60	0.10	3.17	-0.00	-
046	94.44	1.28	0.40	62.91	4.85	42.67	8.67	1.90	2.31	5.52	-0.78	0.66	3.86	0.21	1.81	0.01	4.62	-0.00	-
047	106.67	7.81	0.92	96.25	8.37	42.98	-	2.46	2.44	10.68	-1.23	1.39	8.83	0.71	1.25	-0.01	11.97	0.01	-

Table 7.21: Gold One_1 tailing samples leachate analysis (last collection for first cycle)

Sample	Element																		
	Ca	Si	Ce	Mg	Na	K	Th	Cu	As	Zn	Co	Cr	Ni	Se	P	Pb	Mn	Ti	Fe
048	46.77	-1.31	0.02	0.71	7.01	20.45	0.05	-0.00	-0.21	0.07	0.01	-0.11	-0.07	-0.25	0.14	0.02	0.01	0.00	-0.17
049	115.92	-1.39	-0.03	0.93	6.31	28.34	0.12	0.11	-0.02	0.22	0.05	-0.05	0.03	-0.03	0.08	-0.01	0.07	-0.01	7.30
050	90.62	-3.57	0.00	1.03	1.10	35.45	0.06	0.04	-0.12	0.12	-0.01	-0.07	-0.11	-0.27	0.33	0.07	0.05	0.00	4.00
052	103.56	2.43	0.01	22.69	6.54	38.86	1.01	0.80	0.26	3.50	2.04	0.97	2.57	0.32	0.17	0.03	5.75	-0.00	66.12
053	116.79	1.01	0.04	14.54	5.23	34.55	1.00	0.42	0.07	2.54	0.52	0.81	1.29	0.40	-0.06	0.01	3.38	0.00	54.79
054	93.97	-4.71	-0.03	2.82	10.20	38.13	0.03	0.02	0.04	0.08	-0.01	-0.09	-0.20	-0.30	-0.04	-0.00	0.01	0.00	-0.03
055	83.26	-3.20	0.00	1.74	12.60	37.21	0.02	0.00	-0.18	0.08	-0.02	-0.12	-0.14	-0.24	0.23	0.10	0.01	0.00	-0.04
056	99.79	-0.64	-0.03	3.66	35.67	43.13	0.11	0.00	0.13	0.13	0.04	-0.08	0.02	-0.45	0.10	0.12	0.30	-0.01	-0.37
057	101.82	-4.63	0.08	1.59	8.64	45.53	0.03	-0.01	0.08	0.07	-0.02	-0.08	-0.11	-0.30	0.20	0.01	0.02	-0.01	-0.24
058	104.66	-2.47	0.08	14.19	9.43	34.04	1.52	0.75	0.09	2.70	0.74	0.43	1.00	0.26	0.35	0.04	1.24	-0.01	99.93

Table 7.22: Mogale tailing samples leachate analysis (first collection for second cycle)

Sample	Element															
	Ca	Si	Mg	Na	Cu	As	Zn	Co	Cr	Ni	Se	P	Pb	Mn	Ti	Fe
038	130.17	6.98	18.38	0.90	0.32	0.10	-0.12	-6.09	-9.45	-2.13	-1.01	0.02	3.83	1.36	-0.09	-3.50
038-1	134.79	6.27	3.93	-0.01	0.72	0.26	-0.21	-5.93	-2.80	-6.36	-0.19	-0.37	-3.00	0.80	0.73	-4.09
038-2	-1.23	5.15	-0.45	-0.09	0.84	0.16	-0.56	-5.49	-4.97	-3.94	-0.28	-0.16	29.76	0.79	-0.46	-6.19
039	-6.11	12.96	2.84	0.12	0.62	0.14	-0.39	-3.99	-9.27	2.71	-0.44	-0.19	25.86	1.13	-1.35	6.01
040	75.28	6.46	43.13	0.32	3.01	-0.17	3.38	-2.10	-0.26	3.83	-0.44	0.43	23.05	1.71	1.88	0.00
041	40.58	5.38	6.98	-0.08	2.28	0.15	4.88	-5.79	-2.52	-0.57	-0.91	-0.20	5.50	0.42	-0.31	24.43
042	0.07	7.34	1.51	-0.17	1.53	-0.27	0.63	-4.02	-11.72	-0.58	-0.61	-0.32	21.25	1.17	0.53	4.48
042-1	17.39	10.17	11.62	-0.17	1.94	-0.08	2.93	-4.45	-4.93	-2.71	0.25	-0.45	-11.30	4.10	0.15	22.71
043	43.60	7.79	88.19	-0.05	5.40	3.95	12.21	-1.48	-11.40	13.66	-0.20	4.28	-5.72	19.76	-2.70	0.00
044	47.50	11.06	56.08	0.05	4.59	0.59	7.98	-4.00	-4.50	2.44	-1.18	0.84	-4.93	9.91	-0.65	0.00
045	17.88	3.41	31.29	0.22	2.45	0.51	3.32	-2.68	-5.27	7.59	-0.72	-0.07	9.50	3.34	0.39	0.00
046	54.36	5.11	79.02	0.04	5.22	7.75	10.32	-3.74	-2.06	5.66	-0.07	2.77	26.16	9.26	-1.86	0.00
047	139.62	8.65	50.52	0.20	4.14	1.43	8.17	-3.92	-3.86	1.85	-0.49	0.77	16.21	10.70	0.29	0.00

Table 7.23: Gold One_1 tailing samples leachate analysis (first collection for second cycle)

Sample	Element															
	Ca	Si	Mg	Na	Cu	As	Zn	Co	Cr	Ni	Se	P	Pb	Mn	Ti	Fe
048	55.83	2.44	-0.36	-0.13	1.15	0.28	-0.51	-6.58	-9.03	-5.14	-0.26	-0.42	1.19	0.59	-0.14	6.48
049	68.97	4.81	-0.84	-0.07	1.08	0.32	-0.17	-4.74	-4.69	-5.15	0.58	-0.64	-0.31	-0.12	-1.70	14.59
050	75.42	4.70	0.92	2.36	-0.12	-0.13	0.01	-4.36	-12.12	-4.10	-0.40	-0.54	2.98	0.68	-0.11	21.97
052	60.62	8.94	21.69	0.11	1.12	-0.01	3.35	-3.89	-4.34	1.70	-0.82	-0.69	-4.77	5.44	-2.00	52.60
053	57.52	11.67	13.20	0.01	1.63	0.34	2.31	-2.98	-1.48	-0.90	-0.13	-0.57	7.19	3.93	-0.98	38.79
054	79.40	1.50	7.24	0.13	0.74	0.36	-0.32	-8.58	-14.45	-7.39	-1.13	-0.72	8.61	0.48	1.47	5.65
055	53.66	1.30	0.74	-0.05	0.80	-0.05	-0.17	-5.46	-5.97	-0.79	0.02	-0.62	-4.46	0.51	-0.98	5.85
056	68.24	3.70	6.74	0.01	0.84	0.88	-0.31	-5.42	-0.11	-6.67	-1.42	-0.89	-6.13	0.20	-2.53	8.30
057	73.48	0.67	-0.05	-0.05	1.19	0.38	-0.31	-5.09	-9.70	-0.36	-0.06	-0.87	-0.15	-0.26	-0.76	8.78
058	57.65	5.21	13.71	0.07	1.81	0.00	2.10	-4.54	-3.59	-2.90	-0.40	-0.67	0.54	2.68	-0.10	62.03

Table 7.24: Mogale tailing samples leachate analysis (last collection for second cycle)

Sample	Element															
	Ca	Si	Mg	Na	Cu	As	Zn	Co	Cr	Ni	Se	P	Pb	Mn	Ti	Fe
038	114.44	4.65	9.64	4.50	0.01	0.28	-0.02	-3.96	-43.03	0.34	1.49	-0.12	16.68	1.54	-3.46	4.56
038-1	16.97	2.21	0.49	2.98	0.17	0.55	0.16	7.47	-12.34	-0.22	0.66	0.19	-41.63	0.28	-1.45	2.68
038-2	25.25	0.79	1.03	3.07	0.27	0.54	0.24	-1.48	-31.77	-0.42	0.05	-0.11	-60.53	0.22	-0.97	4.74
039	64.54	3.54	43.19	3.32	0.33	0.02	1.35	-4.13	-6.75	-9.01	0.42	0.33	-64.03	0.27	-0.99	84.71
040	59.81	0.84	71.66	3.66	1.32	0.39	4.39	2.62	-17.39	6.81	0.18	0.24	-69.44	3.81	-2.30	0.00
041	43.75	1.13	24.15	2.99	2.75	0.85	10.95	1.10	-4.29	-2.54	0.19	0.10	4.36	1.73	-1.70	0.00
042	58.59	6.33	96.76	3.51	4.33	0.30	48.91	-0.79	-35.76	20.77	-0.12	0.28	-2.60	27.54	-0.07	0.00
042-1	57.00	5.46	0.00	4.94	6.57	1.45	51.75	23.46	-18.18	51.28	-0.75	1.52	2.92	0.00	-2.84	0.00
043	58.34	0.46	108.80	3.63	5.08	3.07	13.58	3.17	-34.22	15.86	1.43	2.91	-35.12	21.05	-1.49	0.00
044	55.96	0.25	0.00	3.26	5.66	0.50	11.97	9.23	13.69	14.87	-0.02	0.93	11.33	33.52	-3.14	0.00
045	46.33	-0.77	30.92	2.93	1.78	1.86	3.80	-2.18	-28.20	-2.67	0.16	0.71	-8.86	2.84	-2.85	0.00
046	65.22	0.30	0.00	3.61	6.90	14.78	18.30	-1.78	13.74	15.97	1.16	5.86	-50.37	16.04	0.00	0.00
047	62.12	0.27	43.10	3.65	0.98	1.84	5.86	-3.64	-30.15	7.72	-0.59	-0.24	-50.96	6.86	-0.79	0.00

Table 7.25: Gold One_1 tailing samples leachate analysis (last collection for second cycle)

Sample	Element															
	Ca	Si	Mg	Na	Cu	As	Zn	Co	Cr	Ni	Se	P	Pb	Mn	Ti	Fe
048	17.51	-0.46	0.43	3.13	0.52	0.59	0.46	-2.14	-20.78	-0.68	0.88	-0.22	-20.07	-0.46	1.01	5.48
049	78.55	-0.33	0.19	3.03	-0.08	0.62	0.35	3.39	-12.22	4.95	1.17	-0.24	-52.16	0.37	-2.91	5.81
050	47.43	-0.01	1.74	3.25	0.15	0.57	0.40	-1.56	-9.88	-8.72	1.24	-0.27	-103.20	-0.60	-0.53	5.31
052	87.29	1.51	9.30	2.95	0.95	-0.25	1.80	-0.42	-47.58	-2.89	1.01	-0.20	-30.29	1.43	-1.82	18.26
053	92.77	0.48	6.73	2.97	0.42	0.20	1.59	-3.59	-4.03	3.62	0.72	-0.22	-45.76	1.74	-2.76	19.21
054	39.26	0.42	1.01	2.93	-1.25	-0.07	0.18	-0.03	5.24	-3.19	0.40	-0.31	-85.59	-1.21	-3.19	4.61
055	65.20	-0.19	1.06	2.92	-0.63	0.34	0.10	-4.08	-18.20	-0.02	0.24	-0.07	-87.53	-1.45	-1.19	8.41
056	52.22	2.39	2.20	3.21	0.15	0.00	0.28	2.00	-26.78	1.10	0.62	-0.11	-9.53	-0.10	-1.05	4.67
057	38.91	-2.64	0.67	3.01	-0.56	0.57	0.12	6.88	-1.52	-4.33	0.47	-0.22	-44.79	-0.40	-2.65	4.34
058	86.00	-1.76	8.17	2.69	0.41	0.74	1.60	7.34	-35.07	-3.60	1.16	0.15	-64.38	-0.31	-2.71	11.91

Table 7.26: Mogale tailing samples leachate analysis (first collection for third cycle)

Sample	Element																		
	Ca	Si	Ce	Mg	Na	K	Th	Cu	As	Zn	Co	Cr	Ni	Se	P	Pb	Mn	Ti	Fe
038	95.97	1.59	0.00	12.55	2.63	27.81	0.02	0.01	-0.11	0.07	0.03	-0.05	0.04	-0.01	0.02	-0.01	0.30	-0.01	0.71
038-1	3.76	-0.17	0.03	0.16	-3.20	3.10	0.01	0.00	-0.07	0.04	-0.01	-0.04	-0.03	-0.10	0.02	-0.02	0.01	0.01	2.74
038-2	10.55	5.63	0.01	0.18	-9.60	8.78	0.01	0.01	-0.04	0.05	-0.01	-0.04	-0.04	0.03	-0.00	0.05	0.01	0.09	5.43
039	89.07	0.76	0.03	76.70	-7.82	37.94	0.06	0.46	-0.07	1.25	0.82	1.57	1.94	0.21	0.22	0.00	1.47	0.00	-
040	81.95	-0.86	0.04	82.29	-6.79	22.32	0.16	1.49	-0.11	2.98	1.20	1.68	2.99	0.15	0.12	-0.02	1.66	-0.00	-
041	92.03	2.23	0.26	26.38	-8.77	27.22	0.12	2.11	-0.11	12.51	2.56	0.23	5.92	-0.06	-0.01	-0.01	0.80	0.00	35.50
042	93.71	3.03	0.44	80.78	-10.86	28.00	0.35	1.72	-0.17	22.06	3.04	0.51	12.25	0.09	0.01	-0.02	13.51	0.00	75.38
042-1	84.42	1.18	0.40	83.19	-12.26	26.74	0.35	1.76	-0.19	16.76	3.79	0.68	14.08	0.17	0.16	-0.03	17.60	-0.00	-
043	98.11	2.44	0.59	-	-11.21	18.95	0.46	2.93	0.50	9.90	5.70	1.85	14.11	0.37	1.53	0.00	17.07	0.02	-
044	105.83	3.85	0.26	64.76	-10.05	22.49	0.17	2.47	-0.06	5.50	2.44	0.58	5.12	-0.04	0.11	-0.02	6.87	-0.00	-
045	60.93	-1.69	0.27	61.93	-14.67	9.99	0.34	1.82	1.25	4.76	1.97	0.52	4.67	-0.04	0.83	-0.02	3.66	-0.00	-
046	88.55	0.97	0.67	-	-10.07	21.30	0.83	3.68	4.92	9.91	2.45	1.31	9.68	0.17	2.75	-0.01	8.35	0.00	-
047	95.91	1.22	0.34	59.35	-12.31	1.80	0.31	1.27	-0.07	5.01	1.64	0.67	5.20	0.07	0.19	-0.02	6.37	-0.00	-

Table 7.27: Gold One_1 tailing samples leachate analysis (first collection for third cycle)

Sample	Element																		
	Ca	Si	Ce	Mg	Na	K	Th	Cu	As	Zn	Co	Cr	Ni	Se	P	Pb	Mn	Ti	Fe
048	10.81	-4.53	0.01	0.16	-10.90	-1.27	0.00	-0.01	-0.11	0.00	-0.01	-0.08	-0.06	-0.02	0.06	-0.03	0.00	-0.00	-0.16
049	102.46	-2.79	-0.00	0.33	-14.47	27.82	0.03	0.00	-0.09	0.04	-0.00	-0.09	0.01	-0.01	0.01	-0.01	0.03	-0.01	-0.23
050	85.52	-3.60	0.03	0.39	-16.71	19.75	0.02	0.01	-0.13	0.02	-0.01	-0.10	-0.04	0.00	0.02	-0.02	0.02	-0.01	1.08
052	103.67	1.16	0.04	9.69	-12.84	27.53	0.00	0.38	-0.14	1.36	0.54	0.22	1.05	-0.04	0.00	0.01	1.92	-0.01	14.55
053	109.59	1.49	0.04	3.57	-21.38	20.94	0.04	0.09	-0.05	0.59	0.10	0.03	0.29	0.02	-0.06	-0.02	0.68	-0.01	0.88
054	79.37	-5.14	0.01	1.90	-11.83	26.90	0.01	-0.02	-0.15	-0.01	-0.01	-0.10	-0.07	-0.05	-0.03	-0.04	0.00	-0.01	-0.34
055	96.75	-5.03	0.00	1.51	-16.99	25.23	-0.02	-0.02	-0.07	-0.00	-0.01	-0.10	-0.06	-0.16	0.05	-0.01	0.00	-0.00	-0.25
056	80.97	-4.42	-0.00	2.06	-17.22	23.73	0.01	-0.02	-0.14	0.02	-0.00	-0.11	-0.01	-0.04	-0.00	-0.01	0.15	-0.01	-0.39
057	60.74	-4.88	0.02	0.90	-16.06	21.96	-0.01	-0.01	-0.08	-0.00	-0.01	-0.10	-0.07	0.01	0.02	0.00	0.00	-0.01	-0.39
058	95.37	-2.22	0.02	2.96	-26.17	23.55	0.02	0.07	-0.04	0.28	0.05	-0.08	0.06	0.01	-0.03	-0.02	0.14	-0.00	2.86

Table 7.28: Mogale tailing samples leachate analysis (last collection for third cycle)

Sample	Element																		
	Ca	Si	Ce	Mg	Na	K	Th	Cu	As	Zn	Co	Cr	Ni	Se	P	Pb	Mn	Ti	Fe
038	116.82	5.70	0.04	15.19	-4.62	28.31	-0.01	0.00	-0.13	0.08	0.06	-0.03	0.07	0.03	0.01	0.04	0.36	-0.01	0.13
038-1	2.49	14.23	0.04	0.23	-6.66	-10.00	-0.07	-0.00	-0.06	0.05	-0.00	-0.00	0.02	-0.02	0.01	0.05	0.01	0.02	8.12
038-2	4.49	17.26	-0.01	0.25	-5.21	0.91	-0.02	0.01	0.10	0.05	-0.01	-0.00	0.03	0.01	0.08	0.07	0.01	0.15	10.50
039	2.72	7.24	0.00	0.93	-6.25	-0.50	-0.06	-0.00	-0.00	0.06	-0.00	-0.01	0.03	0.13	0.08	0.08	0.03	0.02	4.44
040	82.35	3.14	0.02	61.16	-7.67	16.27	0.25	1.14	-0.09	2.30	0.91	1.40	2.23	0.29	-0.02	0.02	1.36	0.00	-
041	78.24	6.45	0.30	34.90	-4.25	18.13	0.25	2.51	0.00	15.58	3.35	0.35	7.21	0.05	-0.02	0.04	1.05	0.01	42.46
042	86.44	5.05	0.21	44.05	-4.17	25.59	0.13	0.92	-0.03	12.19	1.81	0.30	6.61	0.15	-0.04	0.09	7.87	0.00	14.42
042-1	109.96	5.09	0.33	74.93	-2.09	10.78	0.67	1.61	-0.07	15.66	3.77	0.72	12.72	0.33	0.11	0.01	16.42	0.00	-
043	101.60	6.41	0.41	-	-1.58	25.46	1.03	2.06	0.10	6.98	4.25	1.52	9.60	0.37	0.63	0.01	12.08	0.01	-
044	113.93	7.13	0.12	28.37	-4.36	45.06	0.18	1.17	-0.11	2.53	1.27	0.29	2.31	0.09	-0.01	-0.01	3.17	-0.00	58.55
045	65.45	3.59	0.24	56.79	-0.92	7.82	0.77	1.81	0.87	4.73	1.96	0.62	4.49	0.09	0.66	0.01	3.69	-0.00	-
046	93.56	6.20	0.45	-	-5.89	35.68	1.56	3.06	2.52	8.17	1.59	1.26	7.72	0.29	1.92	0.01	6.97	-0.00	-
047	93.44	5.13	0.26	42.97	-11.80	9.82	0.36	1.05	0.00	3.99	1.31	0.49	3.63	-0.01	-0.06	0.02	5.28	0.00	-

Table 7.29: Gold One_1 tailing samples leachate analysis (last collection of third cycle)

Sample	Element																		
	Ca	Si	Ce	Mg	Na	K	Th	Cu	As	Zn	Co	Cr	Ni	Se	P	Pb	Mn	Ti	Fe
048	3.21	0.70	0.02	0.08	-8.52	-13.50	-0.05	0.01	0.02	0.05	0.00	-0.05	-0.01	-0.08	-0.01	0.02	0.00	0.00	-0.05
049	67.26	2.42	-0.01	0.17	-12.42	3.07	-0.03	0.01	-0.07	0.06	-0.00	-0.04	0.02	0.16	0.06	-0.00	0.02	-0.01	2.20
050	37.00	0.70	-0.02	0.37	-5.92	10.01	-0.04	0.01	-0.03	0.07	-0.00	-0.04	0.00	0.14	0.06	0.04	0.03	-0.00	1.84
052	115.76	6.43	0.03	5.49	-5.77	34.14	-0.03	0.26	-0.02	0.85	0.32	0.17	0.62	-0.03	0.03	0.06	1.16	-0.00	13.67
053	118.03	2.39	-0.00	2.26	-7.73	34.03	-0.05	0.09	0.03	0.42	0.05	0.05	0.22	0.16	0.00	0.05	0.46	-0.00	8.53
054	33.12	0.62	-0.03	0.86	-6.96	5.28	0.03	-0.00	-0.05	0.03	-0.00	-0.05	-0.01	0.01	0.03	0.02	0.00	-0.00	-0.19
055	50.55	0.90	0.02	0.63	-6.20	-2.54	-0.05	-0.01	-0.03	0.04	-0.01	-0.05	-0.01	-0.03	0.00	0.01	0.01	-0.01	1.16
056	41.80	0.98	-0.02	1.14	-4.91	-0.19	-0.05	0.00	-0.03	0.06	-0.00	-0.04	0.01	0.09	0.06	0.07	0.10	-0.01	-0.13
057	24.21	0.70	-0.02	0.49	-8.33	2.91	-0.06	0.01	-0.07	0.03	-0.01	-0.05	-0.03	0.11	0.02	0.02	0.00	-0.00	-0.22
058	99.91	0.92	-0.00	1.84	-11.27	32.60	-0.05	0.08	-0.13	0.20	0.02	-0.03	0.06	0.00	0.02	0.02	0.11	-0.01	3.30

for the first cycle of the samples collected from Gold One_1 show no element analysis error or missing elements.

In Table 7.22 and Table 7.23, the results of the leachate analysis of the first collection for the second cycle indicate that no samples collected from Mogale and Gold One_1 tailings show element analysis error or missing elements. All 23 samples have full elements contents. Similar observation is attained in Table 7.24 and Table 7.25, no samples show element analysis error or missing elements in the leachate analysis of the last collection for the second cycle.

In Table 7.26, the results of the leachate analysis of the first collection for the third cycle of the samples collected from Mogale tailings show that samples 039, 040, 042-1, 044, 045 and 047 exhibit element analysis error of Fe, while only samples 043 and 046 exhibit element analysis error of Mg and Fe. The results presented in Table 7.27 indicate no element analysis error or missing elements in the leachate analysis of the first collection for the third cycle of the samples collected from Gold One_1 tailing.

Table 7.28 presents the results of the leachate analysis of the last collection for the third cycle of the samples collected from Mogale tailings show that samples 040, 042-1, 045 and 047 exhibit element analysis error of Fe, whereas only samples 043 and 046 exhibit element analysis error of Mg and Fe. On the other hand, the leachate analysis of the last collection for the third cycle of the samples collected from Gold One_1 show no element analysis error or missing elements.

General observations show that Fe and Mg contents are largely absent or deficient in some samples collected from Mogale and Gold One_1 tailing, with a few number of samples lacking elemental content of Th and Ca.

Considering the contents of major elements such as K, Ca, Na, Mg, Fe, Al, Si and Mn, result shows that Fe elements were found mostly in the Gold One_1 tailing samples 052, 053 and 058 in high contents, with a lower acidic pH. Fe elements were also released and present in the samples of Mogale tailings, which is the layer with reddish. Gold One_1 tailing samples 054, 055, 056 and 057 pH are more than

5, with high contents of element of Ca, Mg, Na, and K. The major elements contents show no special changes from each of collections. Mn element are rarely found in leachate of Gold One_1 tailing samples but found largely in Mogale tailings. The major contribution of acid neutralisation ability is from element Ca.

The contents of trace elements show that the most of trace elements were released and present in the leachate; especially if the leachate shows acidic, pH is low for those samples from Mogale tailings such as As, Zn, Co and Ni. Gold One_1 sample leachate pH is higher and samples 054, 055, 056 and 057 indicated alkaline. The contents of trace elements are minor, and some of these results show negative values. Most of the trace elements are released in the first collection of the leachate. Therefore, as the number of leaching increased, the content in the filtrate decreases sequentially.

The whole leaching process shows that pH of leachate arranges from 3 – 4.7, which is conductive to the hydrolysis of Fe to generate Fe-OH; thus, Fe content in leachate is not high. The first cycle of leaching Fe is low. The content of Fe element is changed by the content of Ca, to exhibit the ability of Ca to neutralise acid.

7.4.1.4 Residue Chemical Composition Analysis

The residues from the leach column lab experiment were analysed by ICP-MS for geochemical characterisation. Major oxides such as Al, Ca, Fe, K, Mg, Mn, Na and S and trace elements such as Ag, As, Co, Cu, Ni, Pb, U and Zn were tested for all the residues to characterise the contents. Results obtained are arrayed in Table 7.30. Table 7.31 shows the chemical composition analysis results of samples before they are subject to leach column test. The comparison of two results (Table 7.30 and Table 7.31) indicates that some of the trace elements content in the residue increased after few months of free drainage leaching such as Ag, while some elements' content reduced in some samples.

Table 7.30: Residue chemical composition analysis results

Samples	Elements															
	Ag ppm	Al wt%	As ppm	Ca Wt%	Co ppm	Cu ppm	Fe Wt%	K Wt%	Mg Wt%	Mn Wt%	Na Wt%	Ni ppm	Pb ppm	S Wt%	U ppm	Zn ppm
038	2.00	0.50	90.99	0.42	6.22	17.89	1.02	0.12	0.30	0.01	0.02	23.61	124.02	0.42	5.24	17.60
038_1	<2	0.43	49.04	0.03	<2	<2	0.78	0.12	0.06	0.00	0.00	2.03	43.64	0.25	<2	5.21
038_2	<2	0.57	192.53	0.11	<2	1.67	1.05	0.14	0.07	0.00	0.00	3.60	38.00	0.33	2.75	18.48
039	7.62	0.54	59.22	0.31	18.09	14.08	1.00	0.09	0.28	0.01	0.04	51.53	107.15	1.09	<2	37.37
040	10.96	0.52	18.81	0.23	2.33	14.39	0.48	0.07	0.21	0.01	0.01	15.91	72.50	0.32	6.18	15.04
041	<2	0.81	72.05	0.26	12.86	13.79	0.88	0.08	0.25	0.01	0.03	45.45	92.57	0.53	3.76	61.04
042	11.28	1.21	68.00	0.82	68.78	42.31	2.11	0.10	0.52	0.04	2.03	289.62	57.41	1.63	5.30	460.22
042_1	4.59	1.02	76.46	0.61	16.74	10.01	1.57	0.10	0.27	0.01	0.05	70.91	71.30	0.81	2.00	79.10
043	<2	0.66	26.15	0.25	1.53	12.15	0.62	0.07	0.16	0.01	0.01	10.23	54.34	0.32	3.81	9.42
044	<2	0.76	74.09	0.45	70.78	16.88	4.64	0.08	0.16	0.01	0.07	96.22	69.49	0.53	6.88	35.10
045	<2	0.52	8.30	0.18	3.24	15.13	0.43	0.06	0.09	0.00	0.01	10.49	39.41	0.31	<2	10.41
046	<2	0.67	24.99	0.22	14.37	24.86	0.65	0.07	1.48	0.01	0.03	41.50	44.02	0.68	4.23	38.65
047	5.00	0.51	24.53	0.08	9.37	24.41	0.64	0.04	0.10	0.00	0.01	15.97	31.20	0.63	<2	9.11
048	<2	0.33	30.19	<2	2.00	3.12	0.23	0.01	0.08	0.00	0.00	5.60	20.01	0.02	<2	5.78
049	<2	0.66	79.63	0.08	8.57	14.30	0.80	0.02	0.15	0.01	0.02	22.19	32.23	0.48	2.37	15.07
050	5.31	0.48	67.86	0.04	4.21	16.79	0.66	0.02	0.10	0.00	0.01	12.48	31.88	0.26	2.54	9.66
052	<2	0.71	109.49	0.79	7.05	35.10	1.59	0.03	0.15	0.01	0.01	18.48	51.35	0.89	2.63	31.50
053	<2	0.68	89.14	0.63	5.22	22.90	1.36	0.03	0.15	0.08	0.01	19.34	42.87	0.70	1.96	31.14
054	<2	0.70	57.87	0.16	21.62	22.61	0.90	0.02	0.16	0.01	0.04	60.18	33.66	0.52	4.98	119.98
055	3.11	0.71	61.83	0.54	26.64	36.97	1.20	0.03	0.18	0.02	0.07	96.03	54.20	0.66	3.79	126.45
056	5.76	0.60	52.92	0.22	22.58	27.55	0.83	0.02	0.13	0.01	0.04	54.05	31.56	0.64	6.88	69.78
057	<2	0.76	49.02	0.10	21.56	30.15	0.79	0.03	0.19	0.01	0.05	65.37	23.51	0.52	5.52	49.36
058	<2	0.52	57.03	0.13	1.82	7.08	0.48	0.06	0.13	0.00	0.01	11.18	50.17	0.16	<2	12.84

Table 7.31: Raw tailing samples chemical composition analysis results

Samples	Elements															
	Ag (ppm)	Al (wt%)	As (ppm)	Ca (wt%)	Co (ppm)	Cu (ppm)	Fe (wt%)	K (wt%)	Mg (wt%)	Mn (wt%)	Na (wt%)	Ni (ppm)	Pb (ppm)	S (wt%)	U (ppm)	Zn (ppm)
038	0.20	6.94	92.20	0.62	7.00	16.90	1.97	0.50	0.52	<0.01	0.05	16.60	83.20	0.44	7.30	14.00
038_1	n/a	n/a	n/a	n/a	n/a	n/a	n/a	n/a	n/a	n/a	n/a	n/a	n/a	n/a	n/a	n/a
038_2	n/a	n/a	n/a	n/a	n/a	n/a	n/a	n/a	n/a	n/a	n/a	n/a	n/a	n/a	n/a	n/a
039	0.10	5.92	130.20	0.41	17.30	18.10	2.38	0.31	0.43	<0.01	0.06	46.30	63.00	1.03	9.60	32.00
040	0.10	6.43	82.50	0.32	17.80	32.90	2.60	0.36	0.48	0.01	0.04	51.50	51.10	1.02	10.00	42.00
041	0.10	8.25	87.80	0.40	39.40	37.40	2.31	0.38	0.43	0.01	0.07	94.90	43.80	1.08	57.60	175.00
042	0.10	6.74	81.20	0.79	49.90	36.40	3.47	0.36	0.67	0.04	0.14	198.80	26.80	1.29	39.50	346.00
042_1	<0.1	7.64	89.80	0.70	65.10	36.60	3.68	0.41	0.56	0.05	0.10	246.30	35.40	1.49	41.60	299.00
043	<0.1	6.02	96.40	0.40	44.70	37.80	2.95	0.29	0.42	0.03	0.09	98.60	27.50	1.20	42.40	91.00
044	0.10	5.56	123.40	0.63	89.70	52.10	9.05	0.25	0.39	0.02	0.07	141.60	38.90	1.34	34.50	99.00
045	<0.1	4.59	137.10	0.26	34.70	39.40	3.17	0.19	0.27	0.01	0.04	78.60	15.40	1.58	25.70	67.00
046	<0.1	6.14	115.90	0.47	38.50	44.50	3.37	0.27	0.40	0.02	0.07	92.90	28.00	1.72	30.30	99.00
047	-	-	-	-	-	-	-	-	-	-	-	-	-	-	-	-
048	<0.1	4.42	27.00	0.03	3.70	9.80	1.85	0.14	0.19	0.06	0.01	13.20	12.60	0.01	4.00	9.00
049	0.10	3.94	189.70	0.43	23.10	33.50	2.84	0.11	0.26	0.02	0.01	38.10	11.40	1.19	8.30	13.00
050	<0.1	4.71	191.40	1.39	61.50	52.40	4.77	0.15	0.34	0.04	0.02	229.70	28.20	2.04	35.80	145.00
052	<0.1	3.88	92.70	0.51	37.00	34.10	2.99	0.12	0.34	0.03	0.01	61.30	18.00	1.03	20.60	73.00
053	<0.1	4.23	130.30	1.08	28.90	39.80	3.82	0.13	0.38	0.04	0.01	67.70	20.10	1.41	21.20	116.00
054	<0.1	3.88	87.40	0.51	21.50	30.10	2.46	0.12	0.28	0.02	0.01	54.10	14.80	0.78	15.80	90.00
055	<0.1	4.84	127.10	1.16	22.10	25.80	2.83	0.16	0.36	0.03	0.02	57.20	30.60	0.83	18.90	164.00
056	<0.1	3.96	108.70	0.67	22.00	30.10	2.42	0.12	0.25	0.02	0.01	56.10	21.70	0.78	15.30	90.00
057	<0.1	4.62	122.30	0.80	21.90	34.60	2.92	0.15	0.31	0.02	0.02	70.20	30.10	0.92	20.70	97.00
058	<0.1	7.79	114.80	1.27	24.50	42.10	3.16	0.51	0.81	0.03	0.14	88.50	28.80	0.81	31.20	117.00

7.4.1.5 Residue XRD Analysis

The residue samples from leach column tests were also performed for the XRD analysis. Based on this analysis, the results show that the mineral composition of the residue samples have obviously changed compared with the initial un-leached samples. Hole T004 Mogale tailings, as presented in Table 7.32, determine that no Pyrite mineral phase found in the samples. The mineral Muscovite ($KAl_3Si_3O_{10}(OH)_2$), Yoshiokaite ($Ca(Al,Si)_2O_4$), Stishovite (extremely hard SiO_2), Nacrite ($Al_2Si_2O_5(OH)_4$), Caldecahydrite ($CaAl_2O_4 \cdot 10(H_2O)$) were not presented from the results. New mineral phase was found within the samples such as Kaolinite ($Al_2(Si_2O_5)\ (OH)_4$), Sylvite (KCl), Wollastonite ($CaSiO_3$), Potassium Hydrogen Sulfate ($K(HSO_4)\ (H_2SO_4)$). Also, the results obtained from Gold One_1 tailing indicates no Pyrite mineral phase and Caldecahydrite mineral phase. The mineral Kaolinite ($Al_2(Si_2O_5)\ (OH)_4$), Sylvite (KCl), Makatite ($Na_2Si_4O_8(OH)_2.H_2O$), Calcium Aluminum Oxide ($CaAl_2O_4/CaO{\cdot}Al_2O_3$), Sodium Hydrogen Oxalate Hydrate ($C_2HNaO_4.H_2O$), Wollastonite ($CaSiO_3$) and Potassium Hydrogen Sulfate ($K(HSO_4)(H_2SO_4)$) were new minerals phase discovered from the analysis results.

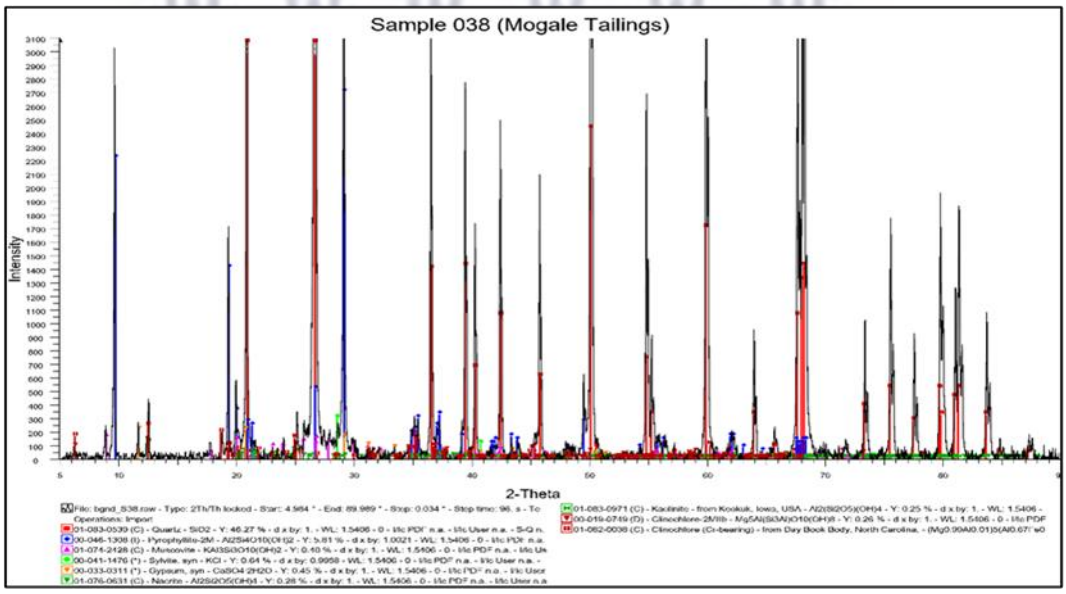

Figure 7.13: Sample 038 XRD analysis results

Table 7.32: XRD analysis results of residue hole T004 Mogale tailings

Samples	Elements														
	Quartz	Pyrophyllite	Clinochlore	Gypsum	Muscovite	Jarosite	Hematite	Nacrite	Kaolinite	Sylvite	Makatite	CAO	SHOH	Wollastonite	PHS
S038	46.27	5.81	0.26	0.45	0.4			0.28	0.25	0.64					
S038_1	50	6.27			0.43	0.48				0.69					
S038_2	47.35	5.94		0.46	0.41	0.45		0.17	0.17	0.65					
S039	55.71	3.5		0.54				0.34	0.3	0.77	0.38				
S040	117.01	2.67		0.41	0.37			0.26	0.23	0.59					
S041	111.82	8.18		0.63	0.57			0.39	0.35	0.9	0.44				
S042	121.57	5.56		1.28	0.62			0.43	0.38	0.98	0.48				
S042_1	92.98	4.25		0.64	0.47			0.33	0.29	0.75	0.37				
S043	61.13	2.79	0.17	0.43	0.31			0.22	0.19	0.2	0.24	0.63	1.04	0.87	2.08
S044	97.03	4.44		0.68	0.49		4.17	0.34	0.3	0.32			1.65		2.08
S045	75.91	3.47			0.38					0.25					
S046	95.40	4.36		0.67	0.48	0.53		0.34	0.29	0.31					1.54
S047	77.44	3.54	0.22	0.54	0.39			0.27	0.24	0.25			0.77		1.66

(In the table above, PHS = Potassium Hydrogen Sulfate ($K(HSO4)(H_2SO_4)$), CAO = Calcium Aluminium Oxide ($CaAl_2O_4/CaO{\cdot}Al_2O_3$) and SHOH = Sodium Hydrogen Oxalate Hydrate ($C_2HNaO_4{\cdot}H_2O$)).

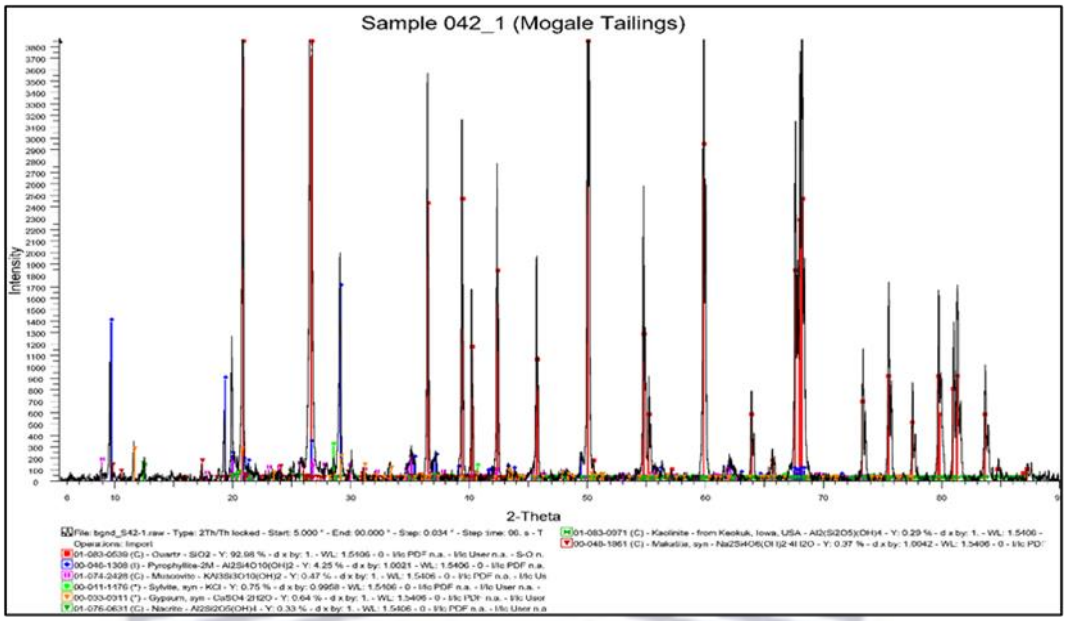

Figure 7.14: Sample 042_1 residue XRD analysis results

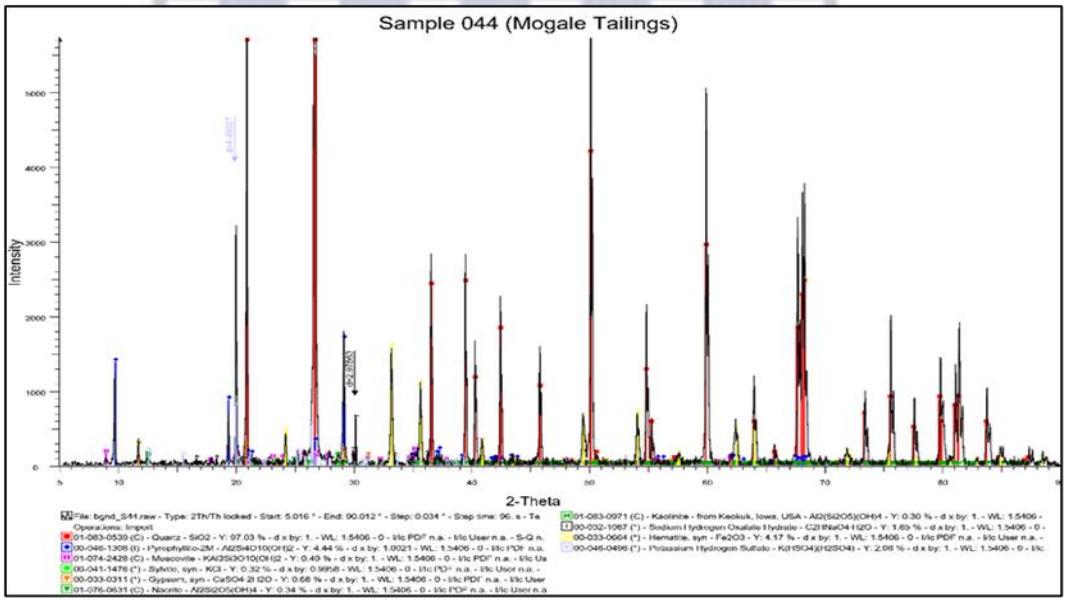

Figure 7.15: Sample 044 residue XRD analysis results

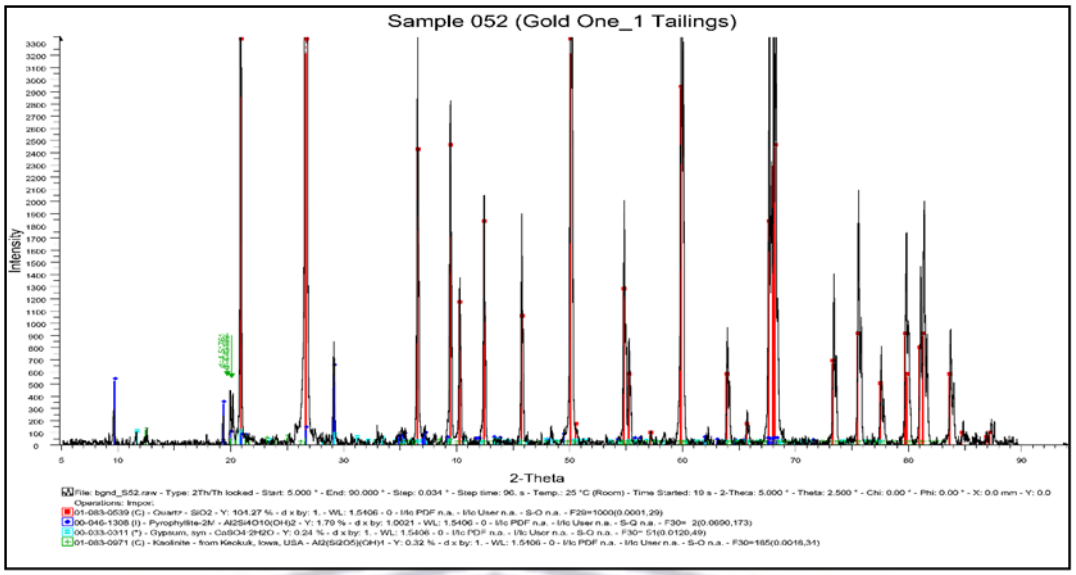

Figure 7.16: Sample 052 residue XRD analysis results

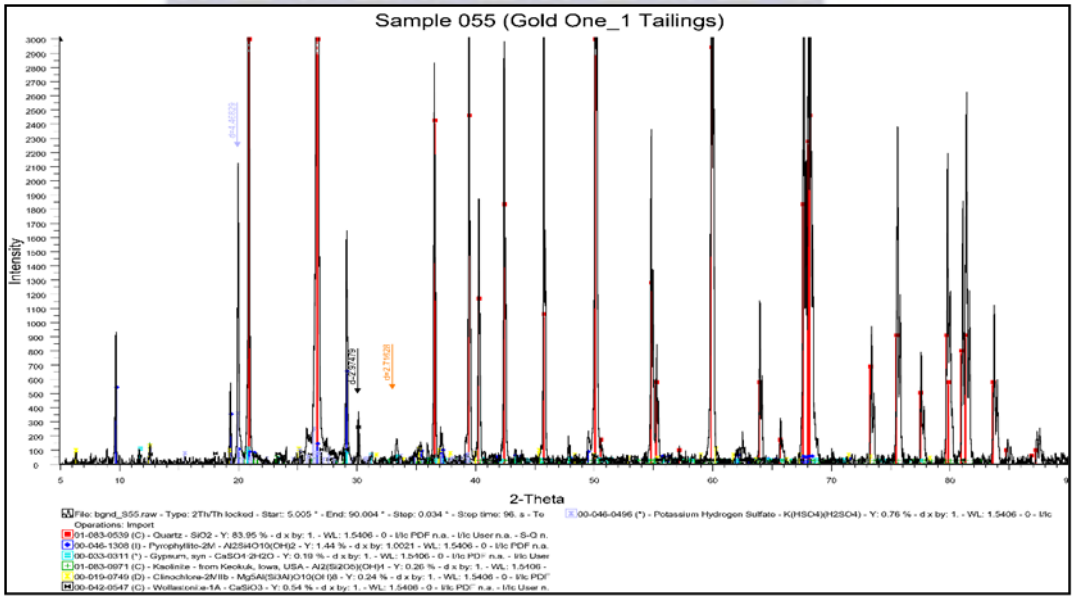

Figure 7.17: Sample 055 residue XRD analysis results

Table 7.33: XRD analysis results of residue hole T001 Gold One_1 tailings

Sample	Elements												
	Quartz	Pyrophyllite	Clinochlore	Gypsum	Muscovite	Iron Oxide	Sylvite	Nacrite	Kaolinite	CAO	SHOH	Wollastonite	PHS
S048	67.17	1.15	0.19				0.22	0.24	0.21		0.67		1.44
S049	96.33	1.65							0.3				0.87
S050	54.93	0.94				0.43			0.17	0.52			0.5
S052	104.27	1.79		0.24					0.32				
S053	87.61	1.5		0.2					0.27				0.8
S054	76.83	1.32	0.22	0.18					0.24				0.7
S055	83.95	1.44	0.24	0.19					0.26			0.54	0.76
S056	59.42	1.02		0.12					0.18			0.38	0.7
S057	60.58	1.04	0.17						0.19			0.39	0.71
S058	71.42	1.22	0.2	0.14	0.36				0.22			0.46	0.84

Finding shows that the duration of the leaching column test is longer enough for those samples to complete acid production process. The mineral composition was changed, and secondary minerals were produced. New minerals are formed in the process of leaching. The newly formed mineral crystallites are not flushed away by the leachate but remain in the solid phase of the sample. The newly discovered minerals are Kaolinite, Sylvite, Makatite, Calcium Aluminium Oxide, Sodium Hydrogen Oxalate Hydrate, Wollastonite and Potassium Hydrogen Sulfate. And the morphology of the pyrite varies greatly at different stages before and after leaching. Pyrite, Delhayelite and Caldecahydrite were not discovered above residue samples.

CHAPTER EIGHT

8. FINDINGS AND DISCUSSIONS

8.1 Introduction

Based on the results derived from the analysis of samples and lab experiments performed, a conceptual geochemical modelling is developed for an extreme problem of AMD in a gold tailing dams in West Rand area, especially the tailings that require immediate re-treatment. In the course of this study, the objectives and expected outcome of the study are achieved in accordance with the findings derived. The findings include the site observation results, data (samples) analysis and lab experimental results, geochemical modelling development, study conclusion and the way forward.

8.2 Findings of the Study

The primary discovery is the determination of the AMD potential in the study area, including the identification of the tailing dams that may begin operation soon, followed by the assessment of the samples' characteristics and evaluation of the factors that control AMD generation, and extended to the validation of the prediction methods for gold tailing dams. The consolidation of these findings eases the establishment of a conceptual geochemical modelling to assess the environmental impacts of gold tailings re-treatment in the future as well paves the way for the development of appropriate recommendation for further treatment techniques of AMD.

As earlier mentioned, site observation offers clear understanding on the ecological impacts of AMD on the study area. Observation demonstrates that ecological environmental contamination, which includes air and dust pollution, water resources contamination, acid mine drainage problems regularly occur in the area. Due to this effect, it is observed that tailing sludge could cause air pollution as it dries, because it got blown away by the wind during the dry and windy seasons. Wind pollution was observed at large rate when there is heavy wind, and this remains a major means of transporting metallic contaminants and radioactive

elements. This is only peculiar to the non-vegetated surface of the tailing dam. Evidently, gold tailing dams' surroundings lack vegetation cover, and therefore tailings are not well preserved. Further environmental observation shows that acid water decanting take place at Randfontein Operation in Gold One_2 tailings, which could affect the hygienic level of ground water resources. Even the adjacent residential area of the tailing is affected and the aquatic life of the streams across West Village residential area is destroyed because the flowing is brownish and with a great iron smell.

Analysis performed yielded relevant findings that determine that side of the tailings is more oxidised than the centre of the tailings dam. The leaching of the tailing dam is visible and more prominent on the side of the dams. The certain depth of the tailing dam has been oxidised due to the capillary movement of water through the soil and the danger it poses to the environment and surface and underground aquifer.

Mine-polluted water has high acid levels because of the presence of sulphuric acid. Beyond a certain concentration, sulphates are acutely toxic. Drinking this water can cause immediate vomiting, often leading to mild to severe levels of diarrhoea. Sensitive individuals can tolerate up to 600mg of sulphates per litre, but at the point of decant, there is (Hobbs & Cobbing, 2007) up to 4 500mg per litre. At high levels, the water will have a bitter and salty taste, which could stop people from drinking it. Mine water also contains toxic heavy metals dissolved by the acid water, including manganese, aluminium, iron, nickel, zinc, cobalt, copper, radium, and uranium–all with varying degrees of toxicity and radioactivity in the case of radium and uranium.

Robinson Lake, a located lake within the study area and next to Mogale gold tailings is unfunctional. This is due to the incapacity of the mining companies to pump and treat water before it overflowed to the surface of the ground in 2002. In addition, a huge volume of partially treated mine water flowed into the Robinson Lake near Randfontein in August 2002. This polluted (unhygienic) water killed the remaining fishes in the lake. In essence, the lake was contaminated because it was used for storage and settling facility for water pumped from the mines when operations were still active in the area. The levels of radioactive uranium in Robinson Lake are 40

000 times higher than the natural uranium levels for the area. Rand Uranium had planned to clean up the lake, but due to the latest crisis the company will have to discharge yet more untreated acid mine water into the lake. Water from the Robinson Lake flows into the Tweelopiespruit, which flows through the Krugersdorp Nature Reserve into a tributary of the Crocodile River, upstream from Hartbeespoort Dam. According to the Department of Water Affairs (Durand, 2012), the Tweelopiespruit which is in the study area, is a Class V, a very high acute hazard.

The tailings were classified into oxidised zone, transition zone and un-oxidized zone. These classified zones are visible through its depth, which are differentiated by the variation of the colour of the tailings compared to its initial state at its deposition. The surface of the tailing dam sampled were completely changed and transformed and no trace of greyish coloration was observed. As we move down the tailing dam, traces of greyish coloration appeared until it becomes wholly grey and sometimes contains blackish grey. A view from the top of the tailing dam visibly showed a whitish coloration that proceeded away from the tailing dam to nearest environment due to salts (susceptibly gypsum) deposited along the seepage pathway.

Better understanding of AMD occurrence mechanism, acid generation, acid transportation, influence factors of acid generation, acid neutralisation, its impact on local environment and communities were better practiced and applied to the study.

8.3 Discussions

The prediction test results together with previous discussions on mineralogical and geochemical characterisation can used to demonstrate a strategic approach towards the establishment of a conceptual geochemical modelling for AMD prediction for the gold tailing dams.

This thesis is a study on the potential of gold tailing dams to produce acid. This process mainly involves three parts, which are mineral composition, element composition and prediction test. The prediction test includes samples Paste pH value, acid-base calculation and leaching experiment. The mineral composition,

element composition and Paste pH value of the sample are the basis for the acid-base calculation and the leaching experiment is to explore the acid production process of the sample. Leaching column test is supplement test to acid-base calculation. During Sobek ABA calculation, the test and calculation of acid-neutralisation potential ANC is the key. Considering the conditions of acid-base reaction and the influence of some of the minerals (siderite) in the sample, the modified acid-neutralisation potential ANC test calculation method was used. ANC results show that the samples with high pyrite content continue to produce obvious acid.

In view of the negative value of the acid neutralisation potential of the sample, the actual acid neutralisation potential of the sample was calculated. NAPP of the samples calculated shows that the large value obviously has the potential of acid generation. Finding demonstrate that sample 040 NAPP value is negative, and the absolute value is very small, therefore, the acid production potential is undetermined and further leaching test is needed. Samples 038, 041 and 048 NAPP values are positive, but the value is not too high, which has the potential for acid production with less opportunities. The remaining NAPP of the samples calculated exhibit high positive values, therefore, the acid production will be generated.

Leach column test was demonstrated with dry and wet cycle Soxhlet extraction and leaching for samples collected from Mogale and Gold One_1 tailing dams. One tailing dam started operating and Gold One_1 will start operating soon. The leachate and residue from the lab experiment were analysed for mineralogical and geochemical composition. The major elements and trace elements in the filtrate showed that Mg and Mn elements in the leaching solution of each sample is slightly high, and the content of Ca is high. During the acid production process of those samples, Mg contributed little to the neutralisation ability of the minerals but Ca among these elements, contributed largely to the neutralisation ability. Moreover, most of the samples are acidic except samples 054, 055, 056 and 057, which are from Gold One_1 tailing dam within 6-10 meters depth. The mineral composition of sample 044 is hematite, and most of the samples' mineral composition are more abundant, including hematite, gypsum, muscovite, jarosite and kaolinite. Comparing the tailing samples with leaching and before leaching, no pyrite mineral

was found in the residue, which are from the leaching test. Some of the new secondary minerals are found from residue XRD analysis.

8.4 Conceptual Geochemical Modelling Development

The outcomes of the study have been fulfilled and the methods applied to this study have been established with a substantial data required to support research selection. For acid generation from the gold tailing dams, following steps of prediction methodologies are applicable.

- Evaluate available data
- Site investigation and observation,
- On-site measurement and experiments
- Samples for ABA
- ABA analysis which is static test
- Interpret data
- Data on mineralogy and geochemistry
- Samples for kinetic test
- Get rate of acid generation
- Data evaluation, including on-site measured data
- Geochemical modelling and risk-assessment, model accurately portrays observations.

CHAPTER NINE

9. CONCLUSIONS AND RECOMMENDATIONS

This study conducted a series of acid generation analysis and tests for the gold tailings samples collected from Witwatersrand area in South Africa. The environment-geochemical conceptual modelling is established and the expected study outcomes are achieved. However, limitation encountered in this study is the practical difficulty of attaining the accurate quantitative analysis of the mineral composition of the samples, which could affect the accuracy of the theoretical calculation value of the mineral acid neutralisation potential of the sample.

9.1 Conclusions

For assessment studies, mineralogical studies and multi-element analysis were used to determine the physical characteristics of the samples. The study performed an overview of minerals and elemental composition of the gold tailing dam. Multivariate statistics was used to characterise the tailing dam based on association, relationship and the compositional patterns of major elements and trace elements present within layers. The IDW interpolation using GIS was able to give an overview of elements spatial distribution with depth in the gold tailing dam.

For prediction studies, geochemical mass balance was used to predict the extent in which the tailings dam has been oxidised over a period. Acid-base accounting (ABA) and leach column kinetic test predicted the potential acidic generation of the gold tailings, together with the metal elements transportation.

The analysis and test results show that the gold tailing dams in the study area have the potential to generate more AMD if exposed to further oxidation. The tailing dam has been oxidised to a depth of 3-4 meters, with significant loss in major and trace elements. It could be said that about 0.164% (±0.02%) of the tailings' materials are leached yearly, and the surface of the tailing (layer 1) shows extreme oxidation. Also, oxidation started within transition zone (4-6 meters depth); and in few years, this lead to complete oxidation.

Overall, the conceptual geochemical modelling, which includes on-site experiments, lab test, mineralogical and geochemical characteristics can be applied to gold tailing acid mine drainage (AMD) prediction. Even in the short period, it could incur a complete prediction methodology for acid mine drainage (AMD) prevention of the gold tailing dams re-treatment.

9.2 Recommendations

Acid-base accounting (ABA) of mineral samples is not an outdated research area. Presently, there is a relatively standard calculation method for acid-base accounting (ABA) of sample based on the Sobek method. Some contradictions in the early methods of acid-base accounting (ABA) led to an improved approach in calculating and monitoring acid production and consumption. In addition, the study of the acid production process or the mechanism of sample acidification is mainly performed through leaching experiments. Therefore, recommendations enumerated below will offer insight on the prospective part of the evaluation of the acid production potential of mineral.

- The interaction between the oxidised zone and transition zone should be given more attention to determine the actual extent of damage.
- The incorporation of data from other tailings dams in the assessment and prediction using the tools employed in this study will give a comparison of results, where remediation process can be based on.
- The mass balance calculation should be done based on individual element since the rate of oxidation and mobility of elements differs. Data from soil and water surrounding the tailings dam should be incorporated into mass balance calculation to determine if there is any trend of AMD heavy metals transport and correlation.
- Considering the magnitude of acid mine drainage (AMD) liabilities and long-term impacts on the environment and financial consequences, therefore, early acid mine drainage (AMD) prediction is needed for the gold tailing dams that will be re-treated in the future. The on-site and lab reaction

of acid-producing and acid-consuming need to be effectively and continually operated.

- With the research on the kinetics of acid production of individual mineral components (A. K. Parbhakar-Fox et al., 2014), there will be more practical and easy determination of acid-base calculation methods. Also, the calculation of the theoretical acid neutralisation capacity of the mineral and the comparison of experimental calculation results is a very important aspect of the research. The theoretical calculation saves time and effort than the experimental calculation; although, one of the difficulties of the theoretical calculation is the accurate quantitative analysis of the mineral composition.
- The evaluation of mineral acid production potential is mainly based on the ratio of AP to NP to classify if there is potential for acid production, non-acid production or uncertain areas. This evaluation method is not universal and only suitable for a certain research area or in a research mining area; therefore, a more scientific evaluation method of acid production potential needs further study.
- The leaching column test is used to study the process of acid production or acidification of mine or tailings samples. The acidification solid phase change is mainly the oxidation and hydrolysis of iron (Dubiková Mária; Cambier Philippe; Vladimı´rSˇucha, 2002), which requires a long-term observation process. It is also a good method to use Soxhlet extraction and leaching experiment to study the changes of the filtrate and to analyse the acid production stage.

REFERENCE

Akcil, A., & Koldas, S. (2006). Acid Mine Drainage (AMD): causes, treatment and case studies. *Journal of Cleaner Production*, *14*(12-13 SPEC. ISS.), 1139–1145. https://doi.org/10.1016/j.jclepro.2004.09.006

Amari, K., Valera, P., Hibti, M., Pretti, S., Marcello, A., Essarraj, S. (2014). Impact of mine tailings on surrounding soils and ground water: Case of Kettara old mine, Morocco. *Journal of African Earth Sciences*, *100*, 437–449. https://doi.org/10.1016/j.jafrearsci.2014.07.017

Andre, B. J., Rajaram, H., & Silverstein, J. (2010). Incorporating geochemical and microbial kinetics in reactive transport models for generation of acid rock drainage. *Abstracts with Programs - Geological Society of America*, *42*(5), 203-.

Baguley, D. (2020). *Tailings dams: Mining and technology sector moves to mitigate tragedy*. AusBiz.

Bisschoff, A. A. (1982). Thermal metamorphism in the Vredefort dome. *Trans. Geol, Soc. S. Afr.*, *85*, 43–57.

Blowes, David W., Jambor John L., H.-F. C. J. (1997). Geochemical, mineralogical and microbiological characerization of a sulphide-bearing carbonate-rich gold-mine tailings impoundment.pdf. *Applied Geochemistry*, *13*(6), 687–705.

Bouiet, M. P. (1997). *A Comparative Mineralogical and Geochemical Study of Sulphide Mine-Taillngs At ' Iwo By* (Issue August). University of Manitoba Winnipeg. Manitoba, Canada.

Brink, A. B. A., & Bruin, R. M. H. (2001). Guidelines for Soil and Rock Logging in South Africa. *Geoterminology Workshop Organised by AEG, SAICE and SAIEG*.

Brough, C. P., Warrender, R., Bowell, R. J., Barnes, A., & Parbhakar-Fox, A. (2013). The process mineralogy of mine wastes. *Minerals Engineering*, *52*, 125–135. https://doi.org/10.1016/j.mineng.2013.05.003

Changul, C., Sutthirat, C., Padmanahban, G., & Tongcumpou, C. (2010). Chemical characteristics and acid drainage assessment of mine tailings from Akara Gold Mine in Thailand. *Environmental Earth Sciences*, *60*(8), 1583–1595. https://doi.org/10.1007/s12665-009-0293-0

Chilean Copper Commission. (2001). *Abandoned Mines: Problems , Issues and Policy Challenges for Decision Makers*.

Coetzee, H, van Tonder, D., Wade, P., Esterhuyse, S., van Wyk, N., Ndengu, S., Venter, J., & Kotoane, M. (2007). *Acid mine drainage in the Witwatersrand: Department of Minerals and Energy*.

Coetzee, Henk., Chirenje, E., Hobbs, P., & Cole, J. (2009). Ground and airborne geophysical surveys identify potential subsurface acid mine drainage pathways in the Krugersdorp Game Reserve , Gauteng Province , South Africa. *11th SAGA Biennial Technical Meeting and Exhibition, Swaziland, 16-18 September 2009, September*, 461–470.

Deloitte Touche Tohmatsu. (2003). *Financial Reporting in the Global Mining Industry*.

Dold, B. (2005). Basic Concepts of Environmental Geochemistry of Sulfide Mine-Waste. In *Latinoamericano de Metalogenia UNESCO-SEG: Vol. XXIV Curso*.

Dold, B., & Fontboté, L. (2002). A mineralogical and geochemical study of element mobility in sulfide mine tailings of Fe oxide Cu - Au deposits from the Punta del Cobre belt, northern Chile. *Chemical Geology*, *189*(3–4), 135–163. https://doi.org/10.1016/S0009-2541(02)00044-X

Dubiková Mária; Cambier Philippe; Vladimı´rSˇucha. (2002). Experimental soil acidification. *Applied Geochemistry*, *17*, 245–257.

Durand, J. F. (2012). The impact of gold mining on the Witwatersrand on the rivers and karst system of Gauteng and North West Province, South Africa. *Journal of African Earth Sciences*, *68*, 24–43. https://doi.org/10.1016/j.jafrearsci.2012.03.013

Eriksson, K.A., Turner, B.R.; Vos, R. G. (1981). Evidence for tidal processes in the

lower part of the Witwatersrand Supergroup, South Africa. *Sedim. Geol.*, *29*, 309–325.

Evangelou, V. P. (1995). *Pyrite Oxidation and Its Control*. CRC Press: Boca Raton.

Ewart, T. I. (2011). *Acid mine drainage in the Gauteng province of South Africa – A phenomenological study on the degree of alignment between stakeholders concerning a sustainable solution to acid mine drainage by* (Issue December). Stellenbosch University.

Ferguson, E. P. M. (1986). Pre-Mine Prediction of Acid Mine Drainage. *Environmental Impact and Management of Mine Tailings and Dredged Materials*.

Frind, E. O., & Molson, J. W. (1994). *Modelling of mill-tailings impoudments* (J. L. J. D. W. Blowes (Ed.); Environmen). Mineralogical Association of Canada.

Gibson, R.L., Wallmach, T. (1995). Metamorphism in teh Witwatersrand Basin: a perspective from the Vredefort Dome. *Circ. Econ, Geol. Res. Unit*, *288*, 30.

Gold - Minerals Council South Africa. (2020). https://www.mineralscouncil.org.za/sa-mining/gold

Gold One International Limited. (2013). *Gold One Tailing Backfill Plant and Pipeline Environmental Scoping Report for Public Comment Report Gold One International Limited*. *27*(107).

Goldfarb, R. J., Nielsen, R. L., Frimmel, H. E., & Minter, W. E. L. (2002). Recent Developments Concerning the Geological History and Genesis of the Witwatersrand Gold Deposits, South Africa. *Society of Economic Geologists*, *9*, 17–45. https://doi.org/10.5382/sp.09.02

Guagliardi, I., Cicchella, D., & De Rosa, R. (2012). A geostatistical approach to assess concentration and spatial distribution of heavy metals in urban soils. *Water, Air, and Soil Pollution*, *223*(9), 5983–5998. https://doi.org/10.1007/s11270-012-1333-z

Hageman, P. L., Seal, R. R., Diehl, S. F., Piatak, N. M., & Lowers, H. A. (2015).

Evaluation of selected static methods used to estimate element mobility, acid-generating and acid-neutralizing potentials associated with geologically diverse mining wastes. *Applied Geochemistry*, *57*, 125–139. https://doi.org/10.1016/j.apgeochem.2014.12.007

Harrison, S., Broadhurst, J. L., van Hille, R., Oyekola, O., Bryan, C., Hesketh, A., & Opitz, A. (2010). *A systematic approach to sulphidic waste rock and tailings management to minimise acid rock drainage formation* (Issue 1831).

Heikkinen, P. M., Räisänen, M. L., & Johnson, R. H. (2009). Geochemical characterisation of seepage and drainage water quality from two sulphide mine tailings impoundments: Acid mine drainage versus neutral mine drainage. *Mine Water and the Environment*, *28*(1), 30–49. https://doi.org/10.1007/s10230-008-0056-2

Hobbs, Phil., Cobbing, J. (2007). *the Hydrogeology of the Krugersdorp Game Reserve Area and Implications for the Management of Mine Water Decant*.

Hobbs, P. J., & Cobbing, J. (2007). A Hydrogeological Assessment of Acid Mine Drainage Impacts in the West Rand Basin, Gauteng Province. *Csir*. https://doi.org/Report no. CSIR/NRE/WR/ER/2007/0097/C. CSIR/THRIP.

Howard, M., & Heymans, J. (2000). *AN INTERNET SERVICE CENTRE ON WATER MODELLING SYSTEMS FOR THE MINING INDUSTRY* (Issue 901).

Hughes, R. (2013). EnvironmEntal Geochemcial Assessment of Waste and Ore. In *Journal of Chemical Information and Modeling* (Vol. 53, Issue 9). https://doi.org/10.1017/CBO9781107415324.004

Hutchision, I. P. G., & Ellison., R. D. (1992). *Mine Waste Management*. Lewis Publishers. INC.

Ian Wark Rearch Instiute. (2002). ARD Test Handbook Confidential Project P387A Prediction & Kinetic Control of Acid Mine Drainage. *Project P387A, Prediction and Kinetic Control of Acid Mine Drainage, May*, 42.

ILISO Consulting Pty Ltd. (2009). *Wonderfonteinspruit Catchment Area Remediation Plan*.

INAP. (2002). Prediction and kinetic control of AMD. In *Project P387A* (p. 42). AMIRA P387A Project.

Jacobs, J. A., Lehr, J. H., & Testa, S. . (2014). Acid Mine Drainage, Rock Drainage, and Acid Sulfate Soils. In *Acid Mine Drainage, Rock Drainage, and Acid Sulfate Soils*. Wiley. https://doi.org/10.1002/9781118749197

Jamieson, H. E., Walker, S. R., & Parsons, M. B. (2015). Mineralogical characterization of mine waste. *Applied Geochemistry*, *57*, 85–105. https://doi.org/10.1016/j.apgeochem.2014.12.014

Jennings, S. ., Neuman, D. R., & Blicker, P. . (2008). *Acid Mine Drainage and Effects on Fish Health and Ecology: A Review* (Vol. 40, Issue 6). https://doi.org/10.1016/j.ejcts.2011.03.013

Kearney, L. (2012). *Mining and minerals in South Africa*. Brand South Africa. https://www.brandsouthafrica.com/investments-immigration/business/economy/mining-and-minerals-in-south-africa

Landers, M., & Usher, B. (2012). Acid metalliferous leaching of a mineral sands deposit: from field to laboratory. *International Mine Water Association Annual Conference 2012*, *17*(6), 478–485.

Lapakko, K. (1994). Evaluation of neutralization potential determinations for metal mine waste and a proposed alternative. *The International Land Reclamation and Mine Drainage Conference*, 129–137.

Lawrence;, R. W., & Scheske., M. (1997). A method to calculate the neutralization potential of mining wastes. *Environ. Geol.*, *32*(2), 99–106.

Lawrence., & W., R. (1990). Prediction of behaviour of mining and processing wastes in the environment. *Doyle FM (Ed) Western Regional Symposium on Mining and Mineral Processing Waste*, 121–151.

Lesaca, R. M. (1975). Monitoring of heavy Metals in Philippine rivers, bay waters and lakes. *International Conference on Heav Metals in the Environment, Symposium Proceedings*, 285–307.

Liefferink, M. (2012). *Integrated Waste Managment Plan for West Rand District Municipality*. http://pmg-assets.s3-website-eu-west-1.amazonaws.com/docs/120530fse-edit.pdf

Lindsay, M. B. J., Moncur, M. C., Bain, J. G., Jambor, J. L., Ptacek, C. J., & Blowes, D. W. (2015). Geochemical and mineralogical aspects of sulfide mine tailings. *Applied Geochemistry*, *57*, 157–177. https://doi.org/10.1016/j.apgeochem.2015.01.009

Lottermoser, B. G. (2010). Mine Wastes: Characterization, Treatment and Environmental Impacts. In *Springer* (3rd Editio). Springer.

MacRobert, C. (2018). *South Africa needs to refresh how it manages by-products from mining*. The Conversation. https://theconversation.com/south-africa-needs-to-refresh-how-it-manages-by-products-from-mining-107019

Marchant, P. B., & Lawrence, R. W. (1991). *Acid Rock Drianage Prediction Manual* (Issue October).

Marescotti, P., Azzali, E., Servida, D., Carbone, C., Grieco, G., de Capitani, L., & Lucchetti, G. (2010). Mineralogical and geochemical spatial analyses of a waste-rock dump at the Libiola Fe-Cu sulphide mine (Eastern Liguria, Italy). *Environmental Earth Sciences*, *61*(1), 187–199. https://doi.org/10.1007/s12665-009-0335-7

McCarthy, T. S. (2006). The Witwatersrand Supergroup. In R. J. Johnson, M.R.; Anhaeusser, C.R.; Thomas (Ed.), *The Geology of South Africa* (pp. 155–186). Geological Society of Soth Africa.

McGuire, M. M., Edwards, K. J., Banfield, J. F., & Hamers, R. J. (2001). Kinetics, surface chemistry, and structural evolution of microbially mediated sulfide minearl dissolution. *Geochimica et Cosmochimica Acta*, *65*(8), 1243–1258.

Meek, F. A. (1981). Development of a procedure to accurately account for the presence of siderite during mining overburden analysis. *2nd Annual West Virginia Surace Mine Drainage Task Force Symposium*.

Méndez-Ortiz, B. A., Carrillo-Chávez, A., & Monroy-Fernández, M. G. (2007).

Acid rock-drainage and metal leaching from mine waste material (tailings) of a-Pb-Zn-Ag skarn deposit: Environmental assessment through static and kinetic laboratory tests. *Revista Mexicana de Ciencias Geologicas*, *24*(2), 161–169.

Miller, S., Jeffery, J. (1995). Advances in the Prediction of Acid Generating Mine Waste Materials. In L. C. Grundon, N. J., Bell (Ed.), *The Second Australian Acid Mine Drainage Workshop* (pp. 33–43). Australian Centre for Minesite Rehabilitation Research.

Miller, S., Robertson, A., Donohue, T. (1997). Advances in Acid Drainage Prediction Using the Net Acid Generation (NAG) Test. *The 4th International Conference on Acid Rock Drainage*, 535–549.

Mine, C. G., & Request, M. (2008). *Tailings and Waste Rock Geochemical Assessment*.

Morin, K. a, & Hutt, N. M. (2001). Environmental geochemistry of minesite drainage: practical theory and case studies. *Environmental Geochemistry of Minesite Drainage*.

Mukherjee, P. K., & Gupta, P. K. (2008). Arbitrary scaling in ISOCON method of geochemical mass balance: An evaluation of the graphical approach. *Geochemical Journal*, *42*(3), 247–253. https://doi.org/10.2343/geochemj.42.247

Naidoo, S. (2017). *Acid Mine Drainage in South Africa: Development Actors, Policy Impacts, and Broader Implications*. Springer. https://doi.org/10.1007/978-3-319-44435-2

Nathan, A. J., & Scobell, A. (2012). How China sees America. In R. J. Johnson, M.R., Anhaeusser, C.R., Thomas (Ed.), *Foreign Affairs* (Vol. 91, Issue 5). Geological Society of Soth Africa. https://doi.org/10.1017/CBO9781107415324.004

Navarro, M. C., Pérez-Sirvent, C., Martínez-Sánchez, M. J., Vidal, J., Tovar, P. J., & Bech, J. (2008). Abandoned mine sites as a source of contamination by

heavy metals: A case study in a semi-arid zone. *Journal of Geochemical Exploration*, *96*(2–3), 183–193. https://doi.org/10.1016/j.gexplo.2007.04.011

Nengovhela, A. C., Yibas, B., & Ogola, J. S. (2006). Characterisation of gold tailings dams of the Witwatersrand Basin with reference to their acid mine drainage potential, Johannesburg, South Africa. *Water SA*, *32*(4), 499–506. https://doi.org/10.4314/wsa.v32i4.5290

Nesbitt, K. (2013). *EMPR for Mogale Gold (Pty) Limited: Randfontein Cluster-Gauteng*.

Nordstrom, D. K., & Alpers, C. N. (1999). Geochemistry of Acid Mine Waste. Reviews in Economic Geology: The Environmental Geochemistry of Mineral Deposits. *Pacific Section Society of Economic*, *6*, 133–160.

Nordstrom D.K., and Alpers, C. N. (1999). Geochemistry of acid mine water. *Economic Geology*, *6A*(In: Plumlee GS, Logsdon Ms (eds.) The Environmental Geochemistry of Mineral Deposits. Part A: Processes, technique and health issues. Society of Economic Geologists, Littleton), 133–160.

Oelofse, S. H. H., Hobbs, P. J., Rascher, J., & Cobbing, J. E. (2002). The pollution and destruction threat of gold mining waste on the Witwatersrand-A West Rand case study. In *Water*.

Paktunc, A. D. (1999). Mineralogical constraints on the determination of neutralization potential and prediction of acid mine drainage. *Environmental Geology*, *39*, 103–112.

Parbhakar-Fox, A. K., Edraki, M., Hardie, K., Kadletz, O., & Hall, T. (2014). Identification of acid rock drainage sources through mesotextural classification at abandoned mines of Croydon, Australia: Implications for the rehabilitation of waste rock repositories. *Journal of Geochemical Exploration*, *137*, 11–28. https://doi.org/10.1016/j.gexplo.2013.10.017

Parbhakar-Fox, A., Lottermoser, B., & Bradshaw, D. (2013). Evaluating waste rock mineralogy and microtexture during kinetic testing for improved acid rock

drainage prediction. *Minerals Engineering*, *52*, 111–124. https://doi.org/10.1016/j.mineng.2013.04.022

Phillips, G.N., Law, J.D.M., Steven, G. (1997). Alteration, heat and Witwatersrand gold: 111 years after Harrison and Langlaagte. *S. Afr. J. Geol.*, *100*, 377–392.

Phillips. G.N., L. J. D. M. (1994). Metamorphism of the Witwatersrand gold fields: a review. *Ore Geol. Rew.*, *9*, 1–31.

Plumlee, G. S. (2009). *The Environmental Geology of Mineral Deposits*. *January*, 1–19.

Pope, J., & Weber, P. (2013). Interpretation of column leach characteristics of Brunner Coal Measures for mine drainage management. *AusIMM New Zealand Branch Annual Conference*, 377–385.

Potgieter, F., & Mendelsoha, C. (2001). *Guidebook to Sites of Geological and Mining Interest on The Central Witwatersrand*. The Geological Survey of South Africa.

Price, W. A. (2009). Prediction manual for drainage chemistry from sulphidic geologic materials. In *MEND* (Issue December).

Revuelta, M. B. (2018). *Mineral Resources: From Exploration to Sustainability Assessment*. Springer. https://doi.org/10.1007/978-3-319-58760-8_6

Rosner, T., Boer, R., Reyneke, R., Aucamp, P., & Vermaak, J. (2001). *A PRELIMINARY ASSESSMENT OF POLLUTION CONTAINED IN THE UNSATURATED AND SATURATED ZONE BENEATH RECLAIMED GOLD - MINE RESIDUE DEPOSITS T Rdsner • R Boer • R Reyneke • P Aucamp* (Issue 797).

Rösner, T., & Van Schalkwyk, A. (2000). The environmental impact of gold mine tailings footprints in the Johannesburg region, South Africa. *Bulletin of Engineering Geology and the Environment*, *59*(2), 137–148. https://doi.org/10.1007/s100640000037

Schippers, A., Kock, D., Schwartz, M., Böttcher, M. E., Vogel, H., & Hagger, M.

(2007). Geomicrobiological and geochemical investigation of a pyrrhotite-containing mine waste tailings dam near Selebi-Phikwe in Botswana. *Journal of Geochemical Exploration*, *92*(2–3), 151–158. https://doi.org/10.1016/j.gexplo.2006.08.003

Setianto, A., & Triandini, T. (2015). Comparison of Kriging and Inverse Distance Weighted (Idw) Interpolation Methods in Lineament Extraction and Analysis. *Journal of Applied Geology*, *5*(1), 21–29. https://doi.org/10.22146/jag.7204

Singh, P. (2014). *The assessment of sediment contamination in an acid mine drainage impacted river in Gauteng (South Africa) using three sediment bioassays in the at the*. *December*. https://ujdigispace.uj.ac.za

Skousen, J., Renton, J., Brown, H., Evans, P. (1997). Land Reclamation Neutralizatin Potential of Overburden Samples Containing Siderite. *Journal of Environmental Quality*, 673–681.

Skousen, J., Perry, E., Leavitt, B., Sames, G., Chisholm, W., Cecil, C. B., & Hammack, R. (2000). *Static tests for coal mining acid mine drainage prediction in the Eastern U.S.* 73–98.

Smith, A., Bridges, J. B. B. (1991). Some Considerations in the Prediction and Control of Acid Mine Drainage Impact on Groundwater From Mining in North America. *The EPPIC Water Symposium*.

Smuda, J., Dold, B., Friese, K., Morgenstern, P., & Glaesser, W. (2007). Mineralogical and geochemical study of element mobility at the sulfide-rich Excelsior waste rock dump from the polymetallic Zn-Pb-(Ag-Bi-Cu) deposit, Cerro de Pasco, Peru. *Journal of Geochemical Exploration*, *92*(2–3), 97–110. https://doi.org/10.1016/j.gexplo.2006.08.001

Sobek, A. A., Schuller, W. A., Freeman, J. R., & Smith, R. M. (1978). *Field and Laboratory Methods Applicable to Overburdens and Minesoils* (p. EPA-600/2-78-054). U.S. Environmental Protecitve Agency. https://doi.org/EPA-600/2-78-054

South African Committee for Stratigraphy. (1980). *Stratigraphy of South Africa* (p.

690).

Stevens, G., Boer, R., Gibson, R. L. (1997). Metamorphism, fluid flow and gold mineralization in the Witwatersrand Basin:towards a unifying model. *S. Afr. J. Geol., 100*, 363–376.

Stevens, L., van Nierop, M., & Clarke, J. (2014). *Climate change framework and operational climate change strategy*. 129.

Stewart, W. (2005). DEVELOPMENT OF ACID ROCK DRAINAGE PREDICTION METHODOLOGIES FOR COAL MINE Submitted In Fulfilment of the Requirements for the Degree of Doctor of Philosophy in Applied Science (Minerals and Materials) University of South Australia February 2005 Table of . *Doctor*, *1*(February).

The Internaitonal Network for Acid Prevention. (2009). *Global Acid Rock Drainage Guide (GARD Guide)*. http://www.gardguide.com

Thompson, J. A. J. (1975). Copper in marine waters: effects of mining wastes. *International Conference on Heav Metals in the Environment, Symposium Proceedings*, 273–284.

Tutu, H., McCarthy, T. S., & Cukrowska, E. (2008). The chemical characteristics of acid mine drainage with particular reference to sources, distribution and remediation: The Witwatersrand Basin, South Africa as a case study. *Applied Geochemistry*, *23*(12), 3666–3684. https://doi.org/10.1016/j.apgeochem.2008.09.002

Usher, B., Cruywagen, L.-M., Necker, E. de, & Hodgson, F. (2003). *ACID-BASE : ACCOUNTING , TECHNIQUES AND EVALUATION (ABATE): RECOMMENDED METHODS FOR CONDUCTING AND INTERPRETING ANALYTICAL GEOCHEMICAL ASSESSMENTS AT OPENCAST COLLIERIES IN SOUTH AFRICA BH Usher • L-M Cruywagen • E de Necker Recommended Methods for Cond* (Issue 1055).

Webber, P.A., Thomas, W. M., Skinner, R. St., Smart, C. (2004). Improved acid neutralization capacity assessment of iron carbonates by titration and

theoretical calculation. *Applied Geochemistry*, *19*, 687–694.

Weber, P. A., Stewart, W. A., Skinner, W. M., Weisenera, C. G. (2004). Geochemical effects of oxidation products and frambiodal pyrite oxidation in acid mine draingae prediction techniques. *Applied Geochemistry*, *19*, 1953–1974.

Weber, P. A., Thomas, J. E., Skinner, W. M., & Smart, R. S. C. (2005). A methodology to determine the acid-neutralization capacity of rock samples. *Canadian Mineralogist*, *43*(4), 1183–1192. https://doi.org/10.2113/gscanmin.43.4.1183

Wels, C., Lefebvre, R., & Robertson, A. M. (2003). An Overview of Prediction and Control of Air Flow in Acid-Generating Waste Rock Dumps. *6th International Conference on Acid Rock Drainage*, 12–18.

Whiteside, H. C. M., Glasspool, K. R., Hiemstra, S. A., Pretorius, D. A., Antrobus, E. S. A. (1976). Gold in the Witwatersrand Triad. In C. B. Coetzee (Ed.), *Mineral Resources of the Republic of South Africa* (Fifth Edit, pp. 39–76). Department of Mines Geological Survey.

Williams, E.G., Rose, A. W., Parizek, R. R., Waters, S. A. (1982). *Factors controlling the generation of acid mine drainage*.

Winde, F., Wade, P., & Van Der Walt, I. J. (2004). Gold tailings as a source of waterborne uranium contamination of streams - The Koekemoerspruit# (Klerksdorp goldfield, South Africa) as a case study. Part I of III: Uranium migration along the aqueous pathway. *Water SA*, *30*(2), 219–225. https://doi.org/10.4314/wsa.v30i2.5067

Yibas, B., Pulles, W., & Nengovhela, C. (2010). *Kinetic development of oxidation zones in tailings dams with specific reference to the witwatersrand gold mine tailings dams* (Issue 1554).

Younger, Paul. L., Banwart, Steven A., Hedin, R. A. (2002). *Mine Water: Hydrology, Pollution, Remediation*. Kluwer Academic Publishers.

Zhao, B., Usher, B. H., Yibas, B., & Pulles, W. (2010). *Evaluation and Validation*

of Geochemical Prediction Techniques for Underground Coal Mines in the Witbank/Vryheid Regions (Vol. 1, Issue 1249).

Zhu, Chen, Anderson, G. (2002). *Environmental Applications of Geochemical Modeling*. Cambridge University Press.

APPENDIX

Table A. 1: Major elements Leco and XRF analysis results, together with LOI, SiO_2, Al_2O_3, Fe_2O_3, CaO, MgO, Na_2O, K_2O, MnO, TiO_2, P_2O_5, Cr_2O_3, Ba, TOT/C and TOT/S. Unit: wt%

Sample	LOI	SiO2	Al2O3	Fe2O3	CaO	MgO	Na2O	K2O	MnO	TiO2	P2O5	Cr2O3	Ba	TOT/C	TOT/S
001	2.02	90.3	4.63	1.42	0.28	0.41	0.03	0.28	<0.01	0.24	0.02	0.041	<0.01	0.02	0.26
002	1.72	90.2	4.56	0.86	0.3	0.29	0.02	0.26	<0.01	0.24	0.01	0.025	<0.01	0.05	0.26
003	5.54	83.4	5.33	3.4	0.24	0.54	0.03	0.25	<0.01	0.18	0.03	0.038	<0.01	0.03	2
004	3.6	85	5.96	2.69	0.27	0.59	0.03	0.25	0.02	0.26	0.02	0.035	<0.01	0.03	1.25
005	5.55	79.2	8.25	3.66	0.53	0.58	0.09	0.4	0.04	0.27	0.03	0.037	<0.01	0.08	1.61
006	5.38	78.5	7.82	3.73	0.85	0.81	0.16	0.39	0.3	0.29	0.04	0.04	0.02	0.13	1.53
007	5.57	77	8.46	3.05	1.7	0.58	0.11	0.37	0.65	0.28	0.04	0.046	0.02	0.2	1.75
007-1	4.62	70.7	9.08	8.77	1.64	0.6	0.14	0.55	0.45	0.28	0.04	0.049	0.02	0.22	1.78
008	2.35	89	3.83	2.34	0.51	0.34	0.05	0.17	0.25	0.25	0.02	0.035	<0.01	0.09	0.96
008-1	2.71	85.9	5.11	4	0.19	0.3	0.04	0.19	0.11	0.28	0.02	0.038	<0.01	0.03	2.19
008-2	7.26	75.7	7.26	2.9	2.75	0.31	0.13	0.34	0.56	0.21	0.04	0.047	0.03	0.16	2.1
009	2.59	88.6	4.69	2.1	0.4	0.31	0.03	0.21	0.08	0.23	0.02	0.034	<0.01	0.04	0.96
010	3.76	84.1	6.73	2.11	1.03	0.09	0.07	0.3	<0.01	0.22	0.03	0.038	<0.01	0.07	0.67
011	2.82	87.9	5.37	1.37	0.37	0.28	0.02	0.27	<0.01	0.23	0.02	0.029	<0.01	0.04	0.64
012	3.43	84.4	6.55	2.5	0.48	0.56	0.04	0.33	0.01	0.21	0.03	0.033	<0.01	0.05	1.17
013	2.23	87.1	6.05	2.21	0.27	0.31	0.05	0.24	<0.01	0.24	0.02	0.028	<0.01	0.03	0.98
014	3.59	82.1	8.45	2.59	0.54	0.64	0.12	0.35	0.02	0.29	0.03	0.036	<0.01	0.05	1.28
015	4.47	80.9	7.49	3.55	0.52	0.56	0.08	0.36	0.06	0.27	0.03	0.035	<0.01	0.06	1.51
016	4.49	81.6	7.21	3.52	0.55	0.49	0.11	0.35	0.05	0.29	0.03	0.035	<0.01	0.04	1.58
017	3.97	79	5.25	9.01	0.55	0.38	0.06	0.23	0.04	0.22	0.02	0.036	<0.01	0.22	1.47
018	3.18	85.3	5.71	3.51	0.48	0.39	0.05	0.22	0.02	0.27	0.03	0.037	<0.01	0.04	1.94
018-1	3.42	82.4	9.85	1.75	0.19	0.4	0.1	0.4	0.02	0.35	0.02	0.057	<0.01	0.05	0.31
019	3.23	82.6	7.78	3.21	0.4	0.46	0.15	0.35	0.02	0.26	0.03	0.035	<0.01	0.09	1.63
020	2.49	87.9	6.29	1.63	0.06	0.1	0.15	0.4	<0.01	0.23	0.01	0.044	<0.01	<0.02	0.26
021	2.78	86.4	7.04	1.83	0.31	0.13	0.17	0.44	<0.01	0.23	0.02	0.041	<0.01	0.04	0.37
021-1	2.59	87.2	6.73	1.2	0.35	0.12	0.16	0.4	<0.01	0.28	0.02	0.045	<0.01	0.02	0.34
023	3.21	82.8	9.4	1.49	0.48	0.11	0.28	0.65	<0.01	0.29	0.03	0.044	<0.01	0.05	0.39
024	2.24	88.4	4.55	2.76	0.21	0.17	0.09	0.23	0.01	0.3	0.02	0.047	<0.01	0.02	1.5
025	3.14	83.9	9.21	1.61	0.36	0.23	0.22	0.55	0.01	0.24	0.05	0.062	0.01	0.04	0.86

Table A.1 continues

Sample	LOI	SiO2	Al2O3	Fe2O3	CaO	MgO	Na2O	K2O	MnO	TiO2	P2O5	Cr2O3	Ba	TOT/C	TOT/S
026	2.41	86.2	7.51	1.55	0.17	0.19	0.19	0.43	<0.01	0.22	0.05	0.048	<0.01	<0.02	0.81
027-1	4.43	76.5	6.97	9.31	0.54	0.48	0.11	0.39	0.04	0.24	0.03	0.044	<0.01	0.08	1.53
028	3.73	82.3	9.78	1.58	0.47	0.27	0.27	0.57	<0.01	0.26	0.04	0.055	<0.01	0.06	1.04
029	4.6	86.2	4.21	3.13	0.44	0.41	0.06	0.36	0.02	0.22	0.03	0.084	<0.01	0.21	0.65
030	2.1	90.1	3.06	2.59	0.28	0.66	0.04	0.24	0.02	0.26	0.01	0.045	<0.01	0.03	1.03
031	2.6	86.7	4.12	3.12	0.52	0.86	0.04	0.31	0.03	0.3	0.02	0.046	<0.01	0.07	1.06
032	2.81	87.6	4.96	2.39	0.7	0.23	0.05	0.35	0.02	0.24	0.02	0.042	<0.01	0.14	0.94
033	2.35	88.7	5.76	1.69	0.37	0.13	0.08	0.26	<0.01	0.26	0.02	0.037	<0.01	0.03	0.83
034	2.96	87.7	5.76	1.97	0.34	0.19	0.12	0.31	<0.01	0.24	0.02	0.046	<0.01	<0.02	1.05
035	2.49	86.7	6.28	2.44	0.32	0.48	0.02	0.35	0.01	0.2	0.02	0.045	<0.01	0.04	1.09
036	2.56	87	5.95	2.38	0.35	0.47	0.05	0.28	0.01	0.19	0.02	0.038	<0.01	0.04	1.11
037	2.41	87.2	5.68	2.48	0.3	0.58	0.03	0.25	0.02	0.21	0.02	0.038	<0.01	0.04	1.17
038	3.42	84.8	6.94	1.97	0.62	0.52	0.05	0.5	<0.01	0.2	0.02	0.04	<0.01	0.08	0.44
039	4.14	85.7	5.92	2.38	0.41	0.43	0.06	0.31	<0.01	0.19	0.03	0.041	<0.01	0.04	1.03
040	3.09	85.6	6.43	2.6	0.32	0.48	0.04	0.36	0.01	0.19	0.02	0.046	<0.01	0.04	1.02
041	3.65	83.6	8.25	2.31	0.4	0.43	0.07	0.38	0.01	0.23	0.03	0.049	<0.01	0.11	1.08
042	4.02	82.8	6.74	3.47	0.79	0.67	0.14	0.36	0.04	0.25	0.03	0.045	<0.01	0.08	1.29
042-1	4.93	80.6	7.64	3.68	0.7	0.56	0.1	0.41	0.05	0.24	0.03	0.034	<0.01	0.08	1.49
043	3.53	85.1	6.02	2.95	0.4	0.42	0.09	0.29	0.03	0.23	0.02	0.037	<0.01	0.04	1.2
044	3.15	79.7	5.56	9.05	0.63	0.39	0.07	0.25	0.02	0.23	0.02	0.047	<0.01	0.03	1.34
045	2.88	88.1	4.59	3.17	0.26	0.27	0.04	0.19	0.01	0.19	0.02	0.041	<0.01	0.04	1.58
046	3.25	85.1	6.14	3.37	0.47	0.4	0.07	0.27	0.02	0.22	0.03	0.043	<0.01	0.07	1.72
048	1.39	91.2	4.42	1.85	0.03	0.19	<0.01	0.14	0.06	0.29	0.02	0.046	<0.01	0.06	<0.02
049	2.77	89	3.94	2.84	0.43	0.26	<0.01	0.11	0.02	0.26	0.02	0.053	<0.01	0.03	1.19
050	5.61	82.1	4.71	4.77	1.39	0.34	0.02	0.15	0.04	0.24	0.02	0.068	<0.01	0.1	2.04
052	2.53	88.8	3.88	2.99	0.51	0.34	<0.01	0.12	0.03	0.24	0.02	0.053	<0.01	0.05	1.03
053	4.27	84.6	4.23	3.82	1.08	0.38	0.01	0.13	0.04	0.25	0.02	0.057	<0.01	0.1	1.41
054	1.96	90	3.88	2.46	0.51	0.28	<0.01	0.12	0.02	0.25	0.01	0.045	<0.01	0.07	0.78
055	3.39	86.1	4.84	2.83	1.16	0.36	0.02	0.16	0.03	0.26	0.02	0.055	<0.01	0.16	0.83
056	2.41	89.4	3.96	2.42	0.67	0.25	0.01	0.12	0.02	0.29	0.01	0.055	<0.01	0.08	0.78
057	2.83	87.2	4.62	2.92	0.8	0.31	0.02	0.15	0.02	0.25	0.02	0.045	<0.01	0.11	0.92
058	3.92	81.1	7.79	3.16	1.27	0.81	0.14	0.51	0.03	0.29	0.03	0.055	0.01	0.14	0.81
059	0.68	92.9	3.73	1.36	0.02	0.24	0.01	0.11	0.01	0.24	0.01	0.05	<0.01	0.04	<0.02

Table A.1 continues.

Sample	LOI	SiO2	Al2O3	Fe2O3	CaO	MgO	Na2O	K2O	MnO	TiO2	P2O5	Cr2O3	Ba	TOT/C	TOT/S
060	3.13	88.1	3.88	3.15	0.33	0.27	<0.01	0.11	0.02	0.28	0.05	0.054	<0.01	0.03	1.22
061	2.11	89.3	3.73	2.81	0.33	0.26	<0.01	0.11	0.02	0.3	0.01	0.047	<0.01	0.02	1.07
062	3.06	88.4	3.8	3.06	0.65	0.27	<0.01	0.12	0.03	0.24	0.02	0.051	<0.01	0.04	1.13
063	3.48	86.6	4.22	3.57	0.69	0.3	0.02	0.13	0.03	0.26	0.02	0.063	<0.01	0.08	1.37
064	3.49	86.3	4.35	3.52	0.73	0.36	<0.01	0.14	0.03	0.25	0.02	0.059	<0.01	0.07	1.04
065	2.8	88.2	3.91	2.95	0.49	0.31	0.02	0.13	0.03	0.25	0.01	0.057	<0.01	0.07	0.91
066	2.95	87.5	4.28	2.72	1.02	0.31	0.02	0.13	0.02	0.25	0.02	0.052	<0.01	0.15	0.87
067	2.44	89.6	3.77	2.44	0.71	0.23	0.02	0.12	0.02	0.27	0.02	0.052	<0.01	0.08	0.84
068	4.13	84.2	6.55	2.54	0.98	0.16	0.04	0.29	0.04	0.25	0.03	0.058	<0.01	0.12	0.84
069	5.27	81.1	7.37	2.92	1.42	0.35	0.04	0.29	0.05	0.23	0.03	0.05	<0.01	0.17	1.29
070	4.06	83.4	7.77	2.33	1.03	0.19	0.07	0.32	0.04	0.27	0.03	0.055	<0.01	0.17	0.88
071	2.29	92	2.73	1.81	0.6	0.1	0.01	0.12	0.02	0.22	0.02	0.047	<0.01	0.05	0.86
072	3.78	86.4	5.01	2.14	1.42	0.13	0.06	0.22	0.03	0.24	0.03	0.056	<0.01	0.36	0.96
073	3.44	87.1	4.28	2.54	1.06	0.13	0.04	0.19	0.02	0.3	0.02	0.072	<0.01	0.19	1.09
074	2.4	89.3	3.74	2.58	0.32	0.15	0.04	0.2	<0.01	0.29	0.02	0.052	<0.01	0.06	1.03
075	2	91.6	3.39	1.72	0.25	0.14	0.04	0.16	0.01	0.25	0.02	0.094	<0.01	0.38	0.77
076	2.69	89.3	3.79	2.79	0.65	0.24	0.01	0.13	0.01	0.24	0.02	0.056	<0.01	0.03	1.06
077	2.52	89.3	4.05	3.21	0.06	0.3	0.01	0.11	0.01	0.26	0.02	0.056	<0.01	0.04	1.59
078	2.42	90.1	3.69	2.69	0.06	0.22	0.01	0.11	0.01	0.29	0.01	0.056	<0.01	<0.02	1.11
079	4.22	79.3	10.87	2.58	0.19	0.66	0.11	0.46	0.02	0.45	0.03	0.058	<0.01	0.06	0.43
080	1.64	92	3.62	2.28	0.03	0.24	0.01	0.12	0.01	0.24	0.01	0.064	<0.01	<0.02	0.84
081	4.18	80.9	9.18	3.26	0.19	0.59	0.08	0.33	0.02	0.33	0.03	0.057	<0.01	0.02	0.51
082	3.27	81.6	10.06	2.82	0.17	0.67	0.1	0.4	0.02	0.38	0.02	0.056	<0.01	0.06	0.55
083	2.51	91.1	3.15	2.19	0.09	0.21	0.02	0.11	0.01	0.28	0.01	0.033	<0.01	0.03	0.96
084	2.62	89	3.58	3.13	0.08	0.26	0.01	0.11	0.01	0.28	0.02	0.058	<0.01	<0.02	1.48
085	2.71	88.1	3.78	3.69	0.08	0.28	<0.01	0.12	0.02	0.32	0.02	0.062	<0.01	<0.02	1.99
086	4.78	79.1	10.12	3.72	0.14	0.67	0.12	0.44	0.02	0.34	0.03	0.057	<0.01	0.07	0.89
087	5.56	77.4	10.59	3.78	0.16	0.65	0.1	0.44	0.02	0.34	0.04	0.052	<0.01	0.07	1.33
088	5.16	79.6	10	3.83	0.17	0.59	0.1	0.39	0.02	0.3	0.03	0.052	0.01	0.09	1.25
089	5.18	79.3	10.24	3.45	0.18	0.58	0.1	0.4	0.02	0.32	0.03	0.054	<0.01	0.06	1.3
090	5.14	79.6	10.07	3.2	0.23	0.57	0.1	0.35	0.02	0.35	0.03	0.049	<0.01	0.07	1.33

Table A. 2: Trace element ICP-MS analysis results-Ba, Be, Co, Cs, Ga, Hf, Nb, Rb, Sn, Sr, Ta, Th, U, V, W, Zr and Y. Unit: ppm

Sample	Ba	Be	Co	Cs	Ga	Hf	Nb	Rb	Sn	Sr	Ta	Th	U	V	W	Zr	Y
001	41	0.9	3.6	0.9	5.2	3	5.7	7.2	2	14.1	1.8	3.6	7	39	1.1	106.5	6.3
002	38	0.9	2.9	1.1	5.2	2.6	4.8	7.2	2	16.1	1.4	3.7	7.4	31	0.7	103.3	6.4
003	39	0.9	49.7	0.9	5.7	3.2	4.3	7.4	2	18.2	1	15.5	53.6	36	0.6	118.3	10.9
004	46	1	36.9	0.9	6.4	3	3.9	8.6	2	18.9	1.2	8	100.9	41	1.1	119	10.8
005	67	0.9	69.3	1.5	8.8	2.9	4	13.8	2	32.3	0.9	10.4	73	47	1	98.4	18.6
006	144	1	65.7	1.4	8.6	3	4.2	13.3	2	48.9	1.1	10.7	50.2	52	1	116.1	11
007	264	3	57.1	2.7	9	3.8	5	13.6	3	67.8	1.6	35.8	68.9	48	1.3	135.2	22.3
007-1	172	0.9	97.1	3	9.7	3.4	4.8	18.1	4	64.8	1.2	19.9	55.9	53	2.5	137.5	18.8
008	115	0.9	33.6	1.4	4.8	4.1	4.3	6.2	1	35.6	1.6	13.8	33.2	33	0.9	156.7	9.2
008-1	34	0.9	51.7	0.8	5.7	5.1	4	6.3	1	19.9	0.9	8.3	30.1	35	1.1	204.7	10.8
008-2	235	0.9	94.1	2.9	9.1	3.4	4.7	12.9	4	70.2	2	54.1	43.1	44	1.4	128.8	30.5
009	58	0.9	25.2	1	5.5	3.1	4.6	6.7	2	23.2	1.5	9	30.5	32	0.9	123.1	9.4
010	53	0.9	4.4	1.1	7.8	3.4	4.6	10.7	1	34.8	1.2	6.1	6.8	38	0.9	120.5	8.2
011	45	1	14.1	0.9	6.4	2.8	3.5	7.6	1	16.8	1.4	5.7	10.7	32	0.7	99.8	7.7
012	51	0.9	21.4	1.2	7.2	3.1	3.8	10.1	2	22	1.2	10.8	13.8	35	0.9	102.8	8.4
013	40	2	23.7	0.9	6.6	3.2	3.1	8.4	2	22	0.8	13.5	27.5	34	0.8	116.2	12.3
014	61	0.9	44.4	1.2	8.2	3	3.5	12	2	36	0.9	9.6	655.5	46	0.9	125.1	12
015	62	0.9	69.6	1.1	8	2.9	3.1	12.2	1	31.6	0.8	10	65.5	42	1.2	106.9	22.2
016	65	0.9	68.5	1.1	8	3.3	3.9	11.9	2	33	0.7	8.2	40.3	39	0.9	141.9	11.5
017	60	0.9	114	0.9	5.7	3.9	4.1	7.5	2	23	0.9	7.7	32.4	32	1.2	160	10.1
018	40	0.9	41.1	0.9	6	3.9	3.4	7.7	1	24	0.7	8.3	31.3	32	1.3	147.5	10.8
018-1	71	0.9	10.4	1.3	10	3.8	3.7	13.1	2	42.8	0.8	8.7	21.3	65	0.9	133	11.4
019	55	0.9	45.3	1	8.1	3.3	3.1	11.5	1	34.2	0.6	8.8	36.5	37	1.2	118.9	11.4
020	64	1	0.9	1	6.8	3.5	3.2	11.9	1	36.7	0.7	4.6	4.4	47	0.7	121.7	8.3
021	75	2	1.3	1.3	7.3	2.6	3.1	13.2	0.9	40.4	0.5	4.9	4.3	40	0.6	108.6	8.1
021-1	73	1	0.9	1.2	7.3	3.8	3.6	12.9	1	41.9	0.6	5.1	4	42	0.6	144.1	8.8
023	104	0.9	1.3	1.7	10	2.9	4.1	20.5	2	61.2	0.7	5.4	5.2	51	0.6	110.8	9.4
024	35	0.9	27.6	0.5	5.6	5.5	4.1	7.1	1	27.5	0.8	6.2	7.6	36	0.8	233.8	10.7
025	89	0.9	26.2	1.5	9.4	3.1	3.5	17.8	0.9	55.7	0.6	16.2	25.7	53	1	115.5	12
026	65	0.9	24.5	1.1	7.6	2.8	3.5	13.5	0.9	44.3	0.6	14.2	22	39	1.1	116.5	10
027-1	69	0.9	125.9	1.1	7.1	3.5	3.9	12.4	4	33.2	0.8	9.1	35.6	40	1.6	144	11.7
028	89	2	30.7	1.5	8.9	2.6	3.1	17.3	1	56.7	0.6	13.6	40	46	1	105.6	11.7
029	63	1	10.5	0.6	4.9	2.9	2.8	9.6	5	23.4	0.6	4.2	7.5	33	1.2	109.3	6.7
030	35	0.9	29.2	0.3	3.4	3.5	3.3	5.7	0.9	17	0.7	4	10.9	26	0.6	135.7	6.9
031	43	0.9	37.9	0.6	4.8	3.5	3.3	6.7	1	18.5	0.6	5.8	33.8	30	1	133.6	9
032	49	2	31.1	0.8	5.7	3	3.4	10.6	2	30.3	1	7.6	35.6	32	0.49	122.7	9.4

Table A.2 continues.

Sample	Ba	Be	Co	Cs	Ga	Hf	Nb	Rb	Sn	Sr	Ta	Th	U	V	W	Zr	Y
033	41	1	18.6	0.9	7.2	4.3	6.3	8.6	2	25.3	1.8	12	33.9	59	1.5	155.2	8.8
034	47	2	19.3	0.9	6.6	3.6	5.3	9.5	1	31.5	0.7	6.8	9.6	56	1.1	137.3	9.1
035	48	0.9	36.2	0.9	6.2	2.3	4.4	8.9	2	16.9	1.8	9.4	75.9	47	0.8	93.1	9.6
036	42	0.9	34.6	1.1	6.2	2.5	4.7	8	2	18.3	1.4	8.5	63	44	0.9	92.7	10.3
037	35	1	36.7	0.8	6.4	2.9	4.3	7.1	1	16.4	1.5	8.8	106.5	39	1.1	102.9	10.2
038	60	0.9	7	0.9	6.9	2.6	4.4	11.6	2	23	1.3	5.9	7.3	37	0.9	95.1	7.7
039	46	1	17.3	0.9	6.1	2.5	3.5	8.4	2	18.5	1.4	7.3	9.6	36	1	100.4	7.9
040	47	1	17.8	0.9	6	3.1	4.1	10.1	2	20	1	9.1	10	41	1.3	100.6	8.7
041	63	1	39.4	1.3	7.4	3	3.9	12.6	2	27.1	0.8	9.3	57.6	45	1.4	110.8	10.7
042	61	0.9	49.9	1	6.7	3.6	3.6	11.3	1	31	0.8	7.4	39.5	43	1.3	122.3	16.6
042-1	63	0.9	65.1	1.1	6.9	3.1	3.5	12.7	2	30.5	0.7	8	41.6	37	1.2	103.1	10.8
043	46	1	44.7	0.8	5.1	2.9	4	8.8	2	25	0.7	7.4	42.4	34	0.8	125.2	10.4
044	41	2	89.7	1.2	4.9	3.9	4.1	8.1	3	24.2	1	8.5	34.5	32	1.9	172.1	10.6
045	29	0.9	34.7	0.6	4.1	3.3	3.2	6	1	18.7	0.7	7.1	25.7	27	1.3	126	8.5
046	40	0.9	38.5	0.9	5.5	2.6	3.9	9	2	23.5	0.7	7.6	30.3	29	1.6	123	11.4
048	53	1	3.7	0.6	3.8	3.3	4	5.8	2	13.7	0.5	3.6	4	40	1	156	6.6
049	20	0.9	23.1	0.3	4	4.6	3.9	3.4	1	14.3	0.6	6.7	8.3	30	1.2	193	7.4
050	34	0.9	61.5	0.5	4.6	5	3.9	4.6	1	19.7	0.6	8.2	35.8	34	1.3	184.1	9.6
052	24	0.9	37	0.2	3.5	4.4	3.4	3.4	2	14.1	0.5	5.1	20.6	31	1	166.3	7.5
053	30	0.9	28.9	0.5	3.6	4.2	3.8	4.2	0.9	18.9	0.6	5.8	21.2	33	1.3	168.4	7.7
054	26	0.9	21.5	0.4	3.5	4	3.2	3.6	0.9	16	0.6	4.7	15.8	28	1.4	163.8	7.7
055	40	0.9	22.1	0.5	4.2	3.9	3.7	4.8	1	22.9	0.6	6.1	18.9	32	2.7	177	9
056	27	2	22	0.4	3.9	4.7	3.5	4	0.9	16.3	0.5	5.6	15.3	26	1.1	175.2	8.4
057	37	0.9	21.9	0.5	4.6	4.3	3.7	4.9	0.9	23.2	0.6	6.6	20.7	28	1.4	159	8.8
058	107	1	24.5	1.4	8.2	3.8	3.7	18.7	2	39.1	0.6	7.9	31.2	44	1.3	143.2	10.7
059	25	1	1.6	0.3	4	4.9	3.7	3.7	0.9	13.6	0.7	3	4.8	31	1	170.2	7.1
060	23	0.9	22.3	0.3	5.5	4.9	3.8	3.4	1	15.2	0.6	8.8	9.6	31	1.2	201.9	7.6
061	22	0.9	29.6	0.3	4.1	4.9	4.1	3.5	0.9	14.7	0.7	5	16.3	33	1.3	203.4	8.3
062	38	1	35	0.3	4.2	4.7	4.4	3.9	0.9	17.8	0.8	5.7	21.7	40	1.2	183.3	8.9
063	38	0.9	56.5	0.5	4.6	4.8	3.8	4.7	2	20.9	0.7	6.3	23.8	37	1.2	187.7	8.7
064	31	0.9	22.5	0.4	4.9	4.5	3.8	4.3	3	18.4	0.6	6.1	18.3	37	0.9	181.2	8.6
065	31	2	18.8	0.4	4.1	4.5	3.7	4.3	3	19.3	0.6	5.6	14.5	33	1.3	176.7	8.1
066	38	0.9	22	0.5	5	4.7	4.2	4.4	1	21.7	0.7	6.5	18.7	30	1.6	178.1	8.6

Table A.2 continues

Sample	Ba	Be	Co	Cs	Ga	Hf	Nb	Rb	Sn	Sr	Ta	Th	U	V	W	Zr	Y
067	31	0.9	22.7	0.4	4.7	3.8	3.6	4.5	1	17.7	0.6	6.1	16.2	33	1.2	184	8.4
068	58	0.9	63.4	1	7.5	4.7	5	9.7	3	36.8	0.7	9	37.1	43	1.2	169	15.1
069	57	2	78	1.1	7	3.9	4.1	9.2	2	40	0.7	10.9	56.5	41	1.2	151.5	16.7
070	55	0.9	61.3	0.9	7.4	3.3	5.7	11.5	2	44	0.7	8.9	52.4	45	1.3	141.7	15.4
071	27	0.9	31.9	0.3	2.6	3.3	4.3	3.7	0.9	21.5	0.5	3.7	14.7	26	1	133.9	7.9
072	40	0.9	24.5	0.6	4.9	2.9	4.6	7.3	2	33	0.5	5.6	14.8	36	1.3	134.3	9.8
073	35	0.9	27.2	0.6	4.5	4.6	5	7.4	1	26.2	0.6	5	10.3	37	1.2	173.9	9.9
074	39	0.9	24.8	0.4	3.7	4.1	4.6	7.8	2	21.5	1	5.8	6.1	33	1	181.8	7.6
075	29	0.9	18.9	0.4	3.4	3.6	4.6	5.1	1	19.5	0.7	4.3	45.1	28	0.8	135.5	8.2
076	22	0.9	18.1	0.3	3.2	3.2	3.4	4.1	1	16.4	0.5	4.9	8.3	36	1	126.8	6.2
077	18	0.9	31	0.3	4.3	3.8	4	3.9	0.9	15.4	0.6	6.2	14.5	35	0.9	171.7	7.5
078	19	0.9	20	0.3	3.3	6.1	4.8	3.7	0.9	14.9	0.7	3.4	7	37	1.1	248.4	7.8
079	74	0.9	16.6	1.6	10.4	3.4	4.9	16.1	1	43.9	0.6	13.6	23.3	64	0.9	129	11.9
080	22	0.9	15.6	0.4	3.5	4	3.6	4.1	0.9	15.7	0.5	3.1	6	33	1	174.2	8
081	62	0.9	16.4	1.1	9.5	3	4.7	12	2	34.1	0.6	9.6	18.3	74	0.7	132.2	11.9
082	73	0.9	24.4	1.2	9.8	3.7	4.9	14.6	1	40.2	0.7	6.1	18.8	60	1.2	140.3	12
083	18	0.9	20.5	0.3	3.1	4.8	4.4	3.8	0.9	14.5	0.7	3.9	9.2	25	1	188.1	7.2
084	20	0.9	28.2	0.2	3.7	4	3.8	3.9	1	20.8	0.7	5.2	9.6	36	1	177	6.3
085	22	0.9	37.7	0.4	3.9	6.3	4.9	4.3	2	18.5	0.8	5.3	13.4	56	1.3	256.3	8.8
086	72	0.9	20.2	1.5	10	3.7	4.2	14.8	0.9	40.8	0.7	6.9	73.8	59	0.8	128.5	14.3
087	66	0.9	59.4	1.4	9.7	3.5	5.9	16.2	1	41.8	0.6	14.9	101.4	50	1.4	123.2	17.5
088	66	0.9	46.5	1.3	8.7	3.1	6.2	13.9	2	40.1	0.8	10.3	89.4	49	1	117.2	14.3
089	72	0.9	86	1.3	10.5	3.6	5.8	14.7	0.9	44.3	0.7	10.4	155.8	46	1	129.4	14.9
090	53	0.9	80.3	0.9	9.8	2.6	5.7	13	2	38.3	0.8	9.9	215	51	1.4	116.3	15.3

Table A. 3: Trace element ICP-MS analysis results- ICP-MS analysis results, La, Ce, Pr, Nd, Sm, Eu, Gd, Tb, Dy, Ho, Er, Tm, Yb, Lu, Mo, Cu, and Pb. Unit: ppm

Sample	La	Ce	Pr	Nd	Sm	Eu	Gd	Tb	Dy	Ho	Er	Tm	Yb	Lu	Mo	Cu	Pb
001	17.1	32.8	3.47	13	1.93	0.41	1.39	0.2	1.18	0.22	0.58	0.1	0.74	0.11	4.2	15.4	91.6
002	16.9	33.8	3.45	12.4	1.99	0.43	1.54	0.22	1	0.23	0.61	0.1	0.7	0.11	1.4	11.7	74.1
003	19.7	37.2	4.14	14	2.62	0.57	2.36	0.38	2.15	0.37	1.21	0.17	1.29	0.16	2.3	282.5	54.8
004	21.9	43.3	4.55	16.6	2.71	0.61	2.26	0.37	2.07	0.39	1.26	0.17	1.04	0.19	3.2	42.6	43.1
005	34.1	68.6	7.4	26.9	4.59	1.13	4.98	0.8	4	0.83	2.36	0.28	1.4	0.2	2.6	41.8	58.1
006	31.2	57.4	6.03	21.6	3.74	0.7	2.79	0.42	2.4	0.45	1.33	0.18	1.38	0.17	2.8	43.4	71.3
007	43	82.2	8.73	31	5.79	1.1	5.22	0.91	4.77	0.9	2.59	0.34	2.05	0.28	2.5	57.9	143.9
007-1	39.5	78.4	8.25	28.8	5.16	1.04	4.49	0.7	3.92	0.8	2.16	0.31	1.84	0.26	2.6	93.6	103.9
008	28	53.7	5.63	18.2	3.23	0.54	2.25	0.36	2.05	0.37	1.07	0.14	1.12	0.13	3.2	32.1	65.1
008-1	27.2	51.9	5.38	18.6	3.18	0.66	2.61	0.37	1.97	0.36	1.21	0.19	1.08	0.18	4.4	53.2	23.5
008-2	49.9	96.8	10.15	38.3	7.37	1.34	7.75	1.31	7.18	1.29	3.57	0.48	2.97	0.4	4.3	62.3	150.2
009	22.6	44.4	4.69	16.3	2.84	0.57	2.3	0.34	1.77	0.36	1.1	0.14	1.06	0.15	4.5	30.1	62.9
010	24.4	43.6	4.57	14.8	2.43	0.51	1.88	0.27	1.42	0.31	0.8	0.12	1.06	0.14	3.8	21	54.6
011	20.4	38.9	4.07	13.6	2.38	0.44	1.83	0.26	1.41	0.27	0.88	0.12	0.76	0.13	2.4	22.6	96.1
012	21.9	41	4.53	15.1	2.59	0.58	2.09	0.31	1.67	0.3	0.94	0.12	0.88	0.15	2.6	33.3	69.6
013	20.3	37.8	4.06	14.6	2.54	0.54	2.21	0.37	2.09	0.43	1.21	0.18	1.21	0.19	1.7	44.3	33.3
014	25.8	51	5.49	18.8	3.59	0.75	2.86	0.44	2.47	0.47	1.39	0.2	1.4	0.21	1.6	46	49.5
015	31.9	63.9	6.95	25.5	4.59	1.16	5.97	0.99	5.3	1.07	2.86	0.28	1.35	0.19	1.9	41.9	43.3
016	25.7	49.7	5.37	19.3	3.2	0.67	2.59	0.38	2.28	0.45	1.25	0.17	1.07	0.17	1.5	38.9	26.6
017	23.2	44	4.57	17	2.69	0.61	2.36	0.35	1.87	0.41	1.07	0.17	1.08	0.16	5.4	52.6	36.7
018	27.3	51.8	5.55	20.1	3.18	0.63	2.57	0.37	2.1	0.44	1.24	0.17	0.99	0.17	3.4	55.5	24.8
018-1	27.6	51	5.38	17.9	3	0.67	2.47	0.36	2.16	0.38	1.18	0.18	1.28	0.2	4.7	28.7	37.8
019	32	58.9	6.51	22.7	3.76	0.76	2.98	0.4	2.33	0.41	1.31	0.18	1.45	0.16	1.2	50.4	36.4
020	24	43.1	4.45	14.9	2.58	0.52	1.75	0.26	1.6	0.3	0.91	0.13	1.11	0.13	6.1	4.4	22.3
021	24.3	44.1	4.57	16	2.3	0.51	1.95	0.27	1.6	0.32	0.83	0.13	0.88	0.12	4.8	4	21
021-1	25.6	46	4.73	16.5	2.57	0.58	2.05	0.29	1.58	0.34	1.09	0.15	0.91	0.14	5.7	3.8	17.9
023	29.6	53.6	5.57	19.2	2.94	0.67	2.35	0.3	1.79	0.36	1.06	0.14	0.99	0.15	3.3	7	25.1
024	21.7	40.6	4.17	14.8	2.4	0.55	2.3	0.34	1.84	0.38	1.27	0.17	1.31	0.18	6.4	8.6	21
025	31.9	57.6	6.07	21	3.45	0.75	2.8	0.42	2.11	0.42	1.34	0.18	1.45	0.18	5.3	308.8	27.4
026	28.3	51.7	5.39	20	2.95	0.65	2.46	0.35	1.83	0.36	1.09	0.15	1.09	0.16	4	218.5	24.3
027-1	28.1	54.9	5.79	19.6	3.45	0.69	2.69	0.42	2.21	0.44	1.23	0.18	1.26	0.18	5.5	69.8	51.9
028	30.3	55.7	5.99	20.6	3.47	0.69	2.74	0.4	2.09	0.44	1.21	0.18	1.16	0.19	3.7	64	34.5

Table A. 3 continues.

Sample	La	Ce	Pr	Nd	Sm	Eu	Gd	Tb	Dy	Ho	Er	Tm	Yb	Lu	Mo	Cu	Pb
029	17.2	32.2	3.43	11	2.05	0.41	1.58	0.23	1.37	0.29	0.71	0.1	0.68	0.11	4.2	32.5	46.6
030	17.6	32.5	3.48	12.6	2.08	0.46	1.6	0.25	1.25	0.24	0.76	0.1	0.59	0.12	4.8	37.3	31.6
031	19.5	37.1	3.9	14.4	2.34	0.51	1.94	0.29	1.82	0.36	0.97	0.12	0.8	0.13	3.8	50.6	60.2
032	23.8	41.4	4.52	16.5	2.63	0.57	2.22	0.31	1.85	0.38	1.07	0.14	0.75	0.14	4.5	39.9	38.4
033	22.6	42.5	4.45	17.8	2.97	0.61	2.35	0.29	1.65	0.32	0.98	0.15	1.05	0.11	3.9	39	37.2
034	23	43.3	4.73	17.5	2.78	0.57	2.4	0.29	1.52	0.34	0.9	0.14	1.02	0.14	5.9	51	16.2
035	22.9	41.9	4.72	16.7	2.97	0.6	2.8	0.33	2.17	0.37	1.09	0.14	0.92	0.13	5.2	37.8	72.5
036	21.2	39.5	4.51	17.3	3.18	0.66	2.62	0.36	1.9	0.37	1.09	0.17	1.06	0.15	3.6	38.3	57.5
037	20.8	40.9	4.49	15.9	3.05	0.62	2.65	0.36	2.06	0.34	1.08	0.16	1.03	0.16	4	46.6	62.9
038	22.1	40.5	4.23	14.1	2.64	0.51	2.04	0.27	1.49	0.25	0.77	0.12	0.77	0.11	2.7	16.9	83.2
039	19.7	35.9	4.09	15.7	2.63	0.5	2.02	0.24	1.22	0.23	0.79	0.12	0.7	0.11	4.1	18.1	63
040	21.3	37.9	4.21	14.8	2.62	0.55	2.24	0.27	1.61	0.29	0.92	0.12	0.91	0.12	4.9	32.9	51.1
041	25.1	49.2	5.72	21.6	3.67	0.79	2.75	0.36	2.13	0.38	1.02	0.16	1.04	0.16	5.1	37.4	43.8
042	26	47.6	5.35	20.8	3.4	0.78	4.09	0.53	3.2	0.62	1.76	0.23	1.15	0.17	4.6	36.4	26.8
042-1	27.4	50.6	5.65	21.5	3.41	0.76	2.64	0.35	1.9	0.35	1.13	0.16	1.01	0.16	1.7	36.6	35.4
043	22.8	43.1	4.76	16.8	3.03	0.63	2.54	0.34	2.24	0.35	1.03	0.17	0.99	0.13	4.5	37.8	27.5
044	25.1	49	5.26	19.7	3.15	0.63	2.71	0.36	2.22	0.36	1.13	0.18	1.1	0.17	5.1	52.1	38.9
045	23.8	42.9	5	19.4	2.78	0.57	2.48	0.29	1.7	0.32	0.81	0.14	0.86	0.13	6.3	39.4	15.4
046	27.4	52.8	5.81	19.6	3.45	0.72	2.85	0.37	2.26	0.38	1.24	0.17	1.1	0.17	4.8	44.5	28
048	13.2	27	2.64	9.9	1.68	0.36	1.41	0.18	1.29	0.25	0.67	0.11	0.69	0.11	6.6	9.8	12.6
049	15.4	27.3	2.89	9.6	1.98	0.4	1.57	0.23	1.36	0.26	0.73	0.11	0.84	0.12	5.9	33.5	11.4
050	18.9	34.6	3.72	14	2.4	0.54	2.2	0.3	1.85	0.33	1.06	0.15	0.98	0.16	7.5	52.4	28.2
052	14.7	28	3.09	10.8	2.06	0.46	1.71	0.24	1.58	0.26	0.78	0.12	0.82	0.12	6.4	34.1	18
053	16	30.3	3.38	11.8	2.05	0.44	1.79	0.24	1.47	0.25	0.71	0.12	0.83	0.12	8.1	39.8	20.1
054	15.4	28.3	3.18	11.7	1.86	0.45	1.55	0.22	1.38	0.25	0.67	0.11	0.79	0.12	5.4	30.1	14.8
055	18.6	34.7	3.72	13.4	2.27	0.52	1.88	0.28	1.74	0.31	0.96	0.14	0.9	0.15	4.6	25.8	30.6
056	16.4	29.5	3.28	12.3	1.97	0.46	1.87	0.23	1.54	0.28	0.78	0.12	0.82	0.13	6.2	30.1	21.7
057	17.4	32.1	3.75	14.8	2.32	0.49	2	0.27	1.72	0.26	0.84	0.14	0.81	0.13	4.3	34.6	30.1
058	23.8	43.7	4.81	18.3	2.9	0.66	2.55	0.34	1.84	0.37	1.1	0.17	0.99	0.15	4.8	42.1	28.8
059	14.8	28	3.02	10.7	1.82	0.4	1.59	0.21	1.22	0.26	0.77	0.1	0.67	0.11	7.4	7.5	12.1
060	15.3	28.5	3.21	11.2	2	0.44	1.66	0.23	1.32	0.27	0.81	0.12	0.86	0.13	6.6	20.9	11.8
061	16.5	30.1	3.21	11	2.04	0.45	1.85	0.23	1.37	0.24	0.77	0.12	0.94	0.12	7.1	23.7	12.1
062	18.2	33.4	3.58	13	2.24	0.5	2.15	0.28	1.69	0.29	0.85	0.15	1.05	0.15	6.7	29	20.5
063	17.8	32.8	3.67	13.9	2.16	0.51	1.98	0.28	1.63	0.28	0.89	0.14	0.87	0.14	8.2	50.4	26.4
064	17.2	31	3.55	12.1	2.2	0.52	1.88	0.25	1.6	0.26	0.85	0.13	0.84	0.12	8.9	30.6	18.3
065	16.3	29.7	3.4	12.3	1.97	0.48	1.83	0.24	1.46	0.26	0.79	0.13	0.81	0.13	8.6	24	22.8

Table A. 3 continues.

Sample	La	Ce	Pr	Nd	Sm	Eu	Gd	Tb	Dy	Ho	Er	Tm	Yb	Lu	Mo	Cu	Pb
066	18	32.3	3.63	13.3	2.23	0.54	2.05	0.26	1.68	0.29	0.79	0.13	0.83	0.13	6.3	30.7	22.3
067	16.3	31.2	3.56	14.3	2.09	0.46	1.78	0.25	1.68	0.31	0.8	0.13	0.91	0.13	6.1	30.6	18.6
068	31.2	60.3	6.91	23.6	4.04	1.01	3.77	0.46	2.83	0.44	1.36	0.2	1.27	0.2	8.5	62.8	51.1
069	38	69.6	8.32	31.1	4.73	1.22	4.41	0.54	3.38	0.57	1.55	0.23	1.52	0.22	4.2	68.1	67.5
070	34.2	67.3	7.47	26.8	4.79	1.02	4.25	0.55	2.98	0.55	1.47	0.21	1.23	0.2	6.6	75.9	41.8
071	17.5	33	3.66	13.6	2.24	0.53	1.92	0.25	1.39	0.29	0.67	0.11	0.89	0.11	9.1	28.7	21.9
072	22	38.6	4.45	15.6	2.36	0.56	2.3	0.29	1.88	0.33	0.83	0.12	0.96	0.14	9.4	55.7	34.2
073	20.2	38.2	4.21	14.8	2.34	0.54	2.19	0.3	2.03	0.35	0.96	0.12	0.9	0.13	9.2	100.5	28
074	15.7	30.8	3.44	11.2	2.04	0.43	1.6	0.22	1.24	0.23	0.86	0.1	0.76	0.11	7.5	36.2	19
075	18	33.8	3.81	14.4	2.4	0.52	1.77	0.27	1.47	0.3	0.85	0.12	0.99	0.14	8.1	37.2	13.4
076	13.9	25.3	2.92	10.7	1.71	0.37	1.37	0.19	0.89	0.23	0.6	0.09	0.67	0.11	9.4	43.2	15.4
077	15	28.7	3.07	10.3	1.8	0.38	1.58	0.21	1.15	0.26	0.77	0.1	0.78	0.11	8.7	34.7	9.1
078	15.3	27.7	3	9.8	1.78	0.36	1.55	0.22	1.44	0.27	0.82	0.13	0.9	0.13	9.2	26.6	18.6
079	27	48.5	5.47	19.7	3.33	0.68	2.76	0.37	2.14	0.43	1.17	0.16	1.17	0.17	4	57.6	24.3
080	15.2	28.8	3.12	10	1.68	0.38	1.64	0.22	1.4	0.29	0.79	0.12	0.82	0.12	9.5	26.4	14.4
081	24.6	44	4.91	18.1	2.88	0.67	2.41	0.35	1.92	0.38	1.15	0.16	0.92	0.16	4.4	25	35.9
082	26	44.9	5.4	18.9	3.05	0.72	2.59	0.35	2.05	0.44	1.19	0.16	1.12	0.18	4.8	42.9	31.5
083	14.8	28	2.99	10.7	1.62	0.4	1.59	0.22	1.34	0.23	0.74	0.11	0.73	0.12	3.4	34.2	15.3
084	18.2	31.4	3.4	12.1	1.83	0.43	1.49	0.19	1.24	0.23	0.67	0.09	0.76	0.12	10	32.5	20.8
085	19.3	32.3	3.55	12.5	2.19	0.47	1.85	0.26	1.75	0.31	0.96	0.14	0.93	0.16	8.4	42.6	11.9
086	25.7	51.3	6.09	23	3.94	0.87	3.35	0.47	2.92	0.5	1.4	0.19	1.38	0.21	4.3	27.7	30.7
087	30.8	58.8	6.63	21.7	3.9	1.01	3.65	0.48	2.62	0.52	1.4	0.22	1.43	0.2	2.7	41.3	26.2
088	26.6	52.7	6.03	18.6	3.73	0.82	2.92	0.45	3.04	0.41	1.39	0.2	1.45	0.18	2.6	43.8	33.7
089	33.1	63.6	6.99	23.5	4.31	0.96	3.5	0.5	3.31	0.55	1.44	0.24	1.49	0.2	2.3	41.1	36.7
090	31.2	62.6	6.9	22.3	4.37	1.01	4.14	0.55	3.11	0.52	1.58	0.22	1.38	0.21	3.2	40.9	30.2

Table A. 4: Trace element ICP-MS analysis results- Zn, Ag, Ni, As, Au, Cd, Sb, Bi, Hg, Ti and Se. Unit: ppm, Au Unit: ppb

Sample	Zn	Ag	Ni	As	Au	Cd	Sb	Bi	Hg	Ti	Se
001	19	0.2	20	45.2	110.2	0.09	0.5	1.9	0.24	0.09	0.8
002	15	0.1	11.2	23.3	271	0.09	0.4	1.8	0.18	0.09	0.49
003	118	0.2	126.9	132.3	404.7	0.4	0.8	1.6	0.13	0.09	0.8
004	124	0.1	123.3	85.3	204.6	0.3	0.5	1.3	0.08	0.09	0.49
005	817	0.09	256.1	102.9	134.9	0.3	0.7	1.4	0.15	0.09	0.49
006	144	0.2	150.9	135.7	186.7	0.3	0.8	1.4	0.17	0.09	0.7
007	260	0.4	149.4	331.9	103.5	0.9	0.7	2.7	0.18	0.1	0.6
007-1	269	0.4	241.5	269.4	1417.5	0.6	2.3	3.6	0.23	0.1	0.8
008	106	0.2	72.4	234.8	84	0.3	0.5	1.3	0.06	0.09	0.49
008-1	80	0.1	119.9	165.6	105.3	0.2	0.8	1.2	0.15	0.09	1
008-2	267	0.4	274.1	471.4	175.6	1.1	1	2.9	0.14	0.09	0.49
009	95	0.2	65.4	119.6	144.1	0.3	0.7	1.5	0.14	0.09	0.6
010	24	0.09	9	192.7	396.7	0.09	0.8	2.1	1.32	0.09	0.6
011	33	0.2	36	116.9	532.9	0.09	0.5	2.1	0.15	0.09	0.5
012	64	0.1	62.1	146.6	270.7	0.09	0.8	2	0.12	0.09	0.7
013	71	0.1	67.4	76.3	84.2	0.2	0.6	1.1	0.1	0.09	0.6
014	177	0.09	133.5	100.1	193	0.2	0.6	1.3	0.08	0.09	0.49
015	538	0.1	229.4	128.2	323.5	0.2	0.7	1.2	0.1	0.09	0.49
016	317	0.09	218.9	92.6	191.8	0.2	0.7	0.9	0.16	0.09	0.6
017	114	0.2	139.7	146.4	322	0.2	1.6	2.3	0.08	0.09	0.6
018	102	0.1	115.7	170	120.6	0.09	1	1.3	0.15	0.1	1
018-1	24	0.1	39.7	61.5	275.6	0.1	0.6	0.8	0.7	0.09	0.49
019	163	0.1	112.9	141.4	237.3	0.1	1.3	1.3	0.24	0.09	0.9
020	4	0.1	9.8	26	69.3	0.09	0.4	1	0.1	0.09	0.49
021	18	0.1	8.1	116.6	66.1	0.09	0.5	0.7	0.06	0.09	0.6
021-1	4	0.1	8.9	15.3	58.1	0.09	0.4	0.8	0.1	0.09	0.49
023	6	0.2	3.8	137.3	126	0.09	0.6	1	0.68	0.09	0.7
024	6	0.2	36.5	110.1	390.9	0.09	0.8	0.9	2.51	0.09	0.7
025	70	0.1	65.2	113	73.4	0.2	0.6	0.9	0.83	0.09	0.6
026	73	0.1	65.4	185.1	106	0.3	0.6	1	0.46	0.09	0.49

Table A.4 continues.

Sample	Zn	Ag	Ni	As	Au	Cd	Sb	Bi	Hg	Ti	Se
027-1	136	0.2	154.7	161.3	831.5	0.5	1.8	2.4	0.19	0.09	0.9
028	98	0.1	91.1	108.5	127	1.3	0.6	1.1	0.51	0.09	0.49
029	63	0.1	41.1	77.1	285.9	0.09	1.1	0.7	1.51	0.09	0.6
030	94	0.09	116.3	47.8	86.9	0.2	0.5	0.7	0.29	0.09	0.7
031	169	0.1	153.8	74.1	408.8	0.3	0.5	1.5	0.41	0.09	0.7
032	145	0.09	77.6	89.7	440.3	0.2	0.6	1.7	0.5	0.09	0.5
033	57	0.1	51.8	118.4	70.5	0.2	0.7	2.2	1.37	0.09	0.49
034	8	0.09	35.7	80.9	94.7	0.09	0.7	1.1	0.36	0.09	0.49
035	144	0.2	109.1	105.9	128.5	0.3	0.7	2.5	0.07	0.09	0.5
036	147	0.2	105.5	97	63.5	0.4	0.8	2	0.11	0.09	0.49
037	148	0.1	113.3	88.4	576.5	0.5	0.7	2.1	0.21	0.09	0.49
038	14	0.2	16.6	92.2	229.5	0.09	0.6	1.8	1.23	0.09	0.49
039	32	0.1	46.3	130.2	125.9	0.09	0.7	1.9	0.05	0.09	0.49
040	42	0.1	51.5	82.5	250.5	0.09	0.7	1.7	0.11	0.09	0.49
041	175	0.1	94.9	87.8	290.6	6.2	0.9	1.5	0.17	0.09	0.49
042	346	0.1	198.8	81.2	130.1	0.09	0.6	1.3	0.12	0.09	1.4
042-1	299	0.09	246.3	89.8	270	0.2	0.8	1.3	0.14	0.09	0.7
043	91	0.09	98.6	96.4	168.7	0.09	0.7	1	0.12	0.09	0.49
044	99	0.1	141.6	123.4	403.9	0.2	1.8	2.5	0.09	0.09	0.49
045	67	0.09	78.6	137.1	174.8	0.2	0.8	1.1	0.12	0.09	0.49
046	99	0.09	92.9	115.9	331.8	0.09	1.3	1.4	0.31	0.09	0.49
048	9	0.09	13.2	27	169.1	0.09	0.4	0.4	0.06	0.09	0.49
049	13	0.1	38.1	189.7	823.3	0.09	0.7	0.5	0.2	0.09	0.49
050	145	0.09	229.7	191.4	149.3	0.6	1.2	1.1	0.42	0.09	1.2
052	73	0.09	61.3	92.7	375.7	0.2	0.8	0.6	0.25	0.09	0.49
053	116	0.09	67.7	130.3	112.1	0.2	0.8	0.6	0.46	0.09	0.49
054	90	0.09	54.1	87.4	125.7	0.2	0.6	0.5	0.2	0.09	0.49
055	164	0.09	57.2	127.1	62.4	0.1	0.9	0.8	0.67	0.09	0.49
056	90	0.09	56.1	108.7	107	0.09	0.8	0.6	0.25	0.09	0.49
057	97	0.09	70.2	122.3	69.8	0.09	1	0.9	0.29	0.09	0.49
058	117	0.09	88.5	114.8	59.6	0.2	0.7	0.7	0.39	0.09	0.49
059	5	0.09	8.2	21.7	140.4	0.09	0.5	0.4	0.17	0.09	0.49

Table A.4 continues.

Sample	Zn	Ag	Ni	As	Au	Cd	Sb	Bi	Hg	Ti	Se
060	11	0.09	35.8	700.2	119.6	0.09	0.8	0.9	0.19	0.09	1.2
061	109	0.09	96	94.3	221.4	0.2	0.7	0.5	0.15	0.09	1.5
062	64	0.09	86.4	95.3	49	0.2	0.9	0.7	0.19	0.09	0.49
063	99	0.09	75	113.5	430.8	0.1	0.9	0.7	0.41	0.09	0.9
064	82	0.09	55.8	102.1	94	0.09	0.7	0.5	0.35	0.09	0.6
065	83	0.09	43.4	93.6	75.1	0.1	0.8	0.5	0.37	0.09	0.49
066	103	0.09	56.8	115.9	117.2	0.09	0.8	0.7	0.27	0.09	0.5
067	66	0.09	49.6	108.8	58	0.09	1	0.6	0.4	0.09	0.49
068	179	0.1	176.6	100.3	97.1	0.3	0.9	1	5.39	0.09	0.7
069	215	0.3	242.2	132.9	130.4	0.7	1	1.3	4.37	0.09	0.49
070	231	0.2	191.8	103.7	219	0.7	1.1	1.6	8.26	0.09	0.9
071	56	0.09	94.2	56.2	58.7	0.2	0.7	0.9	0.55	0.09	0.7
072	85	0.2	58.4	83	75.5	0.2	1	1.3	3.38	0.09	1.3
073	38	0.1	182	91.3	812.1	0.09	0.9	1.1	0.78	0.09	1
074	25	0.09	38.3	84.6	127.8	0.09	0.7	0.8	0.75	0.09	0.7
075	112	0.1	56.8	67.6	324	0.8	0.6	0.7	0.21	0.09	0.49
076	33	0.09	38.4	155.8	134.1	0.09	0.7	0.7	0.29	0.09	0.7
077	24	0.1	58.8	199.3	473.4	0.1	0.8	1	0.14	0.09	-
078	9	0.2	33.2	64	1135	0.09	0.7	1.2	0.21	0.09	-
079	33	0.09	58.6	280.8	536.9	0.09	0.6	1.2	0.9	0.09	-
080	7	0.1	26.7	39	497.1	0.09	0.6	1	0.18	0.09	0.6
081	34	0.09	52.8	232	191.5	0.1	0.7	0.8	0.34	0.09	0.9
082	28	0.1	71.3	64.3	592.6	0.4	0.6	0.9	0.7	0.1	1.1
083	24	0.2	37.7	91.9	1184.1	0.1	0.5	0.9	0.2	0.09	0.7
084	14	0.1	46.4	106.5	331.2	0.09	0.7	1	0.18	0.09	1.5
085	30	0.1	64.8	117.6	581.5	0.1	0.7	1.1	0.18	0.09	1.3
086	122	0.1	86.2	140.8	227	0.09	0.8	0.9	1.04	0.1	0.49
087	176	0.09	163.3	142.1	135.2	0.7	1	0.9	0.78	0.09	0.5
088	175	0.09	161.3	159.1	337.2	0.8	0.9	0.9	0.9	0.09	0.5
089	194	0.1	260	173.2	223.7	0.5	1	0.9	1.13	0.09	0.49
090	404	0.1	300.8	155.4	286.5	0.3	0.7	0.8	2.55	0.09	0.49